LUCAS, M. 1986. *Vibratory response of stator cores of large induction motors operating in an offshore installation*. Robert Gordon's Institute of Technology, MPhil thesis. Hosted on OpenAIR [online]. Available from: https://doi.org/10.48526/rgu-wt-1993236

Vibratory response of stator cores of large induction motors operating in an offshore installation.

LUCAS, M.

1986

The author of this thesis retains the right to be identified as such on any occasion in which content from this thesis is referenced or re-used. The licence under which this thesis is distributed applies to the text and any original images only – re-use of any third-party content must still be cleared with the original copyright holder.

OpenAIR @RGU

This document was downloaded from https://openair.rgu.ac.uk

CC BY NC

VIBRATORY RESPONSE OF STATOR CORES OF LARGE INDUCTION MOTORS OPERATING IN AN OFFSHORE INSTALLATION.

By

Margaret Lucas BSc (Eng) Hons.

This thesis is submitted in partial fulfilment of the requirements of the Council for National Academic Awards for the Degree of Master of Philosophy (MPhil).

Sponsoring Establishment:

School of Electronic and Electrical Engineering
Robert Gordon's Institute of Technology
Schoolhill
Aberdeen AB9 1FR.

Collaborating Establishment:

Britoil plc
150 St. Vincent Street
Glasgow G2 5LJ.

September 1986.

DECLARATION.

I hereby declare that this thesis is a record of work undertaken by myself, that it has not been the subject of any previous application for a degree, and that all sources of information have been duly acknowledged.

During this research the following courses, visits and conferences were attended:

1. Honours level instrumentation course, RGIT.
2. Postgraduate level computing course, RGIT.
3. Industrial visit to Lawrence, Scott and Electromotors Ltd., Norwich, 1984.
4. Seminar on Condition Monitoring of Machinery and Plant, IMechE London, June 1985.

Margaret Lucas
September 1986

INDEX

CHAPTER/

Index (contd.)

ACKNOWLEDGEMENTS.

I acknowledge with gratitude the supervision and encouragement given to me by W.T. Thomson as Director of Studies. I also thank A.J. Low and the technical staff for their construction of the test rig and for their help and advice, B.J. Burnett for the use of his signal processing software, and Mrs. M. Cuthill for the presentation of this thesis.

ABSTRACT

Vibratory Response of Stator Cores of Large Induction Motors Operating in an Offshore Installation

by Margaret Lucas.

The work presented in this thesis is based on theoretical and experimental investigations into the vibration behaviour of stator assemblies of induction motors. The aim is to evaluate the effectiveness of using the Finite Element Method to predict the natural frequencies, mode shapes and vibratory response of a large induction motor stator on an offshore installation. This information of stator vibration behaviour is a prerequisite for the installation of a reliable vibration monitoring strategy to detect motor faults.

Initial studies are based on the analysis of a small (11 KW) motor stator under free and mounted conditions so that a realistic mathematical representation of a motor stator can be verified by comparing calculated with measured dynamic characteristics.

The next stage of the project was to design and develop an original test rig which was a scaled down model of a large (2 MW) induction motor stator assembly. A combined theoretical and experimental investigation of large motor stator dynamic behaviour was carried out and calculated results from a finite element analysis were compared with laboratory measurements.

The finite element models were then developed to include response calculations and the vibration amplitudes due to a simple external forcing function and the fundamental electromagnetic radial forcing function were calculated. Measured response levels were recorded on the frame and core of the test rig for comparison.

Finally an experimental investigation was carried out into the effects of a single-phasing fault on the vibration signal measured on the core and frame of the large stator assembly model.

The main conclusion drawn from this study is that the Finite Element Method is an effective approximation technique for calculating the vibratory response information necessary for reliable motor fault detection by stator assembly vibration monitoring.

CHAPTER 1.

INTRODUCTION

1.1 Condition Monitoring.

Attitudes to plant maintenance in the British industrial sector have been changing as economic pressures and technological advances have encouraged philosophies leading to increased productivity, efficiency and cost effectiveness. In the past, machines were run until they failed and then repaired or replaced. As this was a costly and often dangerous method of operation it became sensible to introduce a formal maintenance policy which included regular planned machine outages. It was hoped that preventative maintenance would reduce the risk of unexpected failures by identifying possible sources of failure and carrying out necessary repairs during machine downtime. However, with the growth of the offshore oil production industry and the introduction of modern stringent safety regulations, there has been a growing awareness among machine operators that a continuous method of assessing the condition of a machine would be advantageous in areas where operation is hazardous and types of failures often cannot be anticipated. The economic benefits of condition monitoring (1), (2) include the reduction of output losses and maintenance costs and a scheme can be incorporated in some form into most industrial maintenance programmes.

On-line conditioning monitoring of rotating machinery is a comparatively new engineering discipline but it has already encouraged many companies to involve themselves in research and certain monitoring techniques have been successfully applied to detect a range of fault mechanisms. For example, monitoring vibration levels on gearboxes and bearing housings can detect mechanical wear or cracks (3), (4), (5), (6) and monitoring electrical line quantities (7) can detect various rotor faults, stator winding faults and unbalanced supply (8), (9), (10), (11). Failure mechanisms which cause most concern, particularly for the offshore operators, are identified in a survey of many of the major industrial organisations by Thomson et al (12). Vincent (13) also analyses the causes of failures in a.c. drives and presents similar findings.

If a fault condition could be detected at an early stage, the future availability of plant could be predicted and outages planned in advance. Hence a condition monitoring strategy providing on-line machine health diagnostics would make economic sense and improve safety offshore.

1.2 Vibration Monitoring of Induction Motors.

In the offshore oil production industry, large (2-10 MW), 11kV, 3-phase induction motors are used to drive sea-water injection pumps, gas compressors and oil exporting pumps. The squirrel-cage induction motor is relied upon by many of the oil companies due to its robust construction and reliability. However the exceptionally hazardous environment on oil production platforms in the North Sea provides extreme operating conditions and special problems for machine operators. Often failures can occur that are not experienced in onshore installations and it is expected that these may be caused by unique vibration problems. For example, vibration problems can be caused by direct-on-line starting producing large transient vibratory forces which act on the stator core and windings. The windings in the slots are also continually subjected to steady-state forced vibrations due to high frequency core vibrations. The combination of transient and steady-state winding vibration causes gradual insulation degradation and can eventually lead to an electrical insulation failure. The operators also believe that vibration problems can occur because the motors are mounted on steel baseplates on a structure which moves. Their reasoning is well founded since in onshore installations the motors are mounted on solid concrete foundations and similar types of failures have not been reported.

Vibration monitoring, as part of a condition monitoring strategy, is a technique which can be applied especially to rotating machines. As all machines which contain moving parts vibrate, information can be collected from the vibrating components which is indicative of the machine's operational well-being.

It is well known that vibratory forces in induction motors are produced inherently by the magnetic excitation forces which are a by-product of the air-gap flux density squared (14). However, induction motors operating offshore will also experience vibrations transmitted to the stator core, frame and windings from drilling operations and sea motion which may influence vibration levels at frequencies being monitored to detect faults. It has been shown that the vibration signature of an induction motor stator core can be analysed to detect faults such as voltage unbalance and broken rotor bars (8). These faults are identified by changes in the measured vibration levels of the principal slot harmonic components. With broken rotor bars, sidebands appear around the principal slot harmonics so that identifying sideband content can indicate that the rotor needs rewinding. The vibration levels of these frequency components can be influenced by stator natural frequencies or drilling operation frequencies occurring at or near a slot harmonic. Fault detection is also affected by the mode shape of the stator assembly as the measured vibration levels change continuously over a modal half wave. Hence the vibration signal should be measured at an optimum sensing position and transducer mounting positions should be carefully selected. For frame vibration monitoring, a suitable measurement position will depend on the type of frame construction and its modal behaviour. The possibilities for core vibration monitoring will depend on the accessibility of the core pack for mounting transducers at good sensing positions.

It appears that a detailed analysis of the mechanical response of the stator core assembly of induction motors is required before any changes in vibration levels due to fault mechanisms can be quantified. The reliability of a monitoring strategy based on stator core vibration will depend on the understanding of the dynamic behaviour of induction motors in their operating environment. Operators must be equipped with a "baseline" machine vibration signature for each machine in its specific environment so that a monitoring system can detect real changes in the signature which can only be due to the inception of a fault mechanism. This baseline must be calculable by the operator when the "healthy" machine is first installed. Therefore an appropriate mathematical analysis of stator assembly vibration must satisfy the following three requirements:

(1) to develop an accurate mathematical model of the stator core including realistic representations of the stator structure and boundary conditions,

(2) to predict accurately the effects of the frame, feet and mounting arrangement on the natural frequencies and mode shapes of the complete stator structure in terms of the influence on fault detection,

(3) to calculate the response of the core assembly to the excitation forces produced in operation.

To comply with these three requirements, the finite element method is used in this study to construct a mathematical model of the stator assembly. The advantage of this numerical approximation technique is its ability to simulate complex boundary conditions so that an accurate representation of the stator can be modelled. Only a few studies of motor dynamic behaviour by the finite element method have been conducted previously and these were concerned with free-body core vibration (see Chapter 2). Therefore one of the main objectives is to assess the effectiveness of the Finite Element Method as a mathematical technique for providing accurate information of stator vibration in an operating environment. This is required as a basic grounding for future work directed towards reliable stator vibration monitoring.

CHAPTER 2.

THE VIBRATION BEHAVIOUR OF INDUCTION MACHINES.

2.1 Construction and Dynamic Behaviour.

To understand the dynamic behaviour of induction motors as influenced by the machine frame, feet and mounting arrangement, it is useful to investigate these characteristics with reference to stator construction. Most induction machines used offshore are large (2-10MW) motors, however previous research into the vibration behaviour of stator cores and frames has mainly been centred on small motors. The resulting mathematical models for calculating natural frequencies and mode shapes are well used in industry in the design of all sizes of stator cores. To appreciate the relevance of these studies in terms of medium or large machines, it is useful to make comparisons between the construction of small and large motor stator assemblies. Also, the dynamic significance of the various stator component parts which contribute to the overall levels and modes of vibration are considered.

In the manufacture of large machines a system of fabricated construction is employed. The core pack laminations are made from low loss electrical sheet steel insulated on both sides. The stampings are assembled in segments separated by radial spacers and ventilation ducts. Segments are built up into a complete core around a shaft, under pressure between large end-plates, while steel tie bars are welded around the core periphery for added rigidity. The endplates support the stator feet as well as serving as pressure plates for the core. Apart from the endplates the rest of the frame usually provides cover for the machine in the form of thin plates and does not add much to the strength of the assembly. This means that vibration transmission between the core and frame of large machines is often entirely through contact between the core ends and the endplates.

The most significant modes of vibration are those due to radial bending so that resistance to large amplitudes of deformation will depend on the core depth behind the slots. The presence of the bars welded along the core back can considerably alter the dynamic behaviour of the core. An experimental study by Bray (15) shows how the addition of discrete longitudinal stiffeners results in a definite difference in many of the natural frequencies of cylindrical shells. The tie bars provide added asymmetry to the stator core and increase the likelihood of finding dual resonances for circumferential and axial modes. Dual resonances are two natural frequencies of differing values associated with the symmetric and antisymmetric mode shape of the same wave number (16). Longitudinal modes of vibration may also be significant in large machines especially if the core is long. If there is axial flexibility, the radial vibration levels along the machine length will not be constant.

The construction of small machines differs most in the design of the frame. Small motors used to be made up of an inner core connected to an outer cylindrical shell by non-rigid ribs (17). This type of construction led to noise and vibration problems due to the lack of structural rigidity. The modern small induction motor is a compact design where the core laminations are an interference fit along the length of a thin lightweight cylindrical frame.

In this case complete solid coupling exists between the core and outer frame for both radial and longitudinal modes which reduces the number of resonant frequencies associated with each core vibration wave number. The frame also adds strength to the stator. In most cases the frame is cast so that the stator feet are integral with the frame and share its motional behaviour. In situ the frame feet tend to become fixed nodal points and if the foundation on which the motor is mounted is very stiff, the stator may be regarded as a partial ring with fixed ends (18, 19). However, in practice the feet may be admitted a degree of flexibility (19) depending on the amount of restraint imposed by the foundation and mounting arrangement.

There is some debate over the dynamic significance of the core teeth and windings and their effects on core vibration. Some researchers believe the teeth act as additional masses contributing inertia but not strength to the core (17, 20, 21). Others allow for free flexing of the teeth by including them as an integral part of the core structure (22, 23, 24). The effects of the windings will depend on the machine size and type of construction. In large machines the heavily insulated formed windings are a radial clearance in the slots and may be free to move although restricted to some extent by the wedges. This movement is often further restricted by the fixing system of the end overhang portion of the winding which may be very rigidly braced (25). The windings of small machines are stacked in the slots and packed tightly by the wedges, allowing for almost no winding movement. In either case, the stator windings will greatly reduce the lateral oscillatory motion of the teeth.

It would seem that an overall view of stator dynamic behaviour will provide the real vibration picture. The various components of the stator assembly must be regarded in their interactive vibratory state rather than as additions to the core pack.

2.2 Theoretical Vibration Analysis of Electrical Machines.

Research involving accurate mathematical methods for determining the natural frequencies of rotating machines has evolved mostly over the past century. As design standards have become more stringent, accuracy has assumed greater importance and the mathematical representations of the vibration condition have increased in complexity. Most of the research has been directed towards manufacturing and design problems in order to avoid mechanical resonances and keep noise levels within British Standards specifications. Nevertheless, the various mathematical models provide an insight into the dynamic nature of machines and attempt to answer the question of how the individual components of a stator assembly contribute to the vibration behaviour of the whole structure.

Most of the published mathematical methods for calculating stator core natural frequencies are derived from elementary thin ring theory. The two basic types of analysis as outlined by Timoshenko (26) and Flügge (27), are most often referred to in the relevant literature.

The energy method in its simplest form is used by Timoshenko. For in plane vibrations, the radial displacement component is approximated by a finite power series and substituted into expressions for kinetic and potential energies. Lagrange's equation for a conservative system gives the appropriate differential equations of motion from which the generalised frequency equation is derived.

Other mathematical models are based on Flügge's bending theory for shells. All the internal and external forces acting on a shell element are resolved to give three force equations. The moments are included to obtain the equation for equilibrium of moments. This three-dimensional stress problem becomes a shell problem by assuming the element is thin. The solution may be based on neglecting the unimportant terms of the fundamental equations of three-dimensional elasticity theory, or on the theories of bars and flat plates.

The application of thin ring theory in its basic form to calculating core natural frequencies has been put forward by some authors (26, 28). In the frequency equation the core teeth are incorporated by increasing the density of the ring but are otherwise ignored. The technique is often used as a rough guide since it is suitable for obtaining a quick approximation.

The limitations of thin ring theory are severe. Many authors have attempted to develop a more accurate model of stator core vibration by considering more realistic approximations of the core structure. The effects of tooth flexibility on the core ring have been investigated by several authors (20, 21, 23, 24). The teeth are typically treated as additional masses attached to the stator core and the analysis is accommodated with the appropriate boundary conditions or correction factors. One author who considers the teeth as an integral part of the core is Finch (22). His mathematical method includes mass and inertia multiplying factors and models the free flexibility of a tooth by constraining it only by its root stiffness.

Another inaccuracy in the use of thin ring theory stems from the fact that many stator cores are thick; i.e. the ratio of ring thickness to ring mean radius is greater than 0·2. Seidal (29) extends the ring vibration analysis by introducing shear and rotational energy contributions and Buckens (30) suggests a shear coefficient of proportionality which is a function of the shape of the ring's cross-section. Both approaches are considered more appropriate for the calculation of core natural frequencies by some authors (21, 22, 31).

One of the very early investigations which applied thin ring theory to electric motors was a study of frame vibration by Den Hartog (19). The more recent theories have included the core and frame as a thick inner ring and thin outer ring (20, 23, 32). The mathematical models have recently become extremely complex with authors extending the natural frequency calculations to include the effects of laminations (33), windings (24) and wedges (22).

The demand for an accurate solution to the stator assembly vibration problem cannot be satisfied by further development of the Energy Method without increasing the complexity of the mathematical equations to unmanageable proportions.

A different approach to the problem is suggested by Thomson (34). He uses the Finite Difference technique based on the work of Ball (35), but recognises the shortcomings of the method in simulating some of the boundary conditions. Shumilov (36) suggested using the Finite Element Method and later Yang (37) and Watanabe (38) showed the real advantages in using the technique, which include its ability to model complex boundaries and the high levels of accuracy attainable.

The main drawback of the traditional mathematical modelling methods is the lack of a real dynamic model of an induction motor stator assembly in its operating environment. The research has been concerned with the analysis of free-body motion, which gives an initial approximation of stator dynamic behaviour but is not representative of the actual vibration condition of a motor in-situ. The results of natural frequency values and associated modes of vibration are compared with free-body stator experimental investigations but are not analysed in terms of in-situ stator assembly dynamic behaviour. The frame and mounting arrangement are likely to play an important role in the response of the core to the excitation forces and affect considerably the modes of vibration into which the stator can deform at its natural resonances.

The Finite Element Method has the ability to incorporate the irregularities of the stator structure and model the restraints imposed by the machine foundations. With the use of a digital computer, the natural frequencies and mode shapes can be calculated for two or three-dimensional analysis and the technique can also provide a forced response solution. For these reasons the Finite Element Method is adopted to carry out the theoretical dynamic investigations in this study.

Since there has been no previous in-depth study of the effectiveness of the Finite Element Method for modelling stator assembly vibration, the technique will be evaluated both in terms of accuracy and its ability to provide the knowledge from calculations, required as the basis of a vibration monitoring strategy.

CHAPTER 3.

THEORETICAL AND EXPERIMENTAL ANALYSES.

3.1 The Need for a Combined Analytical Approach.

The Finite Element Method is to be evaluated as a mathematical technique for predicting the vibration behaviour of a stator core assembly. The purpose of the study is to establish the capability of the method for obtaining accurate calculations of stator natural frequencies and mode shapes which will provide the necessary information for motor operators to carry out fault detection by vibration monitoring.

If the operators are to attain confidence in the calculations and adopt finite element modelling as the basis for a vibration monitoring strategy they will require assurances that:

(a) the Finite Element Method produces accurate and reliable mathematical predictions,

(b) chosen transducer positioning for fault detection based on finite element calculations is suitable for their particular machine and operating environment,

(c) computer costs are reasonable and computer time is minimised.

To comply with these requirements, a complete appraisal of the Finite Element Method with respect to the dynamic analysis of motor stators must be carried out. Firstly, finite element modelling must be shown to be adaptable and accurate and all mathematical predictions must be backed up by experimental evidence. Therefore the theory of the Finite Element Method and the experimental techniques which constitute an appropriate dynamic analysis of a stator assembly for these purposes are set out in this chapter.

3.2 The Finite Element Method.

3.2.1 Introduction.

The Finite Element Method stems from the fundamental mathematical technique of approximating continuous functions using polynomials (44). The basic idea is to find the solution of a complicated problem by discretising the region of interest and replacing the large problem with a series of simpler ones.

Although the name "Finite Element Method" was introduced fairly recently, the technique was used centuries ago by the early mathematicians to determine an approximation of pi. Two polygons were used to describe an upper and lower bound of the circumference of a circle. By increasing the number of sides (or finite elements) on the polygons a closer approximation to a circle was obtained (39).

Modern use of the finite element method was developed mainly by structural design engineers as a practical method for solving elasticity problems. These uses were of a semi-analytic nature, mainly in aircraft design in the 1940's.

Since then engineers and mathematicians have worked separately to develop the technique. The engineers have concentrated on developing the theory in all areas of structural design, including static and dynamic problems. The mathematician's effort was directed towards discovering a convergence proof by the interpretation of the finite element method in terms of well known variational methods and weighted residual methods (40).

With the arrival of high speed digital computers the means of performing the large numbers of calculations was obtained and the diversity of this approximation technique was recognised. Consequently, the theory has expanded to accommodate the solution of many varied and complex engineering problems in all areas of structural and continuum mechanics.

3.2.2 Solution of the Finite Element Problem.

The application of the Finite Element Method to an engineering problem can be viewed as a series of basic steps:

(a) The region of interest is divided into distinct elements over which the main variables are interpolated. The variables are identified with nodal points which may lie along the periphery of the element (typically a triangular or quadrilateral element) or, in some cases, within the element.

(b) For each element certain characteristics are evaluated. A displacement function defines the state of movement within an element. From energy theorems a stiffness matrix can be derived relating nodal forces to nodal displacements.

(c) The stiffness matrix and load vector of each element is then assembled to give the global stiffness and global load vector. These indicate the overall characteristics of the whole region of interest.

(d) The global stiffness matrix and load vector provide a system of simultaneous equations which may be solved to obtain the unknown nodal variables.

The accuracy of the solution is dependent on the choice of displacement function. The displacement function is usually a simple polynomial with coefficients determined by the nodal displacement parameters. It can also be given in terms of shape functions. An appropriate displacement function will satisfy the following conditions:

(i) The function and its first derivative must be continuous over the element.

(ii) The function should allow for rigid body translation or rotation without straining the element.

(iii) The function should allow for uniform strain within the element.

(iv) The function should allow for internal compatibility as well as compatibility of strain or displacement along boundaries between adjacent elements.

Typically triangular elements are used in a finite element mesh. As a simple example, consider two triangular elements with nodal points at the vertices as illustrated in Figure 3.1. If the two elements are joined at the nodal points then the displaced shape conforming to the above conditions is shown in Figure 3.2.

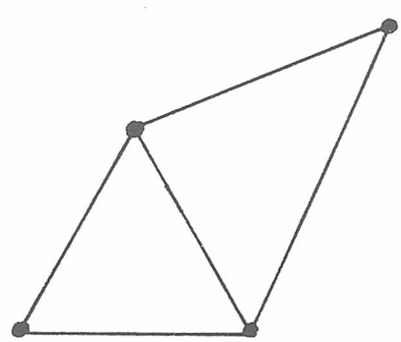

Figure 3.1

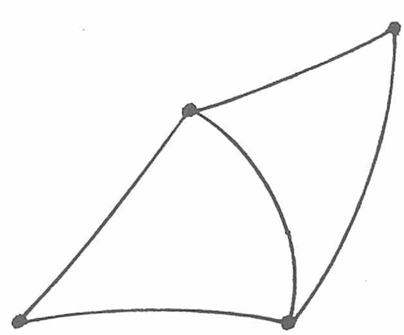

Figure 3.2

Having chosen a suitable trial function, the displacements at any point within the element are derived by the matrix equation

$$\{U\} = [P]\{\alpha\} \tag{1}$$

where $\{\alpha\}$ is the column matrix of the coefficients of the displacement function. For nodal displacement $\{Ue\}$ the matrix equation is

$$\{Ue\} = [A]\{\alpha\} \tag{2}$$

The displacements at any point within the element can be expressed in terms of the nodal displacements of the element by

$$\{U\} = [P][A]^{-1}\{Ue\} \tag{3}$$

At any point in the finite region the strains are given by the matrix equation

$$\{\varepsilon\} = [B]\{\alpha\} \tag{4}$$

The relationship between the strains and nodal displacements is

$$\{\varepsilon\} = [B][A]^{-1}\{Ue\} \tag{5}$$

In this case the matrix $[B][A]^{-1}$ is called the "element strain matrix". If the stress-strain relationship is given by

$$\{\sigma\} = [D]\{\varepsilon\} \tag{6}$$

then stress is related to nodal displacement by

$$\{\sigma\} = [D][B][A]^{-1}\{Ue\} \tag{7}$$

The $[D]$ matrix is an elasticity matrix incorporating the material properties required to relate the stress and strain values in the element. $[A]$, $[B]$, $[M]$ and $[D]$ are matrices of an appropriate order for the system under analysis.

The forces acting on the finite element are described as nodal forces $\{Fe\}$ and are related to the nodal displacements by

$$\{Fe\} = [Se]\,\{Ue\} \qquad (8)$$

$[Se]$ is the "element stiffness matrix" and the product $[Se]\,\{Ue\}$ is the list of generalised forces acting on the element.

The stiffness matrix of an element is determined using the Principle of Virtual Work. A virtual displacement $\{\bar{U}\}$ is imposed on top of the nodal displacement $\{Ue\}$. The resulting virtual strains will be $\{\bar{\varepsilon}\}$ and the virtual strain energy is

$$[SE] = \int_V \{\bar{\varepsilon}\}^T \{\sigma\}\, dV \qquad (9)$$

From equation (5) the virtual strain in terms of virtual displacement is

$$\{\bar{\varepsilon}\} = [B][A]^{-1} \{\bar{U}\} \qquad (10)$$

which may be substituted into equation (9) to give

$$[S.E.] = \int_V \{ [B][A]^{-1}\{\bar{U}\} \}^T [D][B][A]^{-1} \{Ue\}\, dV \qquad (11)$$

in general this simplifies to

$$[S.E.] = \{\bar{U}\}^T[A]^{-T} \int_V [B]^T[D][B]\, dV\, [A]^{-1}\{Ue\} \qquad (12)$$

The external work done on the element by the nodal forces $\{Fe\}$ is given by

$$\{We\} = \{\bar{U}\}^T \{Fe\} \qquad (13)$$

In terms of the nodal displacements, this becomes

$$\{We\} = \{\bar{U}\}^T [Se]\, \{Ue\} \qquad (14)$$

Using the Principle of Virtual Work, the work done may be equated to the strain energy

$$[S.E.] = \{\bar{U}\}^T[Se]\{Ue\} = \{\bar{U}\}^T[A]^{-T}\int_V[B]^T[D][B]dV[A]^{-1}\{Ue\} \qquad (15)$$

which can be rearranged to obtain the element stiffness matrix

$$[Se] = [A]^{-T} \int_V [B]^T [D][B] \, dV \, [A]^{-1} \qquad (16)$$

Once the stiffness matrix for each element over the entire region of interest is determined, the matrices are assembled to give an overall system stiffness matrix $[Ss]$. The element matrices in local axes are transformed into a global stiffness matrix in a global coordinate system. At this point, the boundary conditions are incorporated into the problem and the system equations for the entire region are solved to obtain the unknown nodal displacements. From these primary unknowns, values of stress or strain at any point in the region can be calculated.

3.2.3 Dynamic Analysis.

In a dynamic analysis, displacements, velocities and strains are all time dependent.

The displacement matrix again is given by

$$\{Ue\} = [A] \{\alpha\} \qquad (17)$$

and

$$\{U\} = [P][A]^{-1} \{Ue\} \qquad (18)$$

where $\{U\}$ is the displacement field.

Differentiating equation (18) with respect to time gives the velocity field:

$$\{\dot{U}\} = [P][A]^{-1} \{\dot{U}e\} \qquad (19)$$

where $\{\dot{U}e\}$ is the matrix of nodal velocities. To derive the dynamic equations of motion the Lagrange equation is used:

$$\frac{d}{dt}\left\{\frac{\partial L}{\partial \dot{U}}\right\} - \left\{\frac{\partial L}{\partial U}\right\} + \left\{\frac{\partial R}{\partial \dot{U}}\right\} = \{0\} \qquad (20)$$

In a dynamic analysis the kinetic energy as well as the strain energy must be considered. In this case

$$L = KE - SE \tag{21}$$

R is the dissipation function which is proportional to the relative velocities and dependent on the damping coefficient.

The overall system equations of motion are:

$$[KE] = \{\dot{U}_s\}^T [M_s] \{\dot{U}_s\} \tag{22}$$

$$[SE] = \{U_s\}^T [S_s] \{U_s\} - \{U_s\}\{F_s\} \tag{23}$$

$$[R] = \{\dot{U}_s\}^T [C_s] \{\dot{U}_s\} \tag{24}$$

where:

$[M_s]$ = master mass matrix of the structure.

$[S_s]$ = master stiffness matrix of the structure.

$[C_s]$ = master damping matrix of the structure.

$\{F_s\}$ = total load matrix.

By substituting equations (22), (23) and (24) into the Lagrange equation, the dynamic equations of motion of the structure are derived:

$$[M_s]\{\ddot{U}_s\} + [C_s]\{\dot{U}_s\} + [S_s] \{U_s\} = \{F_s\} \tag{25}$$

or if damping is neglected,

$$[M_s] \{\ddot{U}_s\} + [S_s] \{U_s\} = \{F_s\} \ . \tag{26}$$

If it is assumed that all the displacements in the structure vary sinusoidally in time at frequency ω then,

$$\{\ddot{U}_s\} = - \omega^2\{U_s\} \ . \tag{27}$$

Substituting equation (27) into equation (26) gives

$$-\omega^2[M_s] \{U_s\} + [S_s] \{U_s\} = \{F_s\}$$

or,

$$\left([S_s] -\omega^2 [M_s]\right) \{U_s\} = \{F_s\} \tag{28}$$

where $\{F_s\}$ is a list of the harmonically varying forces which are applied to the system.

The natural frequencies are calculated by determining the frequencies at which the structure will vibrate naturally without any external force being applied.

Therefore $\{F_s\} = \{0\}$.

The natural frequencies will occur when the square matrix

$$| [S_s] - \omega^2[M_s] |$$

has a zero determinant. (39, 40, 41, 42).

3.3 PAFEC.

The viability of the finite element method as a useful analytical tool for solving engineering problems has led to the development of computer packages to cope with the increasing complexity of finite element mesh generation and relevant calculations. One such computer package was developed by PAFEC Ltd., who specialise in finite element software, and is called PAFEC 75 (Program for Automatic Finite Element Calculations). The theoretical analysis of the dynamic behaviour of induction motor stator assemblies in this study is performed using PAFEC.

The finite element package consists of ten computer programs called PHASES. Which Phases are necessary to solve an engineering problem depends on the type of solution required. For a dynamic analysis to calculate natural frequencies four phases are needed; namely Phases 1, 4, 6 and 7. These four programs are executed sequentially to perform a complete analysis and their individual functions are:

PHASE 1 : READ - The data file is read and placed onto backing store.

PHASE 4 : PRE-SOLUTION HOUSEKEEPING - The degrees-of-freedom of the problem are numbered and constrained according to the input constraints.

PHASE 6 : ELEMENTS - The stiffness and mass matrices of all the elements are derived and stored.

PHASE 7 : SOLUTION - The system equations are solved for the primary unknowns.

PAFEC also has a graphics capability which can be included in the analysis by the use of two optional Phases. Phase 3 gives a drawing of the complete structure, depicting all the element boundaries, and Phase 8 draws a graphic solution of the primary unknowns; for a dynamic analysis, the displaced shape of the structure at its natural frequencies.

The input data required by PAFEC is organised into modules describing the structure's dimensions, finite element mesh, boundary conditions and excitation/loading specification. The module headings and standard layout procedure are described in the manual "PAFEC 75 Data Preparation" (43). A control module precedes the input data. Control statements guide the particular job through the various optional paths of PAFEC and can describe the type of information required along with the primary unknowns as printed output.

3.4 Experimental Analysis of a Stator Assembly.

To verify mathematical predictions, a complementary experimental analysis is carried out. There are many resonance testing techniques (44, 45) but the two most applicable to the analysis of stator vibration are Impulse Response and Sinusoidal Resonance tests. Firstly the Impulse Response method is used to identify all the natural frequencies of the structure and indicate which excite radial and longitudinal modes. Once this is known, the structure can be excited at each of these frequencies using the Sinusoidal Resonance Method to determine the associated mode shapes.

3.4.1 Resonance Testing.

An impulse causing vibrational response in elastic systems is characterised by its short duration and wide frequency content. The natural vibratory characteristics of a stator structure can therefore be determined from an impulse response signal containing all the structural natural frequencies. Figure 3.3 illustrates the instrumentation set-up required to determine the response of the stator to a directed impulse. Stator vibratory response is sensed by a unigain piezoelectric accelerometer. The signal is fed through a preamplifier to a B & K Type 2033 high resolution spectrum analyser. The analyser is interfaced to a pdp 11/03 minicomputer, terminal and graphics plotter to obtain hard copies of the response spectra. Impulse tests are carried out at several sensing positions around the core periphery to compensate for any measurements taken at or near a modal node and hence ensure that all resonance frequencies are excited.

Once the natural frequencies have been identified the corresponding mode shapes can be determined by measuring the response around the periphery of the stator structure to a constant amplitude sinusoidal forcing function at each natural frequency. Sinusoidal resonance testing can be performed using single-shaker or multiple-shaker methods to excite the vibration modes. The single-shaker method is appropriate in this study because the stator assemblies are lightly damped and one shaker can provide sufficient force to excite the structural mode shapes.

The instrumentation required to perform a single-shaker sinusoidal resonance test is illustrated in Figure 3.4. The stator structure is radially excited by a B & K electrodynamic vibration exciter driven by a sine generator and power amplifier. To maintain a constant force amplitude, the output level from a force transducer mounted on the structure is used to control the input to the exciter. Vibratory response is sensed by a unigain piezoelectric accelerometer which must have a constant response level itself over the frequency range at which the structure is excited. This requirement must also be satisfied by the transducer mounting stud and mounting adhesive.

There will be some difference between the natural frequency values obtained from the Impulse Response spectra and those obtained from Sinusoidal Resonance tests. In fact the impulse tests can only give an indication of the natural frequency values since the 400 line Spectrum Analyser is, for example, accurate within a bandwidth of $\frac{10000}{400}$ Hz (or 25 Hz) for a spectrum frequency range of 0 - 10 kHz. The Impulse Response spectra are therefore used to indicate where the natural frequencies can be found so that accurate values can be obtained from Sinusoidal Resonance tests.

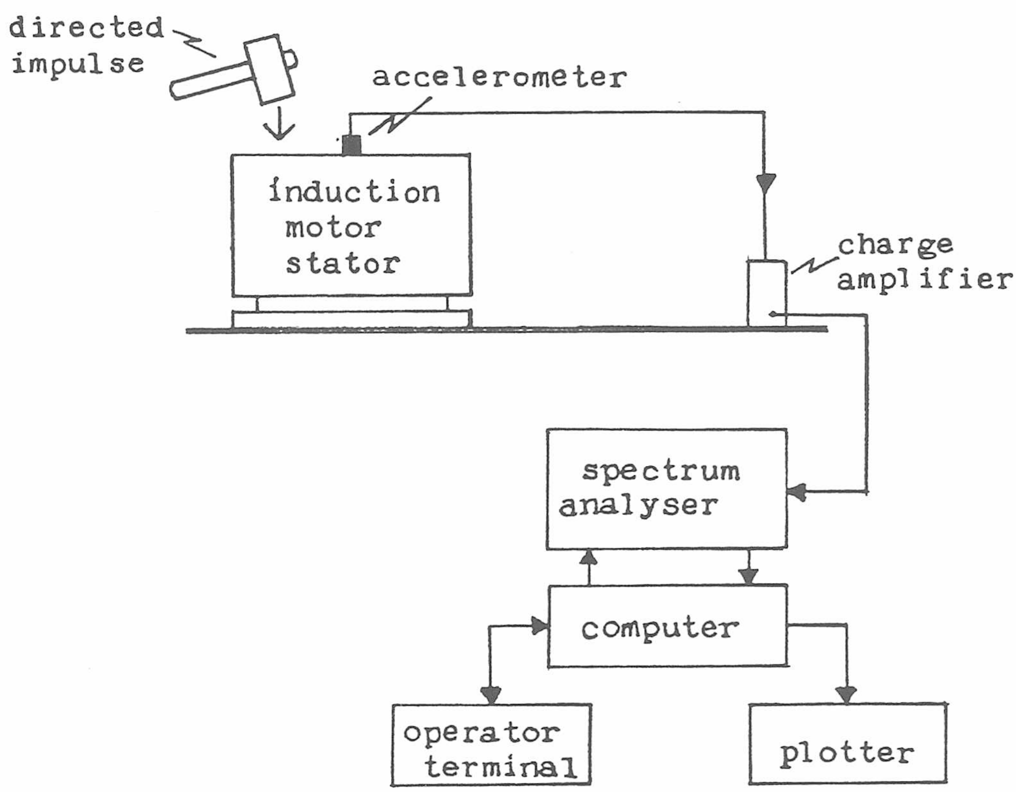

Figure 3.3

Experimental Arrangement for Impulse
Response Tests.

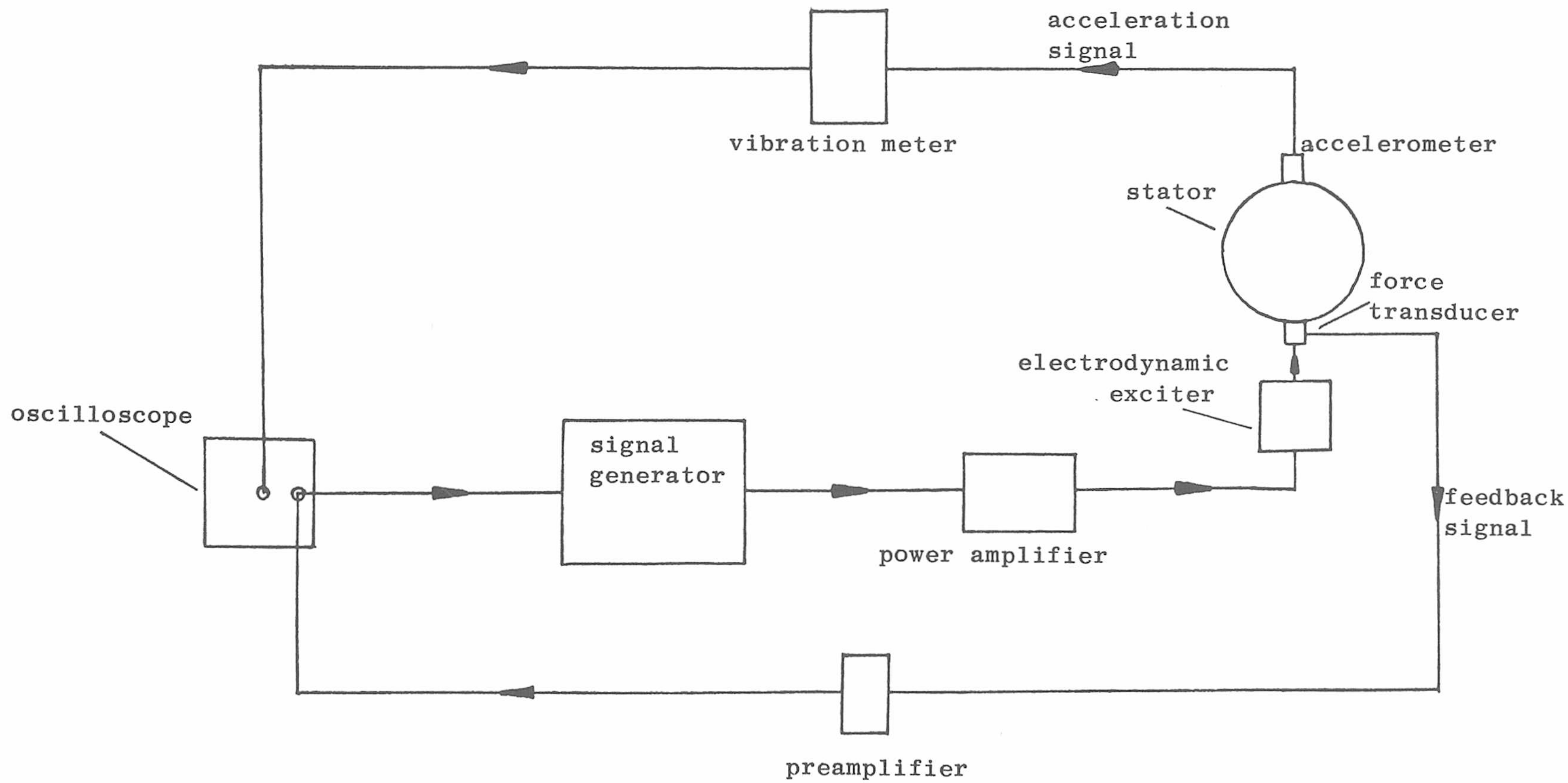

Figure 3.4

Sinusoidal Resonance Test Instrumentation.

CHAPTER 4. THE DYNAMIC ANALYSIS OF A SMALL MOTOR STATOR.

4.1 The Stator Assembly.

The first stage in performing a dynamic analysis of a stator assembly involves a theoretical and experimental investigation of a typical small induction motor. The finite element calculations can be compared with the experimental findings in order to judge the accuracy of the theoretical technique. The stator under examination is the core and frame of a D160M, 11kW motor manufactured by Brook, Crompton, Parkinson Motors. The stator structure comprises annealed steel laminations with 36 slots surrounded by an aluminium frame. The frame is of cast aluminium construction incorporating a thin cylindrical yoke, external ribs and stator feet. A D160M stator core without the frame was also available for analysis. The dimensions and composition of the stator assembly are illustrated in Figure 4.1 .

4.2 The Finite Element Models.

Altogether six finite element models are presented. Throughout, the mesh is made up of curvilinear quadrilateral or triangular isoparametric elements incorporating mid-side nodes where necessary. The model of the complete stator assembly is built up in stages so that the effects of the core teeth, frame, feet and mounting arrangement can be analysed in terms of changes in the calculated values of natural frequencies and their mode shapes.

A description of each of the finite element models is given below:

COR1 (Figure 4.2).

A three-dimensional cylindrical shell based on the dimensions of the stator core but neglecting the teeth.

COR2 (Figure 4.3).

A three-dimensional cylindrical core with the teeth modelled as brick elements with radially tapered sides.

COR3 (Figure 4.4).

A two-dimensional model of the core face including the slot curvature, the semi-closed nature of the slots and the cleating notches on the core back.

ALF1 (Figure 4.5).

A two-dimensional model which consists of model COR3 surrounded by a cylindrical aluminium frame.

ALF2 (Figure 4.6).

Model ALF1 with the aluminium feet added.

ALF3

Model ALF2 with the nodes at the base of the feet restrained to simulate the stator mounting arrangement.

The modelling procedure raises two important points about the finite element analysis.

(i) Since it is the radial component of vibration which is the most significant for measuring vibration levels to detect faults, the emphasis is placed on analysing the radial modes of vibration. These can all be determined from a two-dimensional finite element analysis which is much less time-consuming in computer processing terms than three-dimensional modelling. However, in order to identify the longitudinal modes of vibration, and consider their effects on radial vibration, the first two models are 3D. It was not possible to carry out a three-dimensional analysis of the more complex frame and core models as the computer storage required for the calculations exceeded the allocated running memory of the DEC20 computer.

(ii) The frame ribs are omitted from the finite element models as their effects on the natural frequencies and mode shapes of the stator assembly will be negligible. From cantilever beam vibration theory (26) the calculated fundamental natural frequency of a rib is close to 9·5 kHz and the higher modes are excited above 25 kHz. This means that lower modes of core vibration will not be influenced by rib resonances but will induce small lateral oscillations, in the first beam type mode, in the ribs which will tend to increase the rotational inertia of the structure. However, this mass effect will be negligible since the ribs are short, thin and very lightweight. Therefore, the added complexity to the finite element mesh and the resulting increased computer cost is not justified by the dynamic significance of the frame ribs to the overall structure.

4.3 The Experimental Arrangement.

Impulse Response and Sinusoidal Resonance tests were carried out to determine the natural frequencies and mode shapes of the stator assembly. In order to compare experimental results with those from the finite element analysis, three separate experimental arrangements were analysed:

(1) The stator core pack freely suspended.
(2) The stator core and frame assembly freely suspended.
(3) The stator assembly mounted on a steel bed-plate.

For the analysis of free-body motion, the stator was resiliently mounted, suspended from non-rigid springs, so that none of the degrees-of-freedom of the structure were restrained (Figure 4.7). For the analysis of the mounted stator assembly, the frame feet were restrained by clamps, bolted rigidly onto a thick steel bed-plate.

The accelerometer mounting positions for each of the above test arrangements are as follows:

(1) 24 equally spaced mounting studs around the central circumference and 5 positions along an axial length.

(2) 20 positions around the central circumference of the frame between the feet and 2 positions on each foot. Also 14 axial positions: 7 along the top of the frame and 7 along an axial length 90° around the frame circumference.

(3) As for case (2).

The response of the stator to a directed impulse is plotted on a dB scale and the vibratory response for modal analysis is measured as a radial peak displacement level. The sinusoidal excitation force applied by the vibration exciter during resonance testing has a constant peak amplitude of 19 N (which corresponds to the force level at maximum sine generator output volts).

4.4 Results.

TABLE 1:

Calculated natural frequencies for the freebody analysis of the stator.

Mode m	n	CALCULATED NATURAL FREQUENCIES (Hz). COR1	% Diff.	COR2	% Diff.	COR3	% Diff.	ALF1
0	2	1249	-9.8	1126	-7.8	1036	+9.1	1140
0	2	1254	-10.0	1129	-6.1	1060	+8.5	1159
1	2	1800	-1.1	1780				
1	2	1813	-0.1	1811				
0	3	3588	-12.8	3127	-9.3	2836	+9.2	3125
0	3	3642	-13.4	3153	-10.0	2839	+9.3	3130
1	3	4614	-5.5	4358				
1	3	4768	-7.8	4397				
0	4	7101	-15.1	6028	-14.9	5127	+9.9	5689
0	4	7133	-14.2	6116	-13.6	5286	+7.4	5707
1	4	7316	-14.0	6289				
1	4	7498	-15.0	6374				
0	5	7763	-11.2	6889	-5.4	6513	+0.6	6553
0	5	8410	-12.4	7363	+8.2	8023	+7.7	8689
1	5	8918	-14.9	7593				
1	5	9252	-14.4	7921				

m : longitudinal mode number.

n : radial mode number.

% Diff.: percentage increase (+) or decrease (-) in natural frequency value between each stage of development of the core model, from simple cylinder COR 1 (these values are typical of those calculated from a theoretical approach based on ring bending theory) to the more structurally accurate model COR 2 (with box teeth) to COR 3 (with accurate tooth models) to ALF 1 (with aluminium yoke included).

TABLE 2:

Natural frequencies of the stator core with longitudinal variation (m = 1).

mode n	Natural Frequencies (Hz) COR2	Measured	% Diff.
2	1780	1625	-8.7
2	1811	/	
3	4358	3800	-12.8
3	4397	/	
4	6289	/	
4	6374	/	
5	7593	/	
5	7921	/	

/ : not detected

TABLE 3:

Natural frequencies of the free stator core.

mode n	Natural Frequencies (Hz) COR3	Measured	% Diff.	Response ($m \times 10^{-8}$)
2	1036	1010	-2.5	140
2	1060	1035	-2.4	40
3	2836	2725	-3.9	20
3	2839	/		
4	5127	4725	-7.8	3.0
4	5286	4950	-6.4	10
5	6513	6350	-2.5	3.6
5	8023	/		
6	8146	8150	+0.05	1.0
6	9967	/		

TABLE 4:

Natural frequencies of the free stator assembly.

mode n	Natural Frequencies (Hz) ALF2	measured	% Diff.	Response (m x 10^{-8})
2	1123	1097	-2.3	180
2	1132	/		
3	2831	2820	-0.4	2.8
3	3111	3050	-2.0	2.6
4	4639	/		
4	4825	4970	+2.9	1.6
4	6234	/		
4	6292	5958	-5.3	2.0
4	6745	6545	-3.0	0.01
5	8883	8908	+0.3	0.7

TABLE 5:

Natural frequencies of the mounted stator assembly.

mode n	Natural Frequencies (Hz) ALF3	measured	% Diff.	Response (m x 10^{-8})
2	588	600	+2.0	3.5
2	1153	1130	-2.0	150
3	2421	2870	+15.6	2.7
	2593	/		
3	2601	/		
3	3723	3938	+5.4	0.7
4	5190	5100	-1.7	3.0
4	6110	5980	-2.1	1.1
4	7346	7236	-1.5	0.02
5	7755	/		
5	9354	9280	-0.8	0.3
5	9767	/		

4.5 Discussion.

The results highlight three main areas of interest to the study of induction motor vibration behaviour:

(1) The effects of the various components of the stator assembly on the natural frequencies and mode shapes of the structure.

(2) The possibilities for accurate and realistic mathematical modelling of stator vibration using the Finite Element Method.

(3) The capability of finite element analysis to determine the natural frequencies and mode shapes of a stator assembly in situ, which would aid the understanding of modal deformation expected around frequencies being monitored to detect motor faults.

Recent research into the analysis of induction motor faults (46) has centred on identifying unique changes in the vibration signature recorded on the stator assembly. Broken rotor bars (47) and rotor eccentricity (46) are detected by studying changes around the principal slot harmonic frequencies. These harmonics typically lie within the frequency range 500 Hz to 2.5 kHz depending on the motor under observation. In this study, the finite element analysis refers to the first 4/5 radial modes of vibration or, in other words, the 2nd to 5th/6th ring modes of bending, extending up to frequencies just below 10 kHz. This ensures that any natural frequency occurring at or near an important principal slot harmonic is calculated.

Table 1 presents a comparison between the calculated natural frequency values of the first four mathematical models, which constitute the free-body dynamic analysis of the stator. The changes in the natural frequencies as the stator assembly model develops can be explained as follows:

4.5.1 Effect of Stator Teeth.

The effects of including the core teeth in the mathematical analysis can be determined by comparing the calculated values for COR1 and COR2. The results show a significant decrease in natural frequency values. When the core vibrates at a resonance, small lateral vibrations are induced in the teeth, which tend to increase the rotational inertia of the structure. The stiffening effect of the teeth is small and since tooth resonances occur at much higher frequencies the overall mass effect due to tooth vibration results in a general decrease in natural frequency values.

4.5.2 Three-Dimensional Modelling.

The finite element analysis calculates four natural frequencies for each ring mode of vibration. The lower two frequencies are components of the dual resonance exciting pure radial deformation whereas the two higher frequencies excite radial deformation combined with axial variation. The mode shapes of the two 3D models (Figures 4.8 and 4.9) show that at these two higher frequencies, axial variations produce a central nodal circle around the core periphery where no vibratory response would be detectable. During the experimental analysis only two of these frequencies were detected (Table 2) and the vibratory response of the core at both these frequencies was very low compared with the response at the corresponding pure radial bending frequencies. Pure longitudinal natural frequencies were not excited in the frequency range under investigation. The effects on core vibration of axial variations due to coupled radial and axial modes are negligible. For this reason, it is unnecessary to carry out 3-dimensional theoretical studies since all the responsive radial natural frequencies can be determined from a two-dimensional analysis.

4.5.3 Calculated Values from 3D and 2D Models.

Comparing the calculated natural frequencies of models COR2 and COR3 for radial modes of vibration, there are in the main considerable decreases from the 3D model to the 2D model. These reductions are attributable to COR3 being a much more accurate model of the stator core, which includes the cleating notches, slot curvature and the semi-closed geometry of the slots. These results highlight the errors which can occur from simplifying the core boundaries for easier mathematical modelling. Two-dimensional finite element analysis increases the scope for accurate modelling of the stator structure which will increase the reliability of the calculations.

4.5.4 Effect of Stator Frame.

The calculated values of core and frame natural frequencies are higher than those of the core alone. The vibration behaviour is characterised by an increase in the bending stiffness of the stator due to the solid coupling which exists between the core and frame. This more than compensates for the added mass of the yoke which is lightweight aluminium.

The four mathematical models presented in Table 1 all have very similar vibration characteristics. In each case the natural frequencies excite conventional radial ring modes with a phase displaced dual resonance predicted for each wave number. However, when the frame feet are taken into account, the vibration behaviour of the feet affects the mode shapes of the structure at resonance and introduces non-conventional deformation at some natural frequencies. Modes of vibration are further influenced by the stator assembly mounting arrangement which causes the base of the feet to become fixed nodal points.

Tables 3,4 and 5 present comparisons between measured and calculated resonance frequency values determined from the three experimental arrangements and their corresponding finite element models. The associated mode shapes are illustrated in Figures 4.10 to 4.12. Natural frequencies were found experimentally from impulse test spectra (Figures 4.13 to 4.24), and from sinusoidal response measurements.

The Finite Element Method calculates all the structural resonances. It is usual to accept the most responsive frequency of a wave number as being the natural frequency and to consider the less responsive component of the dual resonance and any other frequencies associated with that wave number as being parasitic resonances (48). In some cases the parasitic resonances predicted by finite element analysis could not be detected experimentally. In other cases the response to the forcing function at these frequencies was significant. Since vibration monitoring is sensitive to stator vibration levels, natural frequencies and all other responsive resonances are important. The most responsive frequency (or natural frequency) for each wave number is underlined in Tables 3, 4 and 5, and levels of vibration at all the responsive resonance frequencies are recorded as maximum displacement values.

4.5.5 Core Pack Vibration.

Table 3 shows two frequencies calculated for each wave number. The corresponding mode shapes (Figure 4.10) are the conventional dual resonances of each ring bending mode. The problem which arises from the theoretical predictions is that the first calculated value of a mode is not always the natural frequency. This is not so important at low modes (i.e. $n = 2,3$) as the two frequencies of the dual resonance are close, separated by only a few Hertz. For n = 4, 5 and 6, the phase displaced mode shapes are well separated. At n = 4 the second calculated frequency is the natural frequency whereas at n = 5 and n = 6, only the first frequencies were detectable. It is important for vibration monitoring purposes to know where the natural frequencies occur and the precise shape of deformation around the core at a responsive frequency. Transducer positioning can then be carried out, knowing in advance on which part of the modal wave it will be at a particular frequency. In the analysis of free core vibration, the greatest magnitudes of core displacement are excited by the first two natural frequencies which suggests that these are most likely to affect vibration levels at frequencies monitored to detect motor faults.

4.5.6 Free Stator Assembly Vibration.

Table 4 and Figure 4.11 represent the free-body vibration behaviour at resonance of the stator assembly. The value of n assigned to each frequency indicates the ring bending mode closest to the deformed shape of the stator structure. For n = 2 and 3 the calculated frequencies are dual resonances of each mode with the feet and frame having little effect on core deformation but causing an increase in natural frequency values and a decrease in measured response levels. At higher frequencies, non-conventional mode shapes are excited. For instance, at n = 4 four parasitic resonances are calculated. Figures 4.11 (f) and 4.11 (h) are the two components of the dual resonance both of which could be detected experimentally. The other three parasitic resonances are excited by lateral oscillation and bending deformation of the frame feet. Only one of these frequencies was detected. The vibratory response around the frame was extremely low but the frequency excited a higher response at the frame feet measurement positions. The natural frequency at n = 4 was the fourth calculated value which again highlights the difficulty in predicting the most responsive resonance.

At n = 3, the two components of the dual resonance excite similar vibration amplitudes at their bending wave maxima which implies that in complex structures one component at a particular mode number is not necessarily dominant.

4.5.7 Vibration Behaviour of a Mounted Stator Assembly.

Resonance frequencies and mode shapes of the stator assembly mounted on a steel bed-plate are presented in Table 5 and Figure 4.12 .

Again, parasitic resonances other than the phase-displaced component of the dual resonance are predicted by the mathematical analysis. In this case deformation of the whole stator structure cannot be affected by free lateral oscillation of the frame feet as they are restrained along their base. The parasitic resonances are due to deformation of the feet similar to the first bending mode of a cantilever beam (26) where the restrained base of a foot represents the fixed end of a beam. The resonance frequencies which are influenced by frame deformation excite coupled beam-type and ring-type modes of vibration. In the experimental analysis of the stator assembly only one of these resonances was detected but the response levels were very low and the mode shape was difficult to construct from the vibration measurements.

If the results in Table 5 are compared with those in Table 4, the changes in the dynamic behaviour of the stator due to the effects of mounting the assembly can be analysed. For n = 2 and n = 3 there is an increase in the natural frequency values due to the stiffening effect of restraining the structure. However the mode shape associated with the mounted structure at both mode numbers is phase displaced from the mode shape of the free structure. Another discrepancy arises at the third and fourth modes where the dual resonance components occur in reverse order between the two dynamic conditions. At $n = 4$ the natural frequency excites the displaced dual resonance component under both free and restrained conditions which leads to a reduction in the natural frequency value at this mode.

The other main difference between free and restrained vibration behaviour is in the resemblance of core deformation to ring bending mode shapes. Fixed boundary conditions cause more distortion and restriction in the modes of vibration at resonance producing unique vibration characteristics which are largely dependent on frame construction.

4.6 Conclusions.

This study shows that the free-body dynamic characteristics of a motor stator assembly do not reflect the dynamic characteristics of a motor installed in its operating environment. The stator assembly is a complex structure and must be modelled accurately to achieve realistic and credible resonance evaluations.

The outcome of the theoretical and investigative dynamic analysis is that it illustrates the need for thorough groundwork involving a complete knowledge gathering exercise before stator dynamic predictions for a particular motor adequately justify the application of a quantative vibration monitoring strategy.

The Finite Element Method has proved to be an accurate mathematical technique. The errors involved are, in the main, between two and three percent and do not tend to become much larger at higher modes which is a problem encountered using most of the standard theoretical techniques (26, 28, 34). Finite element analysis is capable of calculating all the structural resonances and providing graphic illustrations of all the associated mode shapes.

In order to be a wholly effective analytical tool, the responsive nature of the assembly needs to be determined. Natural frequencies should be distinguishable from the parasitic resonances and/or frequencies exciting very low level vibration. For this to be achieved sinusoidal response calculations must be introduced into the theoretical analysis.

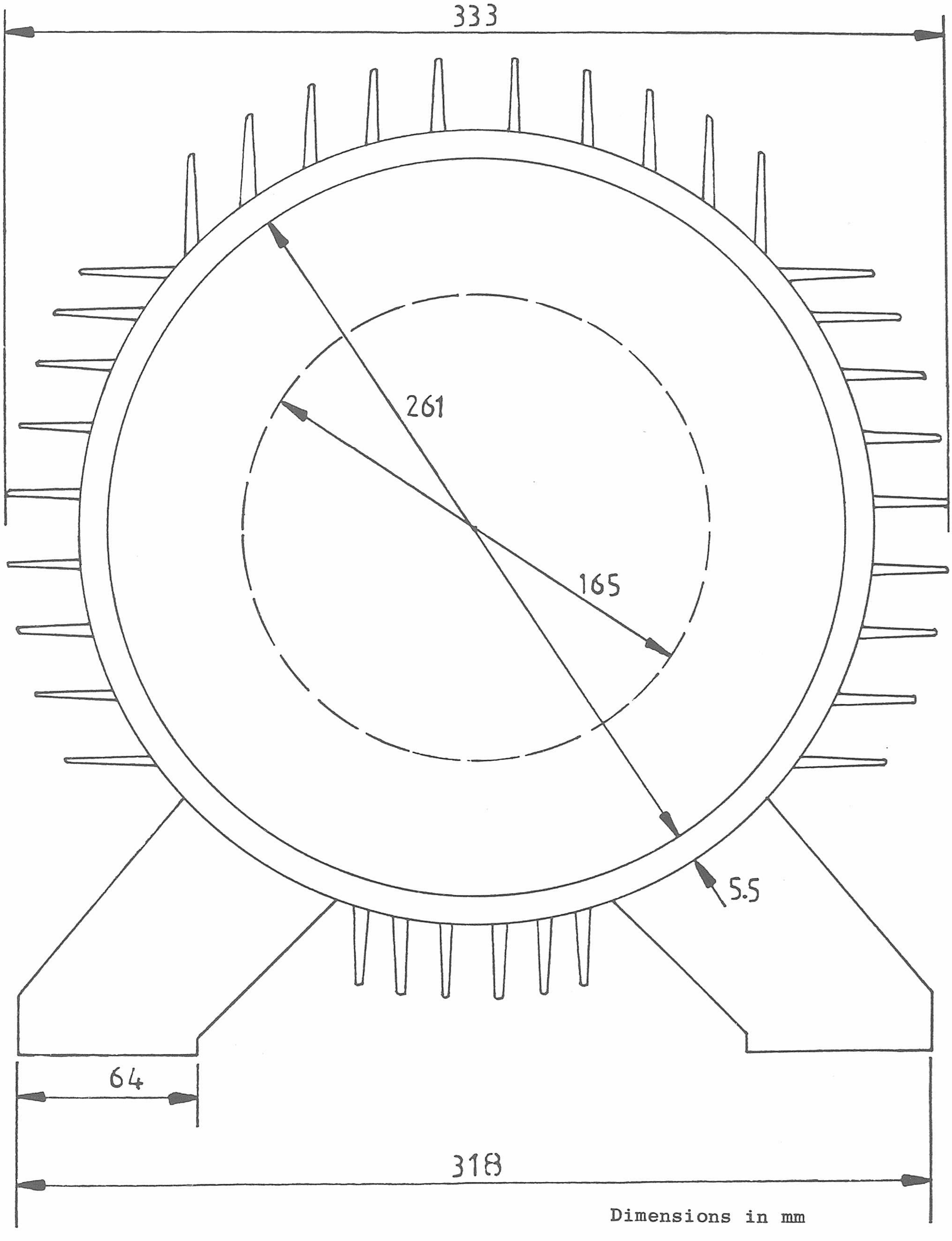

Figure 4.1

Small Induction Motor Stator Assembly.

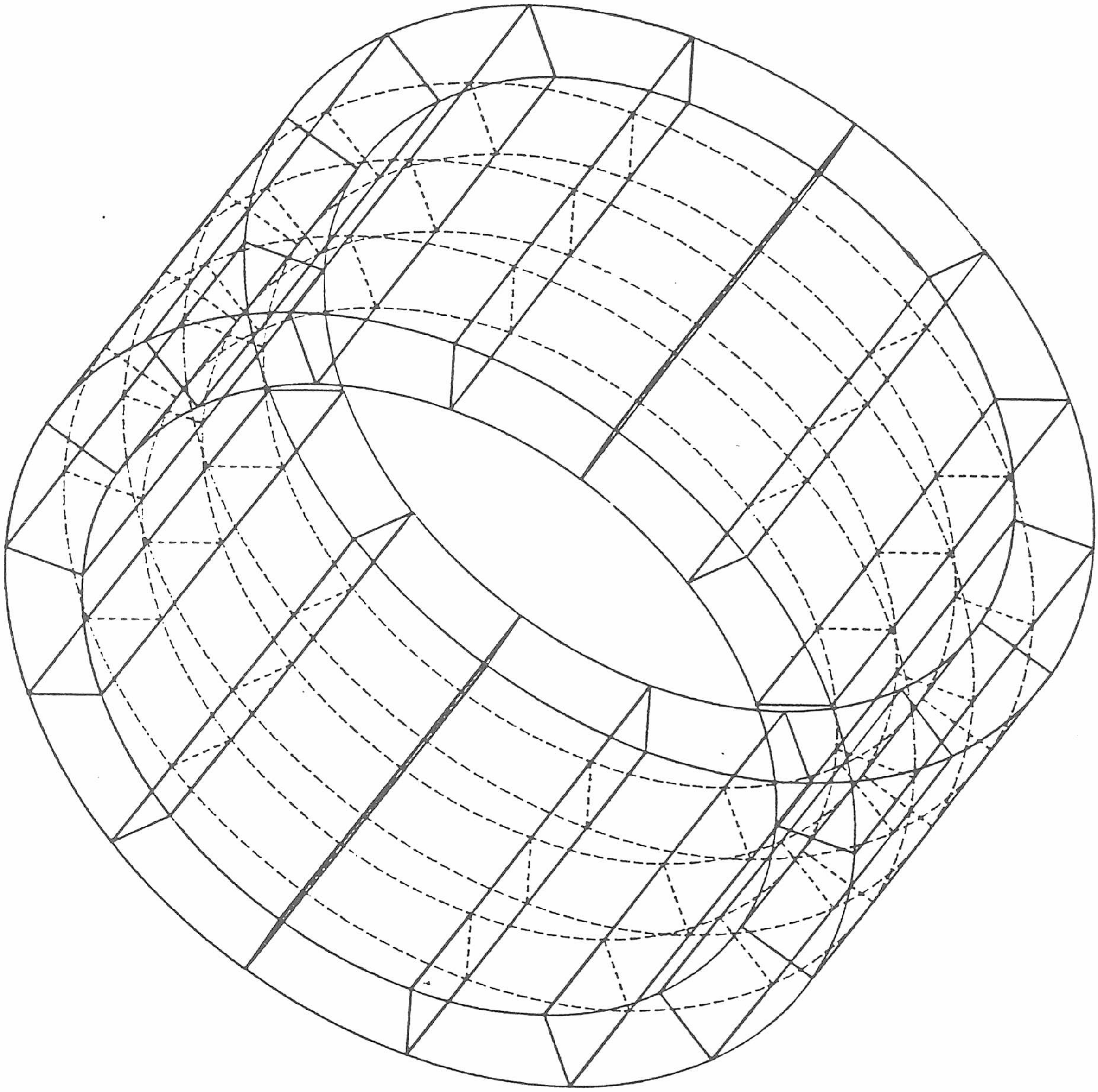

Figure 4.2

COR1.

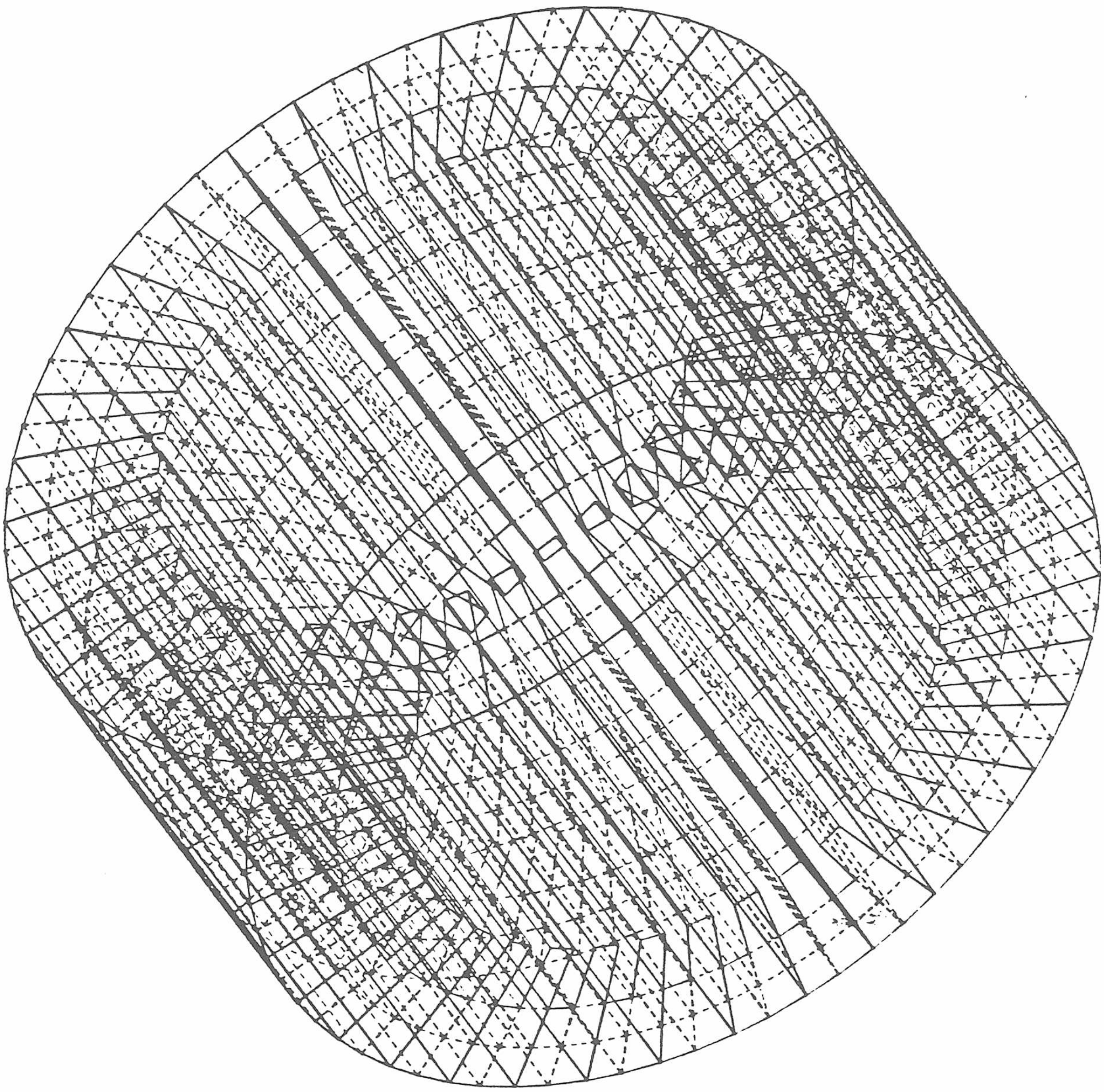

Figure 4.3

(a) COR2 (3D).

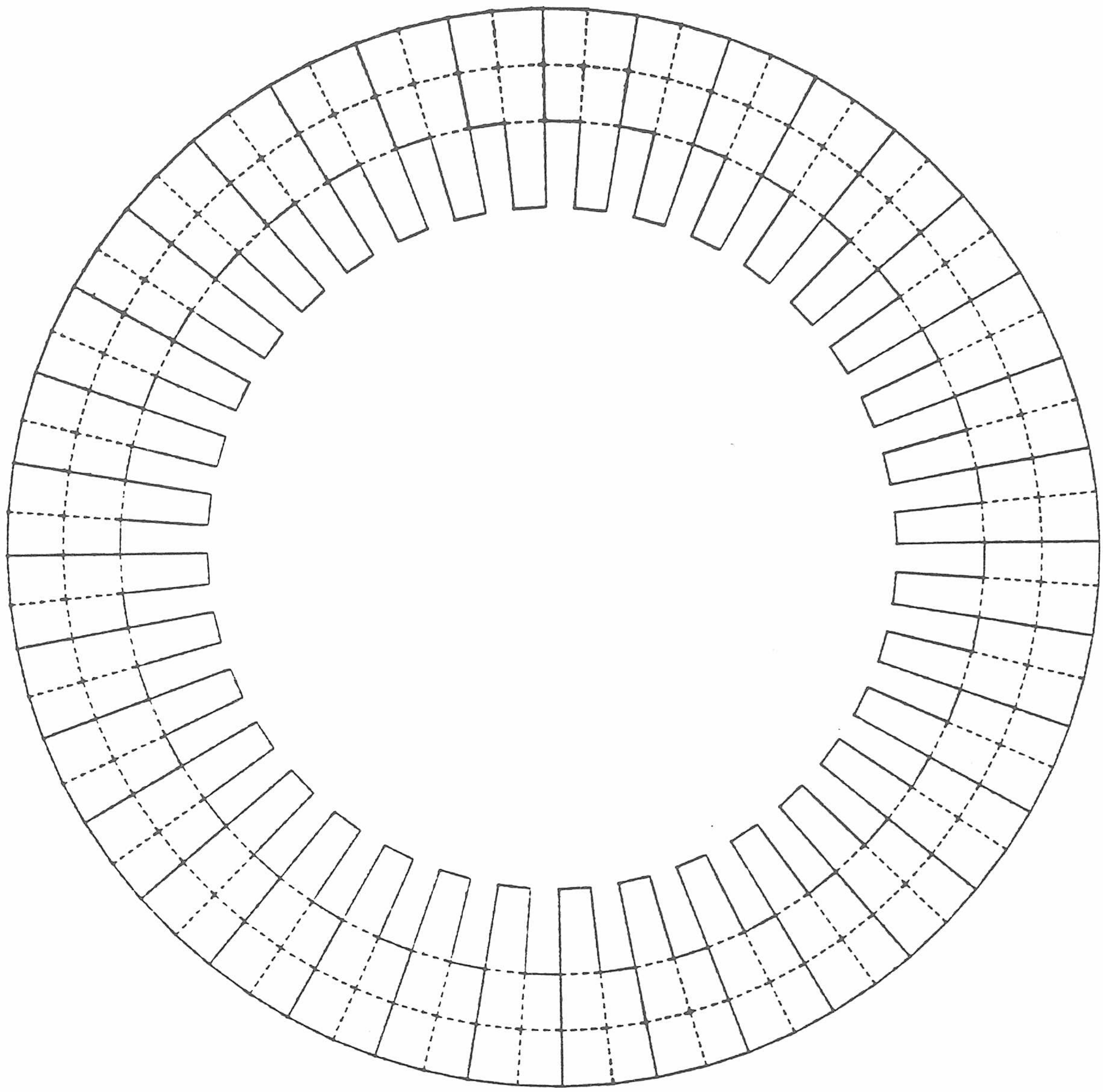

Figure 4.3

(b) COR2 (2D View).

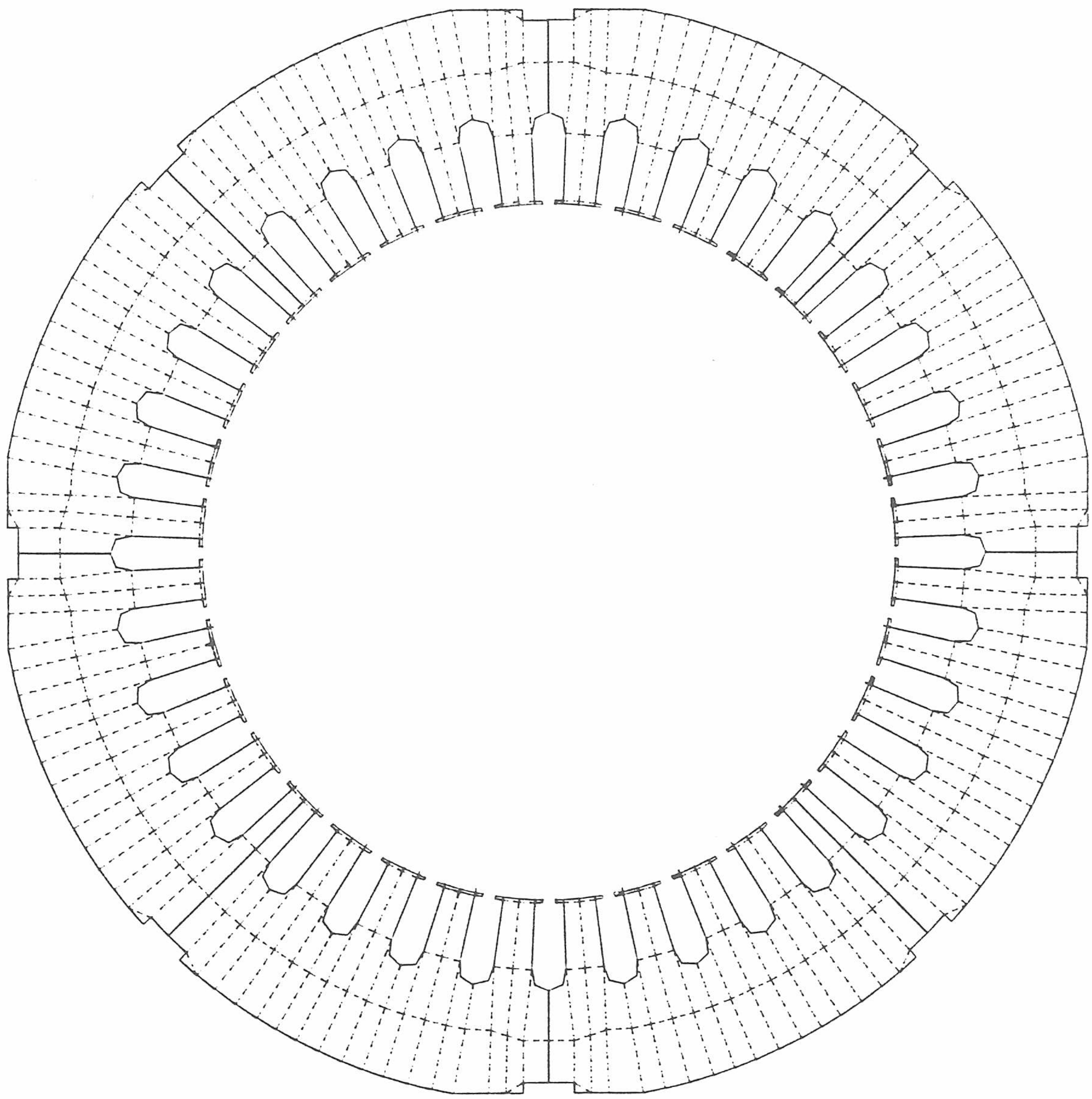

Figure 4.4

COR3.

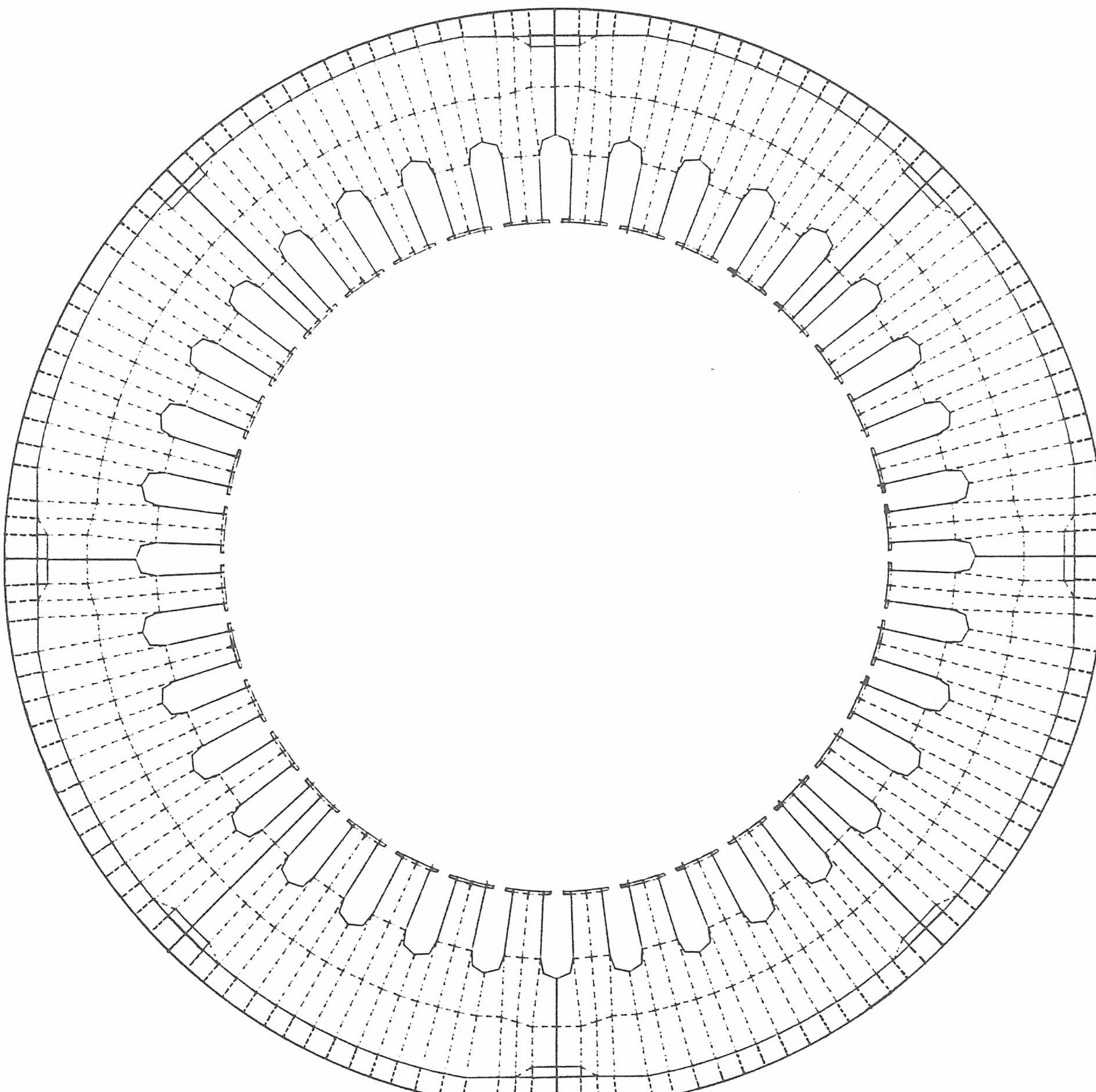

Figure 4.5

ALF1.

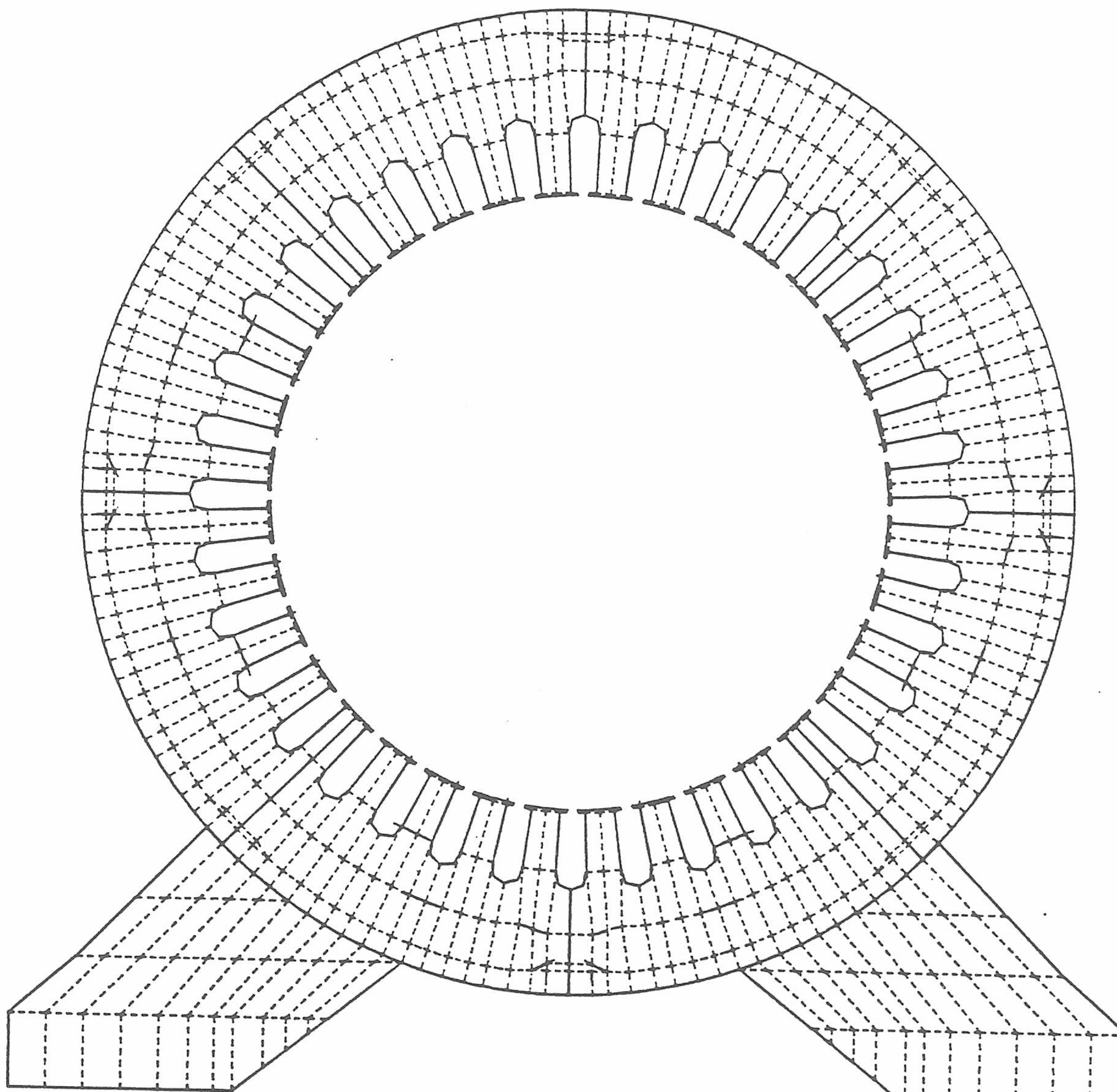

Figure 4.6

ALF2.

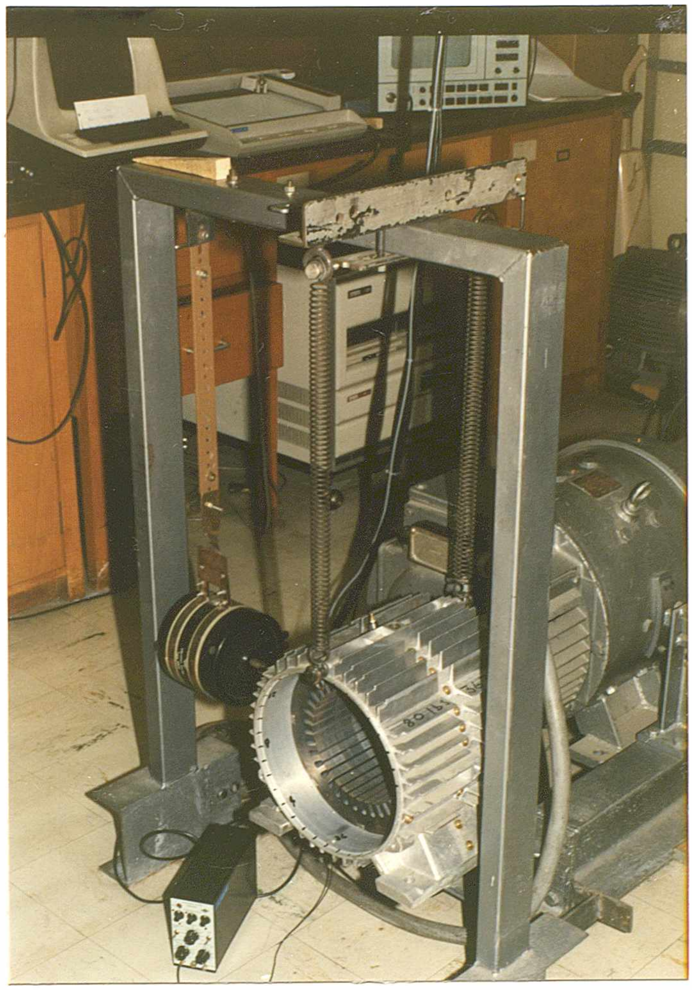

Figure 4.7

Experimental Arrangement for Free-Body Analysis.

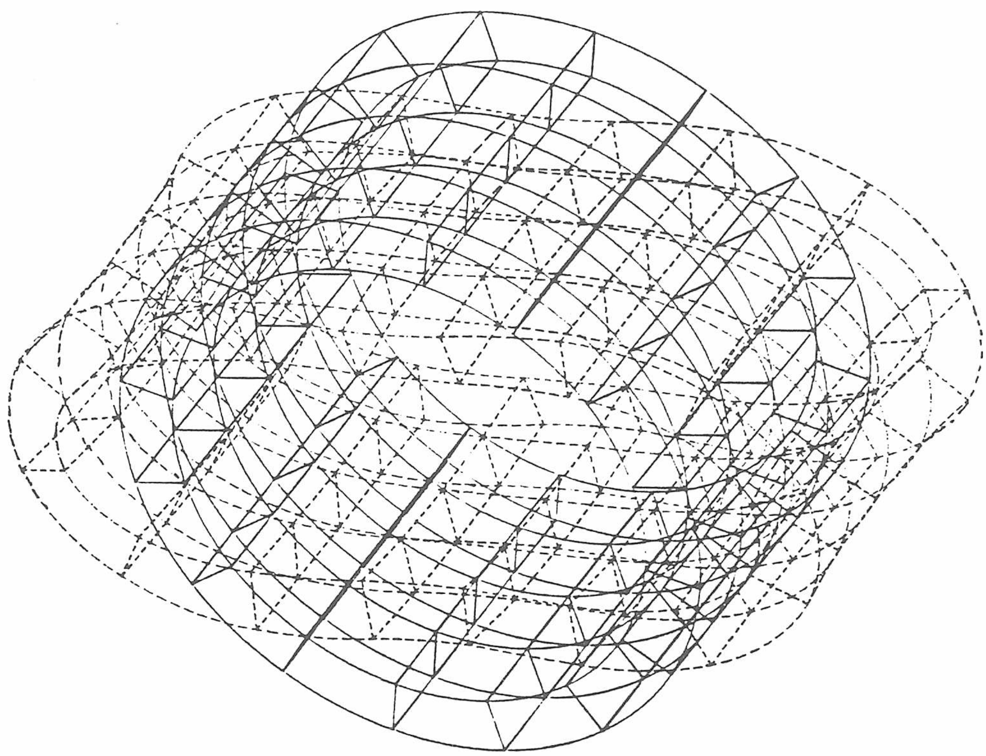

(a) f_n = 1249 Hz.

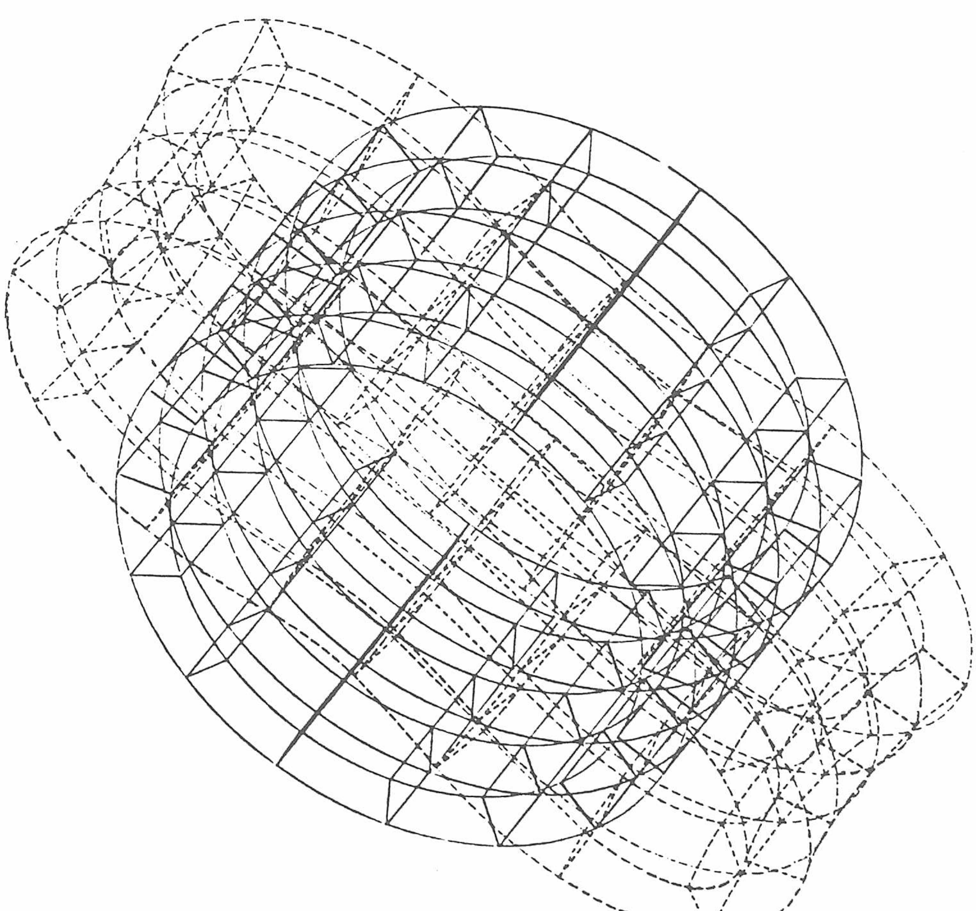

(b) f_n = 1254 Hz.

Figure 4.8

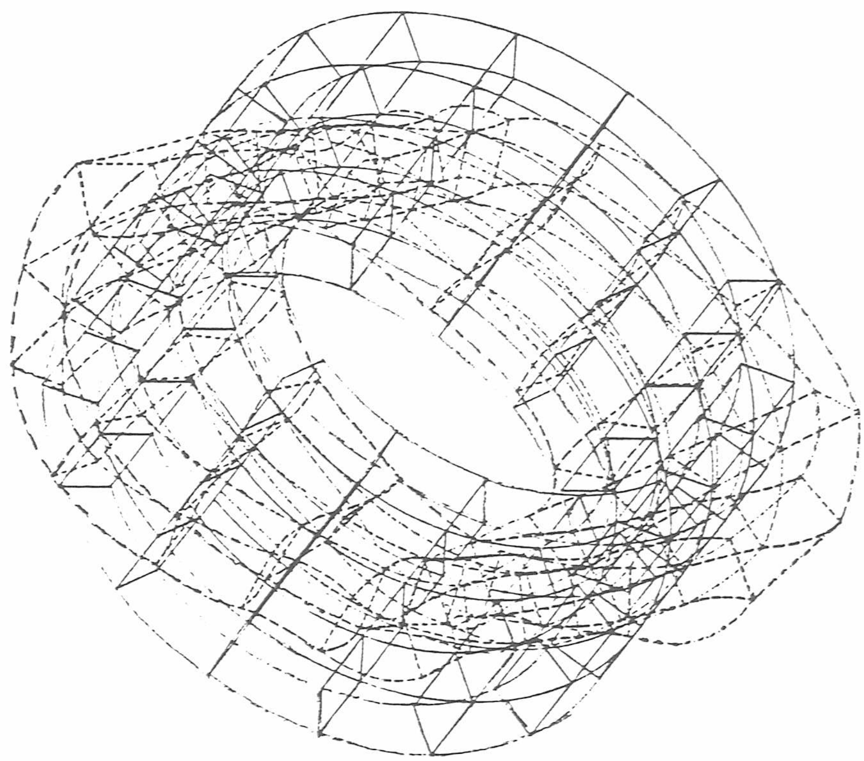

(c) f_n = 1800 Hz.

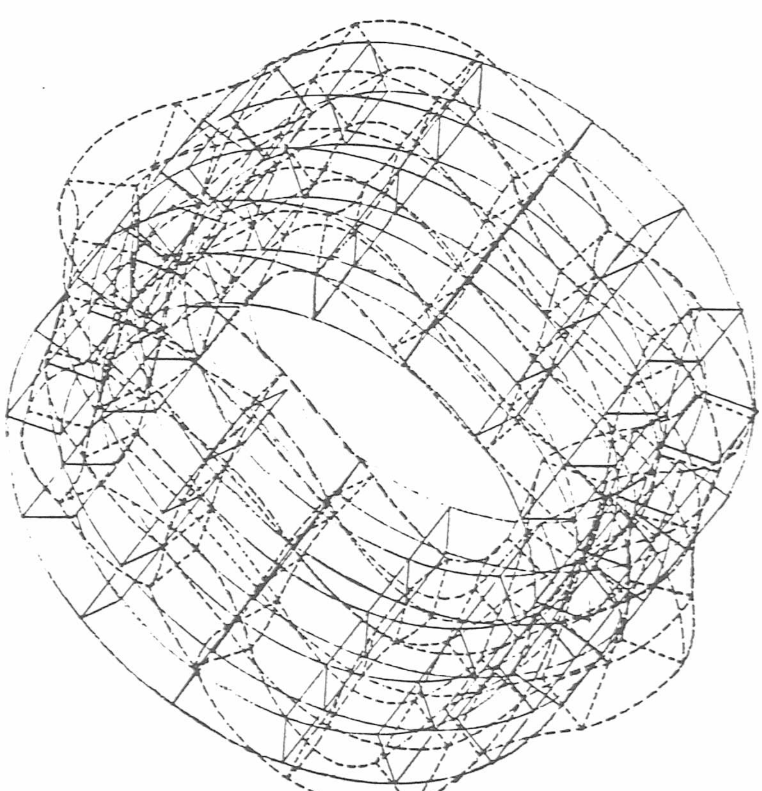

(d) f_n = 1813 Hz.

Figure 4.8

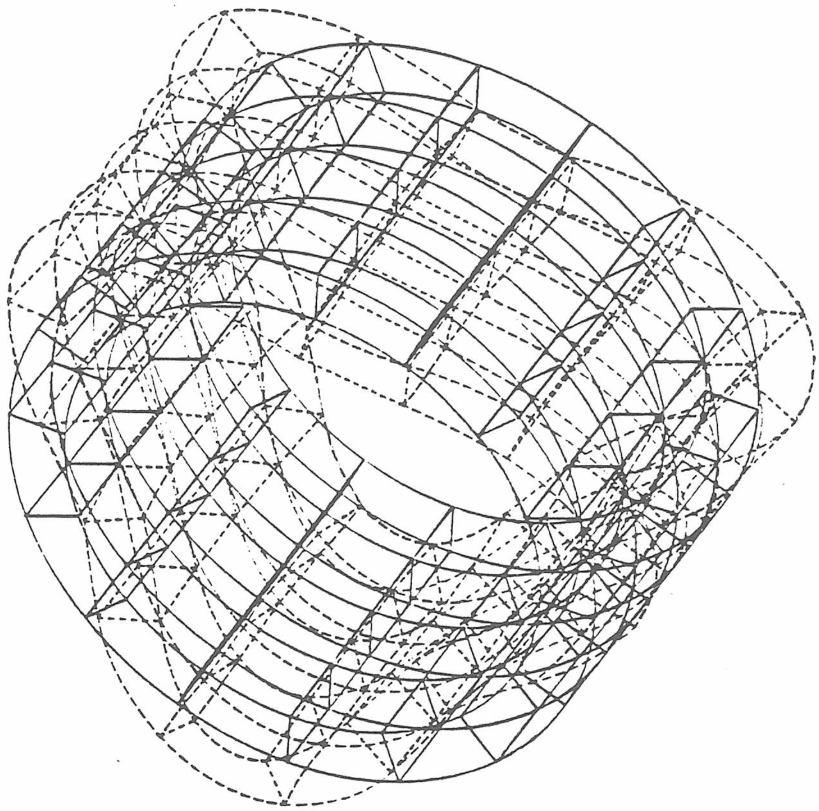

(e) f_n = 3588 Hz.

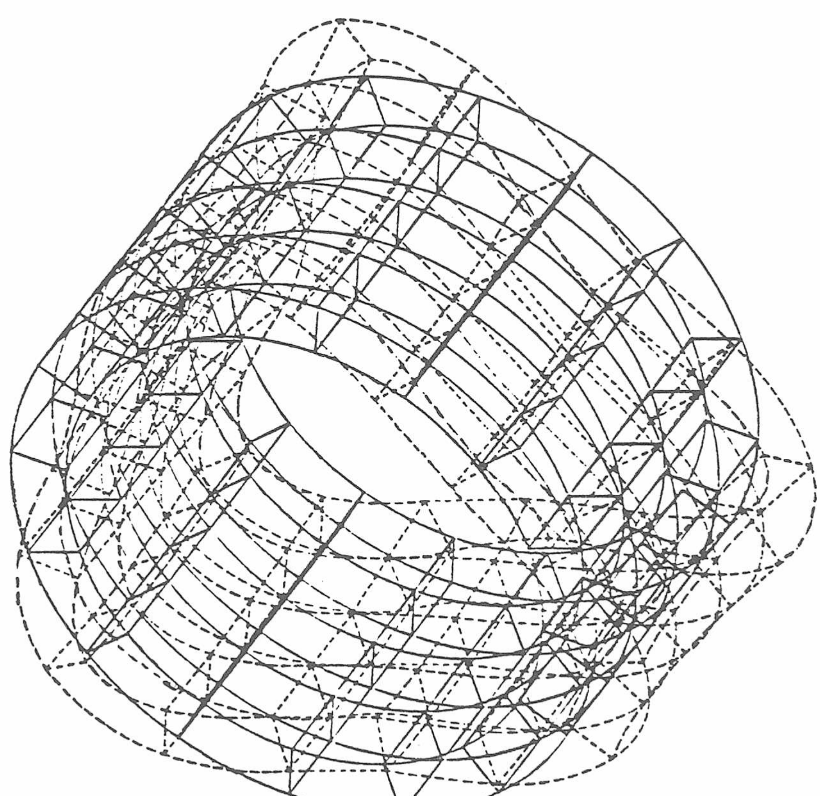

(f) f_n = 3642 Hz.

Figure 4.8

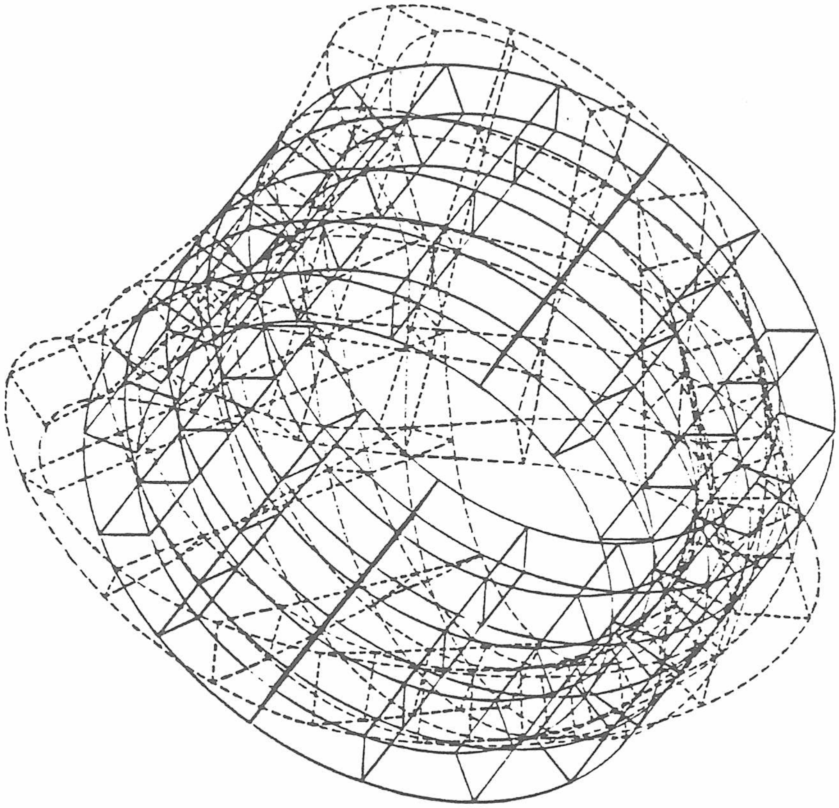

(g) f_n = 4614 Hz.

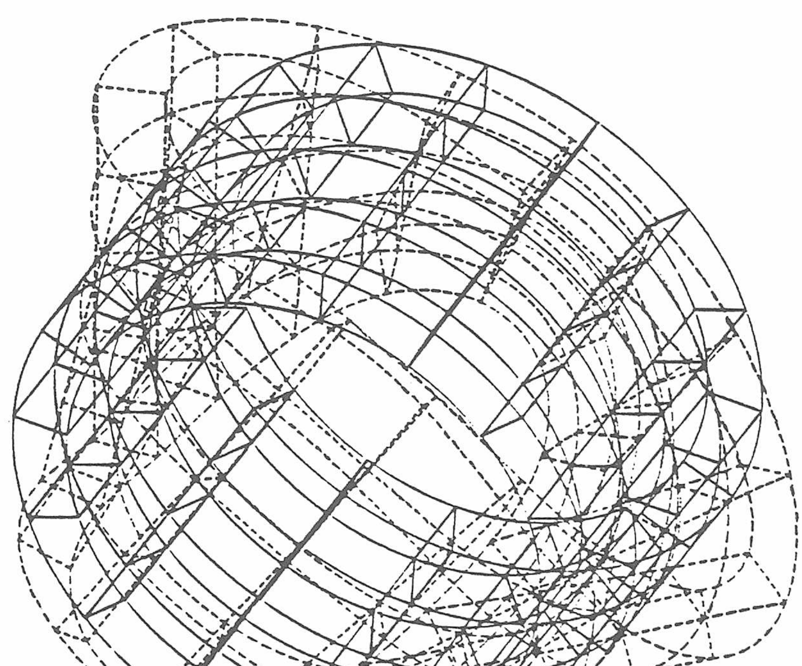

(h) f_n = 4768 Hz.

Figure 4.8

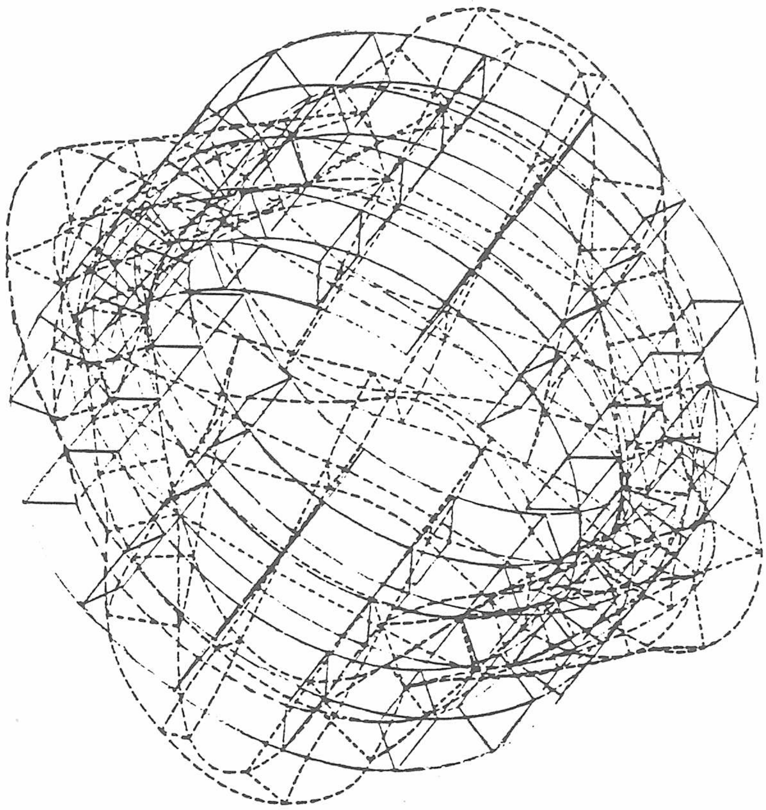

(i) f_n = 7101 Hz.

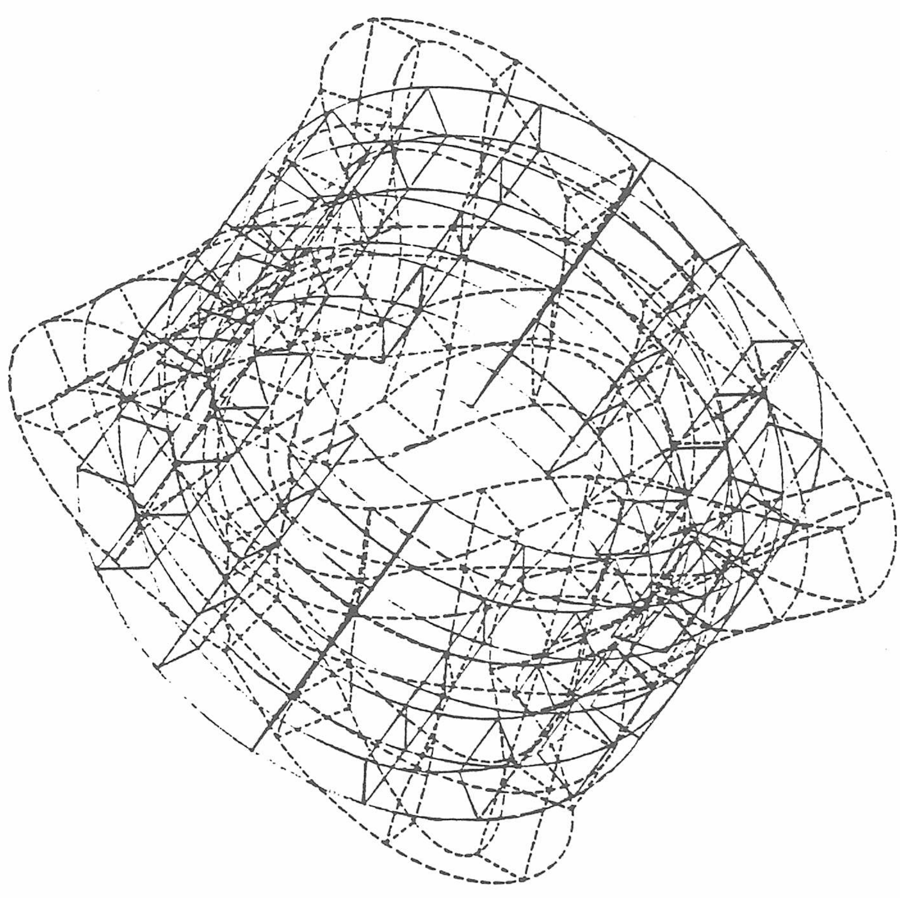

(j) f_n = 7133 Hz.

Figure 4.8

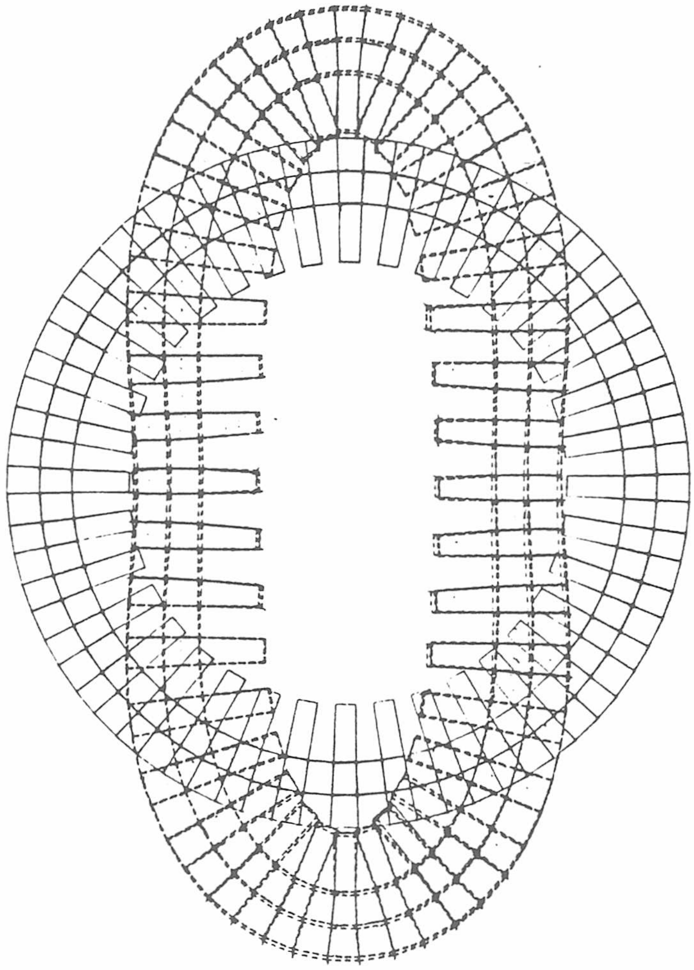

(a) f_n = 1126 Hz.

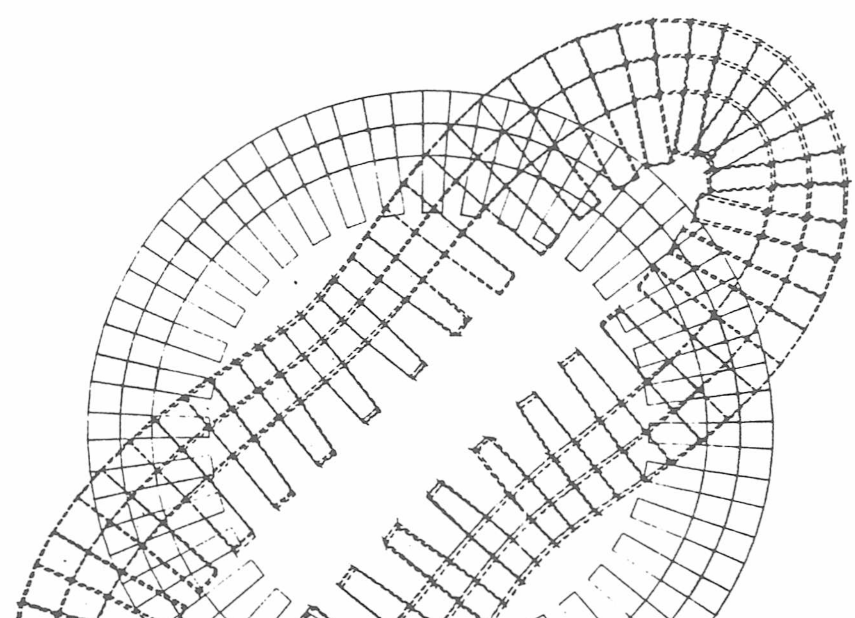

(b) f_n = 1129 Hz.

Figure 4.9

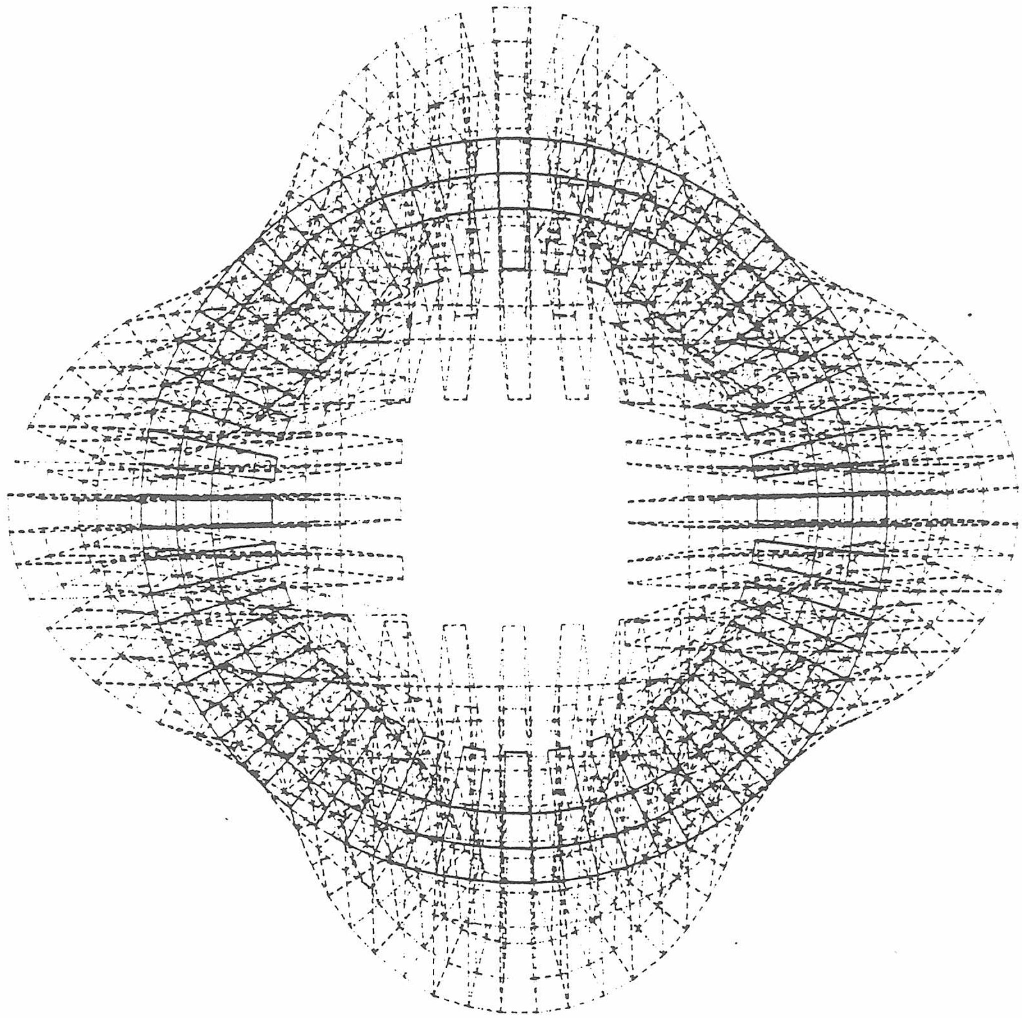

(c) f_n = 1780 Hz.

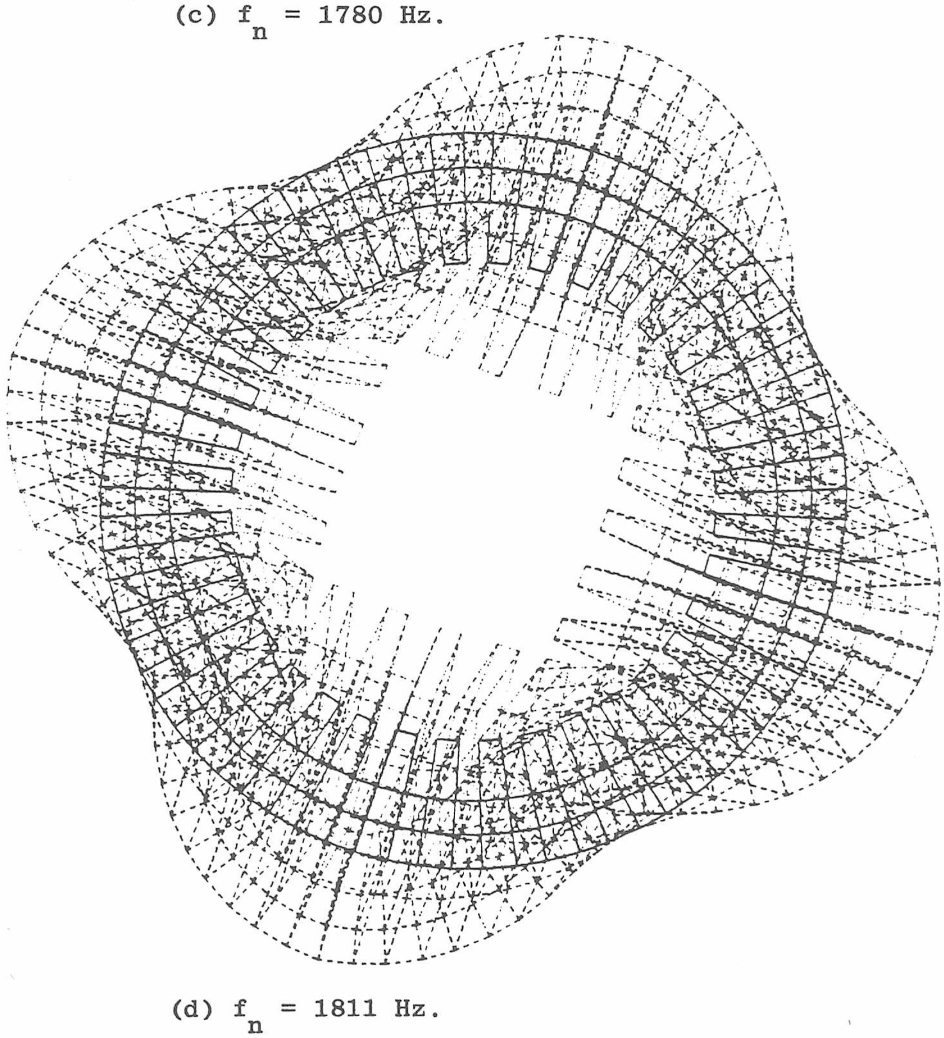

(d) f_n = 1811 Hz.

Figure 4.9

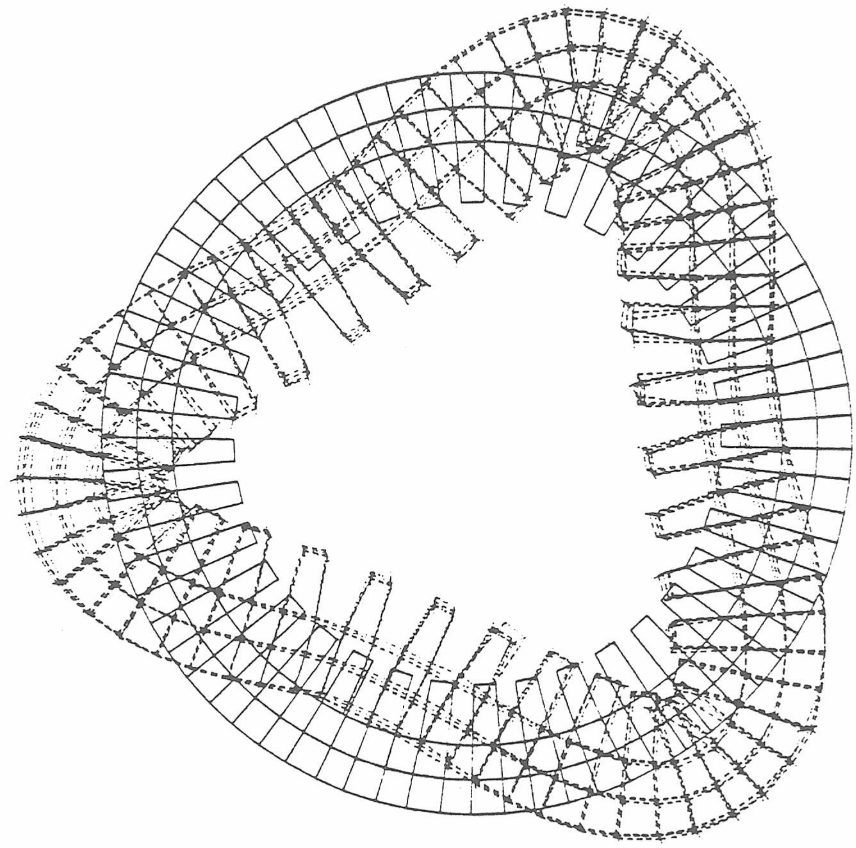

(e) f_n = 3127 Hz.

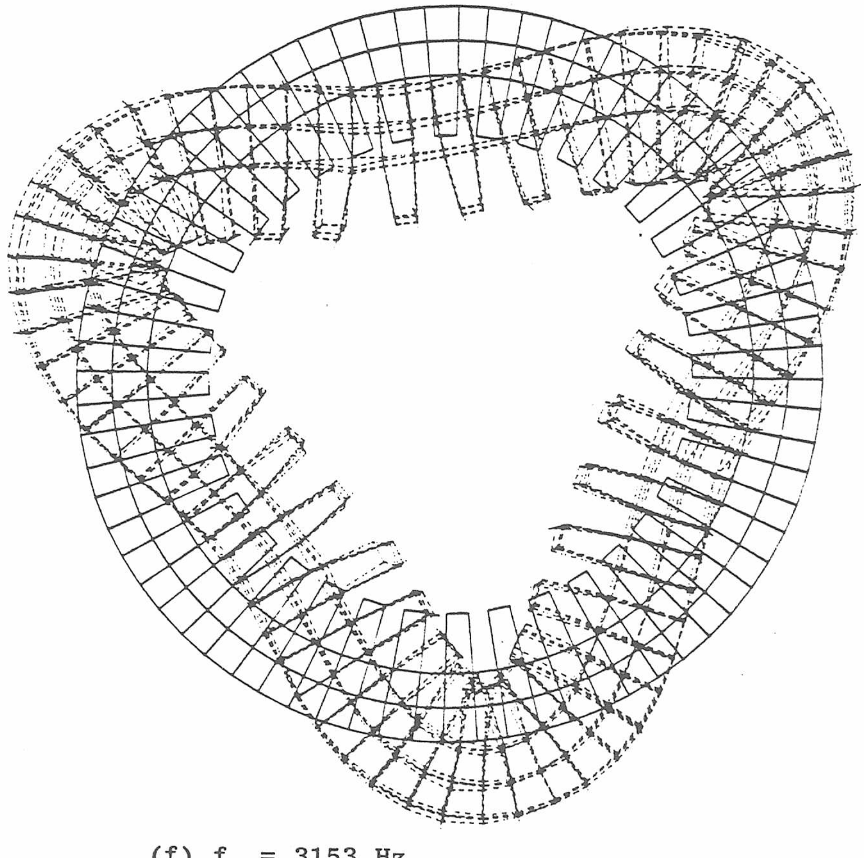

(f) f_n = 3153 Hz.

Figure 4.9

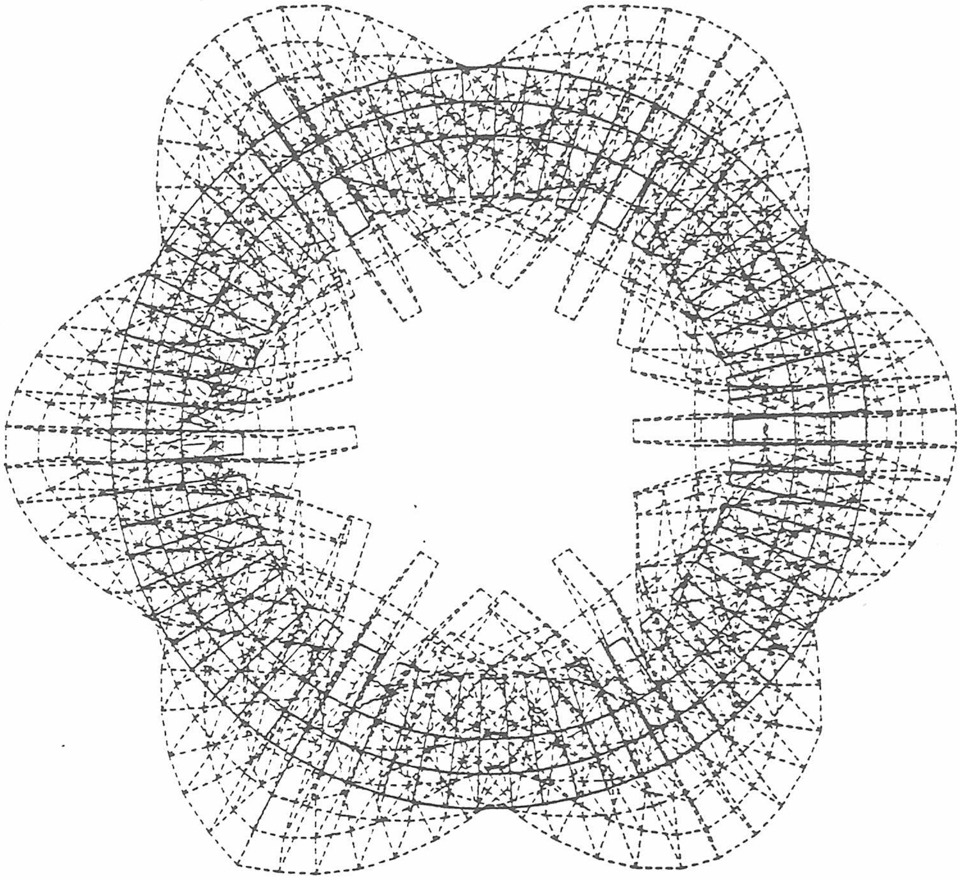

(g) f_n = 4358 Hz.

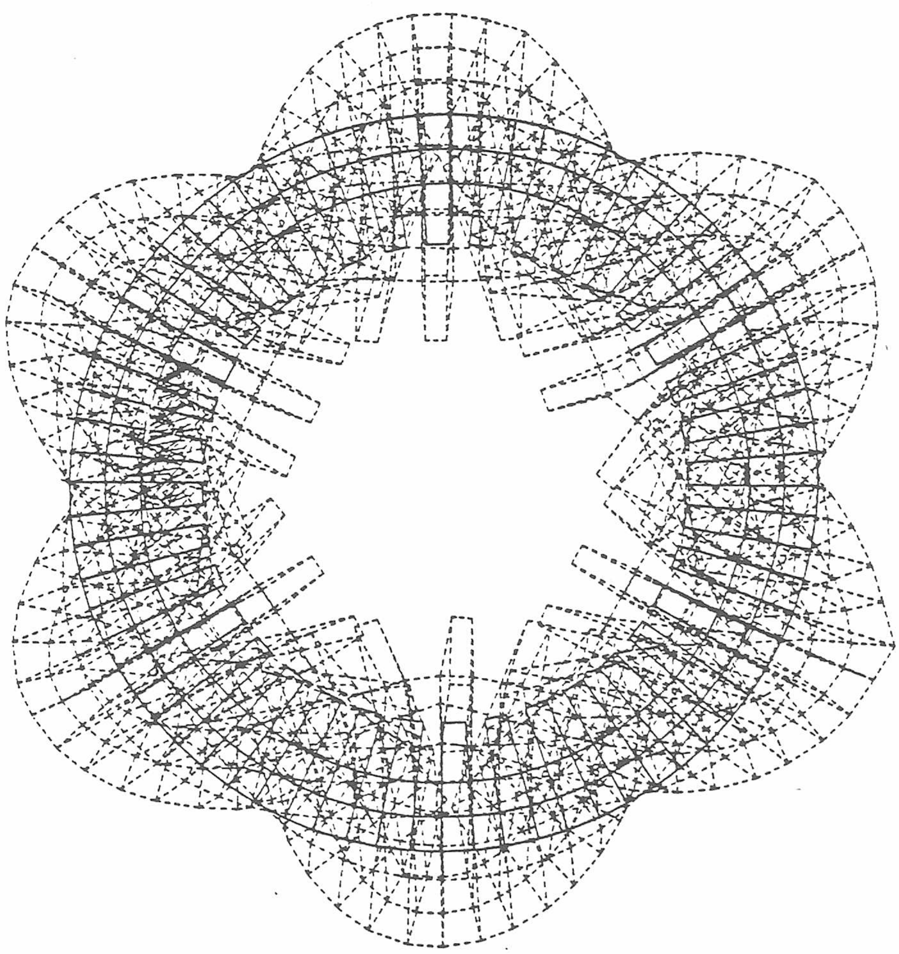

(h) f_n = 4397 Hz.

Figure 4.9

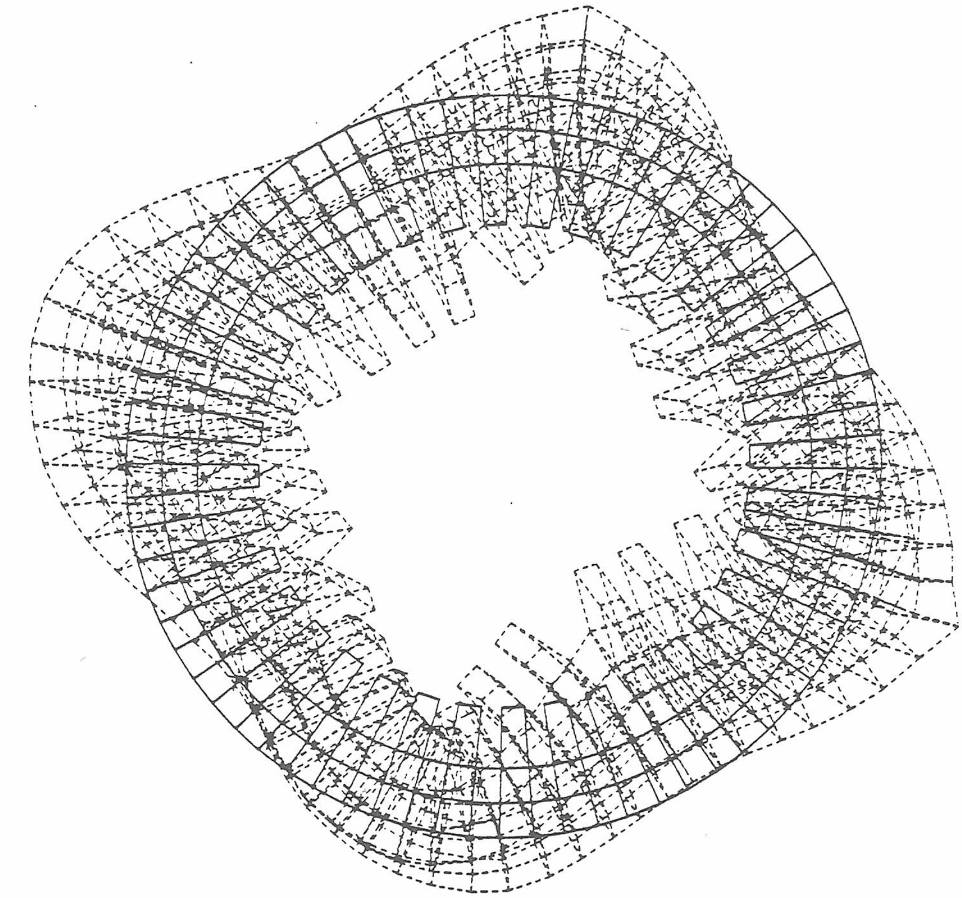

(i) f_n = 6028 Hz.

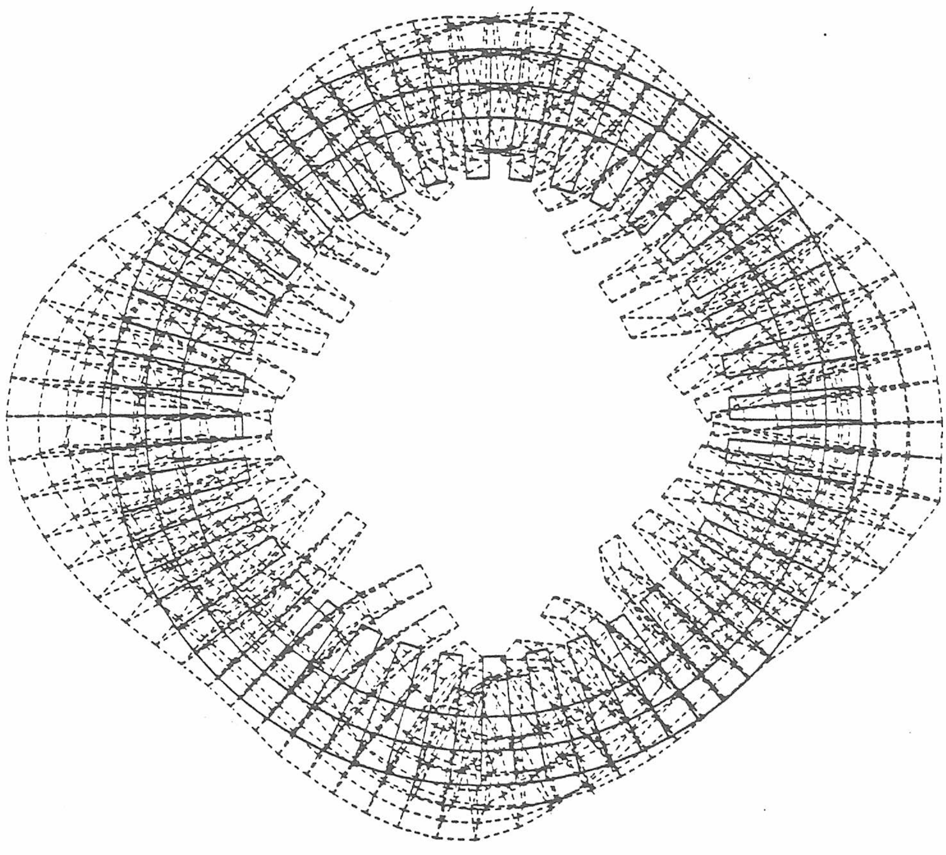

(j) f_n = 6116 Hz.

Figure 4.9

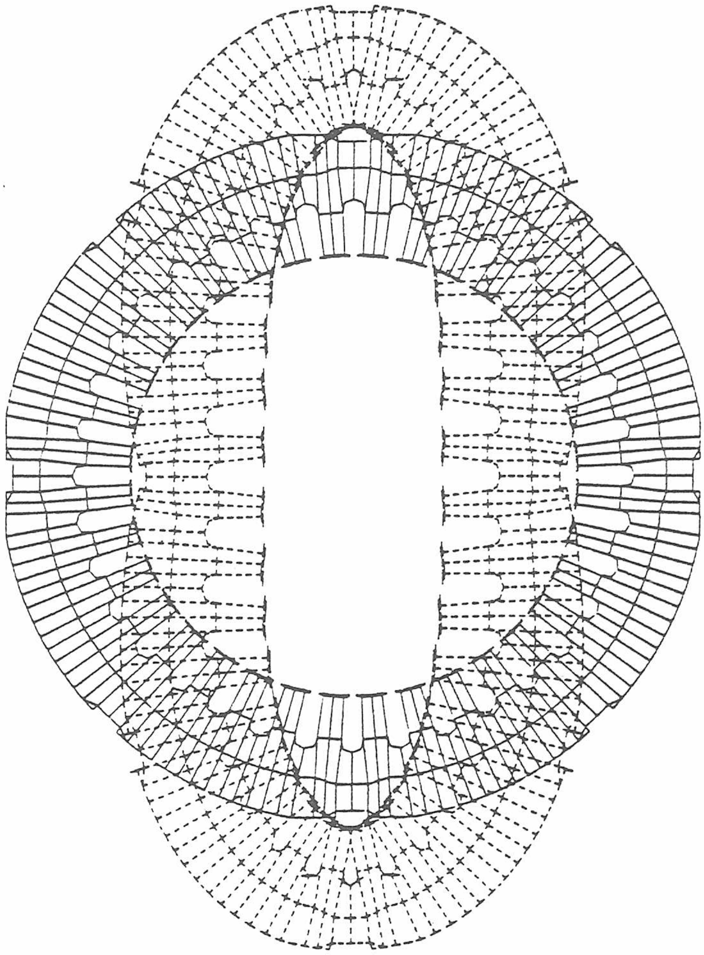

(a) f_n = 1036 Hz.

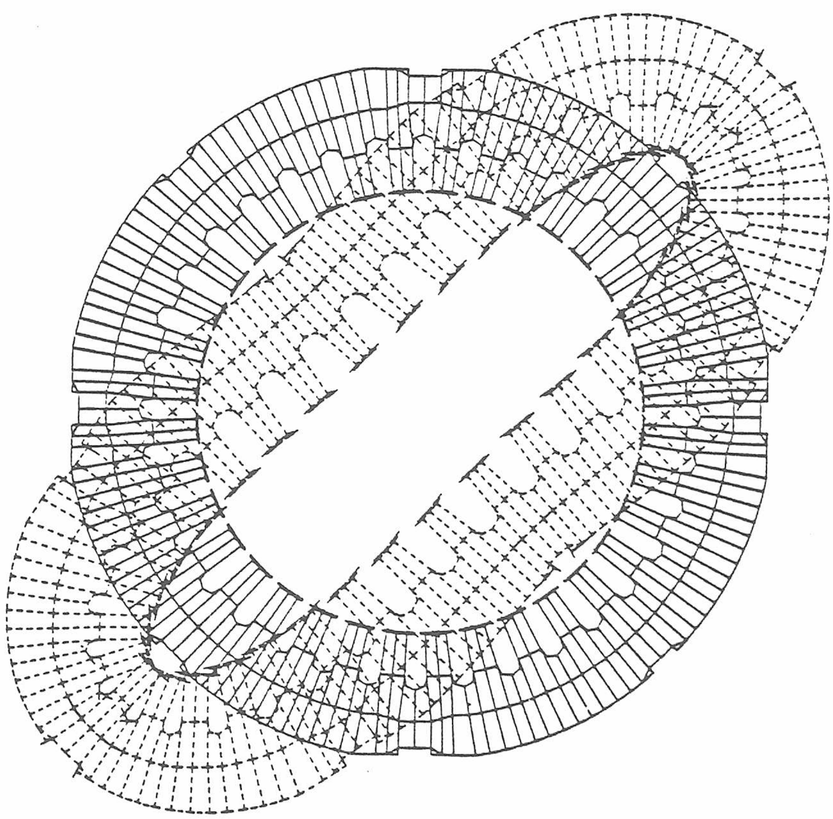

(b) f_n = 1060 Hz.

Figure 4.10

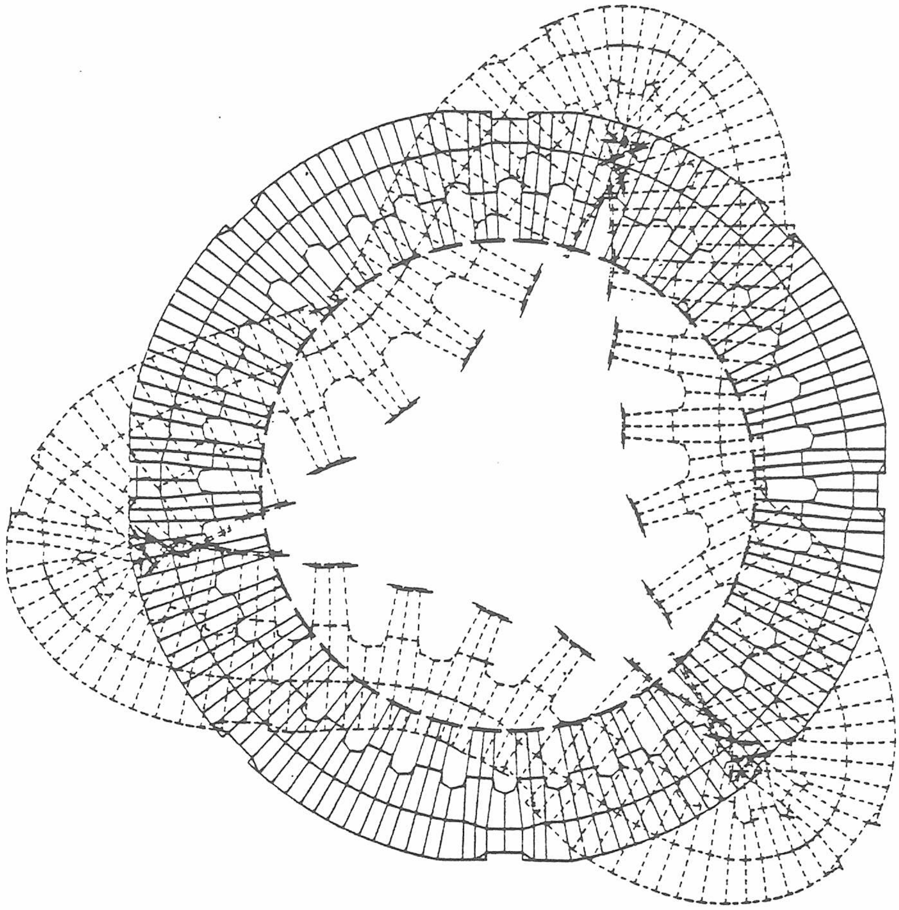

(c) f_n = 2836 Hz.

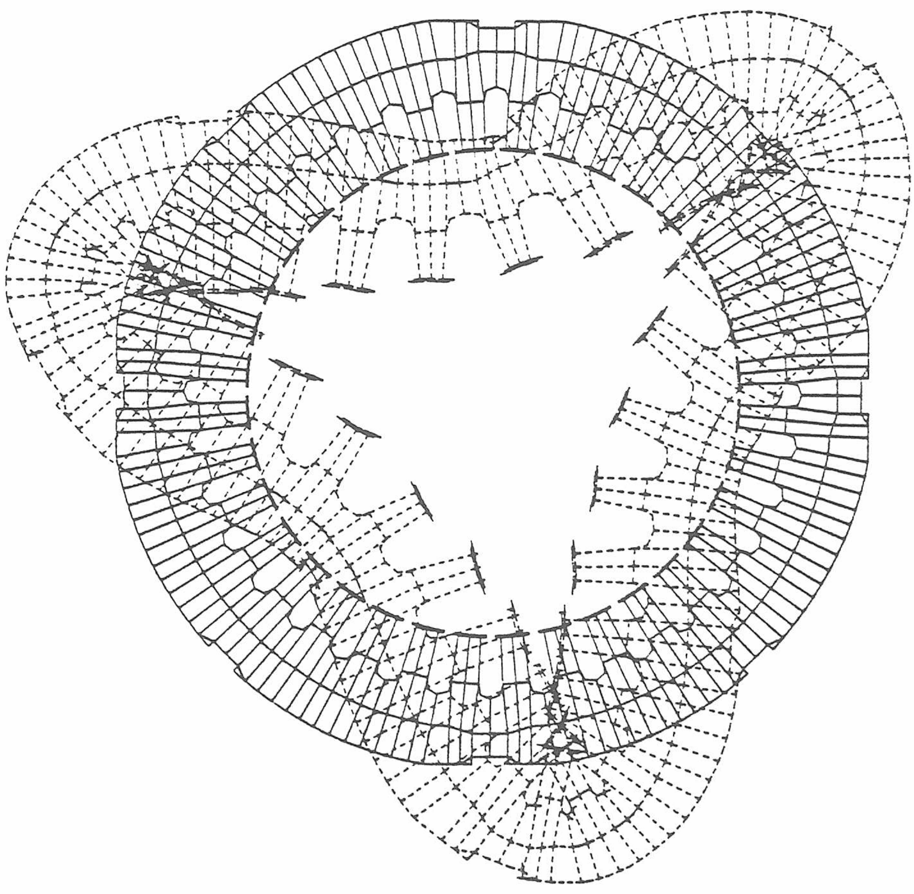

(d) f_n = 2839 Hz.

Figure 4.10

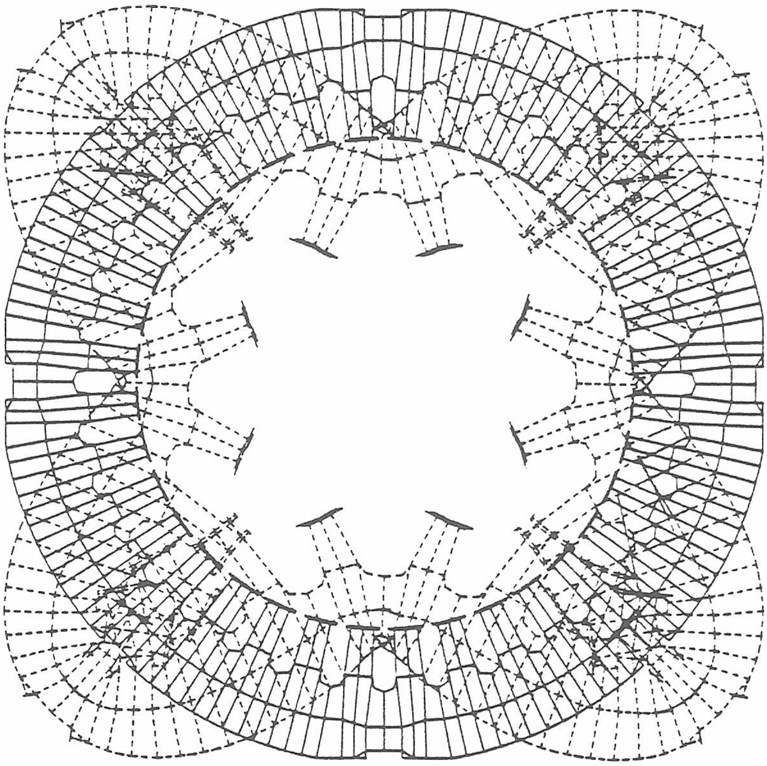

(e) f_n = 5127 Hz.

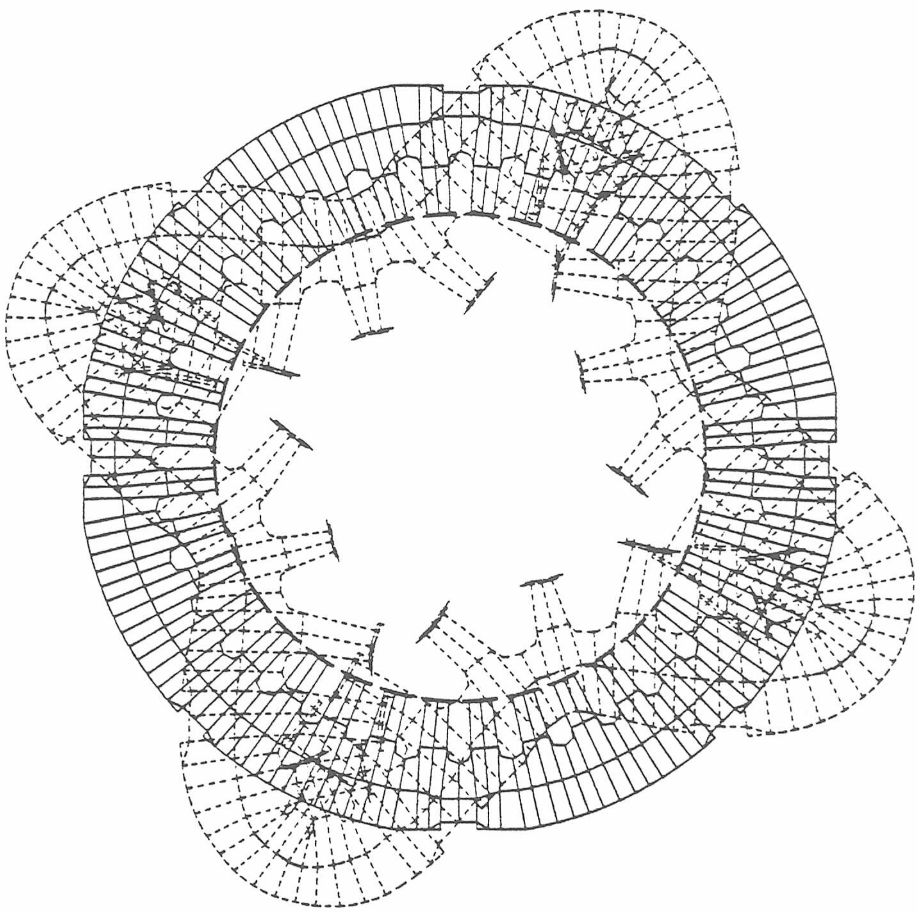

(f) f_n = 5286 Hz.

Figure 4.10

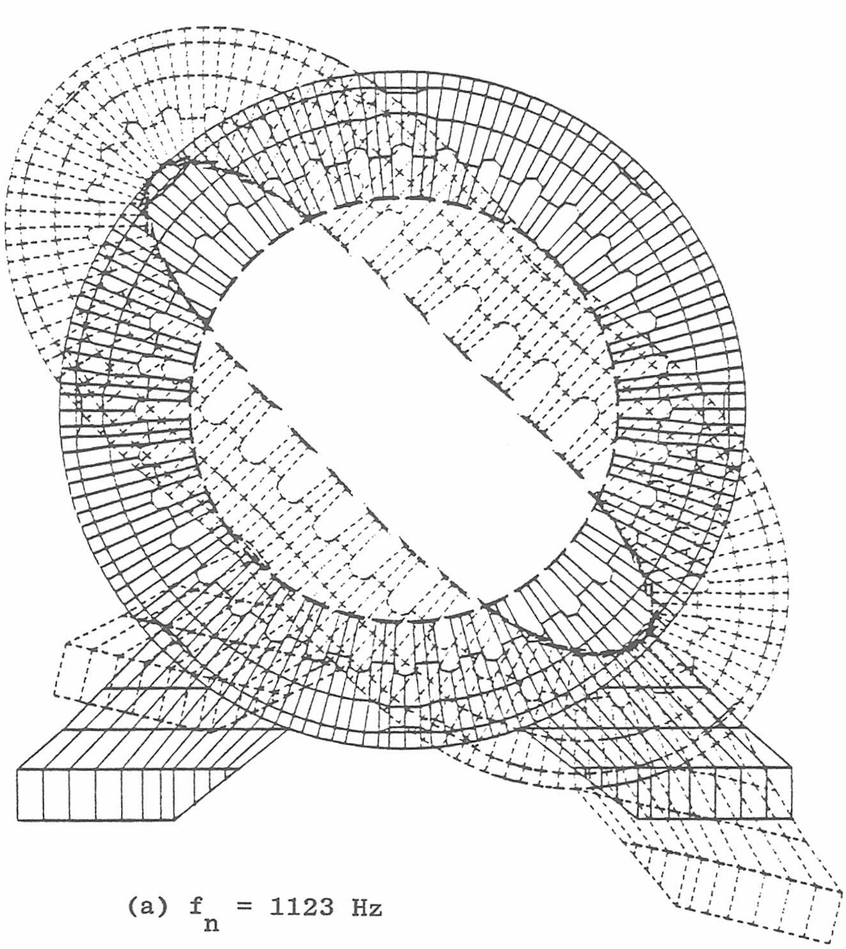

(a) f_n = 1123 Hz

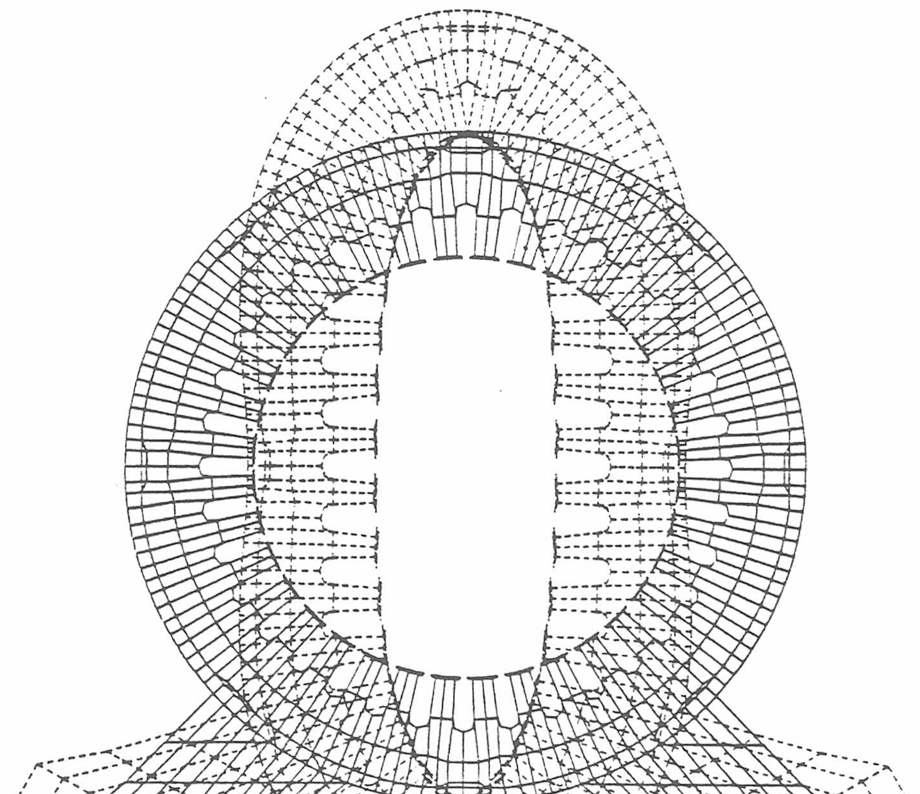

(b) f_n = 1132 Hz.

Figure 4.11

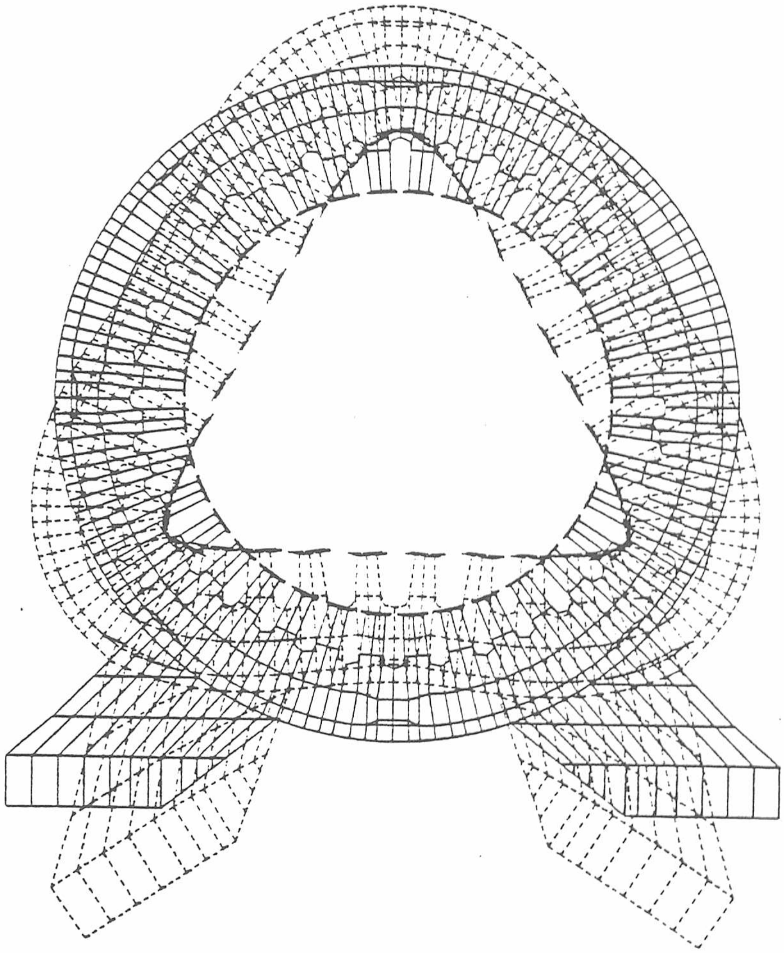

(c) f_n = 2831 Hz.

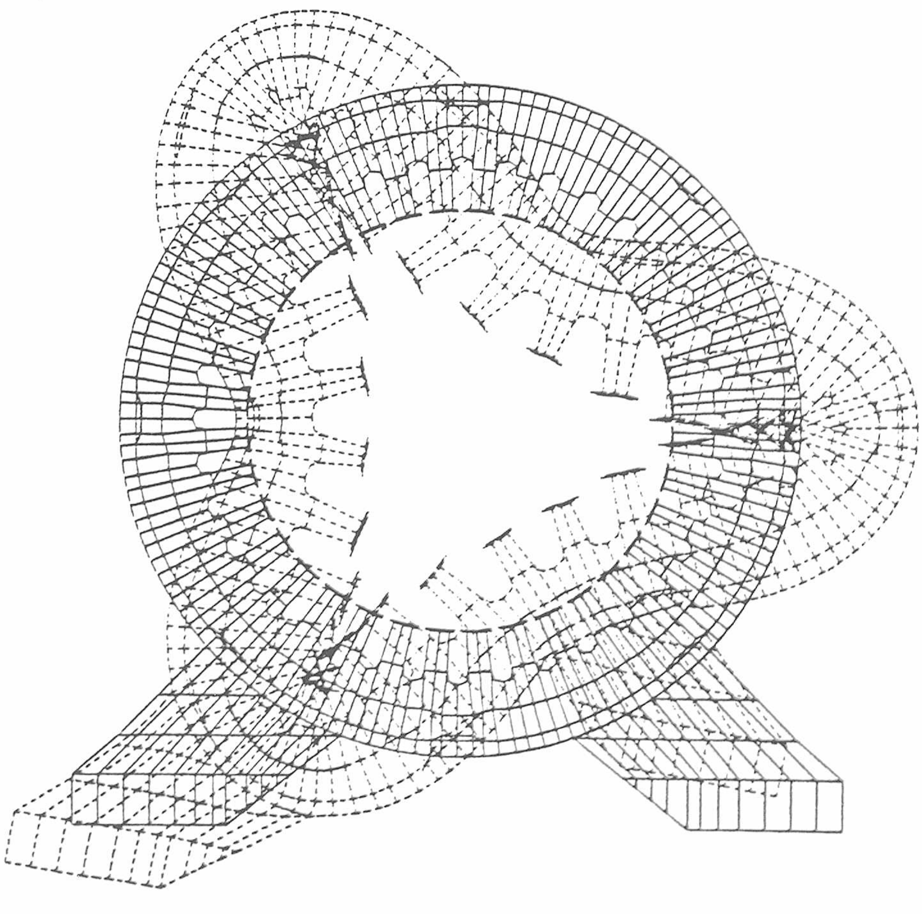

(d) f_n = 3111 Hz.

Figure 4.11

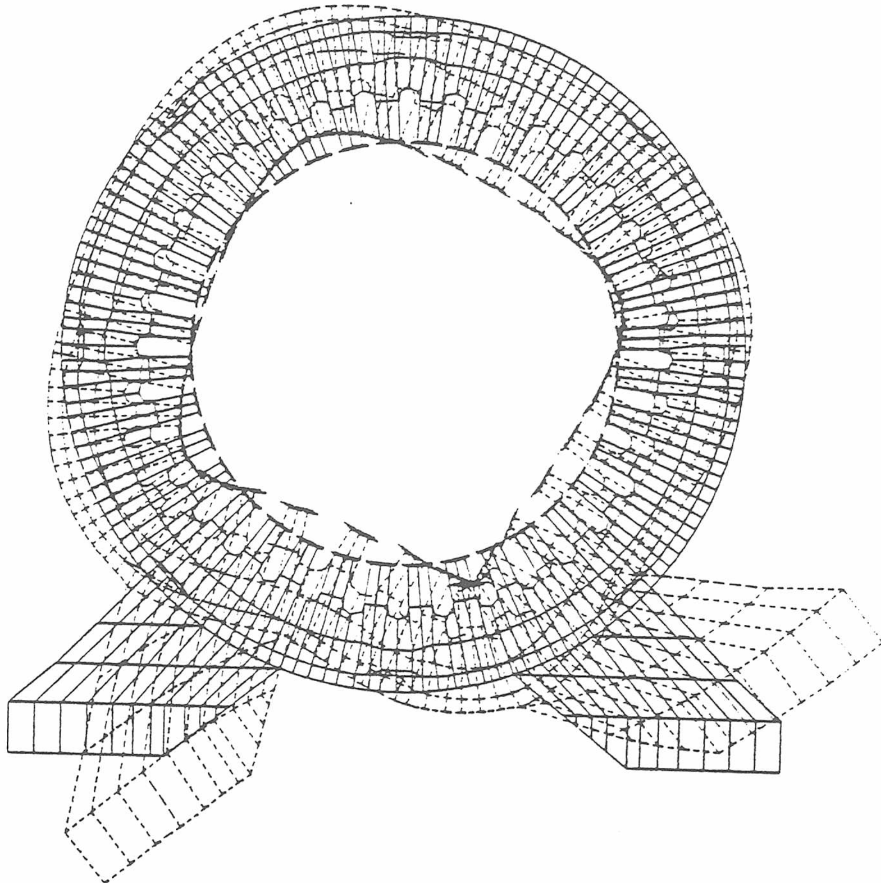

(e) f_n = 4639 Hz.

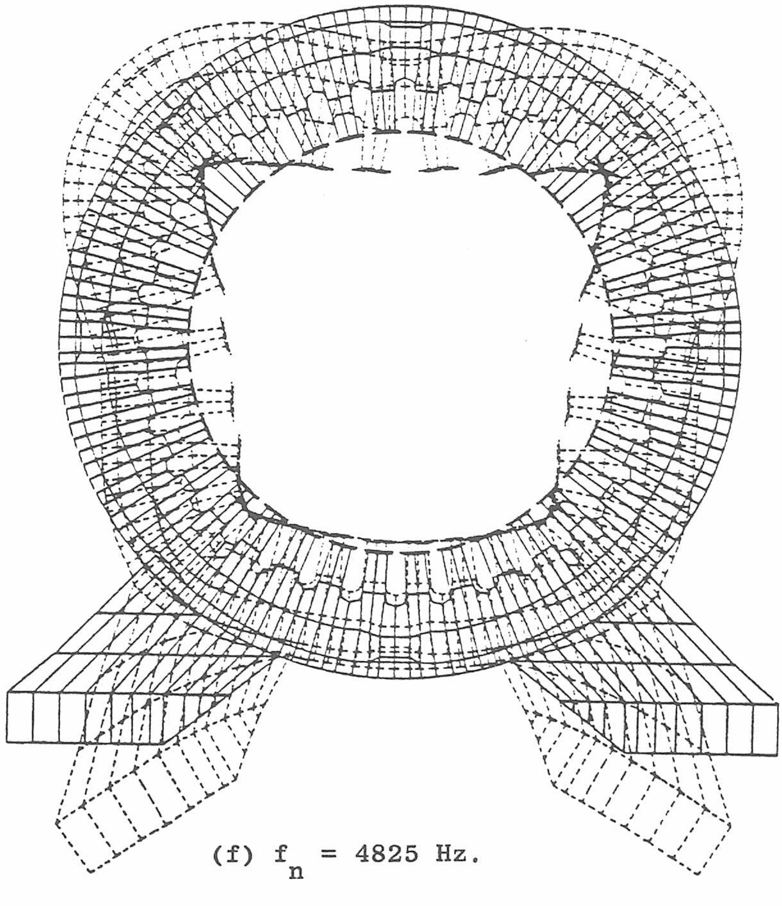

(f) f_n = 4825 Hz.

Figure 4.11

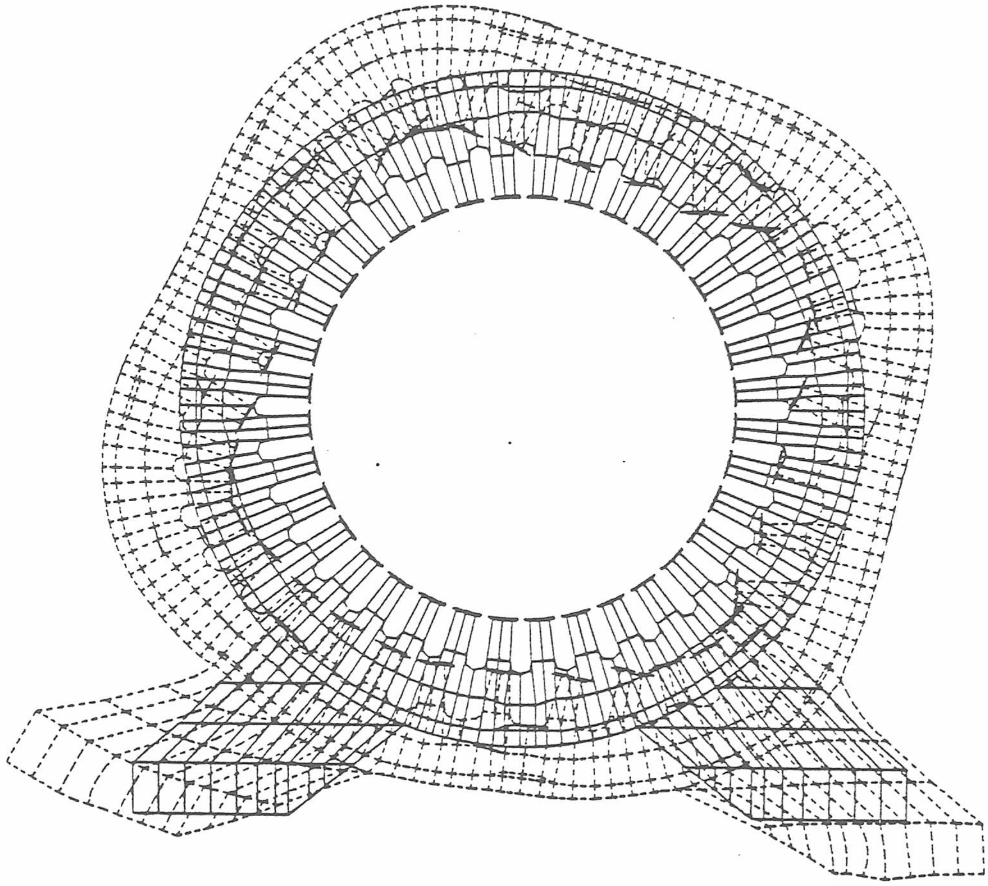

(g) f_n = 6234 Hz.

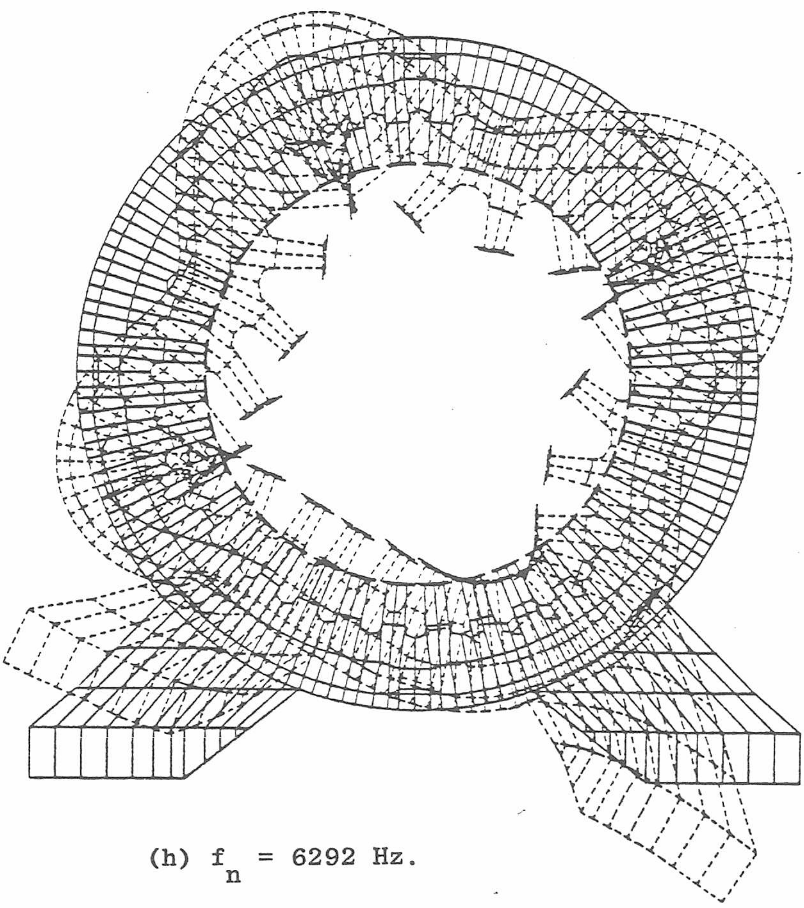

(h) f_n = 6292 Hz.

Figure 4.11

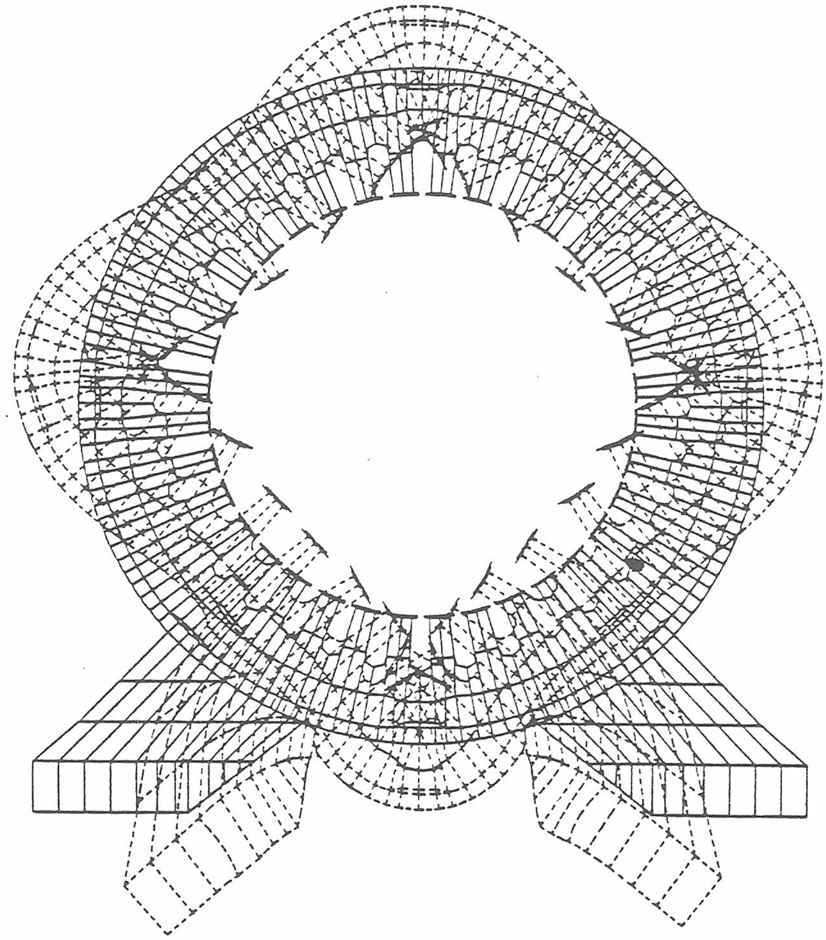

(i) f_n = 6745 Hz.

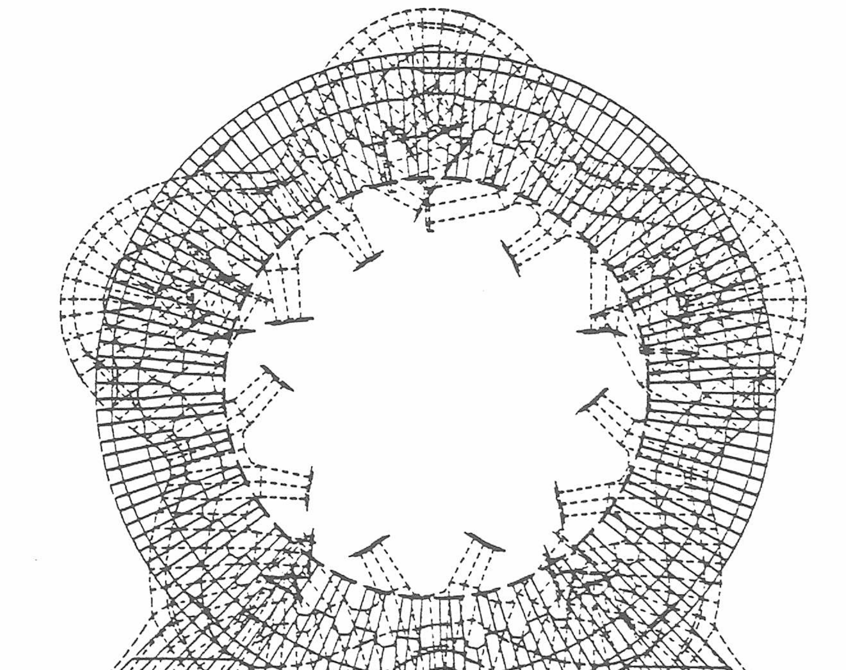

(j) f_n = 8883 Hz.

Figure 4.11

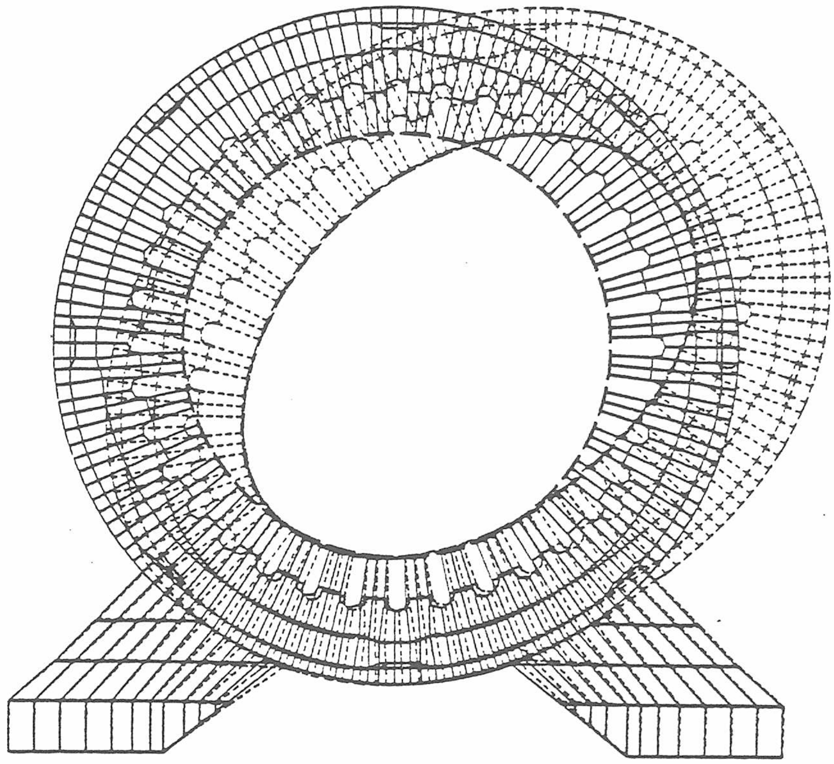

(a) f_n = 588 Hz.

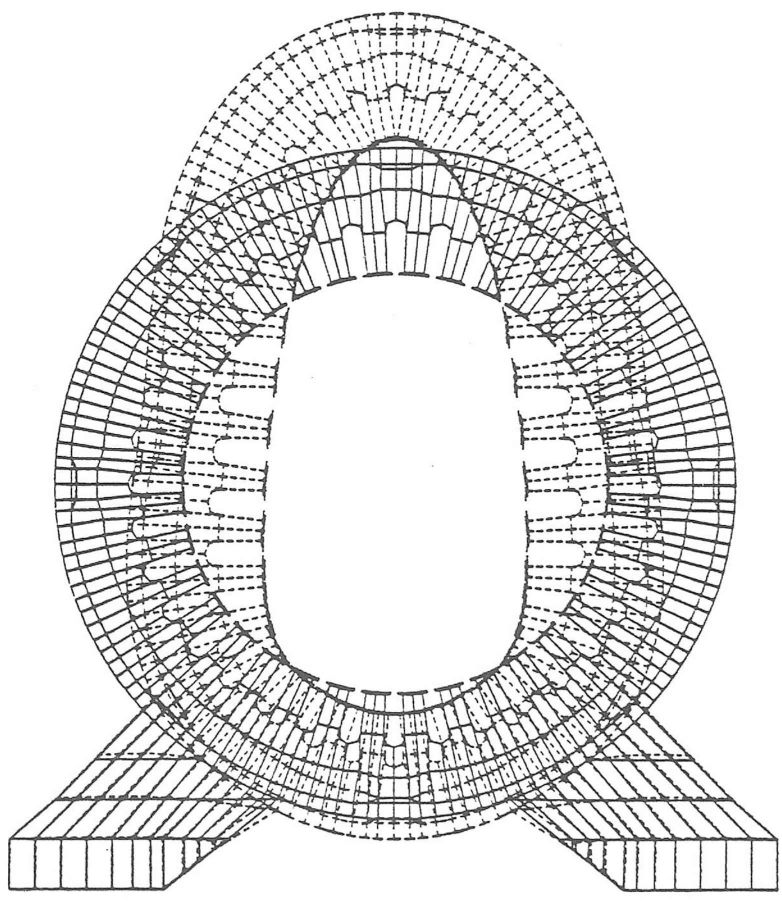

(b) f_n = 1153 Hz.

Figure 4.12

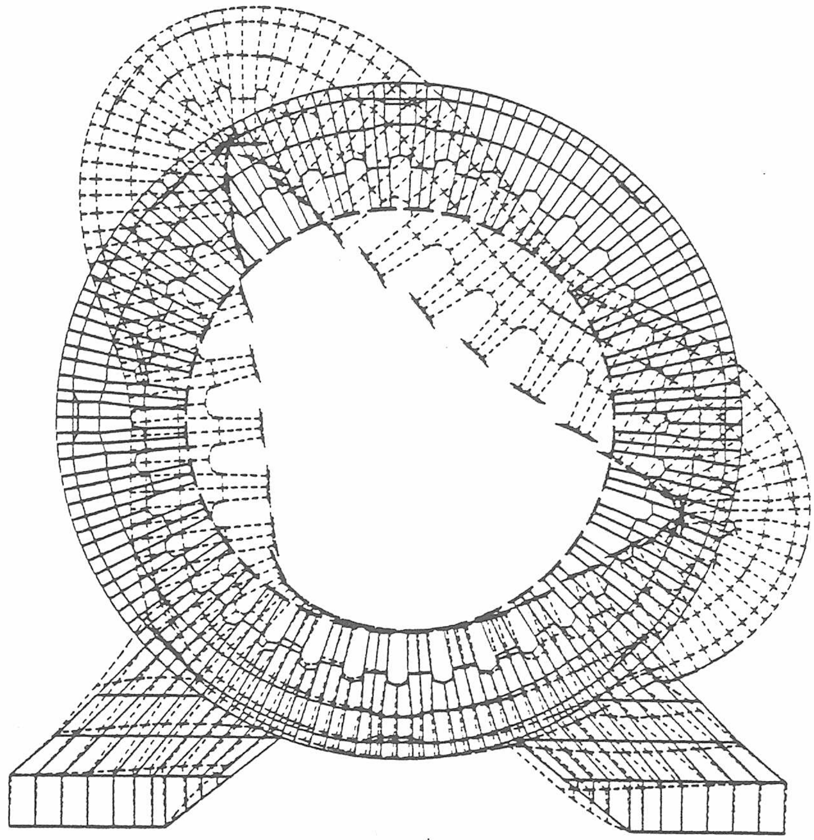

(c) f_n = 2421 Hz.

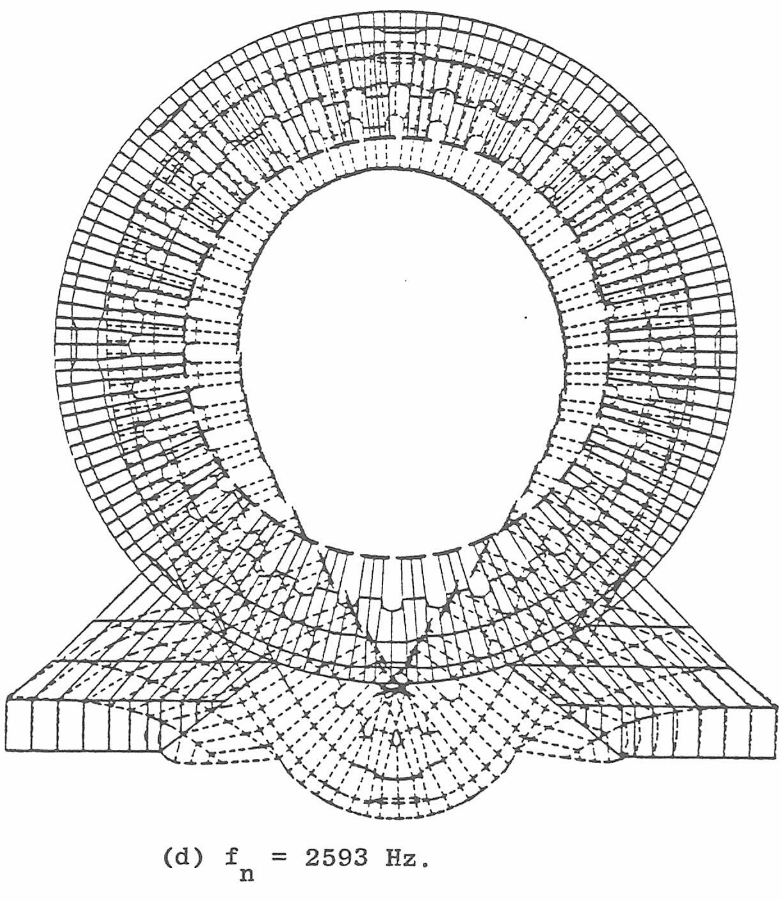

(d) f_n = 2593 Hz.

Figure 4.12

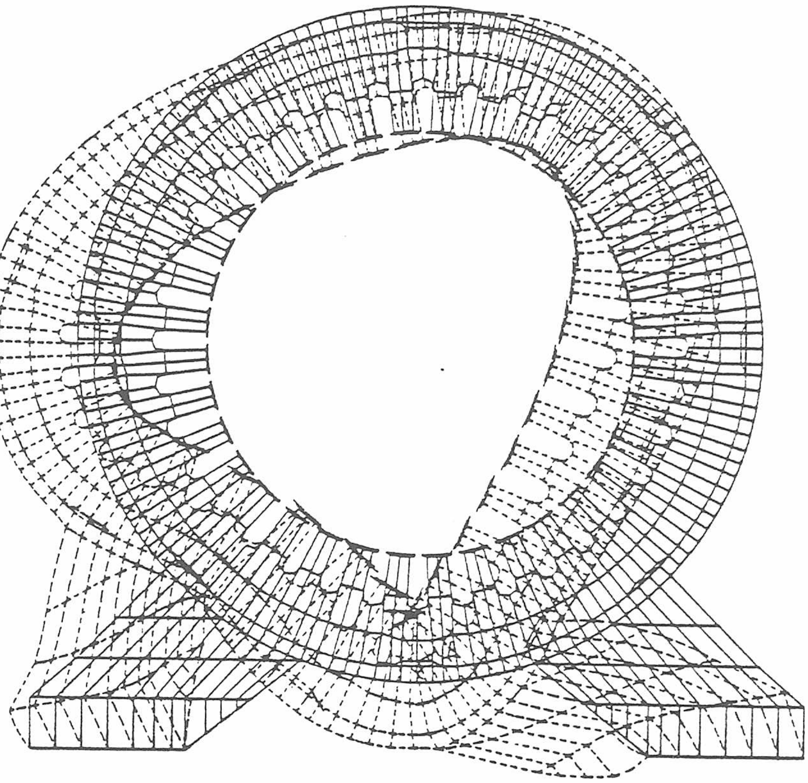

(e) f_n = 2601 Hz.

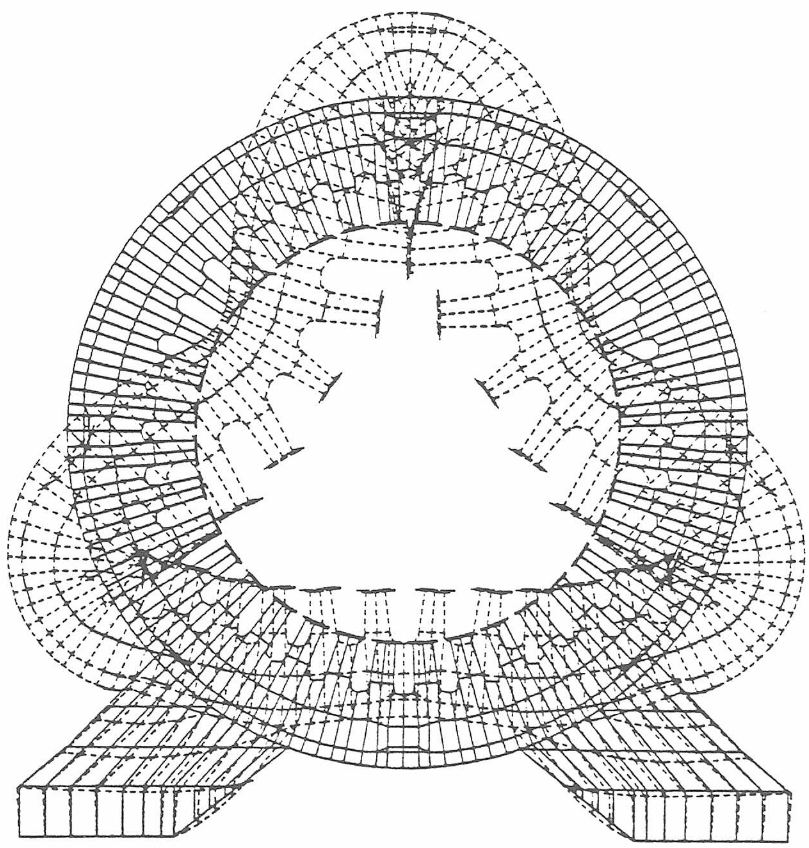

(f) f_n = 3723 Hz.

Figure 4.12

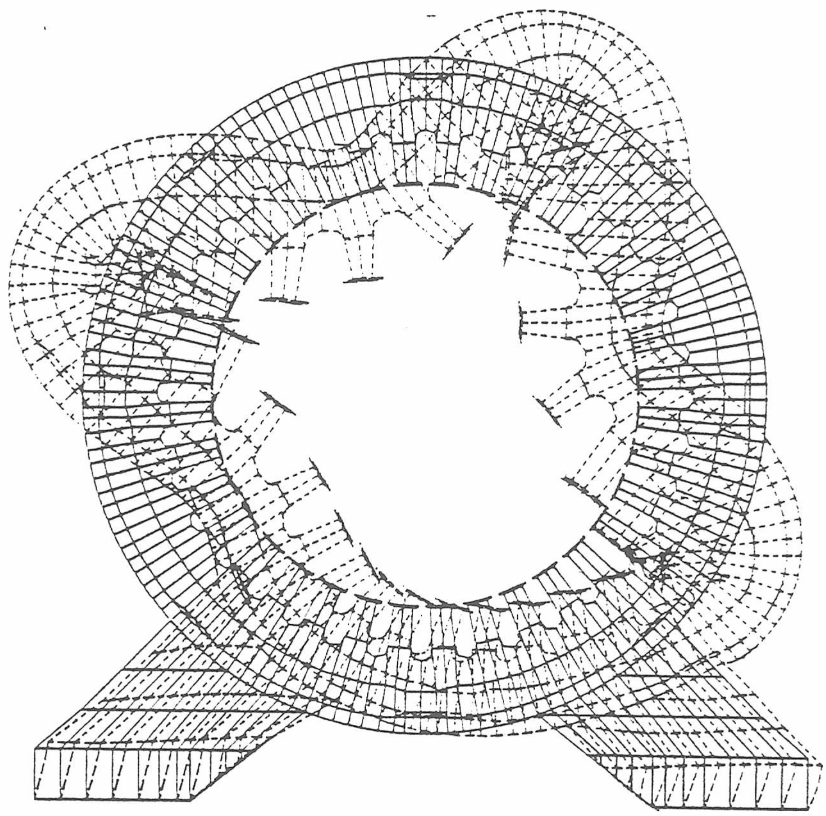

(g) f_n = 5190 Hz.

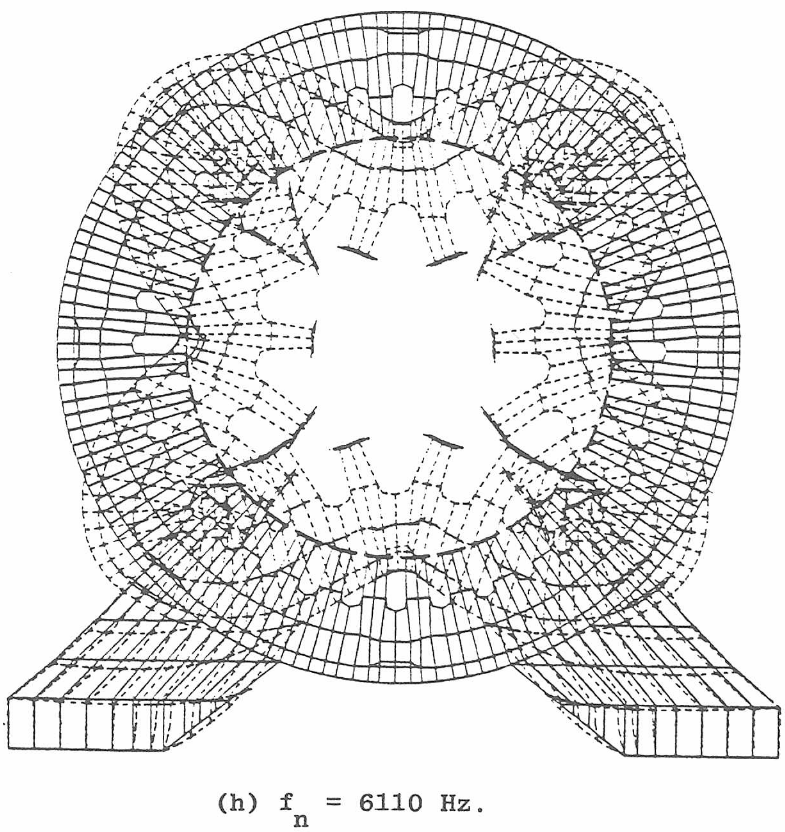

(h) f_n = 6110 Hz.

Figure 4.12

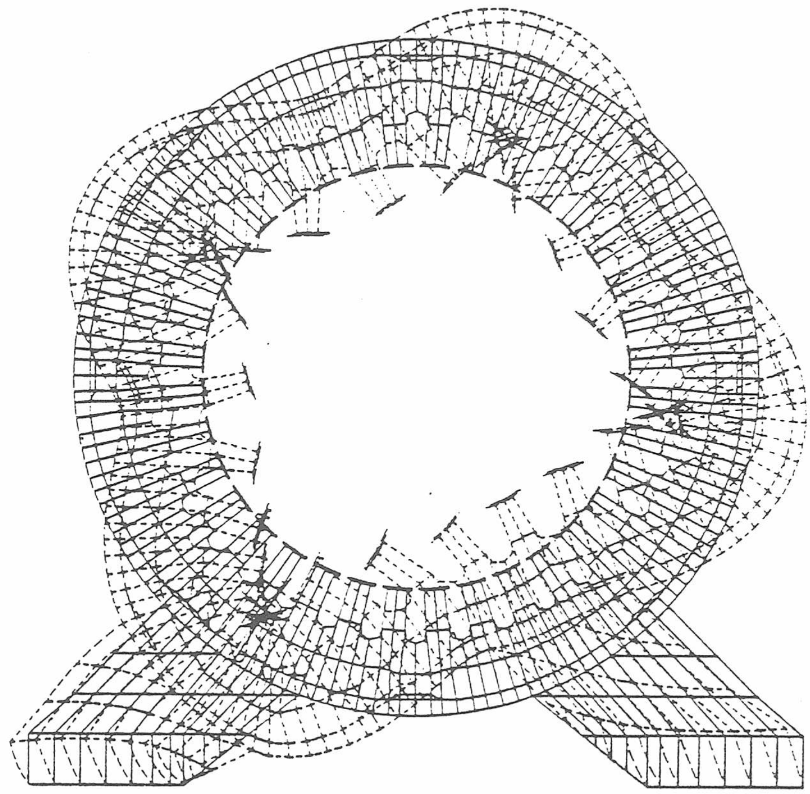

(i) f_n = 7346 Hz.

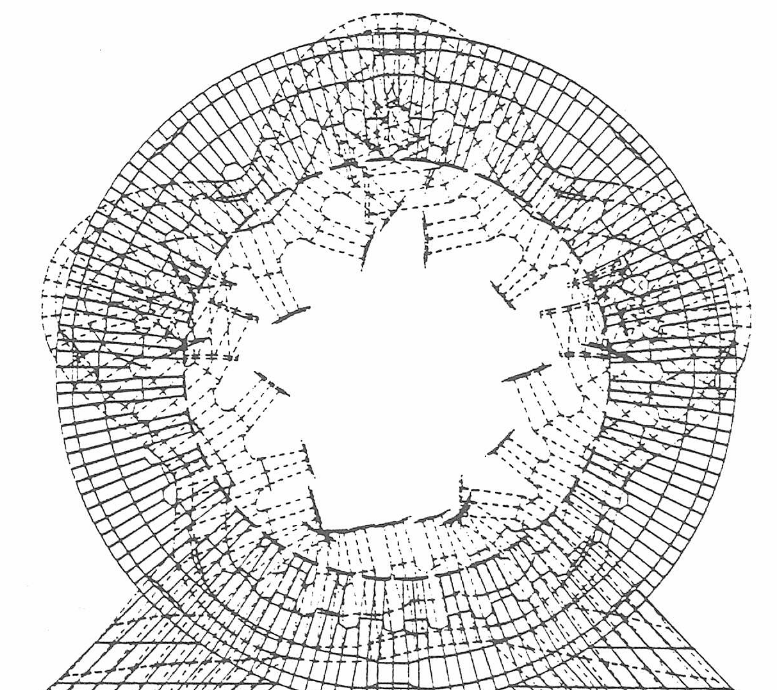

(j) f_n = 7755 Hz.

Figure 4.12

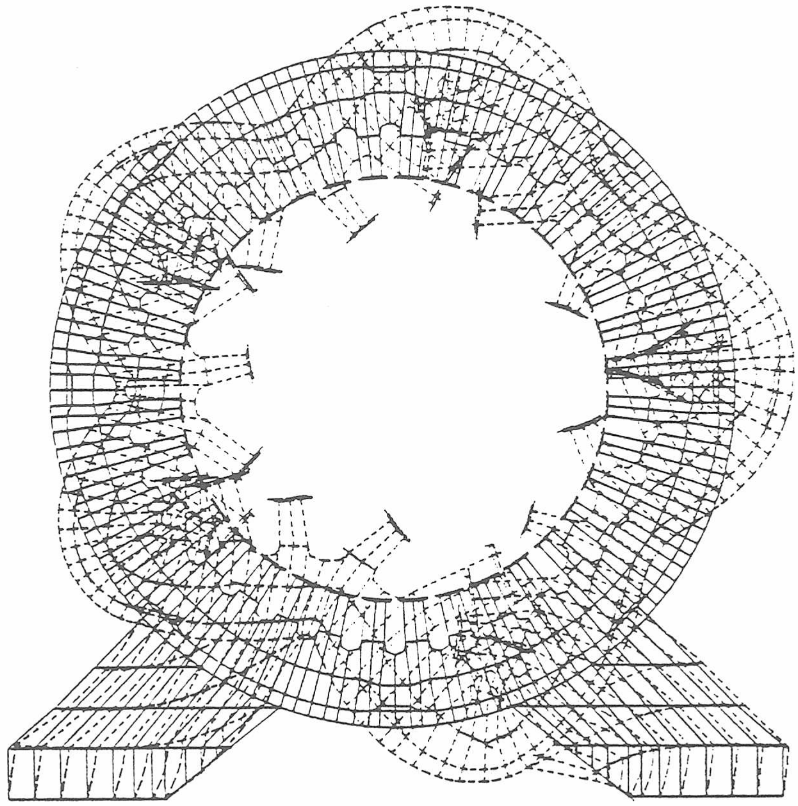

(k) f_n = 9354 Hz.

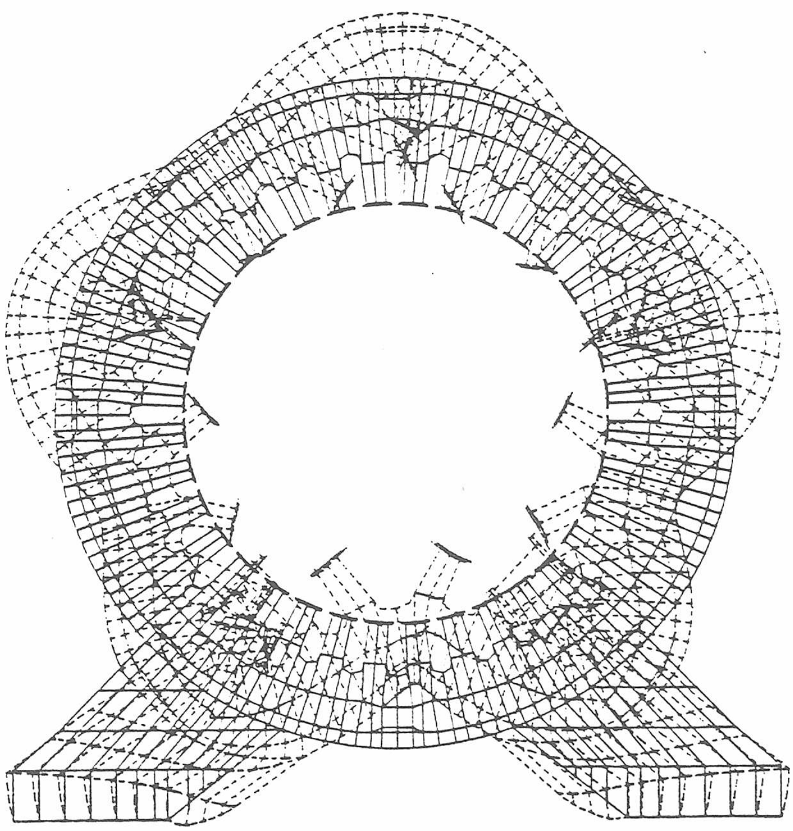

(ℓ) f_n = 9767 Hz.

Figure 4.12

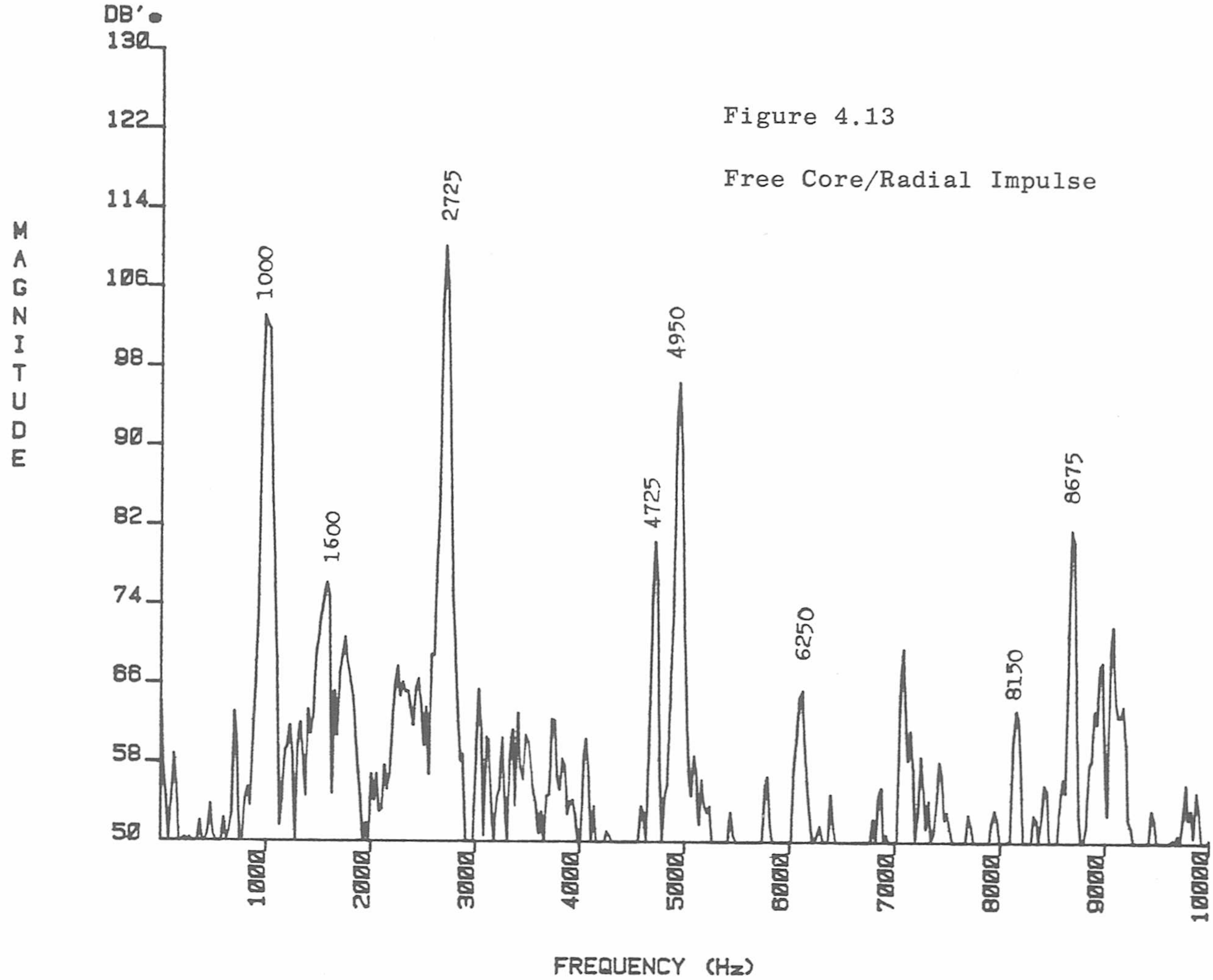

Figure 4.13

Free Core/Radial Impulse

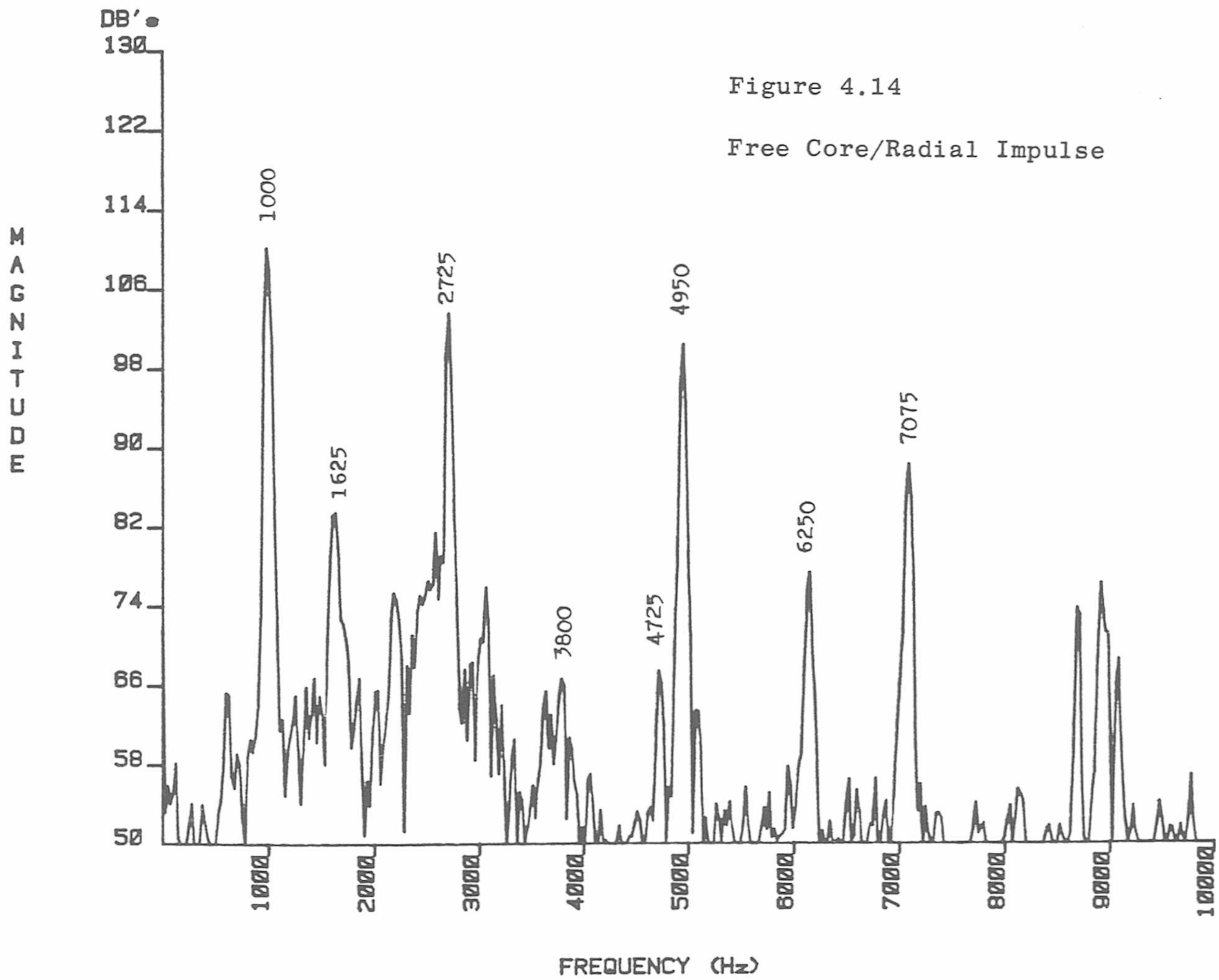

Figure 4.14

Free Core/Radial Impulse

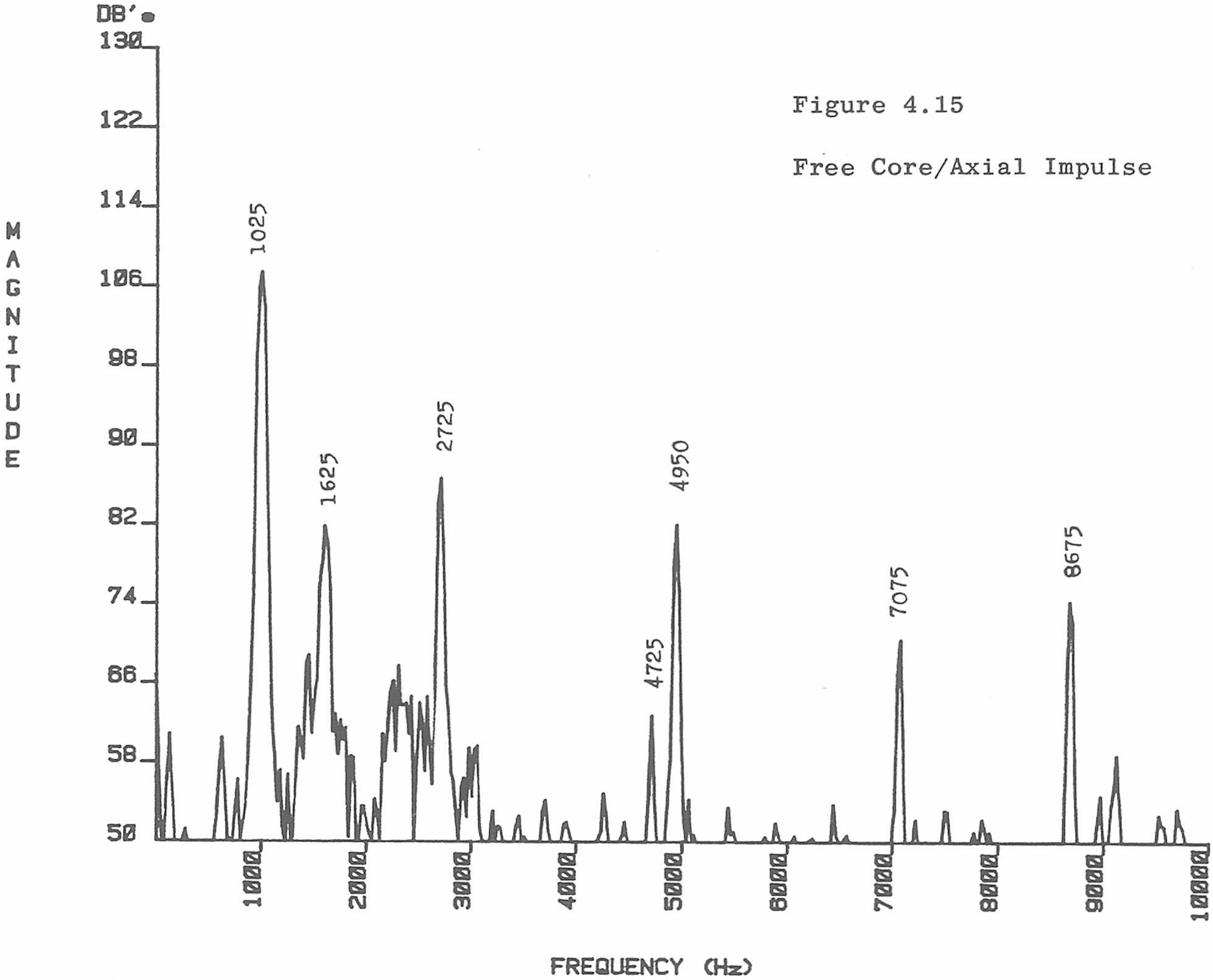

Figure 4.15

Free Core/Axial Impulse

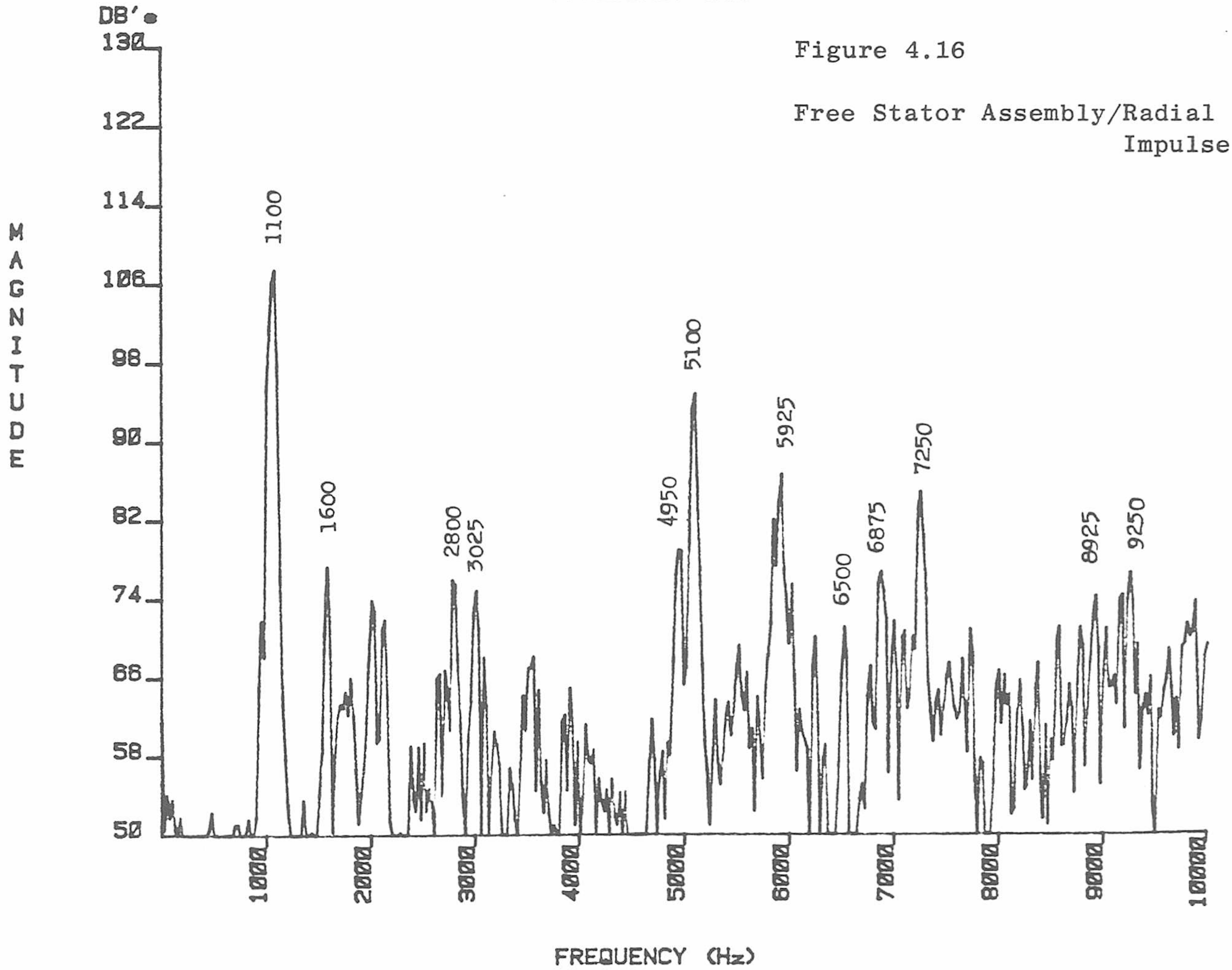

Figure 4.16

Free Stator Assembly/Radial Impulse

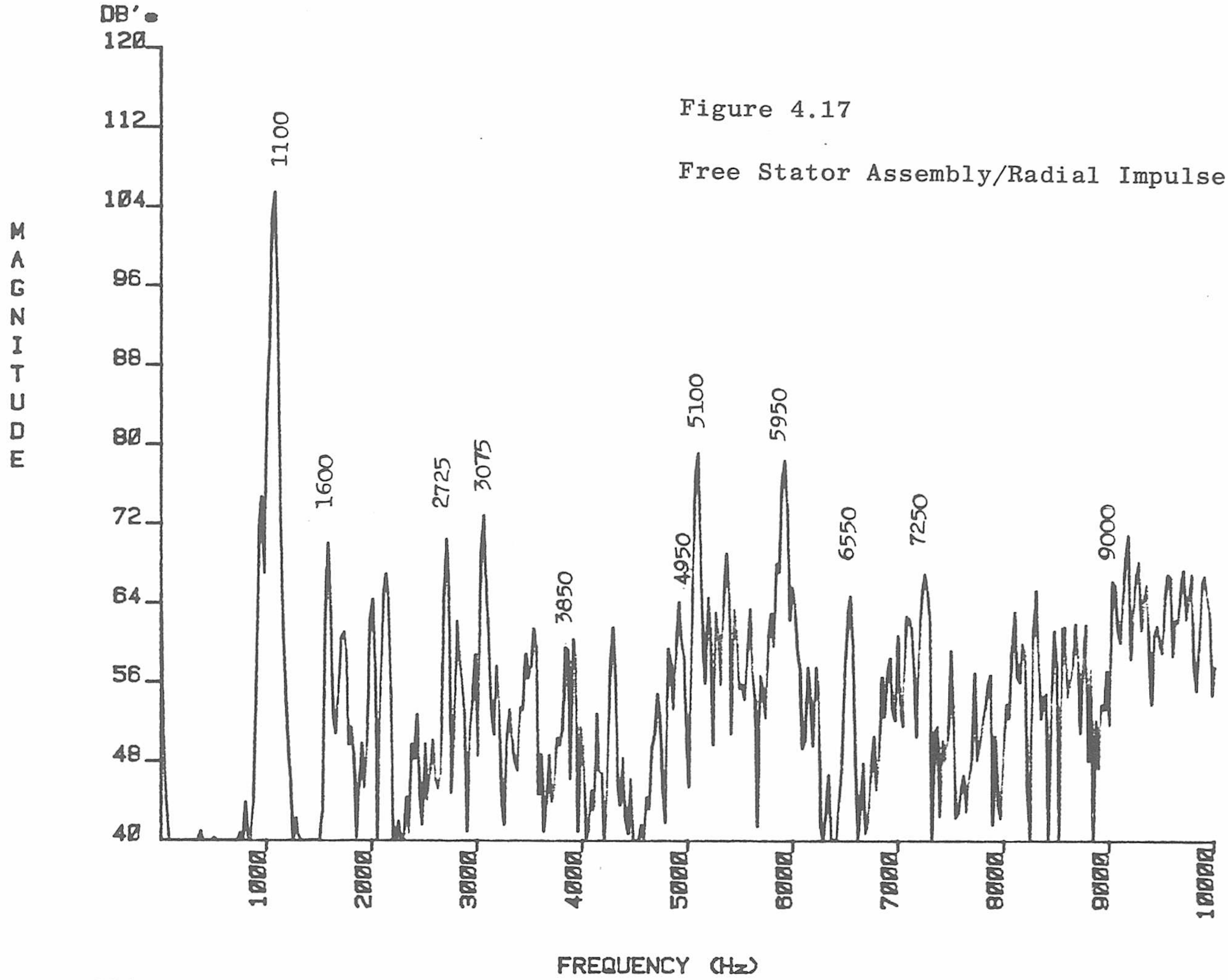

Figure 4.17

Free Stator Assembly/Radial Impulse

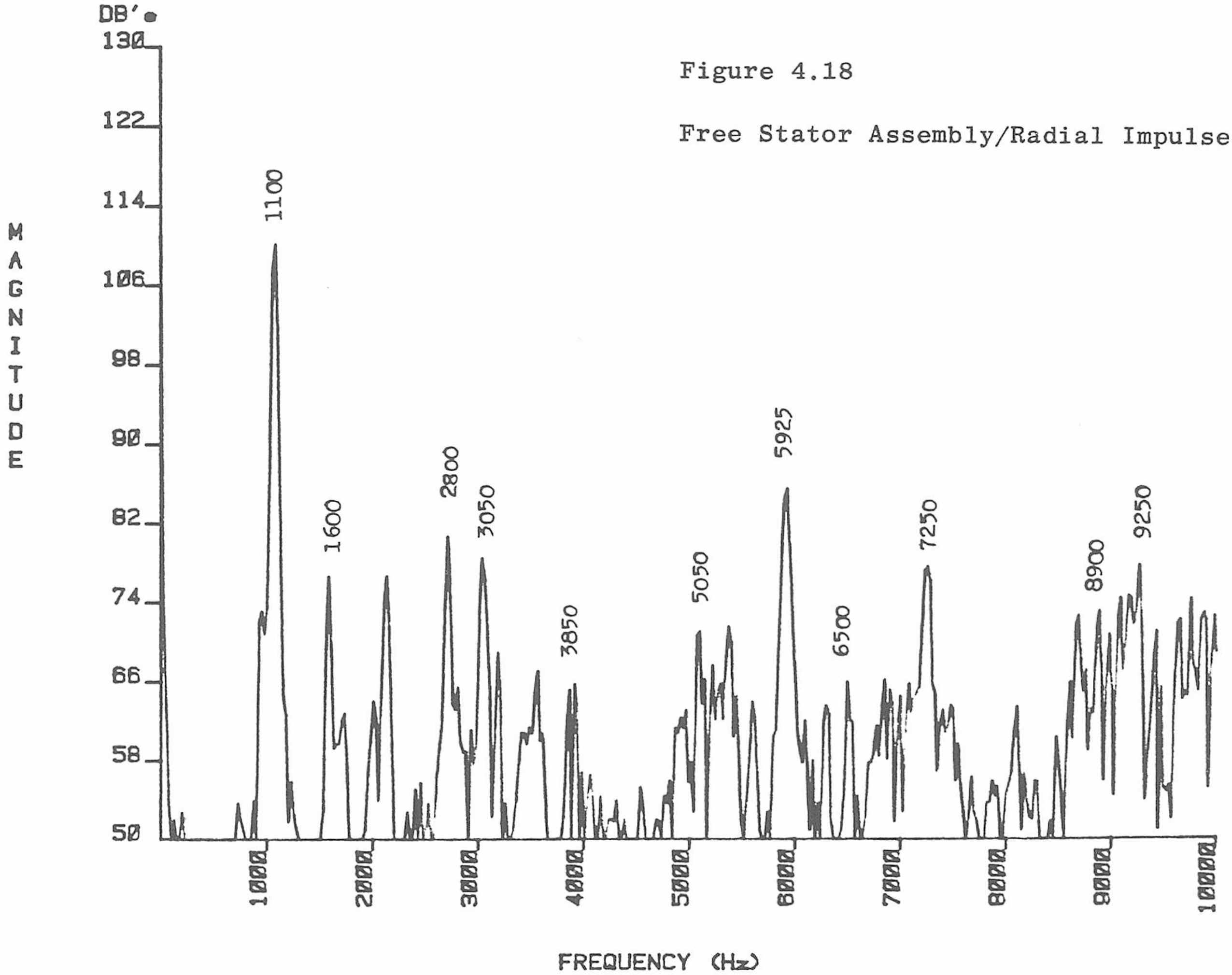

Figure 4.18

Free Stator Assembly/Radial Impulse

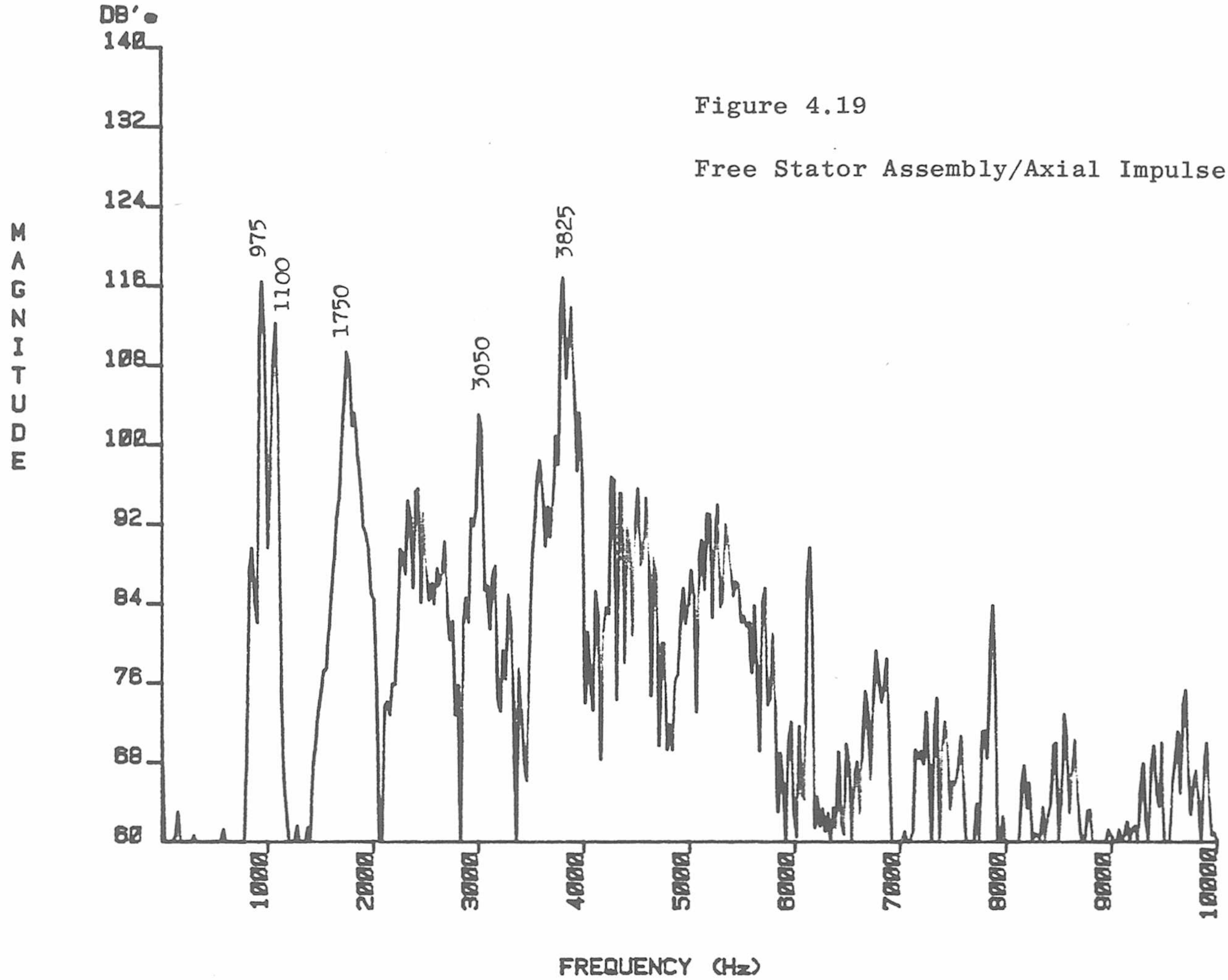

Figure 4.19

Free Stator Assembly/Axial Impulse

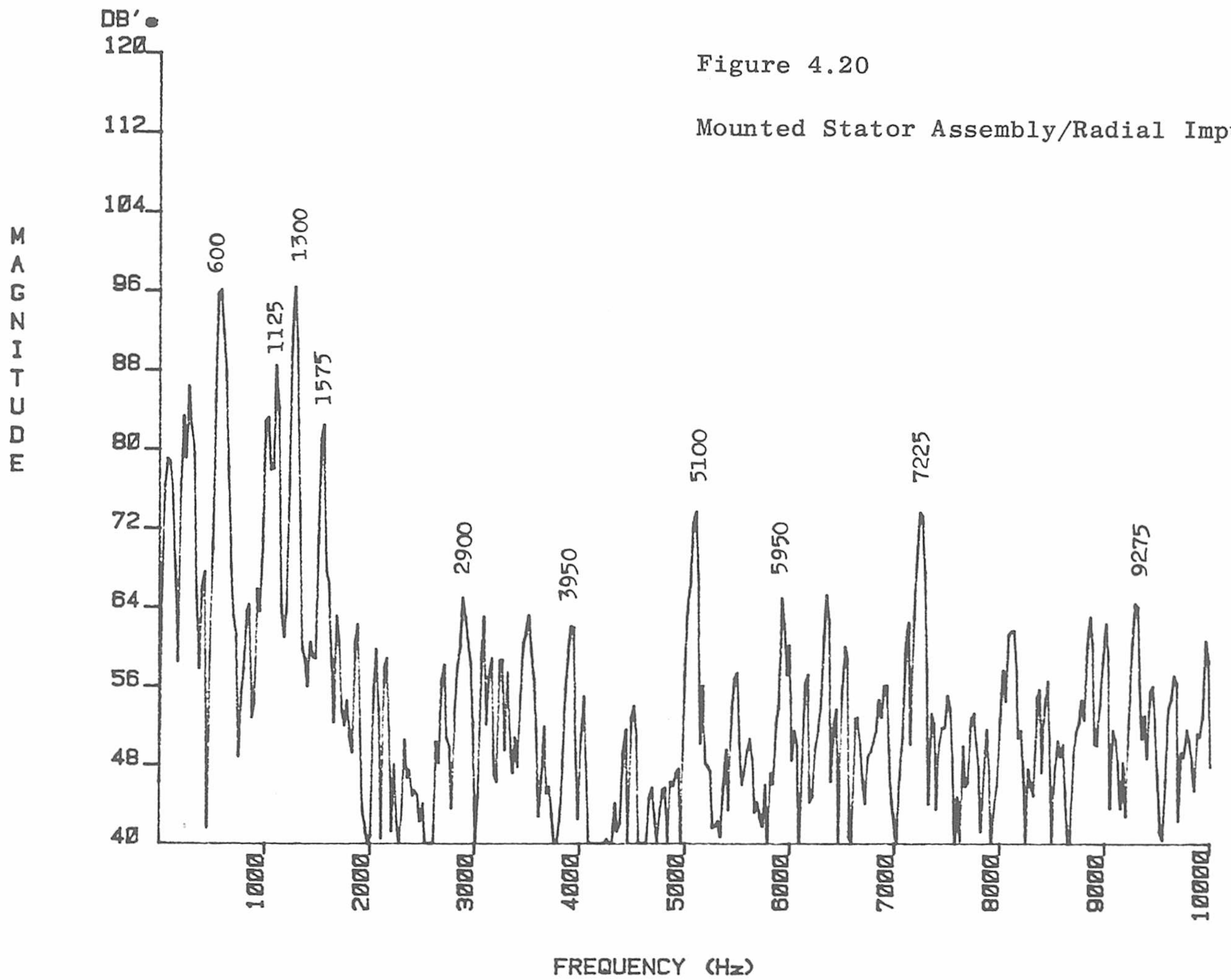

Figure 4.20

Mounted Stator Assembly/Radial Impulse

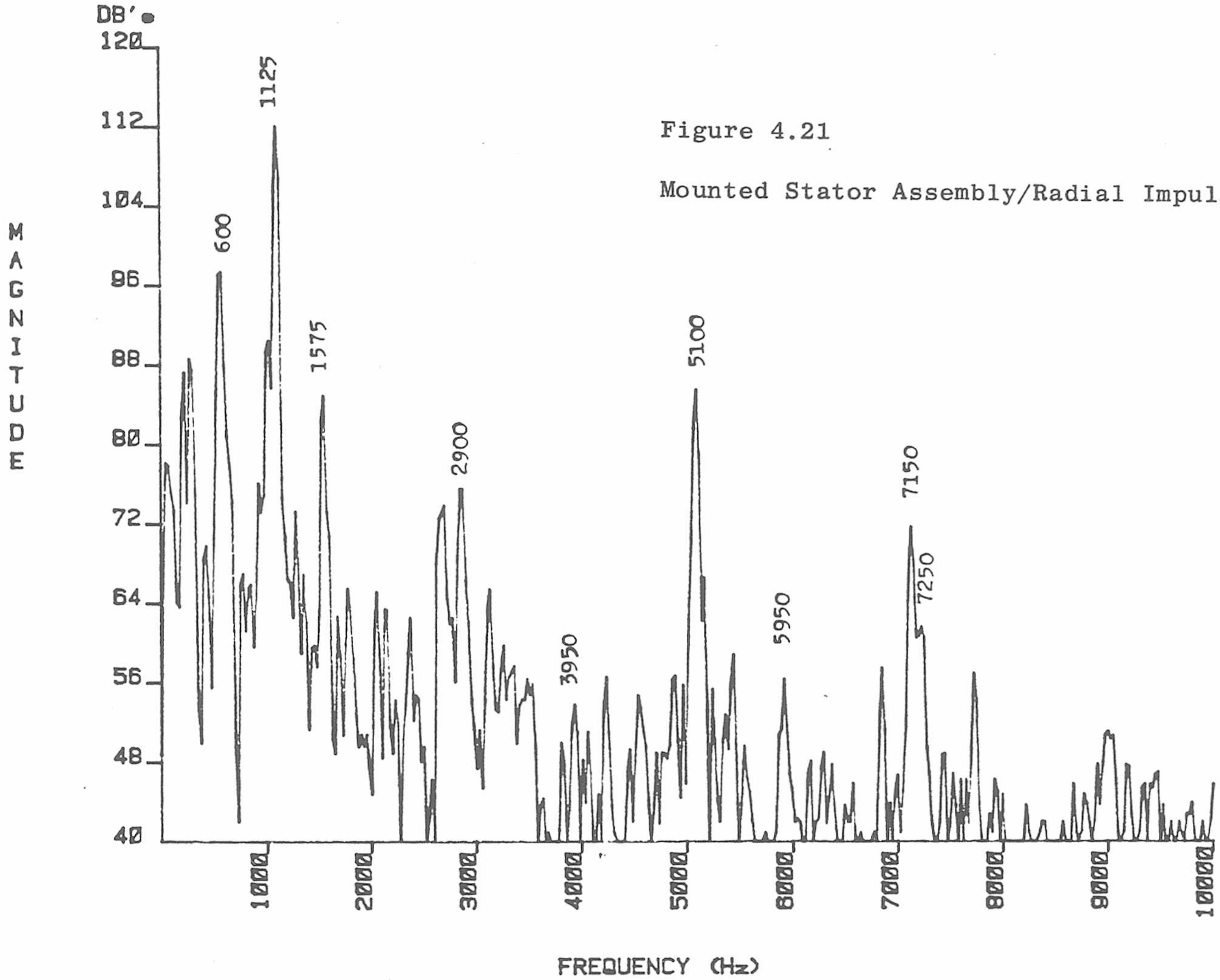

Figure 4.21

Mounted Stator Assembly/Radial Impulse

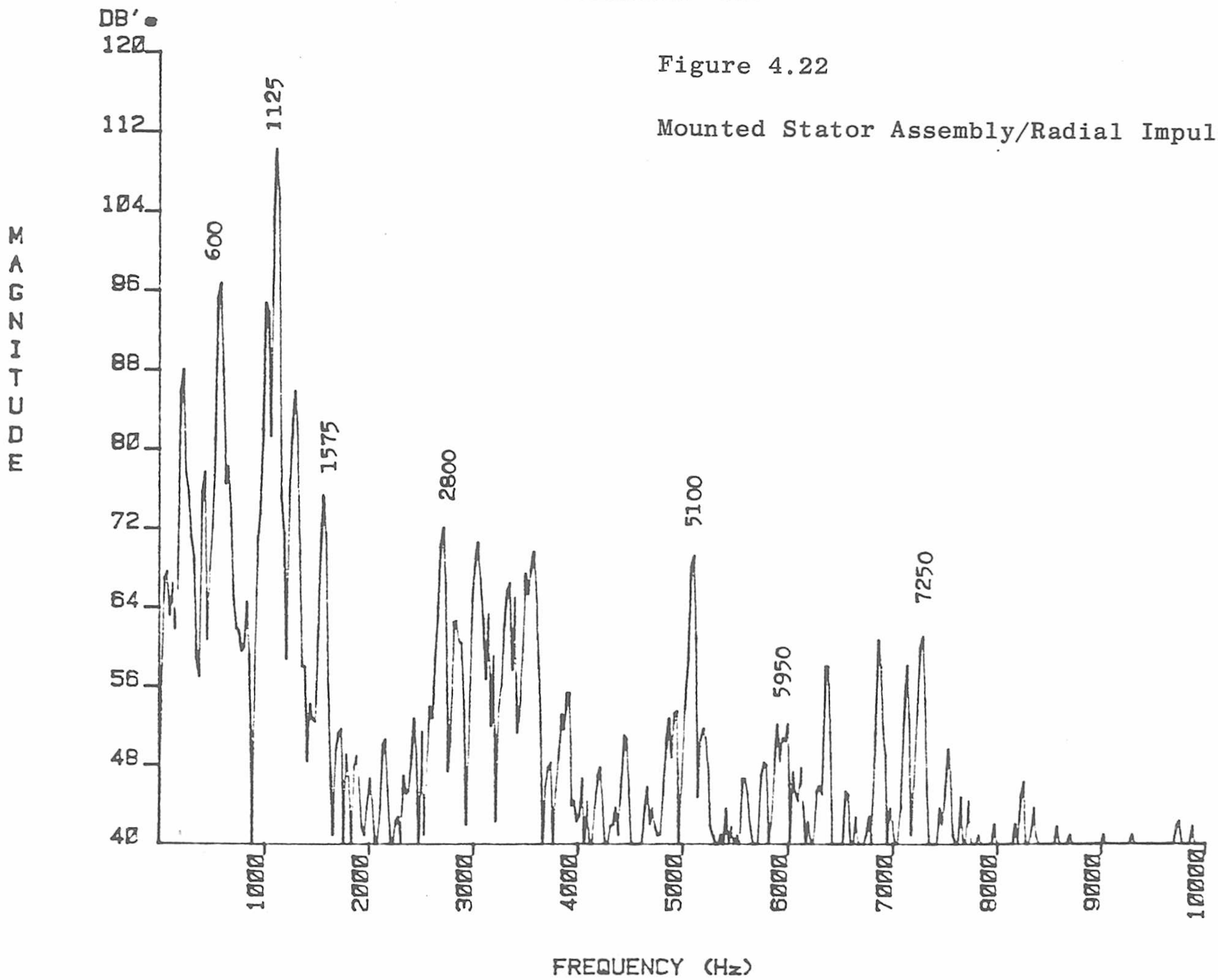

Figure 4.22

Mounted Stator Assembly/Radial Impulse

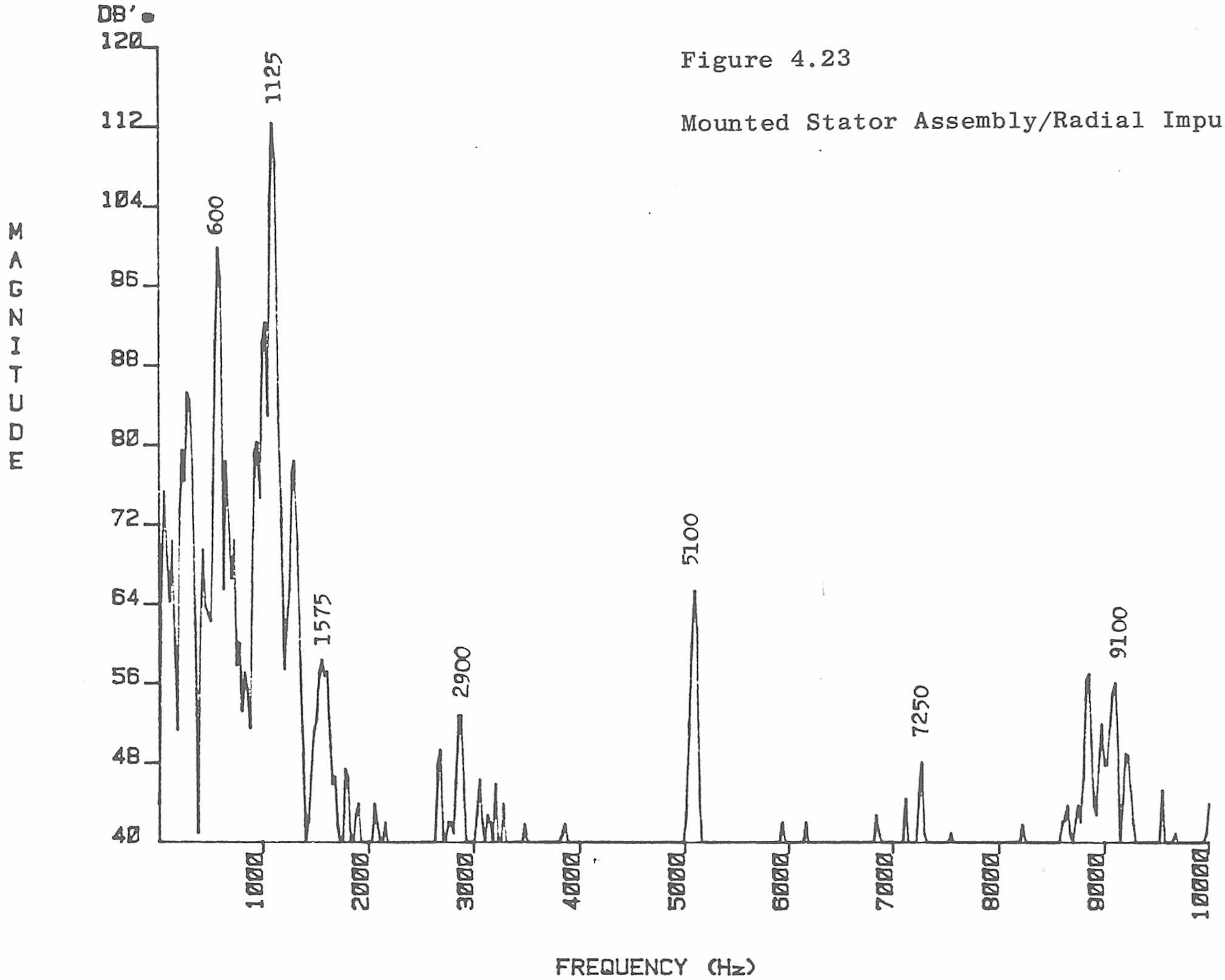

Figure 4.23

Mounted Stator Assembly/Radial Impulse

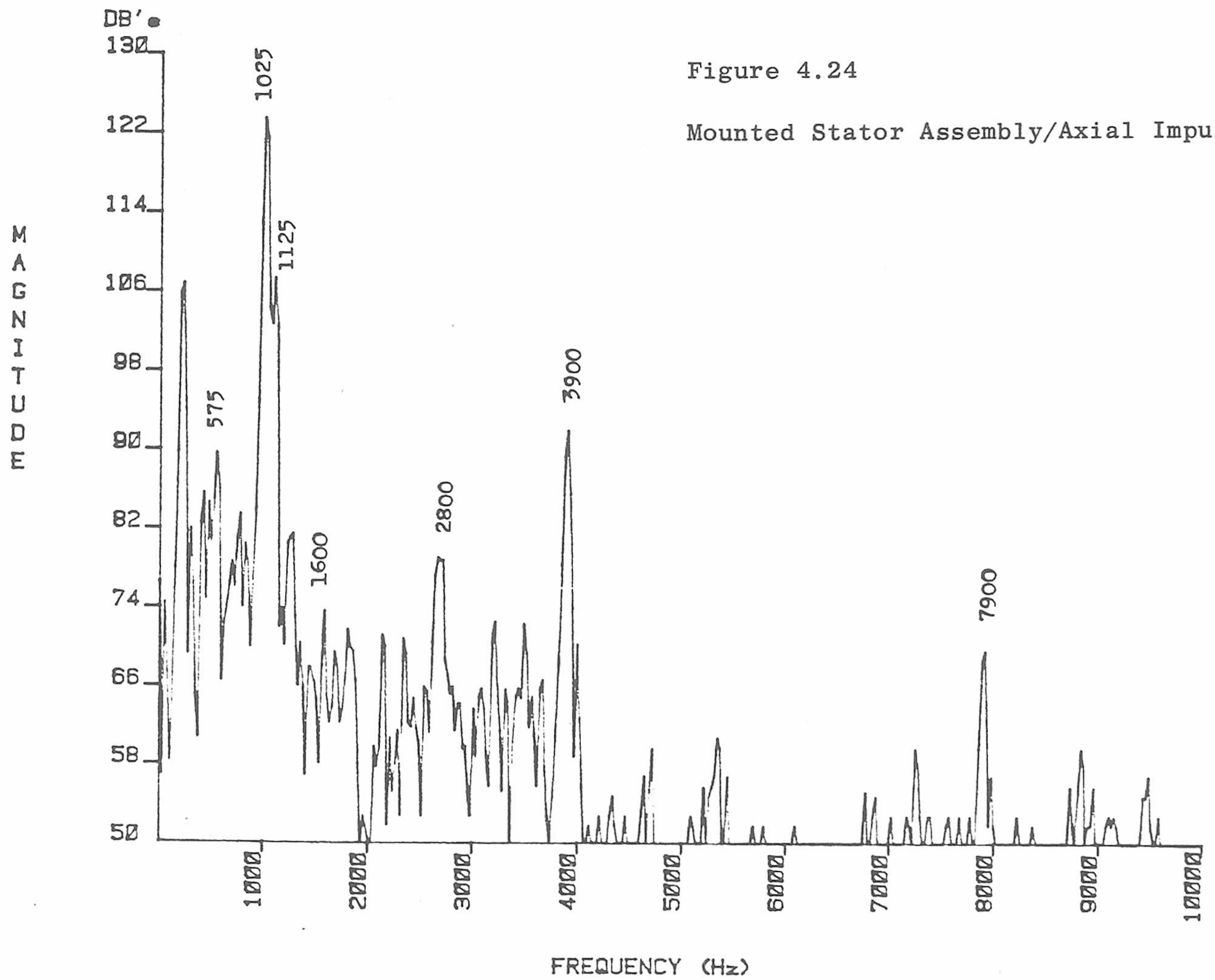

Figure 4.24

Mounted Stator Assembly/Axial Impulse

CHAPTER 5. THE DYNAMIC ANALYSIS OF A MODEL OF A LARGE INDUCTION MOTOR STATOR.

5.1 Vibration Analysis by the Use of a Model.

The next stage of the project was to design and develop an original test rig based on the construction of a typical large induction motor. The purpose of the stator model was to provide an experimental rig which could undergo resonance testing in the laboratory, in order to compare theoretical predictions of vibration behaviour with experimental findings. To meet these requirements, the new test rig is a scaled-down model of the stator assembly of an actual 2 MW induction motor used in offshore operations. Although the resonance frequencies and deflection amplitudes of the model will be atypical of the corresponding large machine, the modes of vibration will be illustrative of the interactive vibration behaviour of the stator assembly components of a large machine and will demonstrate the differences between small and large stator dynamic characteristics. The model, therefore, is not being used to predict large motor natural frequency values, but rather to verify whether finite element analysis can predict the natural frequencies of a complex stator assembly model and predict the vibration modes of a large motor type of stator structure.

Urusov (49) and Baudry (50) have investigated the use of plastic models for the analysis of stator vibration behaviour. Although the scale models were tested primarily to determine stator natural frequencies, they also predicted the modes of deformation at resonance. In a following discussion paper, Barton (51) describes the feasibility of using scale steel models to indicate the natural frequencies and vibration behaviour of full-size stators.

Findings from an experimental dynamic analysis of the test rig will be indicative of the vibratory characteristics of large motor stators. The results of the theoretical study will show whether or not finite element modelling is appropriate for the analysis of large machines.

5.2 The Stator Assembly Model.

The stator assembly illustrated in Figure 5.1 is built up around the D160M stator core used in the previous analysis (Chapter 4) and is approximately a 4 : 1 scale model of a 2 MW motor stator assembly. A fabricated construction process is used for the stator frame. Each of the frame components is cut from steel plate and machine finished before being welded together. Firstly, four core bars are welded at equally spaced positions around the core back. Core bars add rigidity to the stator and the number will depend mainly on the size of the motor (typically 12 bars will be welded to the core of a 2MW motor). In this case four core bars are sufficient to stiffen the structure without completely restricting vibratory response around the core back. These support the two endplates which are welded onto the core bars at either end of the core. Four circular rods join the endplates at their corners, adding rigidity to the structure. Steel blocks welded to the base of the endplates provide stator feet for mounting the assembly onto a bed-plate. The completed stator frame is an enclosed construction with side panels bolted at equidistant intervals along the width of the endplates. The test rig was developed with removable side panels so that there is access to accelerometer mounting positions round the core back and along the core bars for vibratory response measurements. The construction and dimensions of the model are illustrated in Figure 5.2 .

5.3 Finite Element Analysis.

The finite element models which constitute the theoretical dynamic analysis of the new stator assembly are described below:

(1) END 1 (Figure 5.3)

The endplate is modelled using triangular and quadrilateral isoparametric elements. The free body natural vibration of an endplate is determined from this analysis.

(2) END 2

The endplate is restrained at its base at nodes corresponding to the feet mounting positions.

(3) STR 1 (Figure 5.4)

Models END 1 and COR 3 are coupled through the core bars to model the stator assembly. STR 1 is a free-body analysis.

(4) STR 2

The stator assembly model is restrained at the nodes corresponding to feet mounting positions.

(5) EPC 1 (Figure 5.5)

This model of the stator assembly comprises END 1 and a core with simplified boundaries, neglecting cleating notches, semi-closed slot geometry and slot curvature. EPC 1 is a free-body dynamic analysis.

The finite element calculations from model COR 3 and those from the analysis of an endplate are presented in order to assess the effects on the natural frequencies and mode shapes of the stator structure of coupling between the core and endplate through the core bars.

In Chapter 4 it was found that simplifying the core boundaries for mathematical modelling caused considerable errors in the natural frequency calculations. However, it is possible that if the core is part of a larger structure, the errors involved from these simplifications may not be as significant. EPC 1 is modelled so that the results can be compared with those from model STR 1 and differences in the calculated values can be viewed in terms of reduced computer costs and simplified modelling procedures as well as accuracy.

5.4 Experimental Analysis of the Stator Model.

The experimental analysis of the stator assembly, to determine the natural frequencies and mode shapes, involved the use of Impulse Response and Sinusoidal Resonance tests for two experimental arrangements:

(1) The stator assembly freely suspended,
(2) The stator assembly mounted on a steel bed-plate.

The free-body analysis of the stator involved resiliently mounting the structure by connecting non-rigid springs to the ends of the core. For the latter arrangement, the steel blocks acting as stator feet were bolted onto the steel bed-plate to provide a rigid fixing at the assembly base.

The accelerometer mounting positions consist of 28 mounting studs equally spaced around the central core periphery with one stud on each core bar. 6 equally spaced positions along the top and 6 equally spaced positions down one side of an endplate were chosen as measurement positions, as were 5 positions including the mounting stud on a core bar. Mounting studs on the core back were permanently fixed using an epoxy adhesive. For the measurement of endplate vibration, the mounting stud was fixed to the transducer which was positioned on the structure using bees-wax as a temporary adhesive. Both epoxy resin and bees-wax are suitable adhesives for stator resonance testing as they exhibit constant response properties over the frequency range at which the stator assembly is tested.

The stator assembly was excited radially at the central mounting stud on one of the side core bars. For this reason and also for access to the core transducer positions, the frame panels were removed for all the sinusoidal resonance tests and for some of the impulse tests. A set of impulse tests was performed on the stator with the frame panels bolted onto the endplates to make sure that any changes in structural natural frequencies due to enclosing the frame could be analysed experimentally.

5.5 Results.

TABLE 6.

Calculated Endplate Natural Frequencies.

Mode m	FREQUENCY (Hz) FREE ENDPLATE	RESTRAINED ENDPLATE
2	* 771	517
2	958	* 1265
3	2487	2416
3	* 2488	* 3076
0	4093	3564
4	4144	* 4219
0	5111	
0	5125	
4	* 5152	4941
0	6232	5315
0		6214
5	* 7086	* 7295
5	7108	7775
6	* 9443	* 9325

TABLE 7.

Free Stator Assembly Natural Frequencies.

mode m	n	Natural Frequencies (Hz) Calculated	Measured	% Diff.	Response (m x 10^{-8})
*2	*2	889	907	+2.0	58
2	2	1069	1015	-5.0	22
2	2	1774	1806	+1.8	4.5
	3	2177	/		
	*3	2177	2105	-3.3	2.0
		2587	2560	-1.0	1.9
*3	*3	2947	2755	-6.5	4.9
3	3	2982	2963	-0.6	2.7
	*4	4307	4305	-0.05	1.8
	3	4715	4680	-0.7	1.6
	3	4759	4825	+1.4	8.2
4	4	4835	5006	+3.4	3.6
*4	*4	5300	5350	+0.9	7.7
6	6	5496	5620	+2.2	
			FROM IMPULSE TESTS		
		5816	/		
		5852	5935	+1.4	
		6071	/		
		6314	6335	+0.3	
		6819	6940	+1.7	

TABLE 8.

Mounted Stator Assembly Natural Frequencies.

MODE m	MODE n	Natural Frequencies (Hz) Calculated	Natural Frequencies (Hz) Measured	% Diff.	Response (m x 10^{-8})
2	2	619	605	-2.3	3.2
*2	*2	1098	1030	-6.2	19.1
0	2	1117	1043	-6.6	22.8
0	*3	1945	1880	-3.3	1.6
0	3	2081	/		
		2523	2552	+1.1	0.9
3	3	2766	2760	-0.2	7.1
	*3	3236	3155	-2.5	0.9
	3	3621	3578	-1.2	0.8
*3	*3	3918	3875	-1.1	1.2
		4951	4850	-2.0	4.7
4	4	5005	5060	+1.1	0.7
*4	*4	5272	5246	-0.5	0.5
*4	*4	5943	5943	0.0	1.1
	4	6018	/		

Calculated	FROM IMPULSE TESTS	% Diff.
6284	/	
6376	6350	-0.4
6850	6950	+1.4
8459	8250	-2.5
8532	/	

TABLE 9.

Comparison Between Calculated Natural Frequencies of Two Finite Element Assembly Models.

Calculated Natural Frequencies (Hz) STR1	EPC1	% Diff.
889	883	-0.67
1069	1045	-2.24
1774	1836	+3.38
2177	2188	+0.50
2177	2195	+0.82
2587	2741	+5.62
2947	3026	+2.61
2982	3032	+1.65
4307	4332	+0.58
4715	4716	+0.02
4759	4785	+0.54
4835	4860	+0.51
5300	5298	-0.04
5496	5534	+0.69
5816	5830	+0.24
5852	5898	+0.78
6071	5984	-1.45
6314	6297	-0.27
6819	6989	+2.43

m : Plate inner ring bending mode number.

n : Core ring bending mode number.

* : Symmetric component of mode number.

% Diff.: Percentage increase (+) or decrease (-) in value.

5.6 Discussion.

The interaction of core and endplate vibration means that the dynamic behaviour of a large motor stator structure is more complex than that of a small motor assembly. Core and endplate resonances can have a significant effect on each other and on the whole structure's vibration behaviour. Every resonance frequency, whether it is due mainly to core characteristics, endplate characteristics or whole structure vibration, excites some form of deformation in all parts of the stator assembly. Coupling of the modes exists through the core bars and their positioning influences the interactive behaviour of the core and endplate. Therefore to understand the modal behaviour of the stator structure as a whole it is useful initially to calculate core and endplate resonance frequencies separately.

The relevant stator core modelling and analysis was referred to in Chapter 4. The calculated and measured values were presented in Table 3.

The calculated endplate resonance frequencies are given in Table 6 and the corresponding mode shapes are illustrated in Figures 5.6 and 5.7 .

5.6.1 Endplate Vibration.

Free endplate resonance frequencies are influenced by two types of modal behaviour:

(1) Modes of vibration associated with ring bending. The inner circumference of the plate deforms in the conventional ring modes with a displaced dual resonance predicted for every wave number.

(2) Extensional modes of vibration associated with plate bending.

The value of m in Table 6 is the mode number of the ring bending mode. A value of $m = 0$ is therefore assigned to extensional plate bending type mode shapes. An asterisk (*) indicates the symmetric component of a dual resonance.

The modal behaviour of an endplate is restricted by restraining the feet positions but the wave patterns of the inner circumference remain identifiable as ring bending modes. However, as was found in Chapter 4 for the restrained stator assembly, the symmetric and antisymmetric components of the dual resonances occur in reverse order at some modes between the free and restrained vibratory conditions. In this case at $m = 2$ and $m = 4$.

The effects of restraining the base of the endplate on the resonance frequency values are recorded as percentage differences. There is no general trend of frequency increases or frequency decreases. For some mode shapes, the increased bending stiffness of the structure plays the dominant role in determining the resonance frequency, whereas for other mode shapes the structure's increased rotational inertia is more important. The resulting effects are most obvious at $m = 2$ where the antisymmetric mode shape is dependent on plate-edge oscillation and the symmetric mode shape is dependent on plate-edge bending.

As well as extensional, in-plane vibration the endplates will also exhibit transverse vibration properties exciting out-of-plane deformation. The analysis of such vibration behaviour is well-known and well documented (52, 53). Transverse natural modes occur at much lower frequencies than their extensional counterparts but will not have any effect on stator assembly radial vibration levels and are therefore not relevant to vibration monitoring.

5.6.2 Free Stator Assembly Vibration.

Table 7 presents a comparison between calculated and measured resonance frequency values of the free stator assembly. A number m identifies a plate ring bending mode and n identifies a core ring bending mode. An asterisk indicates a symmetric mode shape. The free stator assembly mode shapes are illustrated in Figure 5.8 . The maximum vibration amplitudes measured during resonance tests are also recorded in Table 7.

The complex stator assembly produces modes of vibration which are difficult to categorise. The mode shapes can be made up of a combination of the following vibratory characteristics:

(i) core circumference radial bending,
(ii) plate inner ring bending,
(iii) plate edge extensional deformation,
(iv) core bar bending.

If at a resonance frequency one particular mode of vibration is dominant, very distorted mode shapes may be excited in parts of the structure. This is especially true at higher modes where the pure uncoupled waveforms are complicated and easily distorted by coupling. For this reason the values of mode number assigned to most resonance frequencies are only a guide to the identifiable ring-type bending waveforms excited at those frequencies.

At $m = 2$, $n = 2$ three modes of vibration are excited. The first resonance frequency lies between the first core natural frequency and the first frame natural frequency. The resultant is a structural natural frequency exciting a pure coupled symmetric bending mode. At the second resonance frequency the core anti-symmetric mode is excited and dominates the stator assembly vibration. At the third frequency two opposing antisymmetric modes are excited with the endplate component dominating. At each wavenumber the resonance frequencies are excited by mainly core vibration, mainly frame vibration or a combination of the two. The mode shapes are dependent on the closeness of the structural resonances to core or endplate resonance frequencies and the interaction of core and endplate vibration. Responsive resonances tend to occur at frequencies near stator core natural frequencies and the core in general dominates the assembly vibration behaviour.

The effects of the tie bars have been neglected in the stator assembly model. The assumption was that the tie bars would restrict the out-of-plane modal behaviour of the endplates at transverse resonance frequencies but would have little effect on extensional vibration and negligible effect on core radial vibration. The assumption would appear to hold true since there is good agreement between calculated and measured natural frequency values and mode shapes.

5.6.3 Restrained Stator Vibration.

As was predicted by the analysis of endplate vibration, the restraints imposed at the base of the stator assembly have a considerable effect on endplate modes and as a result, core ring bending modes tend to be distorted. The mode shapes (Figure 5.9) show very little vibratory motion around the base of the endplate which restricts the ability of the stator structure to assume conventional modal wave patterns. To understand the vibration behaviour of a motor stator mounted on a steel bed-plate, the resonance frequencies and mode shapes must be viewed in terms of core and endplate interaction.

There are various factors influencing the overall behaviour at each resonance frequency. Most have already been encountered as separate determinants of natural frequency values or modal deformation which are characteristic of one or all components of the stator structure. For example: dual resonances, inertial effects, stiffening effects, plate edge extension, plate ring bending, core circumference bending and plate restraining effects. Mounted stator assembly vibration encompasses all of these factors and each natural frequency and mode shape is affected to some extent by all of them. Although plate mode shapes and core mode shapes are differentially distinct, the structural resonance frequencies exciting them cannot be predicted by the analysis of either core or endplate vibration alone.

5.6.4 Frame Panel Vibration.

Having assumed previously that transverse motion of the endplates is not important to the analysis of radial assembly vibration, it is precisely this type of vibration behaviour which will affect vibration levels measured on the side panels and top panel. If the presence of the frame panels does have any effect on the assembly natural frequencies, it would be possible to identify changes in the impulse spectra. For this reason, a series of impulse tests was performed on the stator assembly with the frame cover panels bolted onto the endplates. The frequency spectra obtained from impulses directed at and measured at various positions on the panels are very similar to the spectra obtained on the stator assembly with the panels removed. (Compare Figures 5.16 to 5.19 with Figures 5.20 to 5.23). The same assembly natural frequencies are excited and no additional responsive frequencies are detected. It can therefore be concluded that the frame covers have a negligible effect on stator assembly resonance frequencies and that the natural frequencies of a frame panel under these particular boundary conditions are most likely not excited in the frequency range covered by this study.

Calculations carried out using Warburton's transverse analysis for a plate with built-in boundaries (52) predicts that the first natural frequency will occur at 57 kHz. The actual value will in fact be lower than this. The plate edges have some flexibility so that assuming built-in boundaries is an upper limit approximation. However the value does indicate that the stator assembly frame plates will not introduce extra assembly resonance frequencies within the frequency range of this dynamic analysis or affect the values associated with the assembly without its cover.

5.6.5 Simplifying the Finite Element Model.

If a motor operator commissions a complete dynamic study of a newly installed machine as a prerequisite to instituting a vibration monitoring strategy, consideration of computer costs may be especially important. Hence it is sensible to establish where approximations can be made to the finite element mesh which will have a negligible effect on the calculated dynamic characteristics of the stator assembly.

Calculated resonance frequency values for the stator model EPC1 are given in Table 9. A comparison with results calculated from the more structurally accurate model STR1 is presented. Values obtained from the model that simplifies the boundaries match closely in most cases with those of the more complex model. During the study of free-body core vibration in Chapter 4, these same boundary approximations led to large errors in the computed results. It would seem therefore, that in large stator structures where complex interaction of assembly components is involved, the dynamic significance of accurate modelling of the slots and notches is considerably reduced. The modelling procedure of EPC1 requires less input data and less computer processing time than STR1.

These factors must be weighed against any loss of accuracy before validating the simplifications, In this instance, the finite element model EPC1 is a feasible alternative.

5.7 Conclusions.

Several conclusions can be drawn from this study:

(1) The vibration behaviour of a large motor stator is more complex than that of a small motor.

(2) Structural resonance frequencies and mode shapes are influenced by core and endplate natural frequencies and mode shapes but cannot be predicted from an analysis of core or endplate vibration alone.

(3) Structural resonance frequencies and mode shapes are influenced by the boundary conditions. Restraining the frame feet leads to distortion of the deformed assembly at resonance.

(4) The interactive vibration behaviour of the core and frame is caused by coupling through the core bars so that the number and positioning of core bars will determine the shape of the distorted modes at structural resonances.

(5) The frame panels which enclose the stator assembly do not affect the structural resonance frequencies.

(6) The Finite Element Method performs well as an analytical tool for the study of vibratory characteristics of large motor stator structures. Error margins between calculated and measured natural frequency values are small and all the calculated mode shapes excited by responsive resonance frequencies could be found experimentally.

(7) Computer cost reduction by introducing boundary approximations into the finite element mesh can be a feasible proposition if care is taken to make simplifications only where the dynamic significance to the overall structure is negligible.

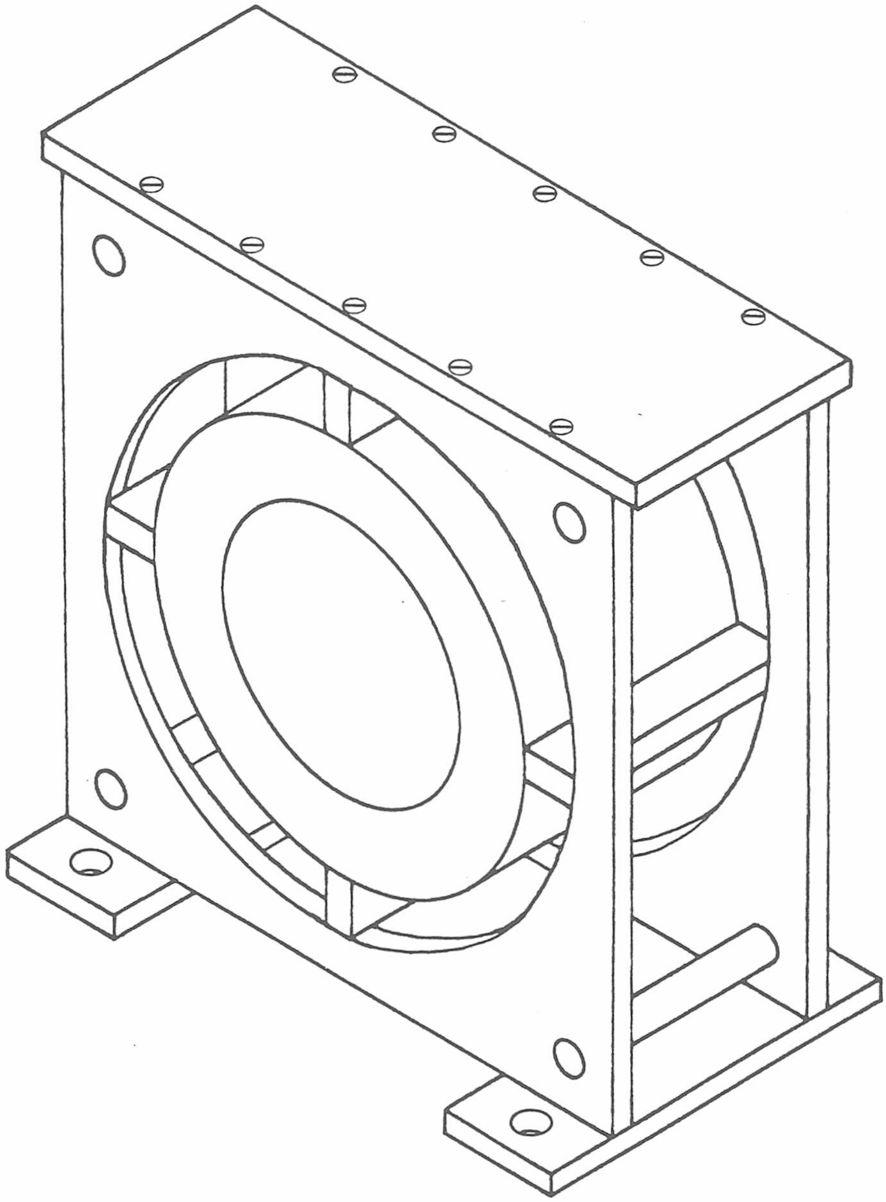

Figure 5.1
Large Motor Stator Assembly Model.

SCALE 1:3
All dimensions in mm.

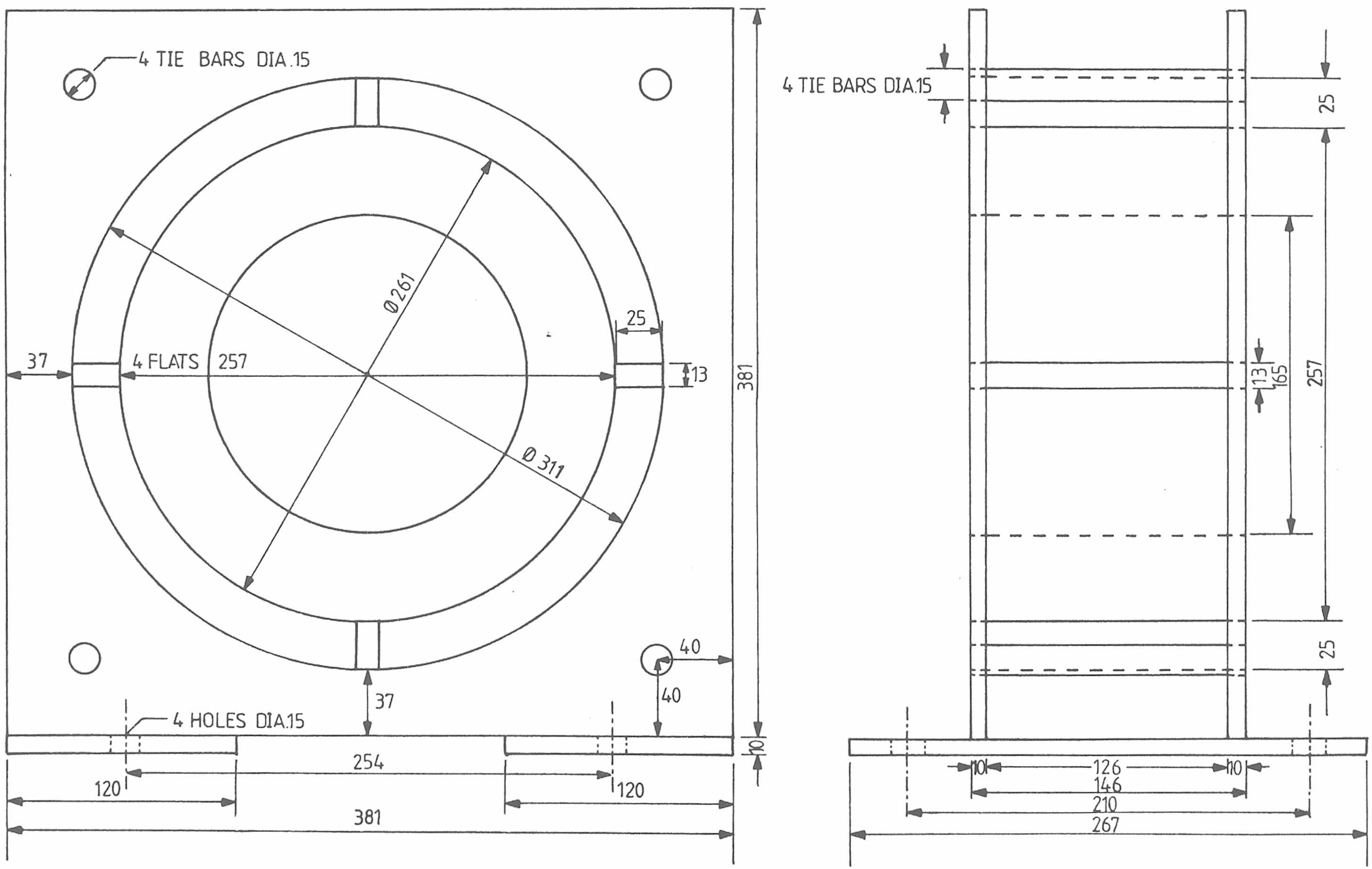

Figure 5.2 Dimensions of Stator Assembly Model.

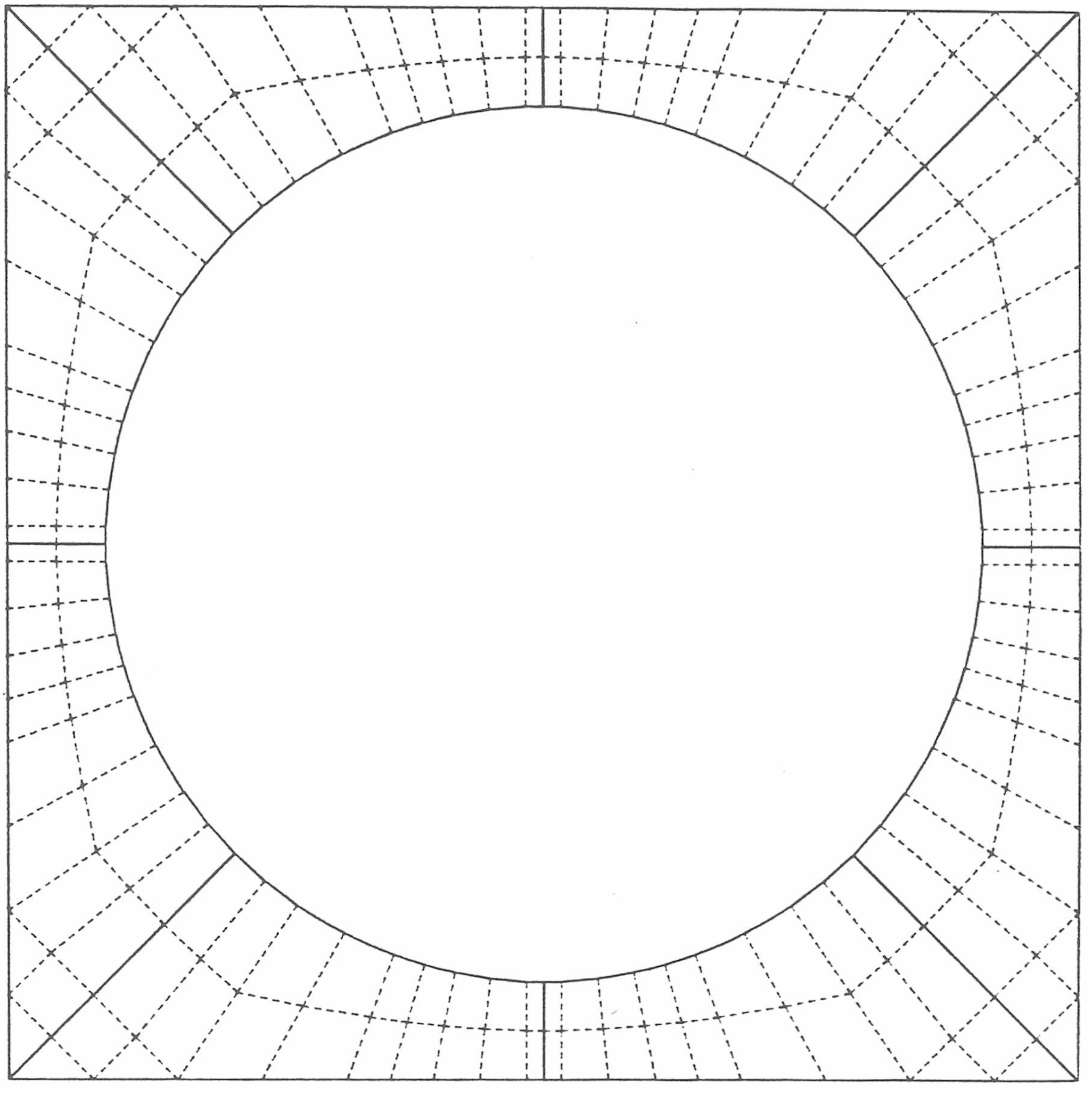

Figure 5.3

END1.

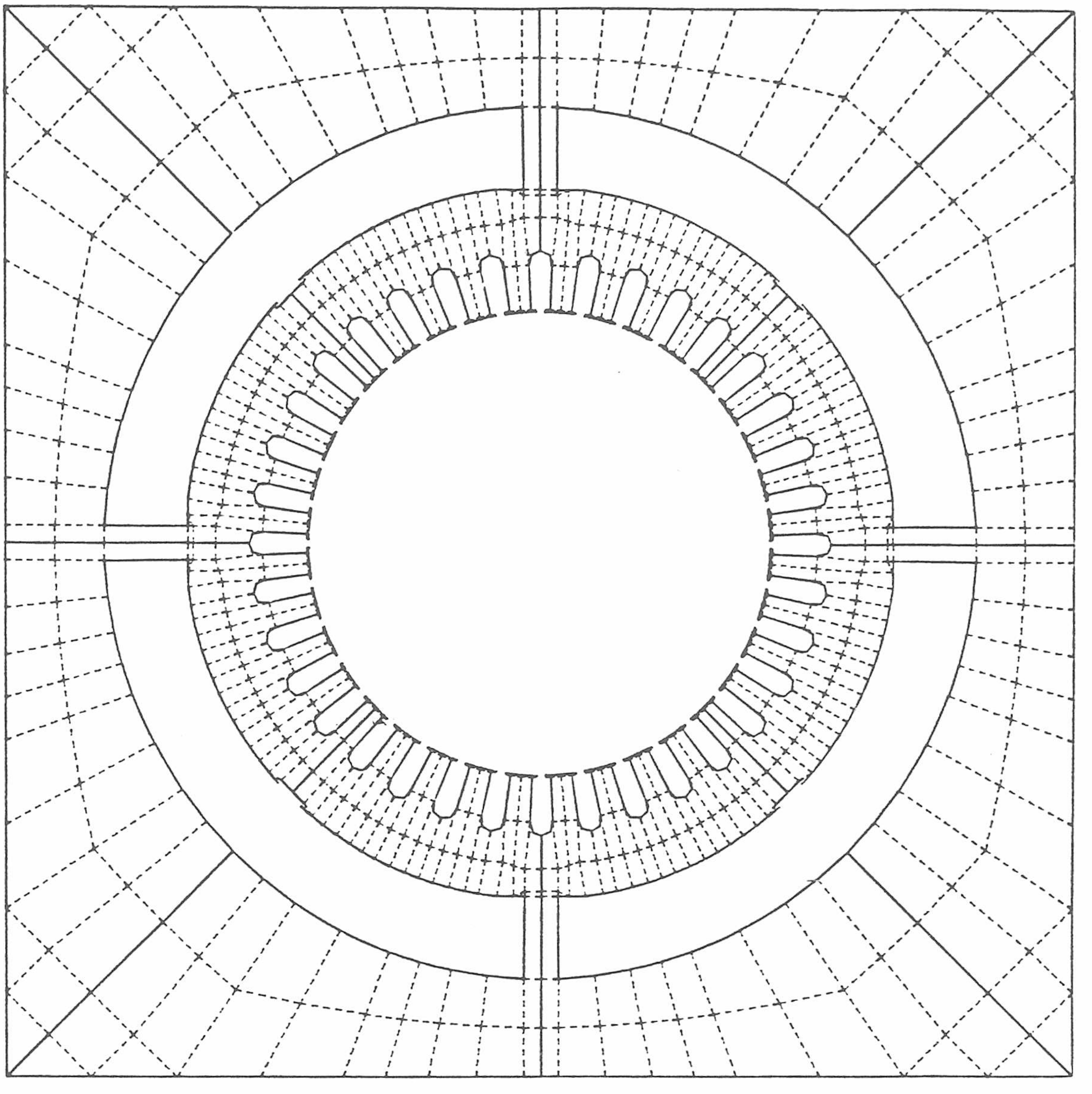

Figure 5.4

STR1.

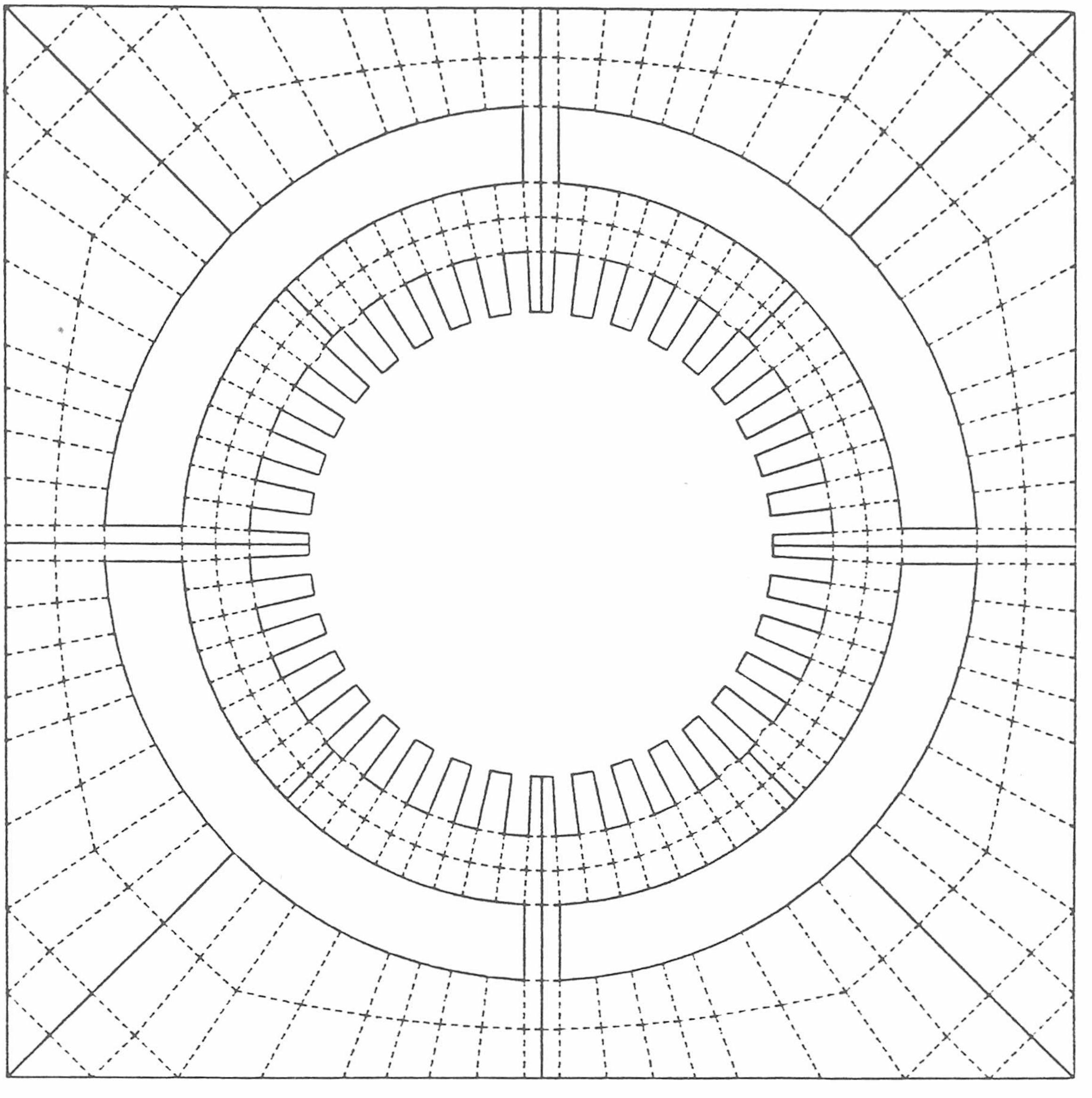

Figure 5.5

EPC1.

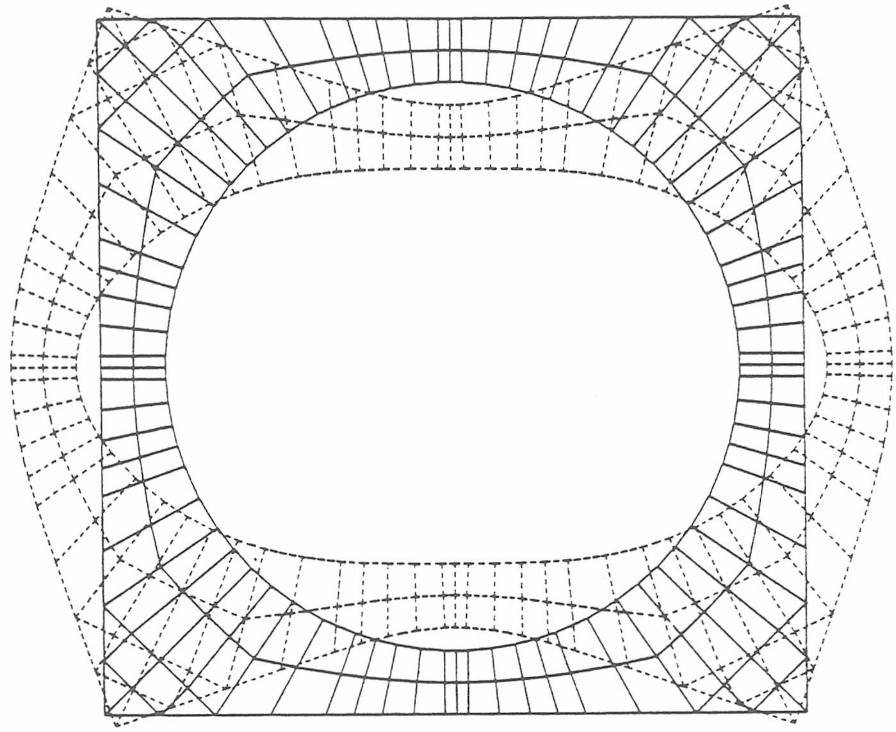

(a) f_n = 771 Hz.

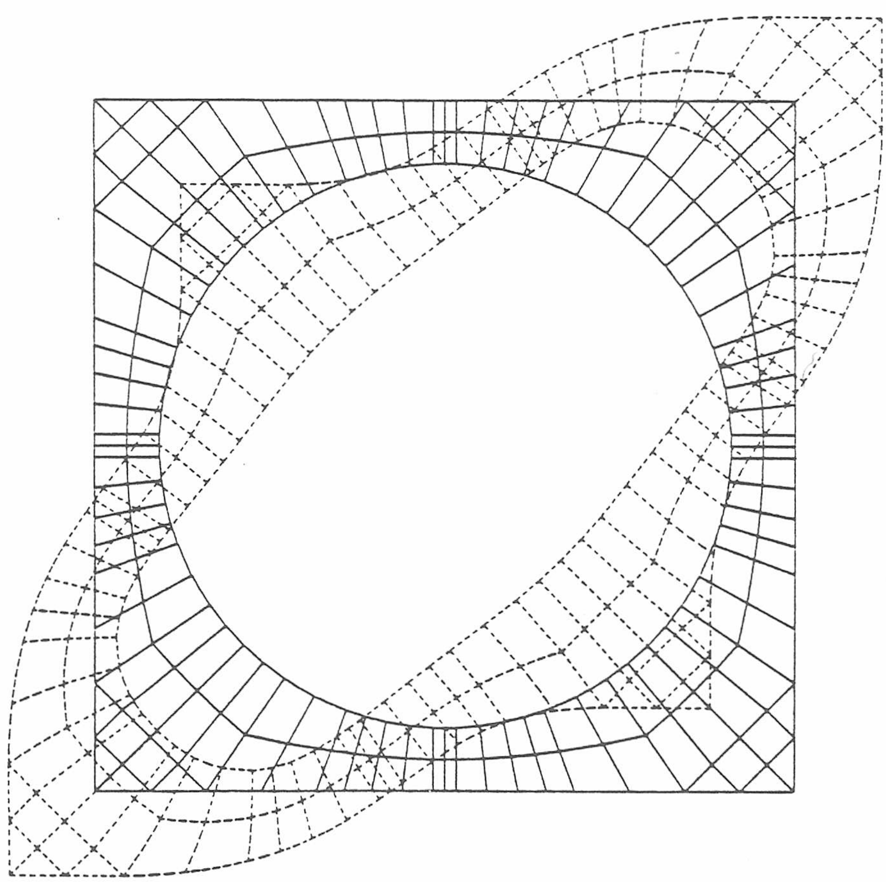

(b) f_n = 958 Hz.

Figure 5.6

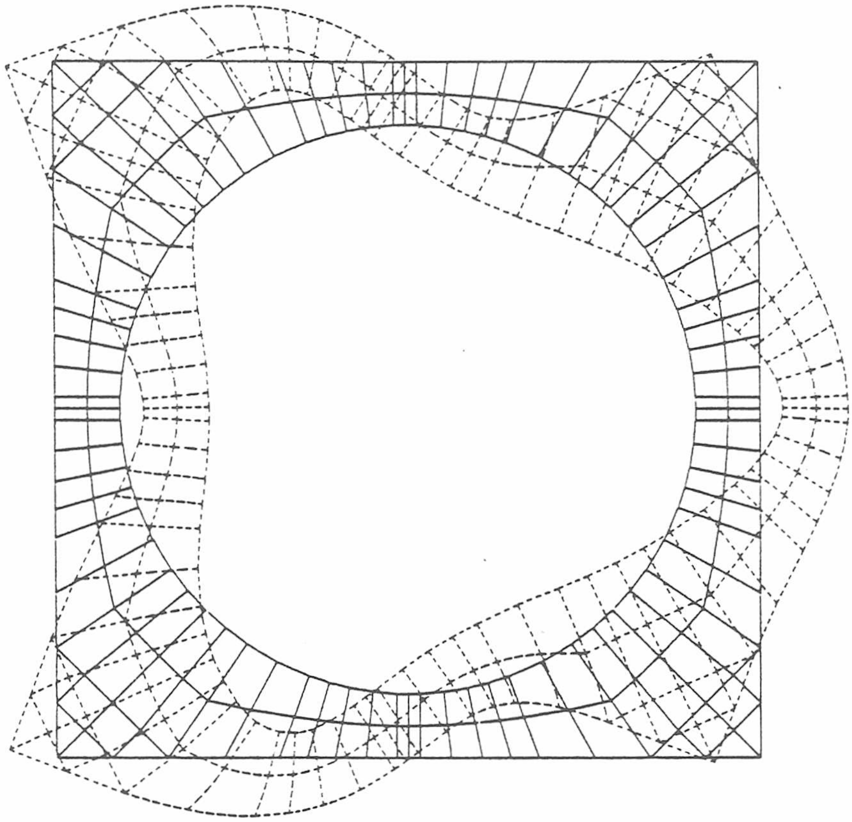

(c) f_n = 2487 Hz.

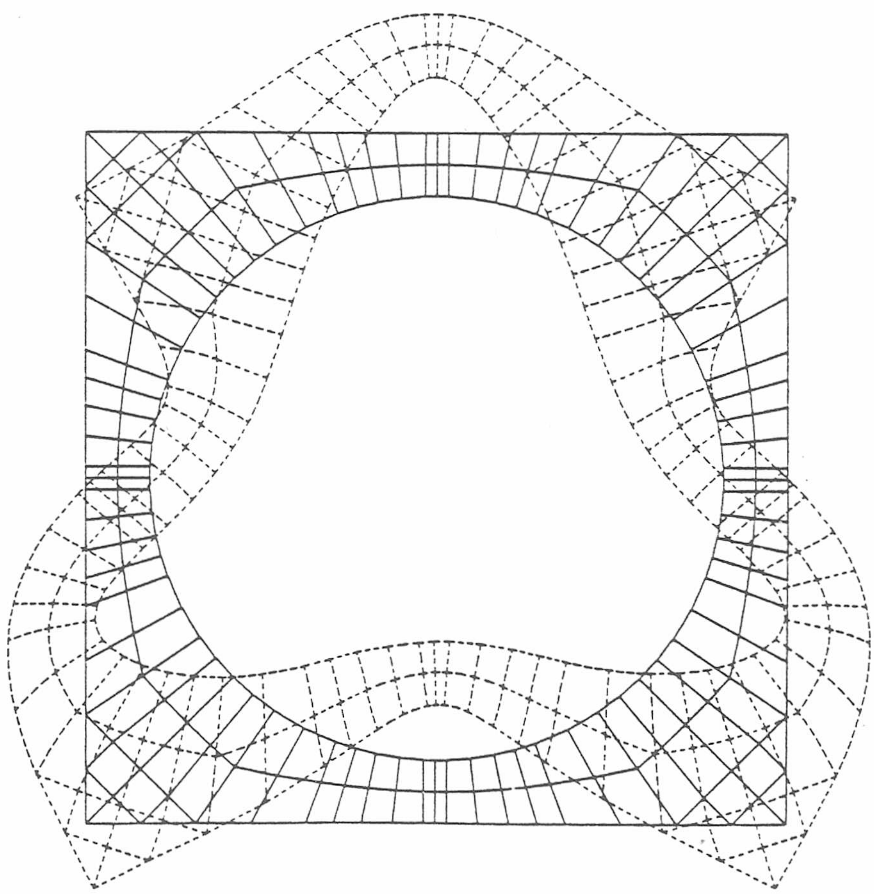

(d) f_n = 2488 Hz.

Figure 5.6

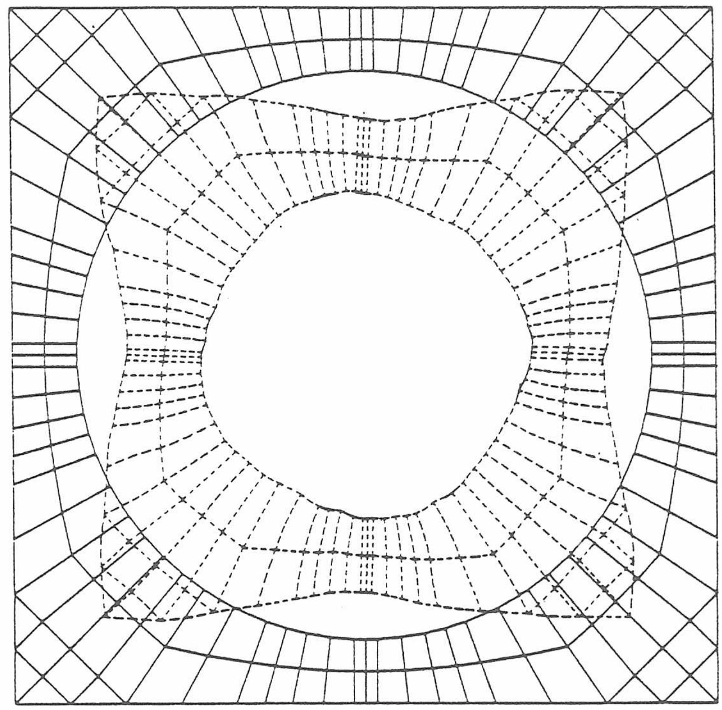

(e) f_n = 4093 Hz.

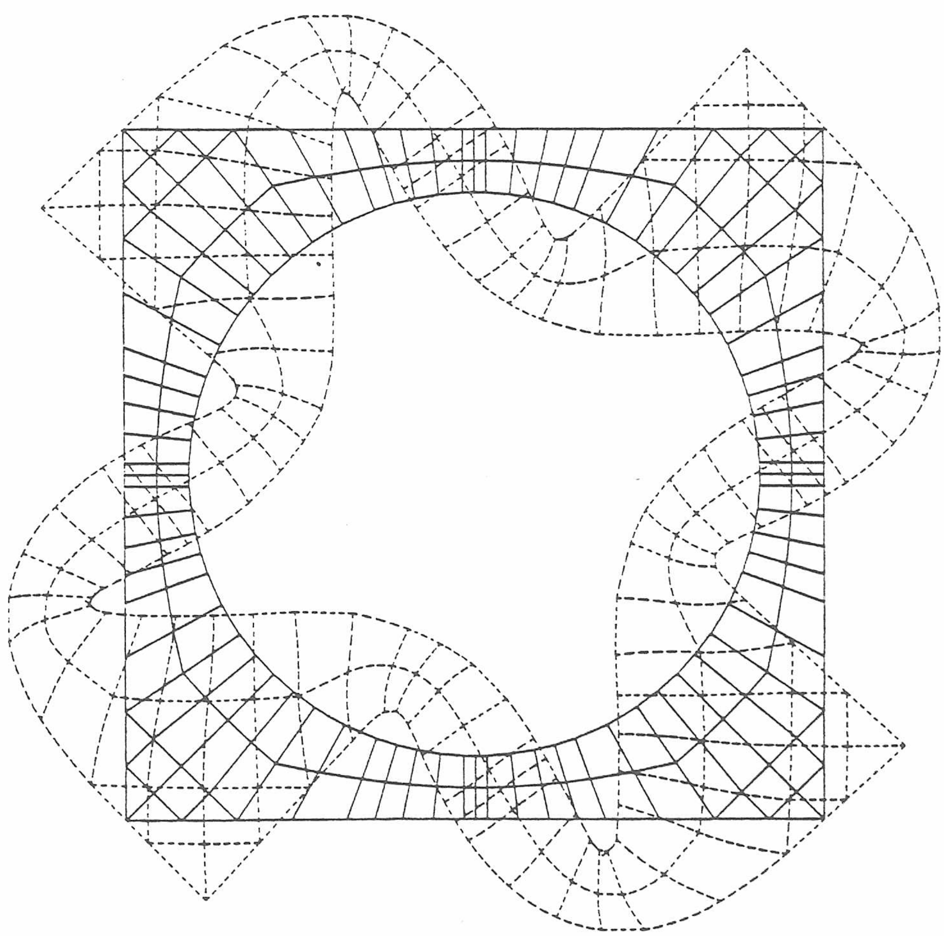

(f) f_n = 4144 Hz.

Figure 5.6

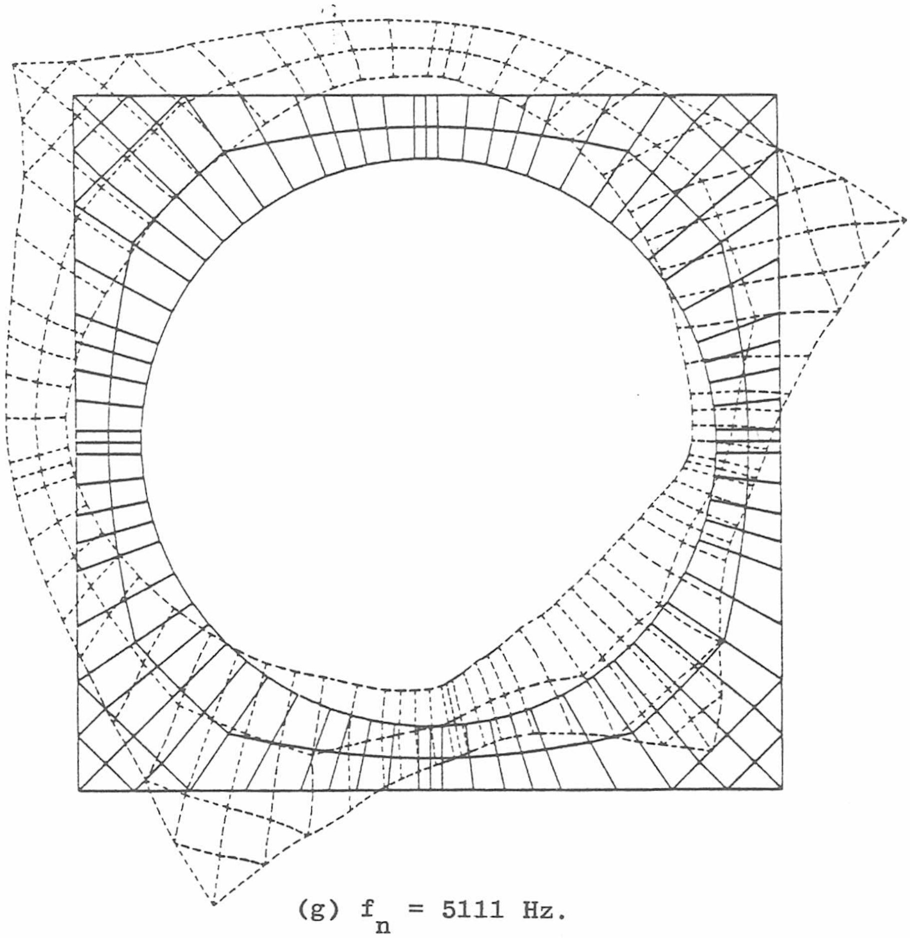

(g) f_n = 5111 Hz.

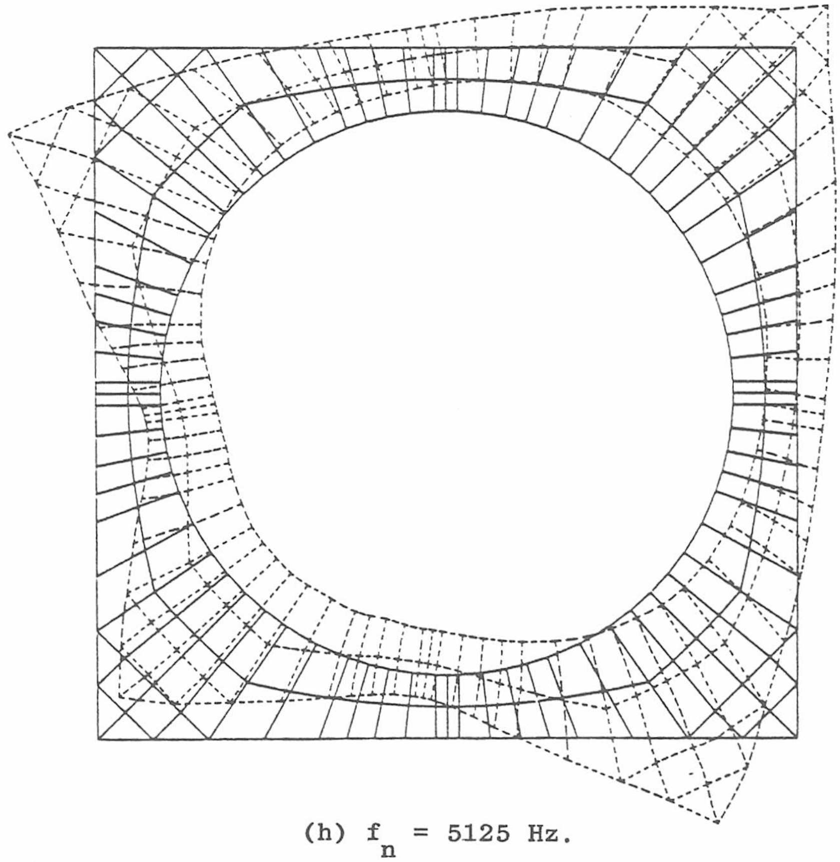

(h) f_n = 5125 Hz.

Figure 5.6

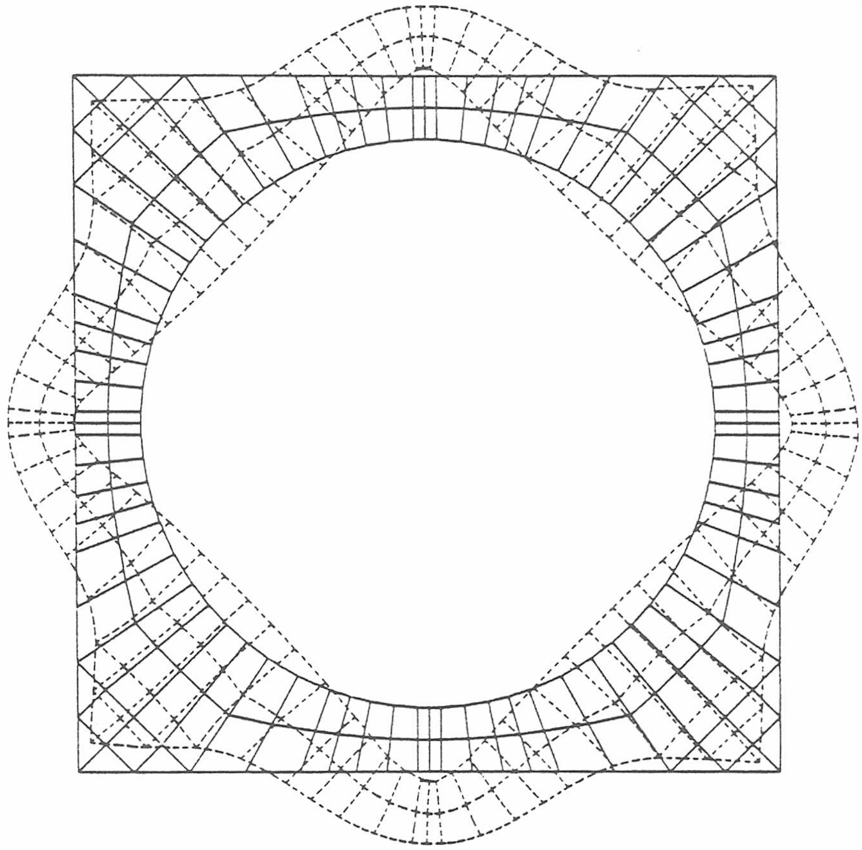

(i) f_n = 5152 Hz.

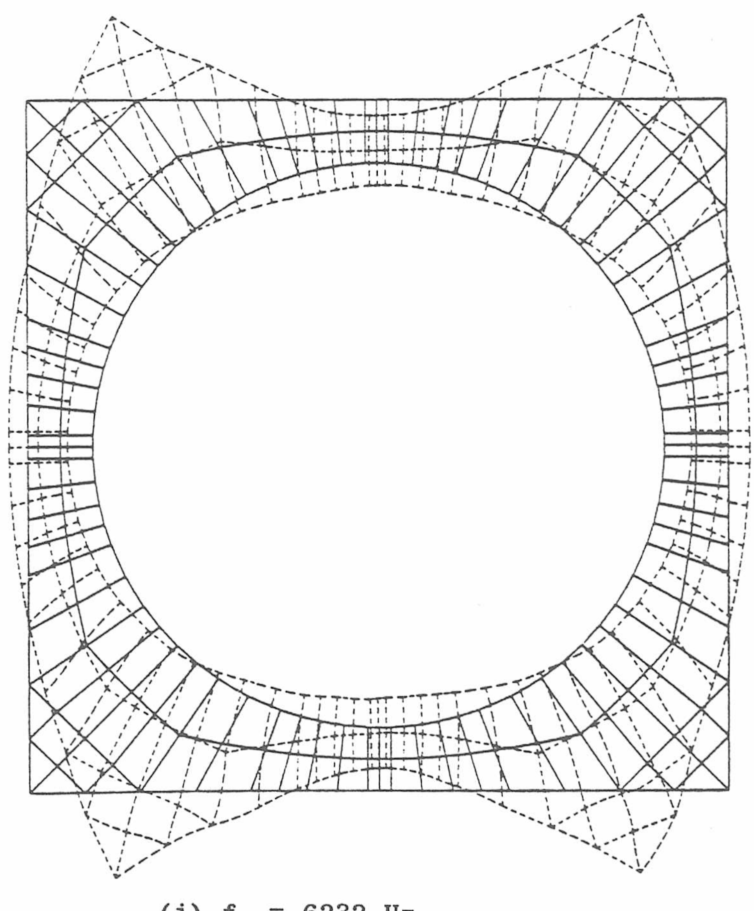

(j) f_n = 6232 Hz.

Figure 5.6

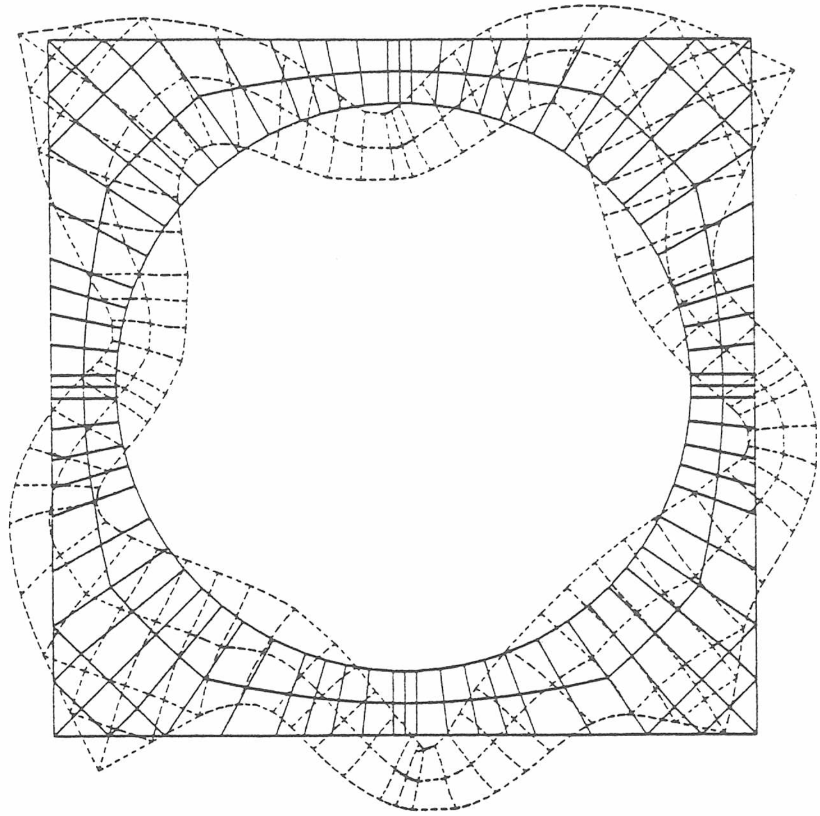

(k) f_n = 7086 Hz.

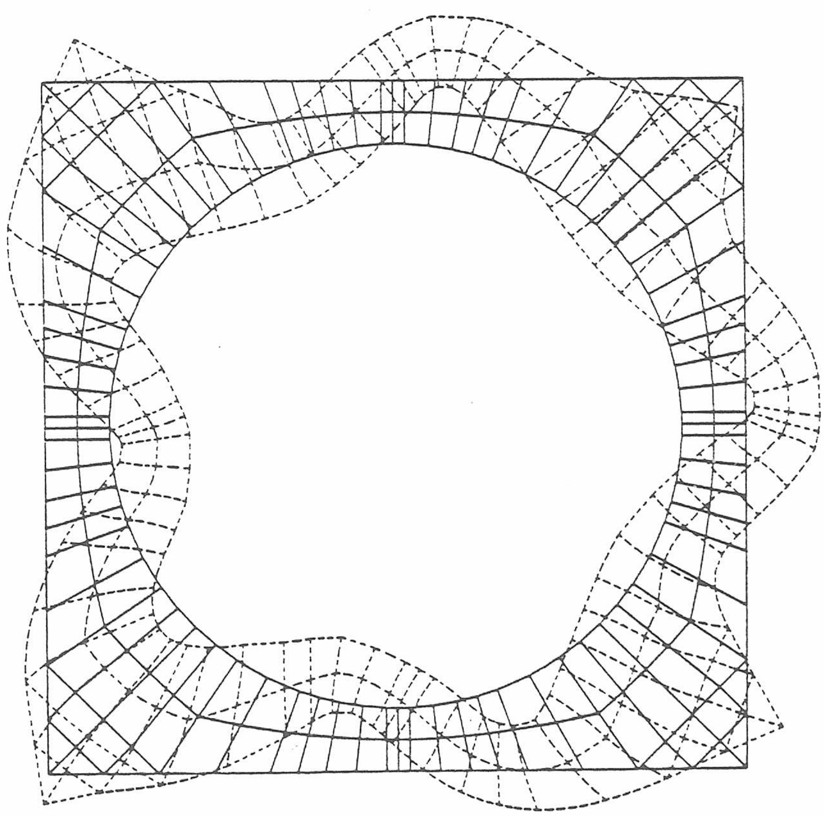

(ℓ) f_n = 7108 Hz.

Figure 5.6

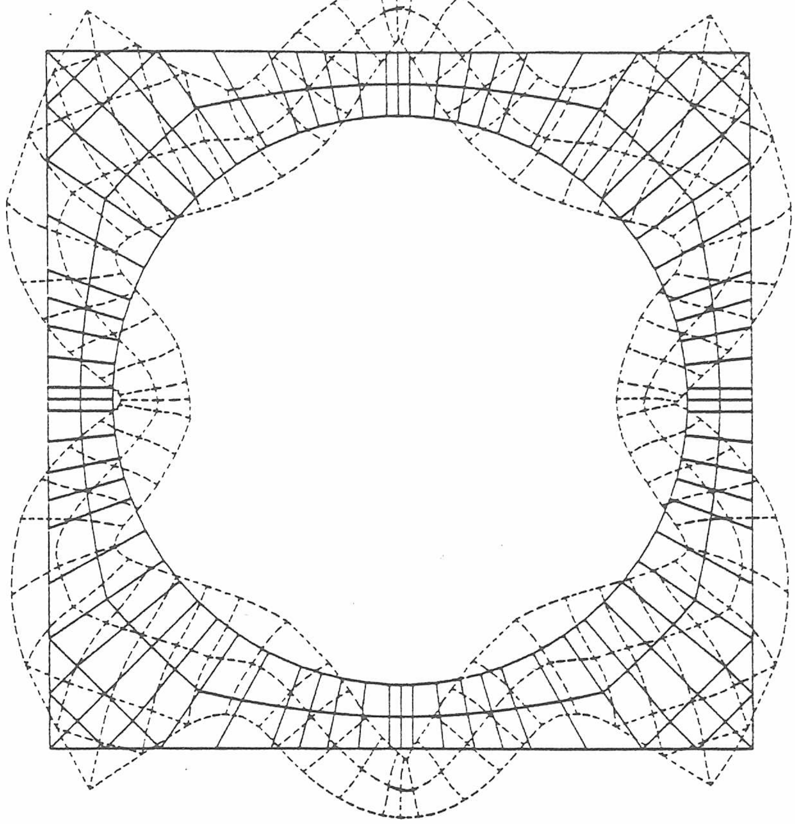

(m) f_n = 9443 Hz.

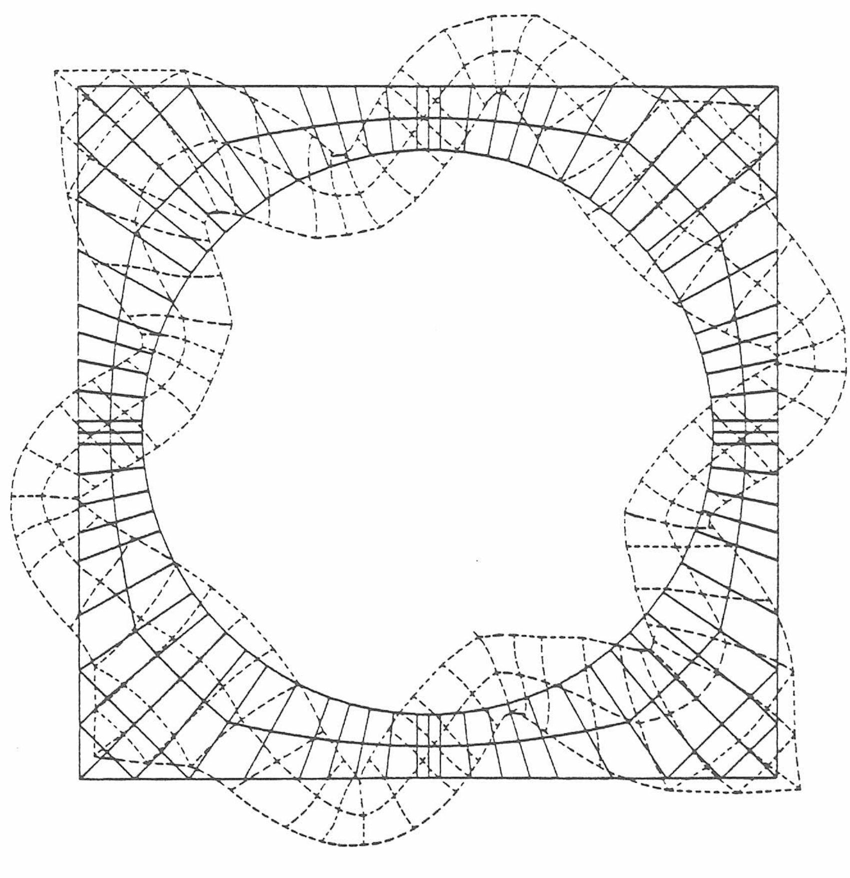

Figure 5.6

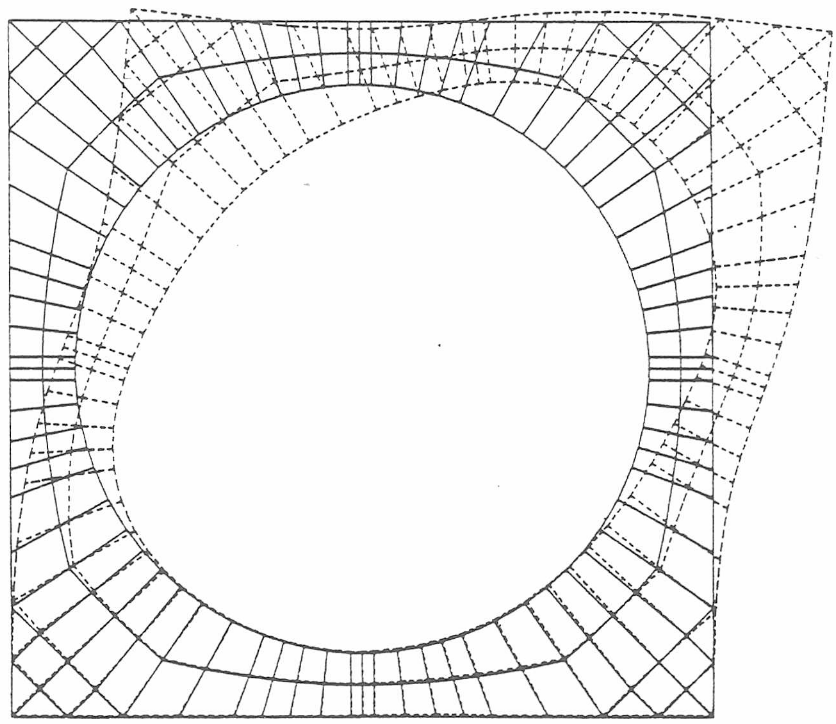

(a) f_n = 517 Hz.

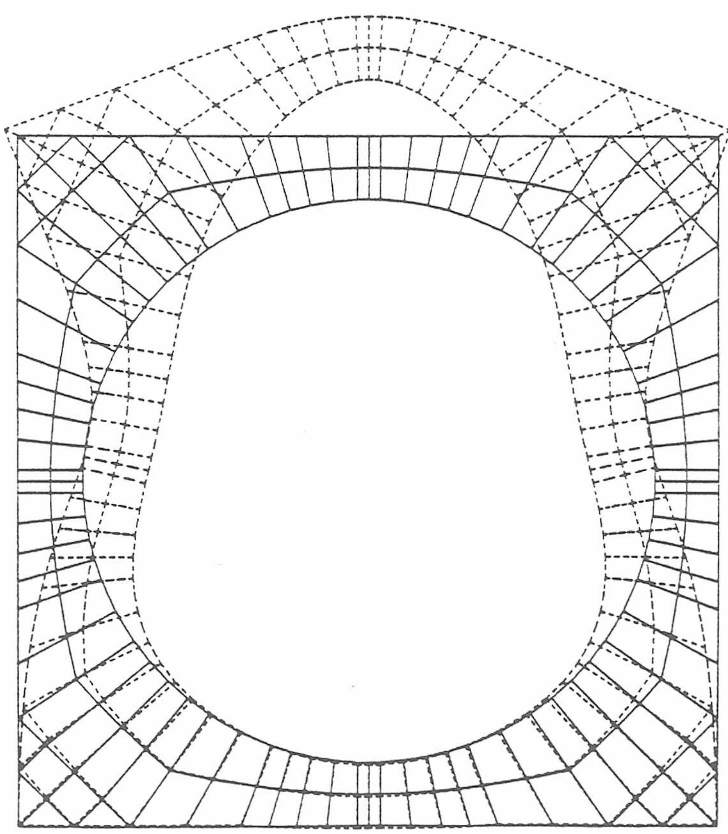

(b) f_n = 1265 Hz.

Figure 5.7

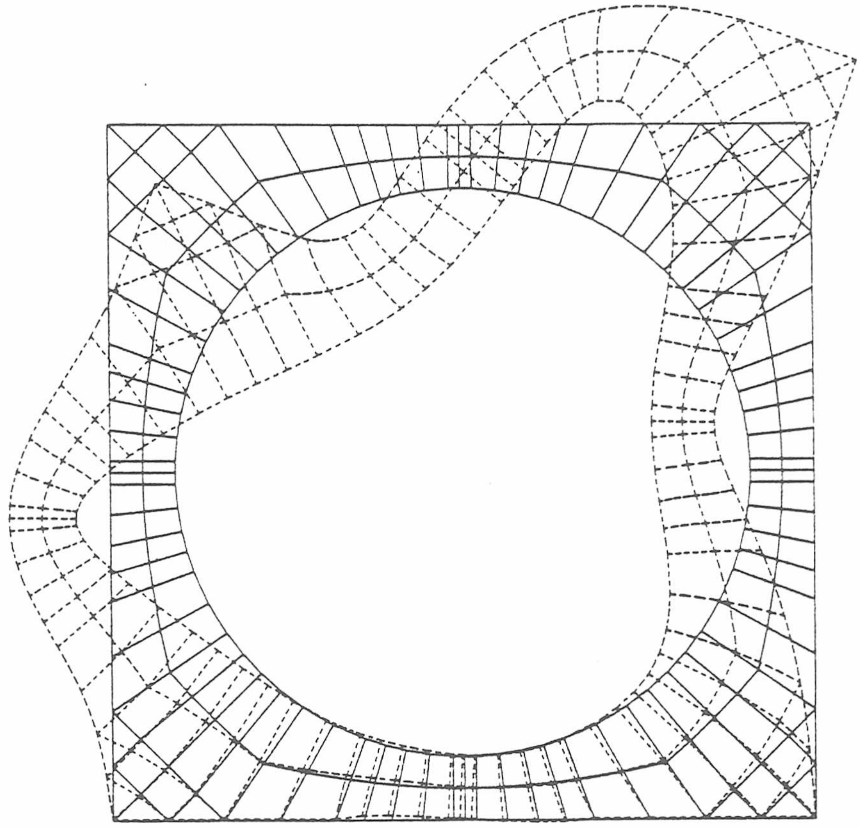

(c) f_n = 2416 Hz.

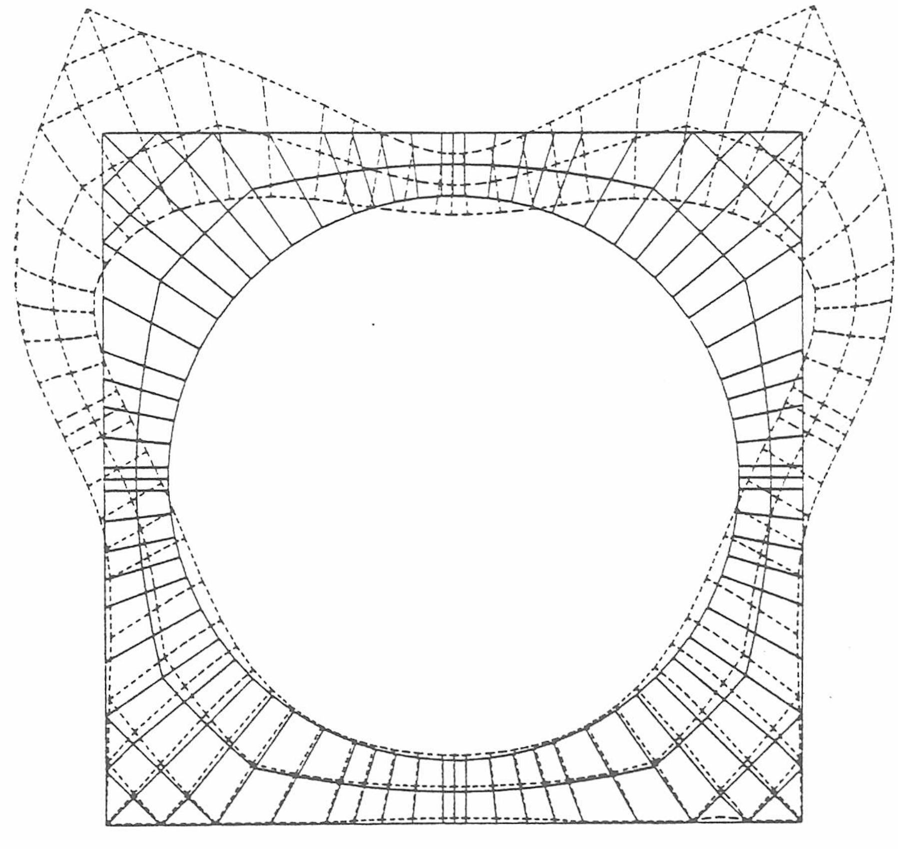

(d) f_n = 3076 Hz.

Figure 5.7

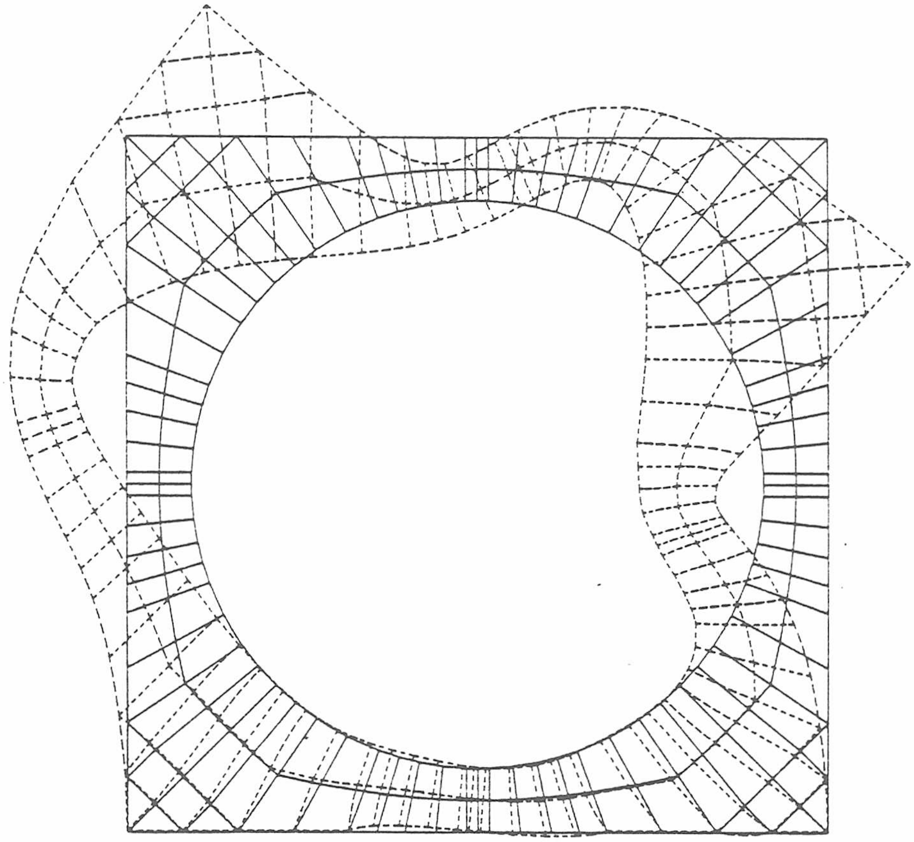

(e) f_n = 3564 Hz.

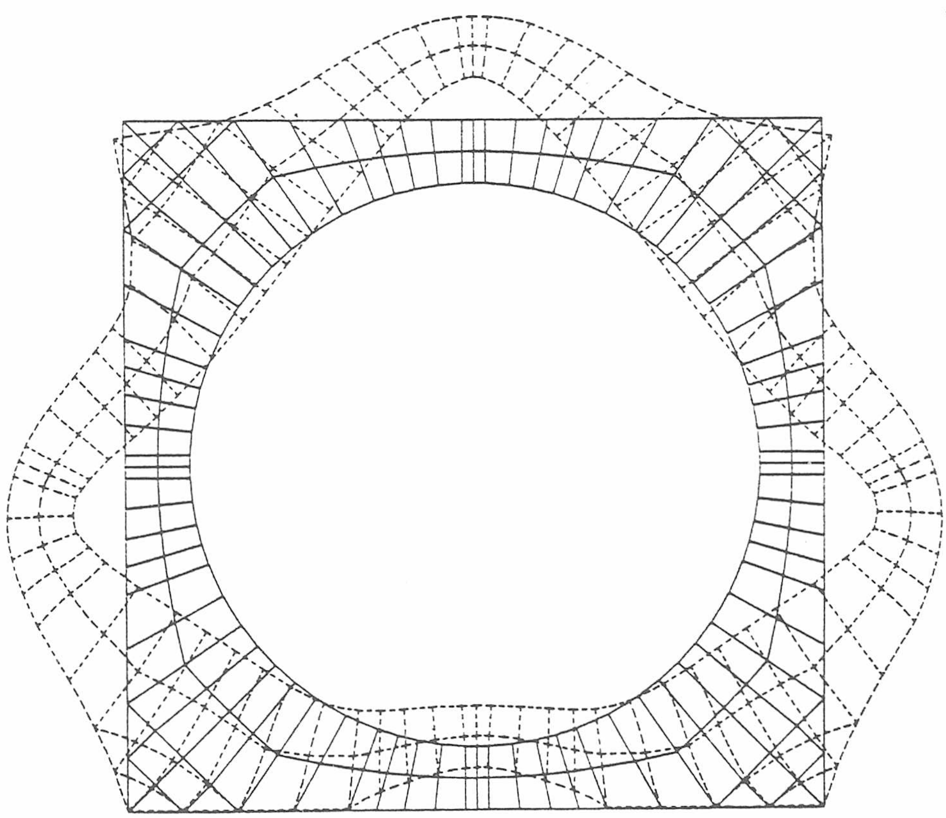

(f) f_n = 4219 Hz.

Figure 5.7

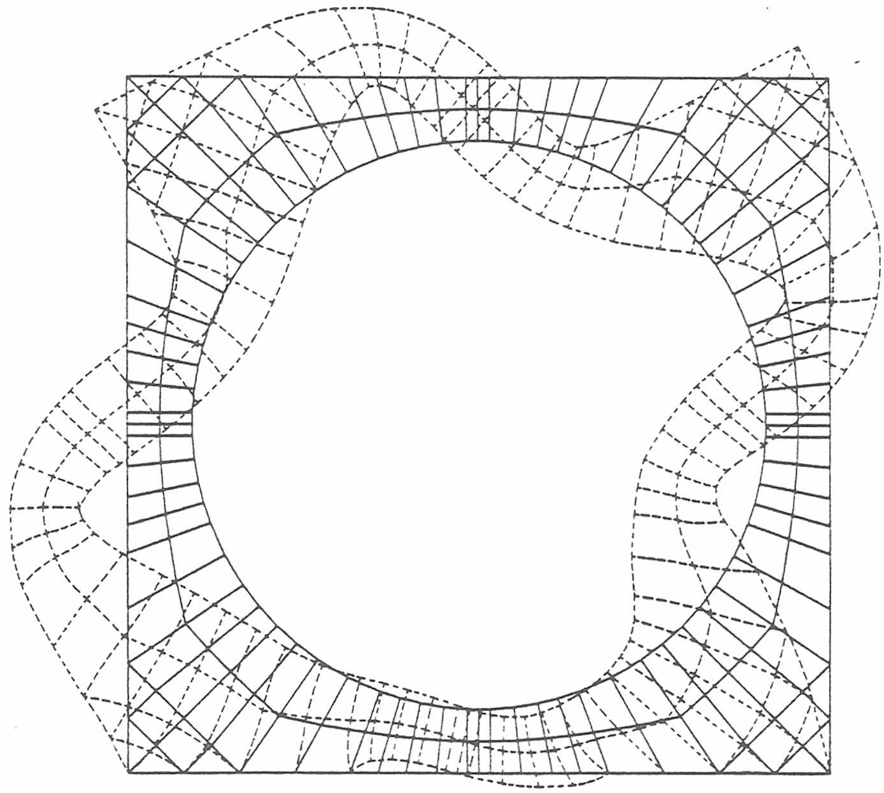

(g) f_n = 4941 Hz.

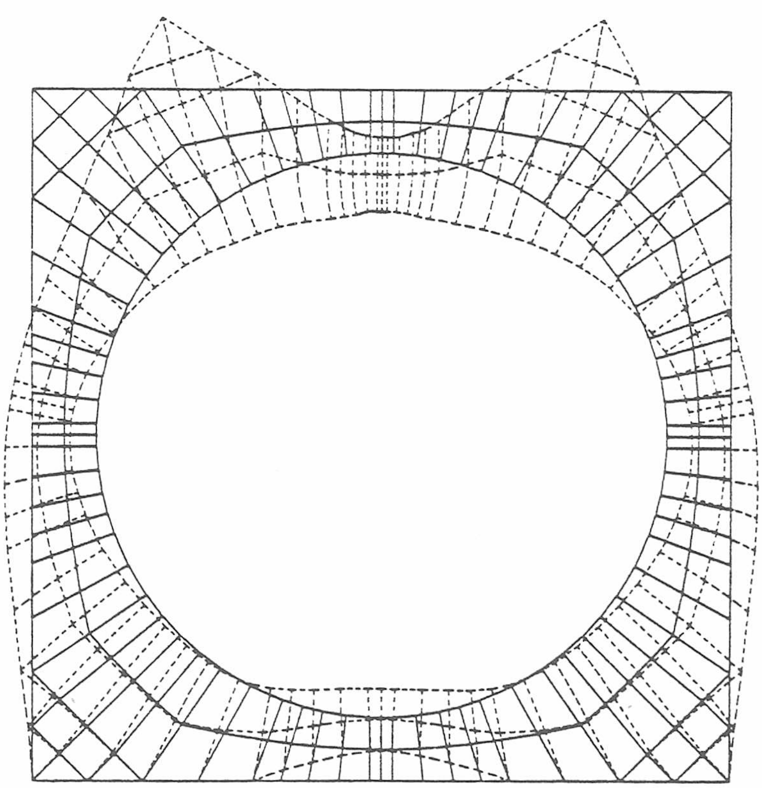

(h) f_n = 5315 Hz.

Figure 5.7

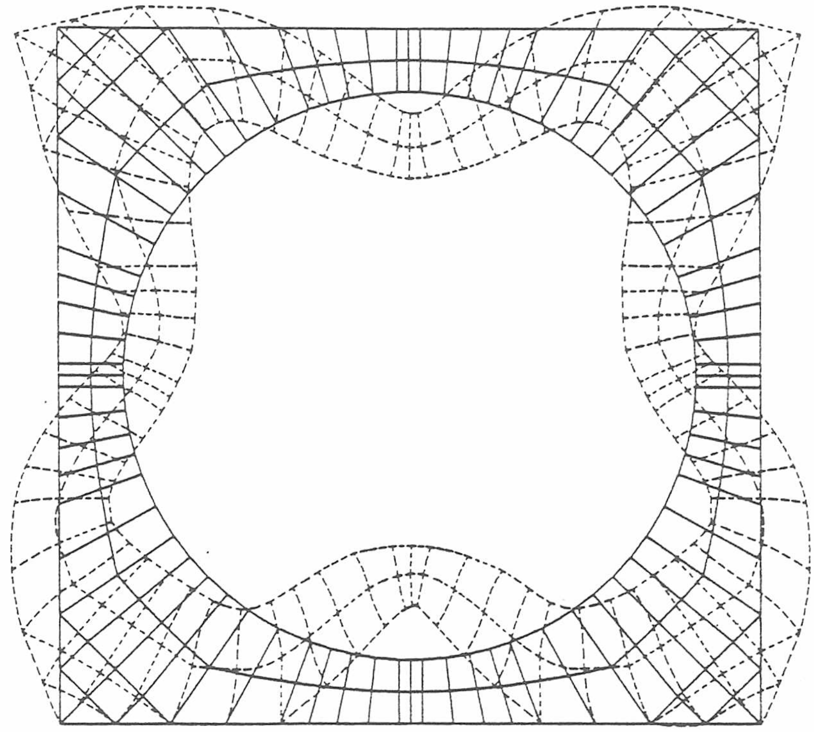

(i) f_n = 6214 Hz.

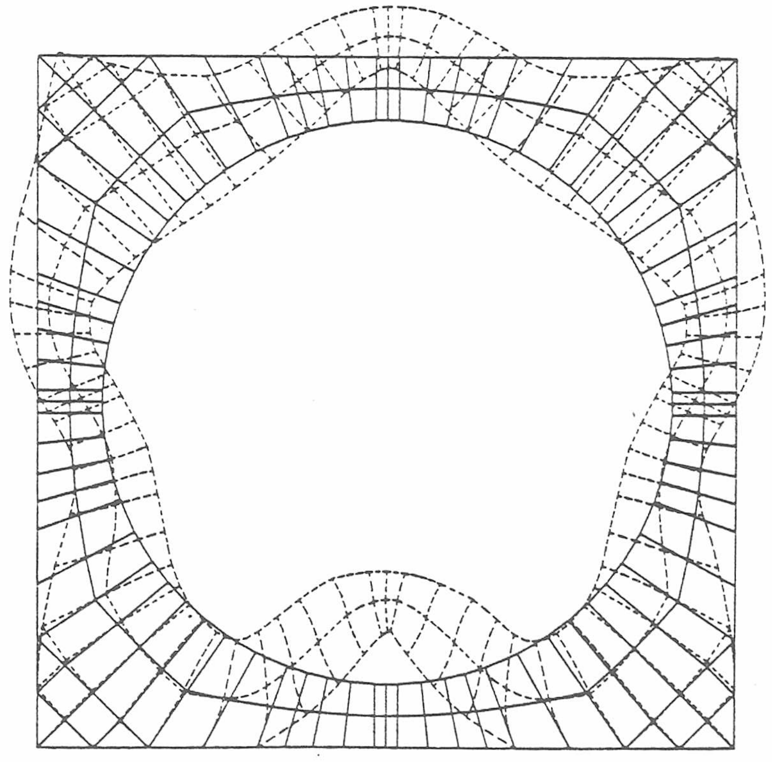

(j) f_n = 7295 Hz.

Figure 5.7

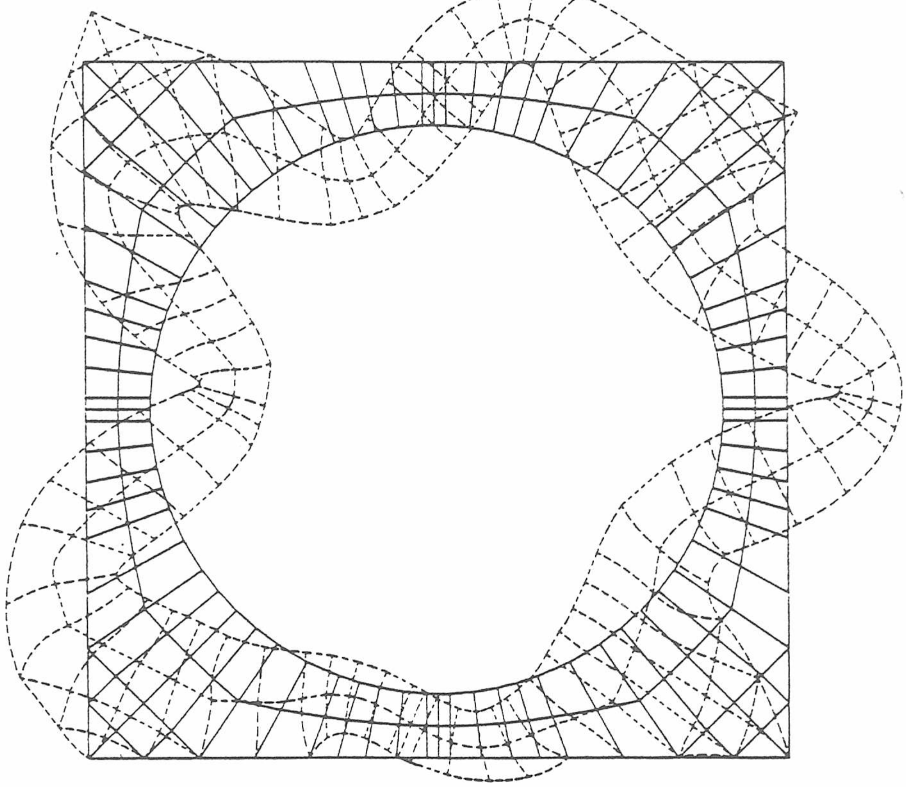

(k) f_n = 7775 Hz.

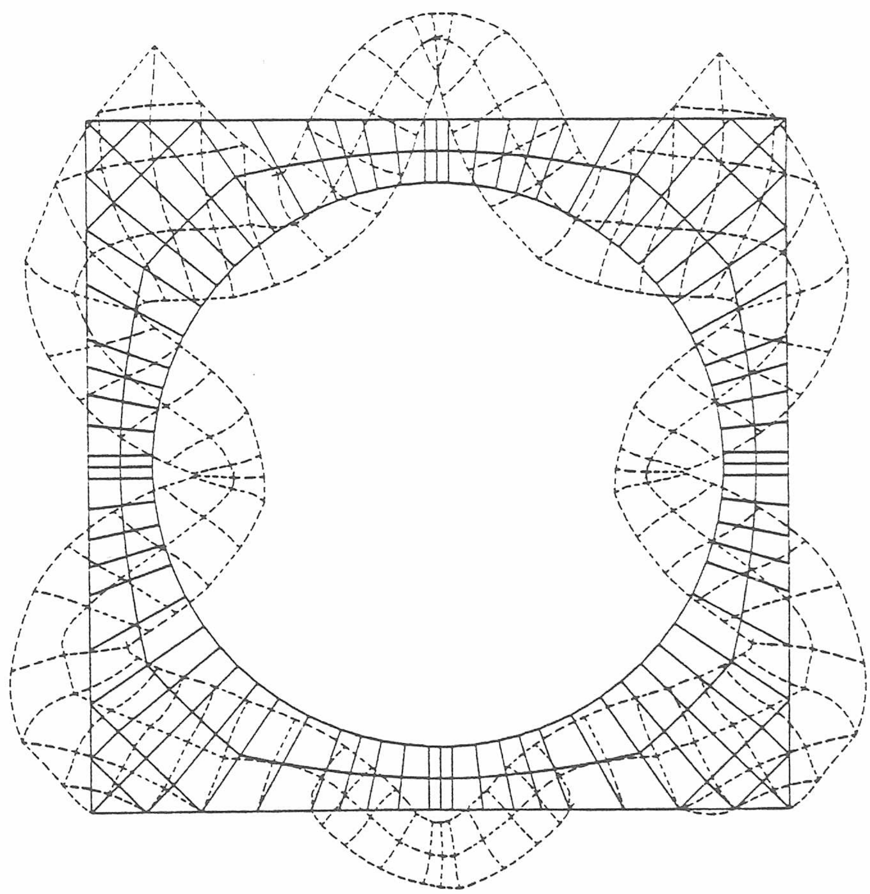

(ℓ) f_n = 9325 Hz.

Figure 5.7

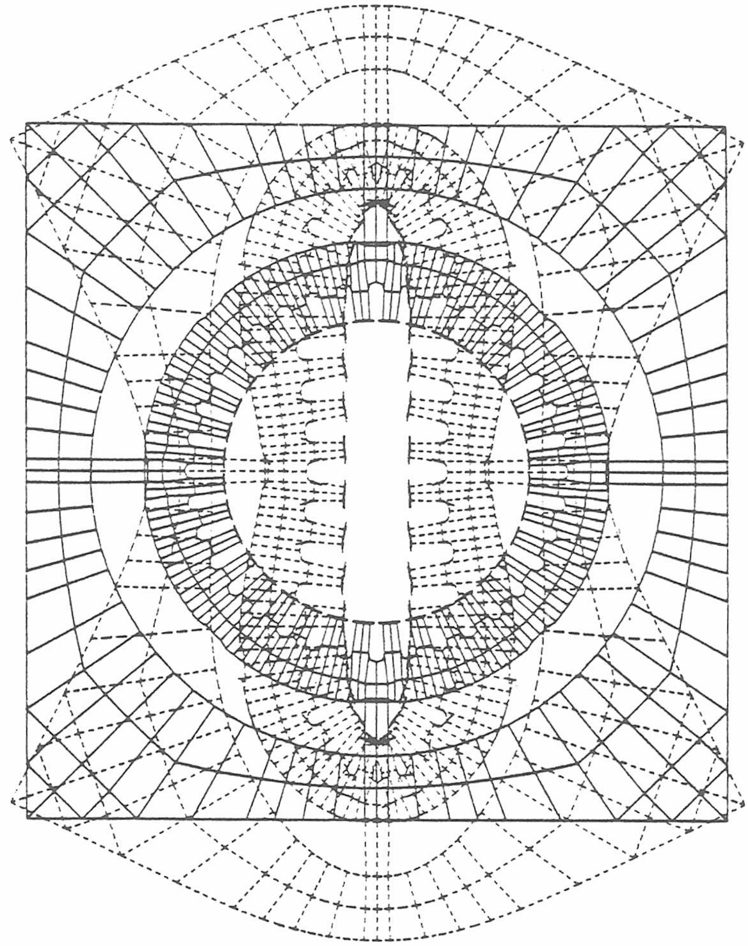

(a) f_n = 889 Hz.

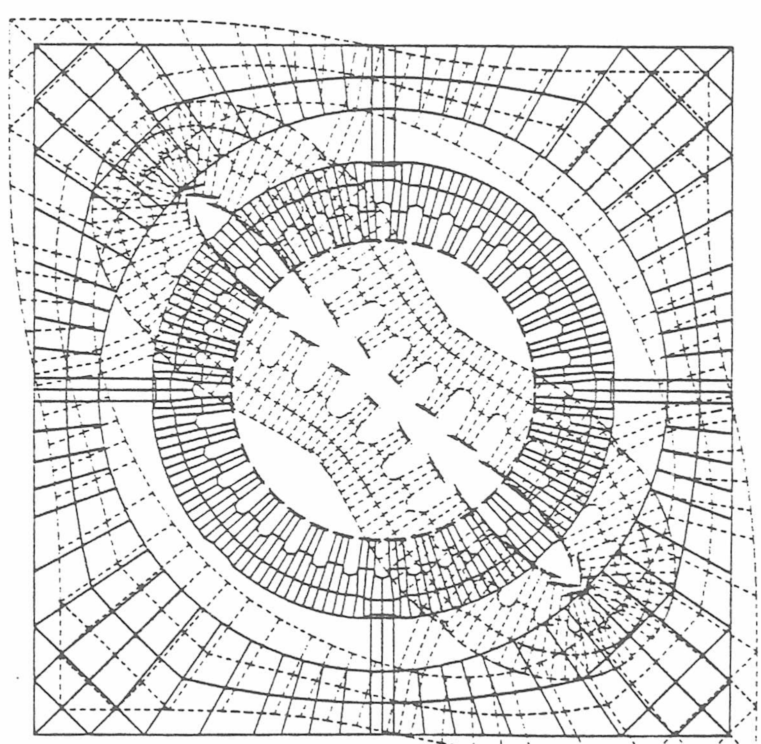

(b) f_n = 1069 Hz.

Figure 5.8

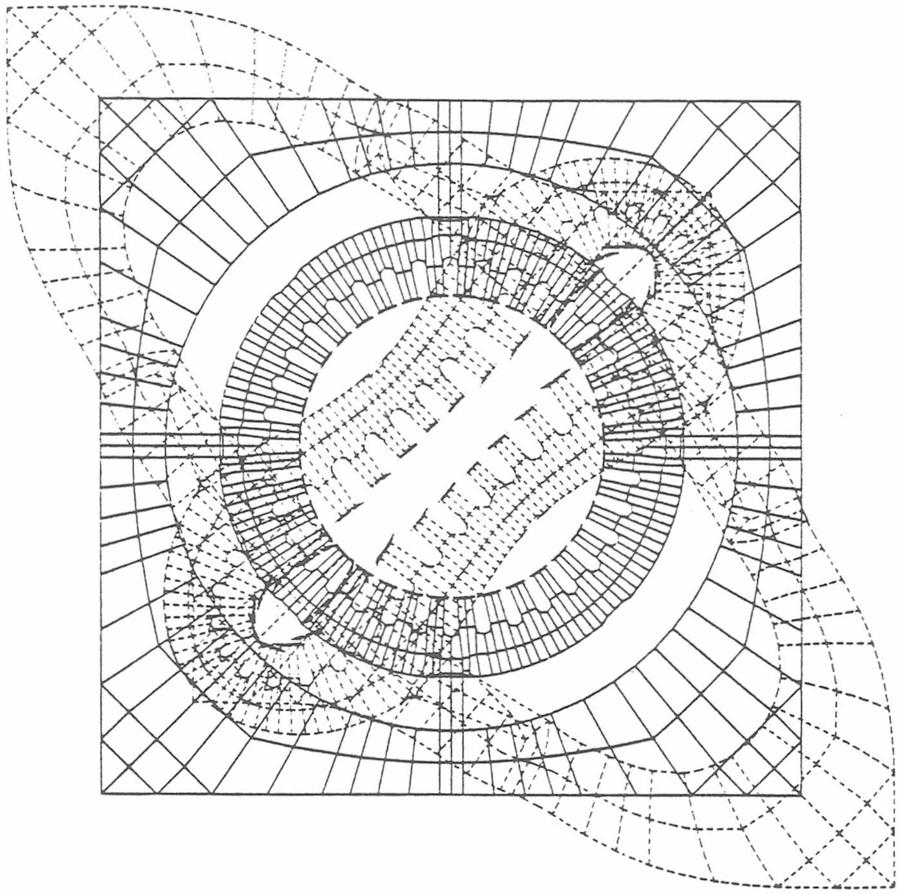

(c) f_n = 1774 Hz.

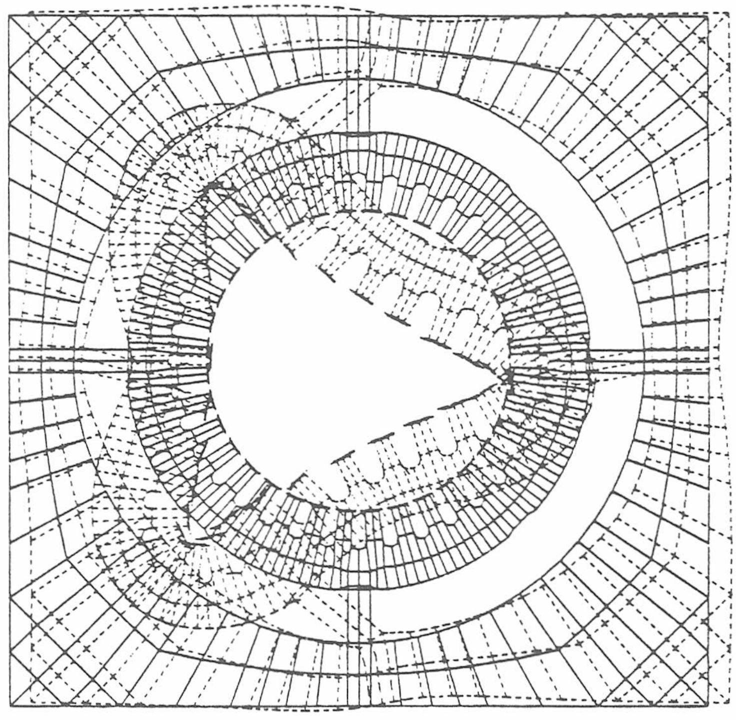

(d) f_n = 2177 Hz.

Figure 5.8

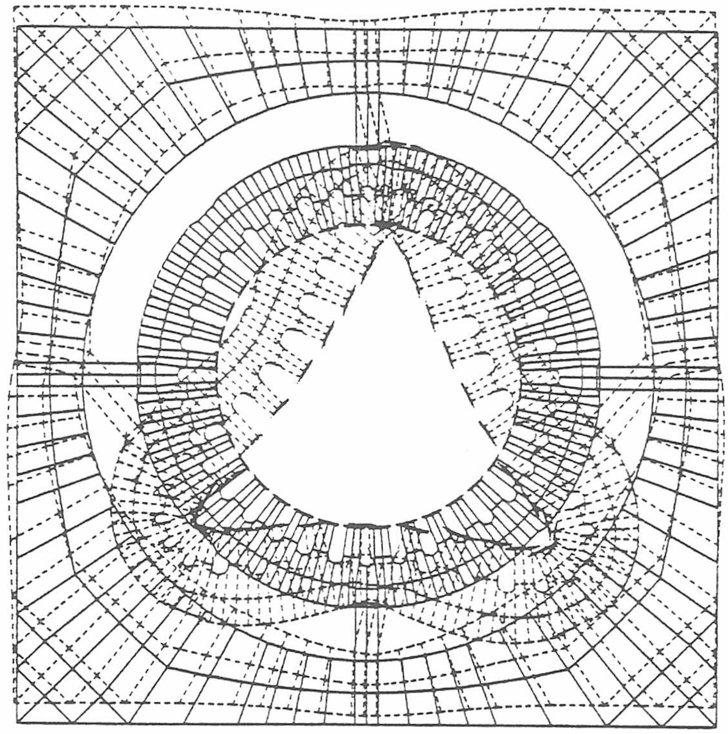

(e) f_n = 2177 Hz.

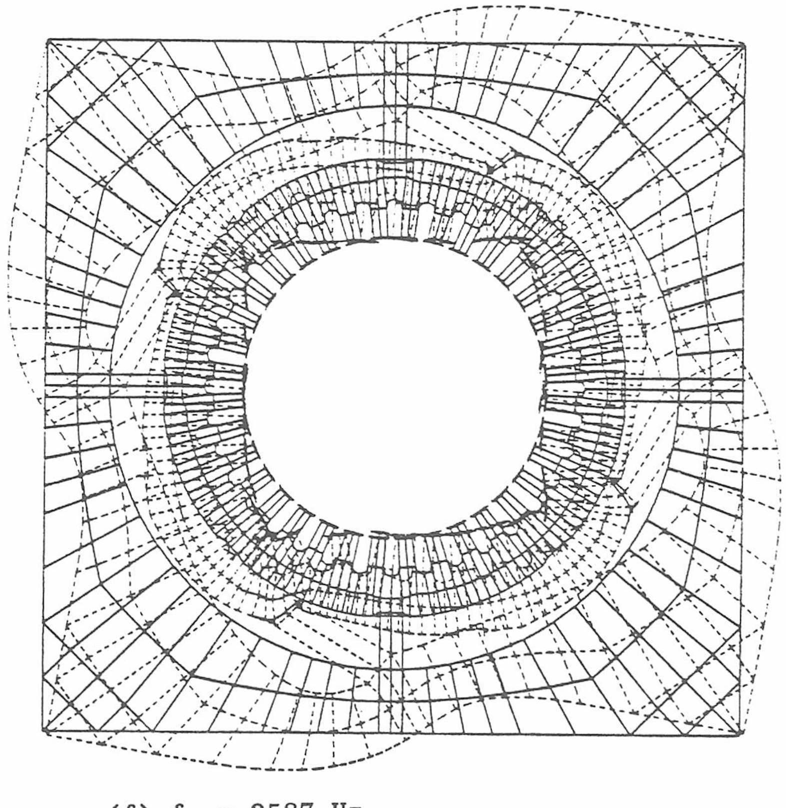

(f) f_n = 2587 Hz.

Figure 5.8

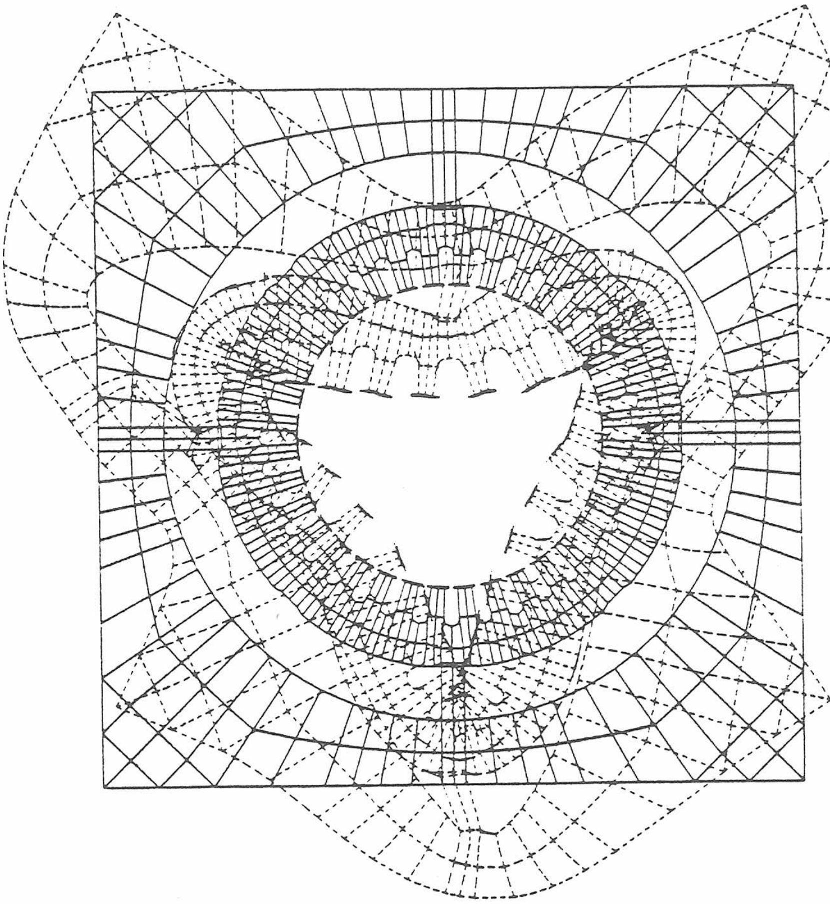

(g) f_n = 2947 Hz.

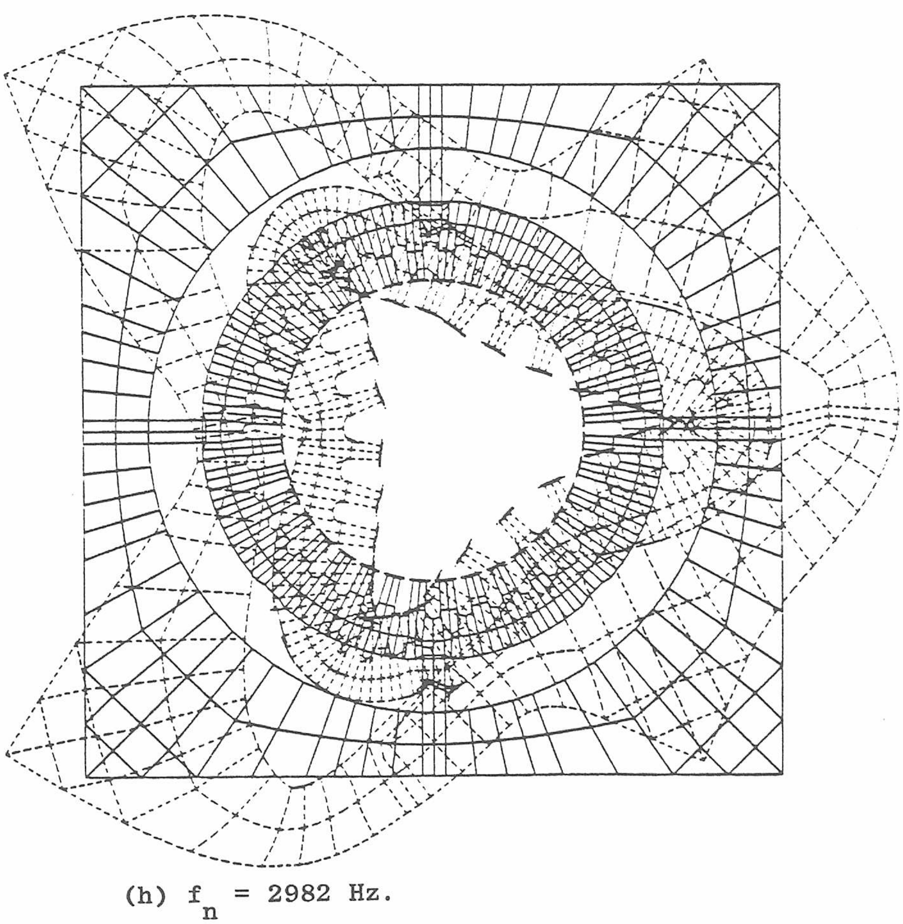

(h) f_n = 2982 Hz.

Figure 5.8

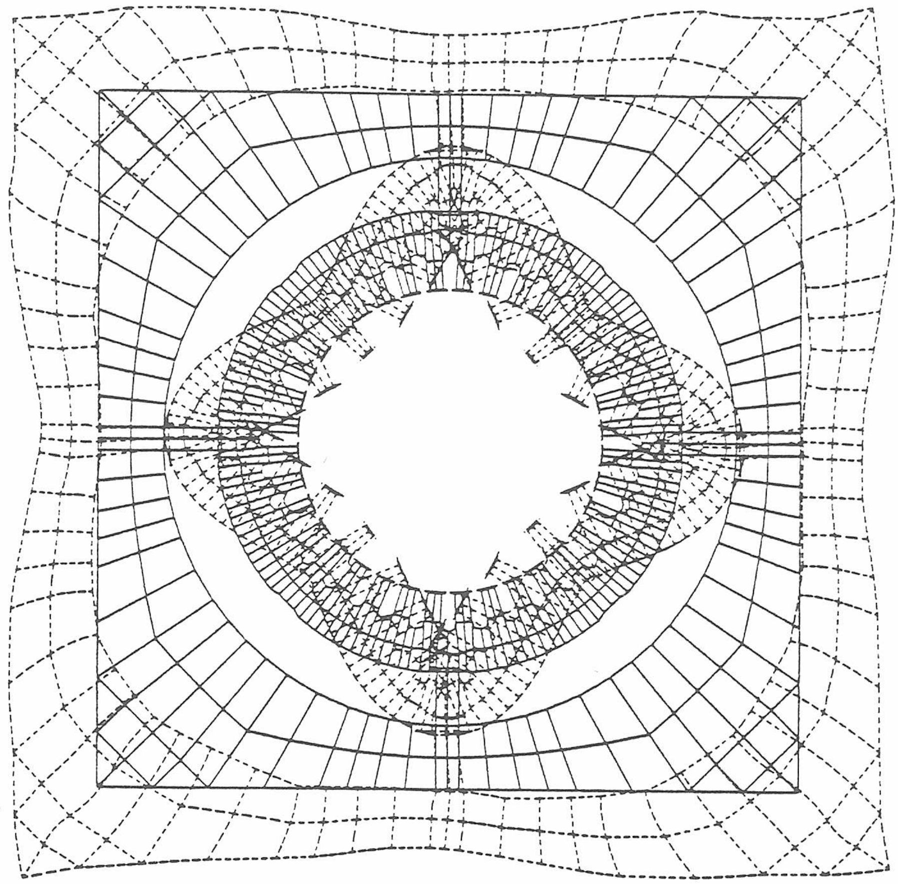

(i) f_n = 4307 Hz.

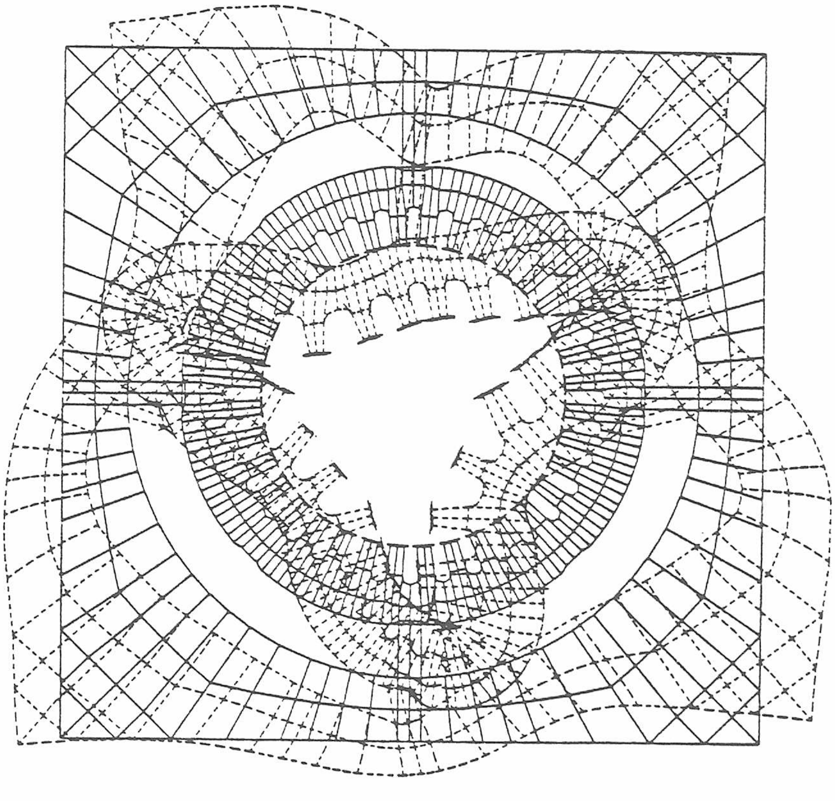

(j) f_n = 4715 Hz.

Figure 5.8

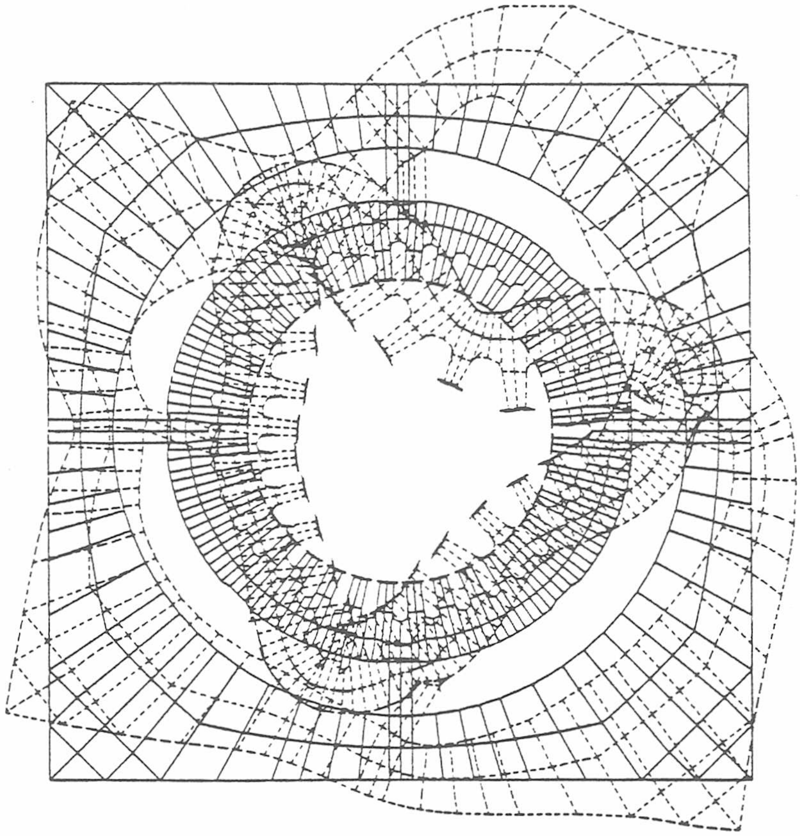

(k) f_n = 4759 Hz.

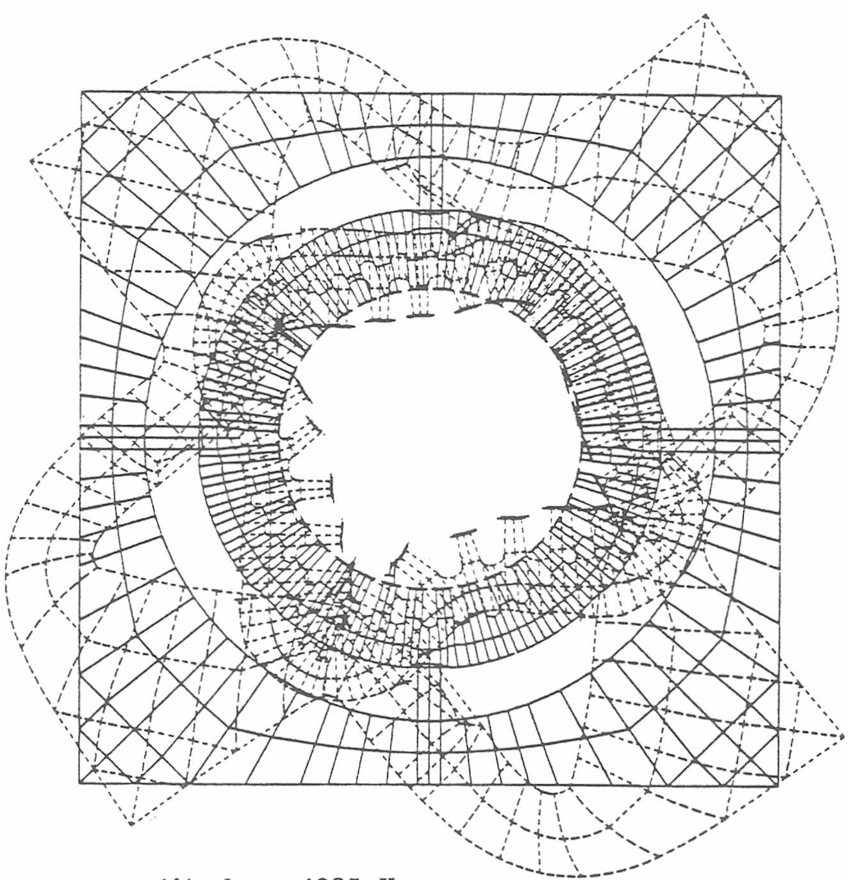

(ℓ) f_n = 4835 Hz.

Figure 5.8

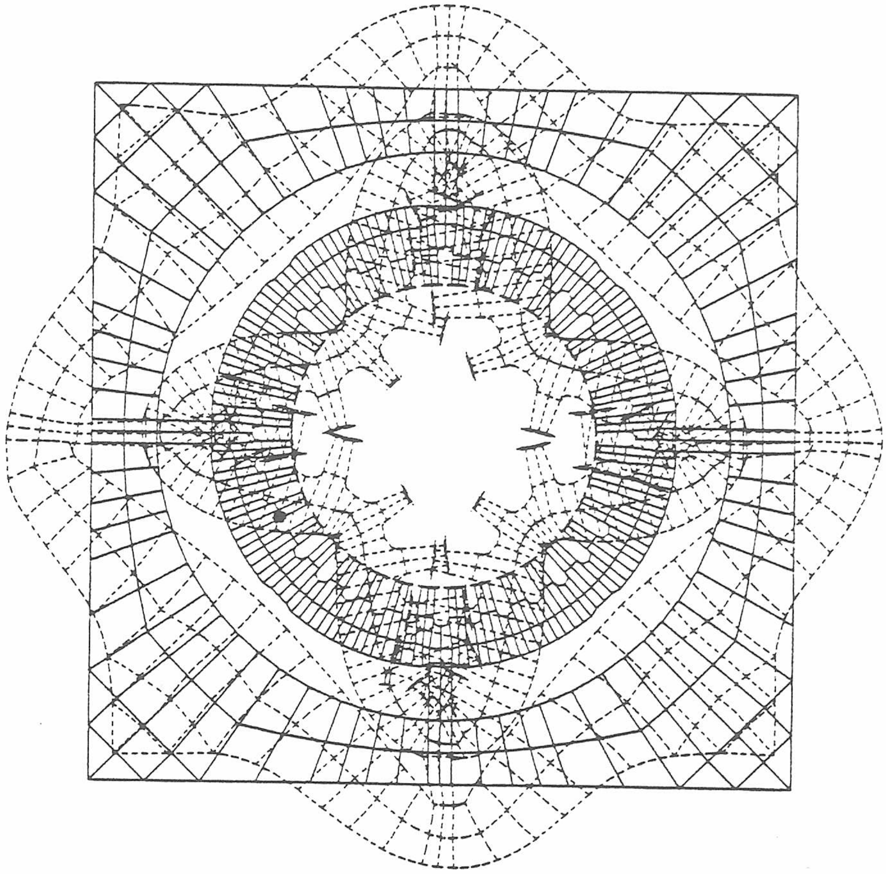

(m) f_n = 5300 Hz.

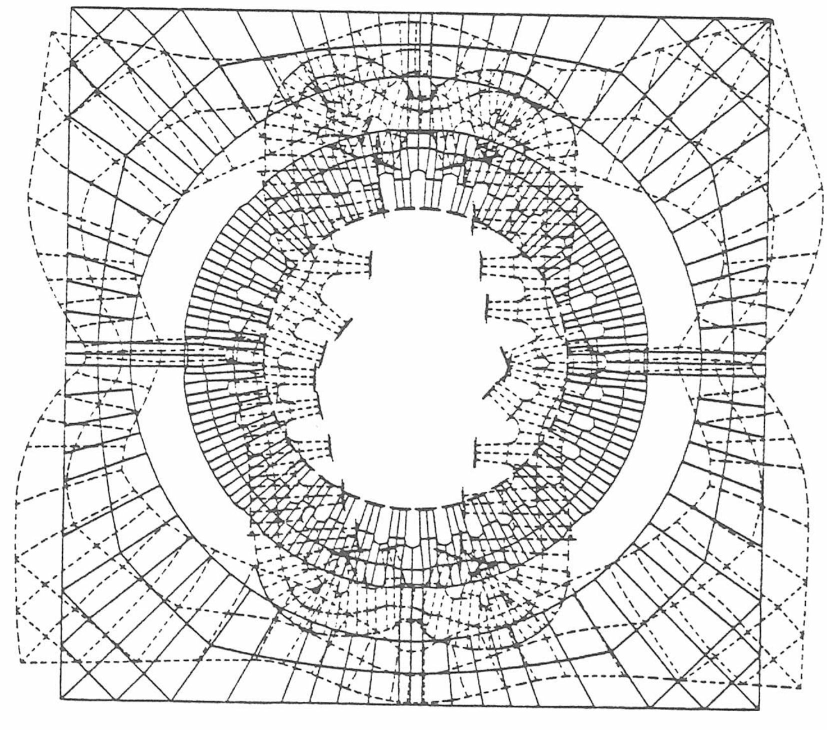

(n) f_n = 5496 Hz.

Figure 5.8

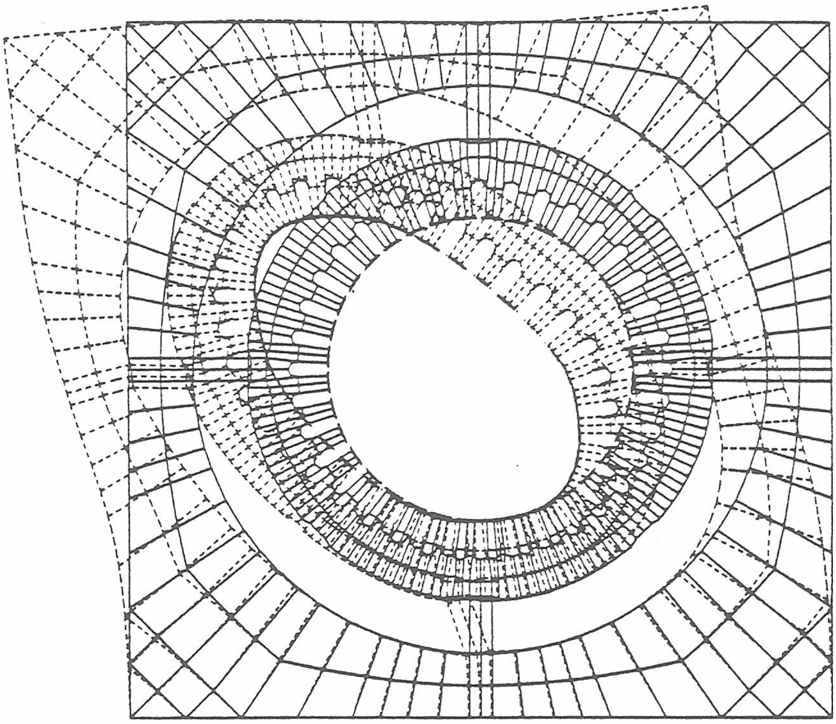

(a) f_n = 619 Hz.

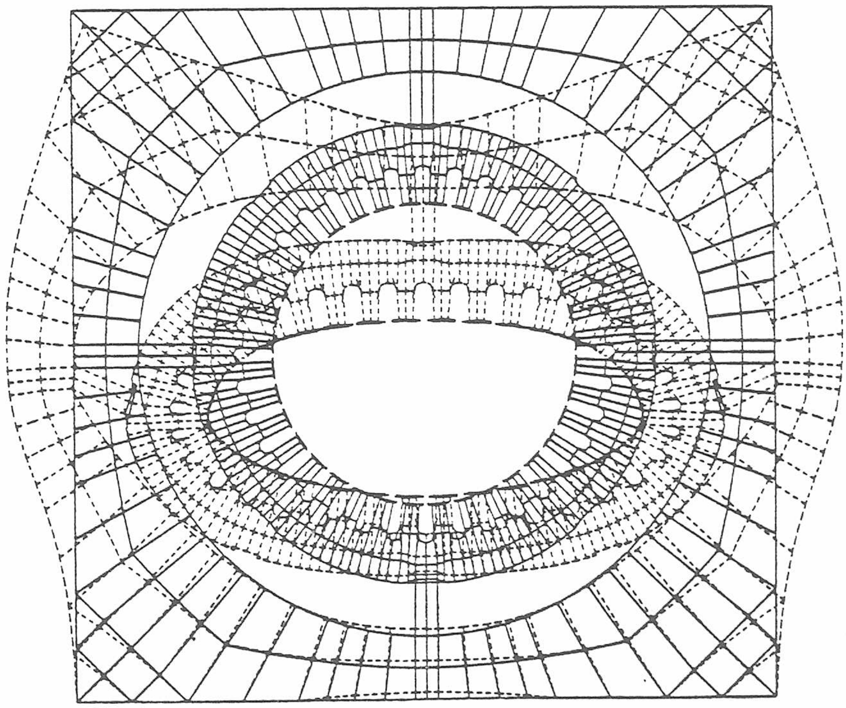

(b) f_n = 1098 Hz.

Figure 5.9

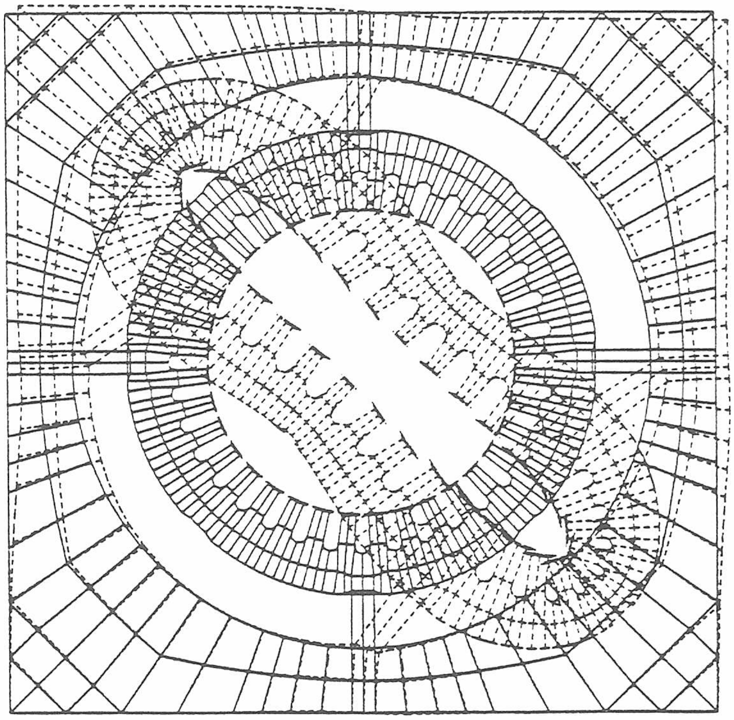

(c) f_n = 1117 Hz.

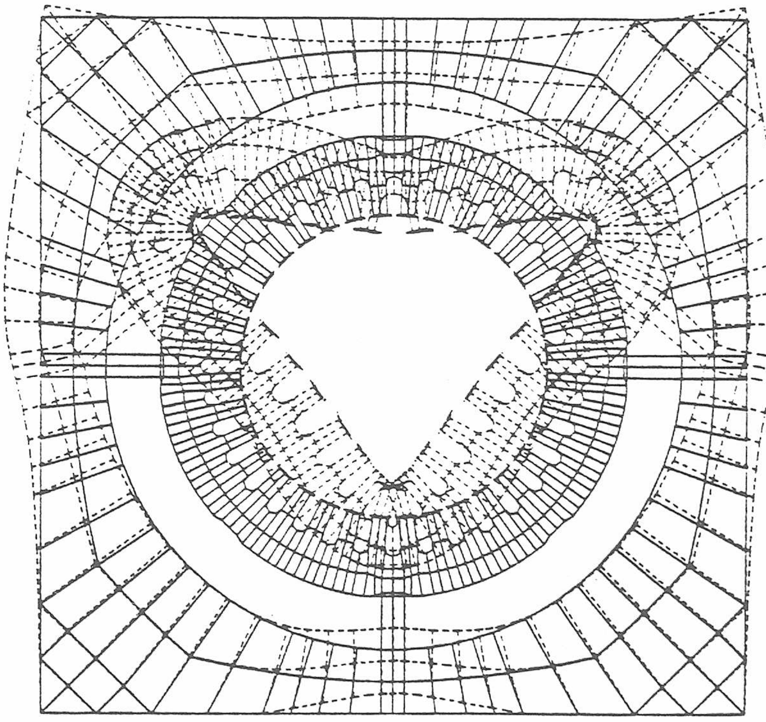

(d) f_n = 1945 Hz.

Figure 5.9

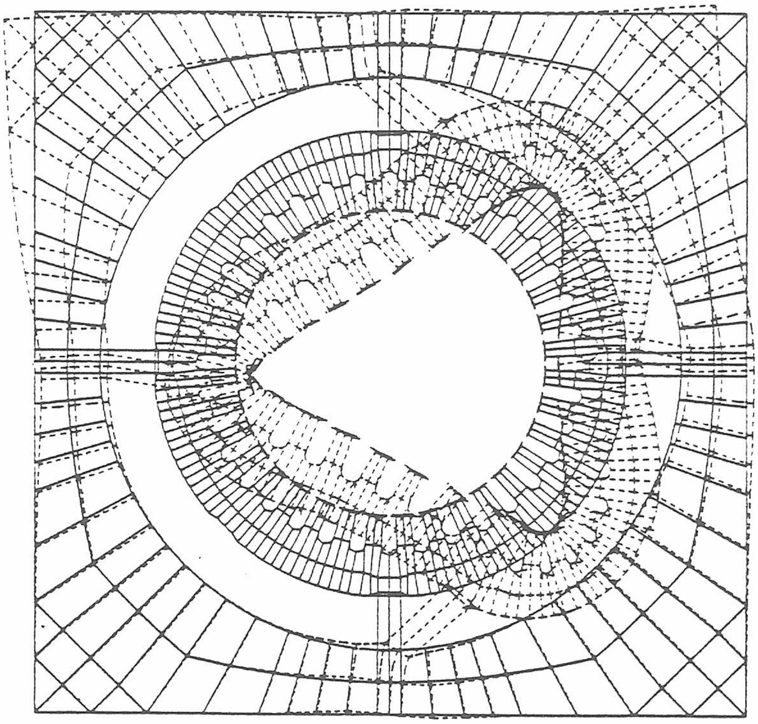

(e) f_n = 2081 Hz.

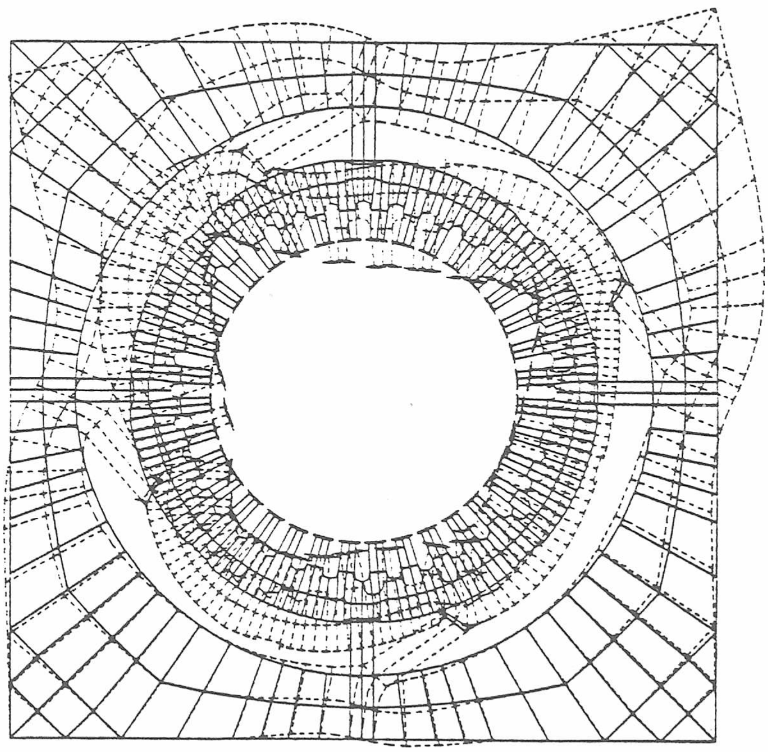

(f) f_n = 2523 Hz.

Figure 5.9

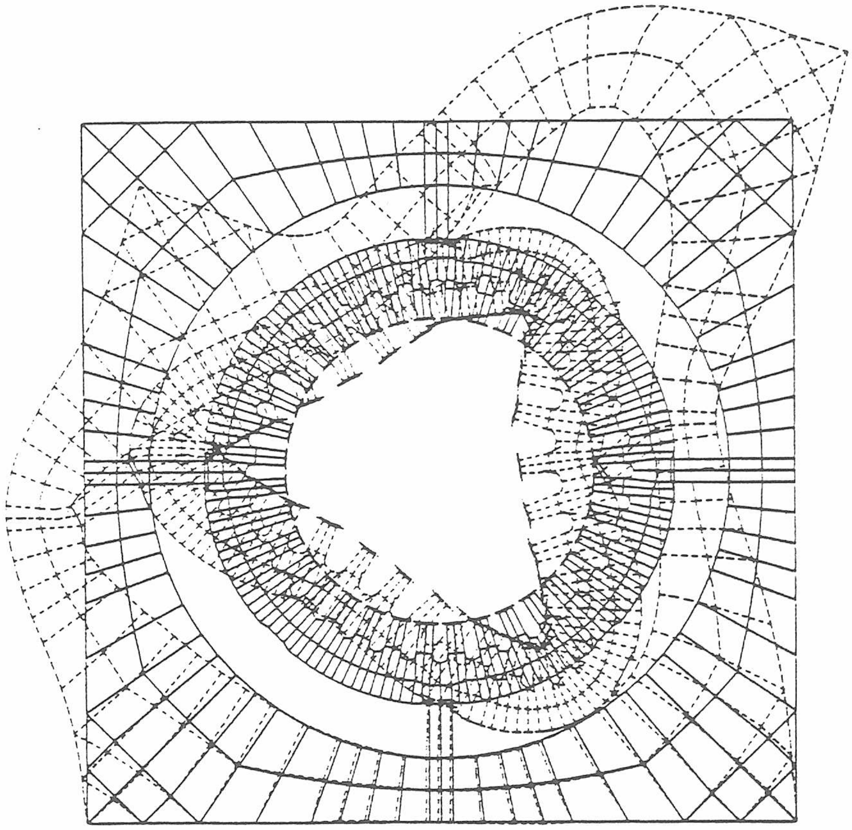

(g) f_n = 2766 Hz.

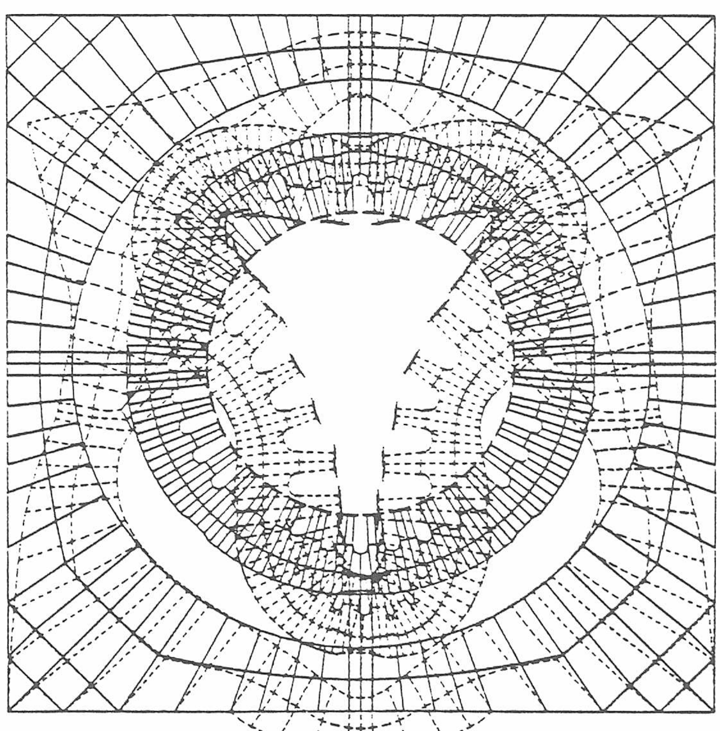

(h) f_n = 3236 Hz.

Figure 5.9

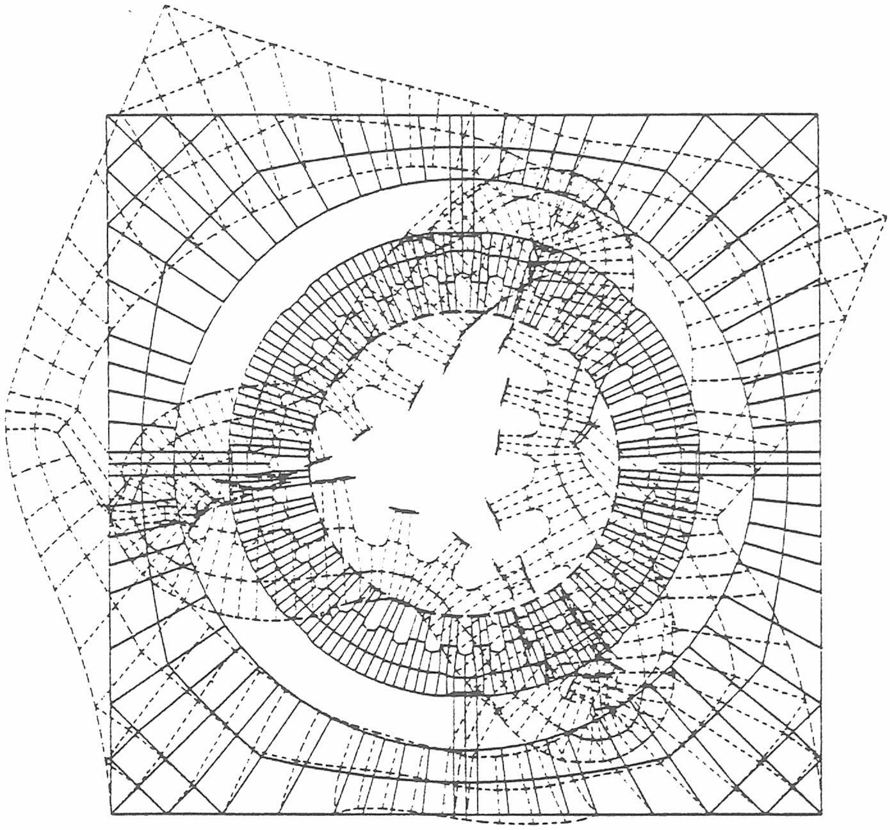

(i) f_n = 3621 Hz.

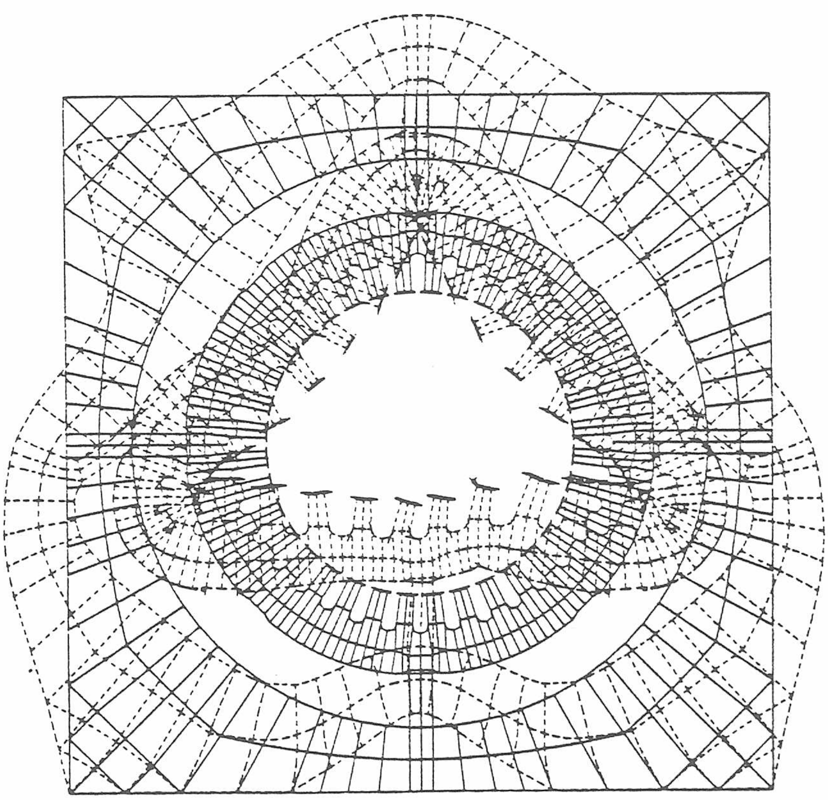

(j) f_n = 3918 Hz.

Figure 5.9

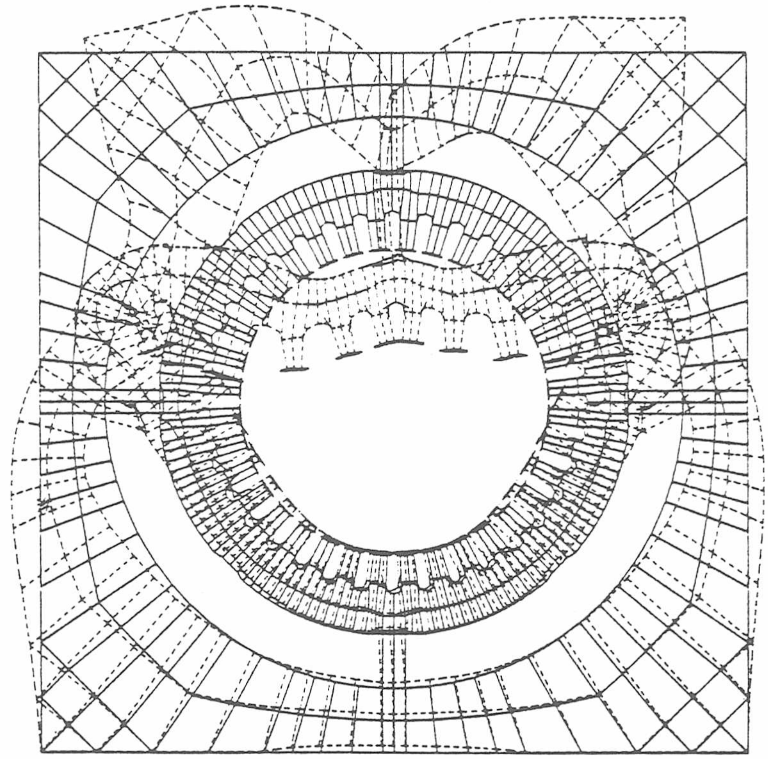

(k) f_n = 4951 Hz.

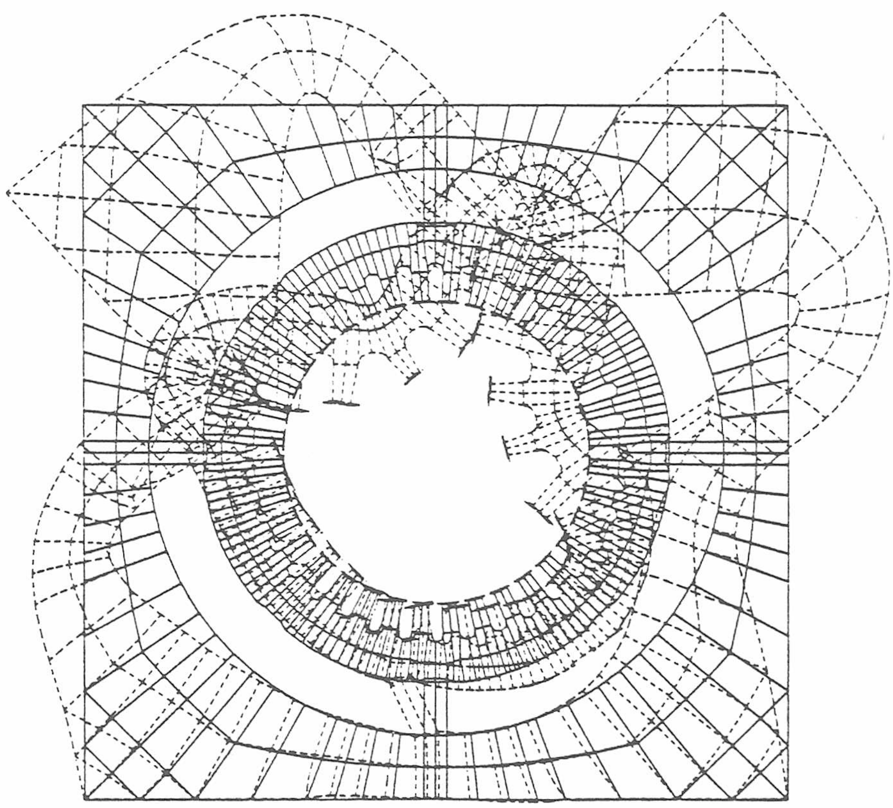

(ℓ) f_n = 5005 Hz.

Figure 5.9

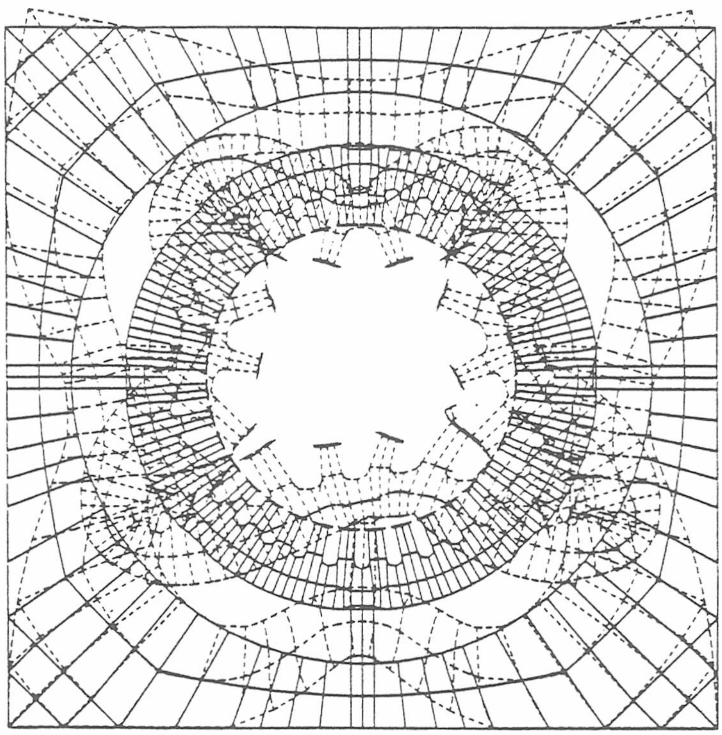

(m) f_n = 5272 Hz.

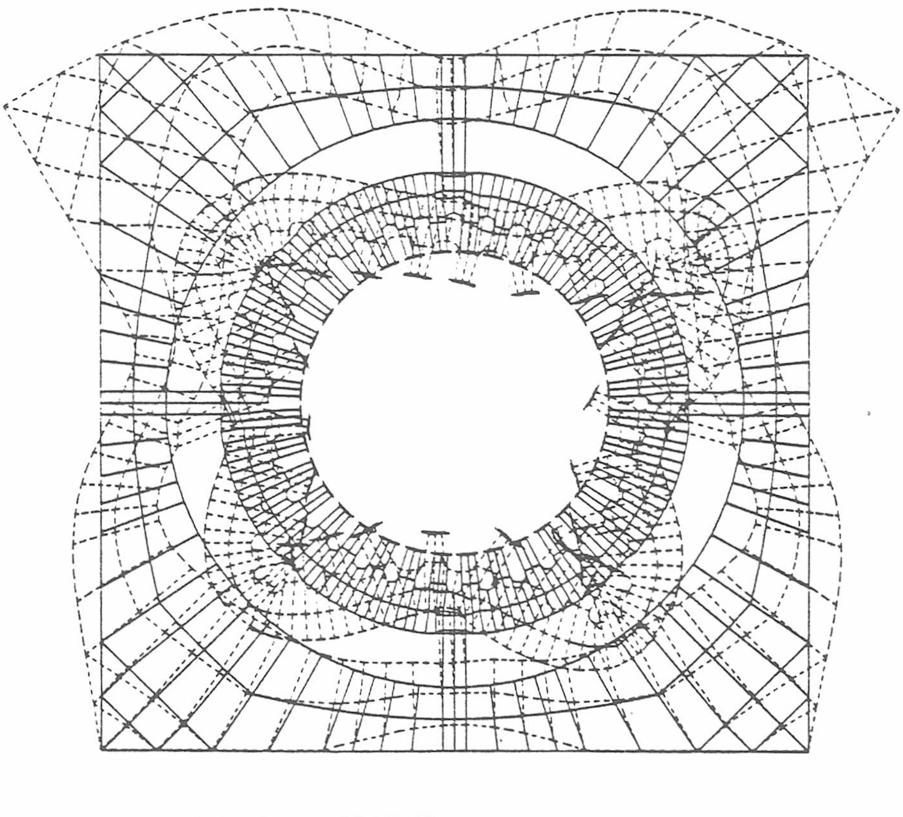

(n) f_n = 5943 Hz.

Figure 5.9

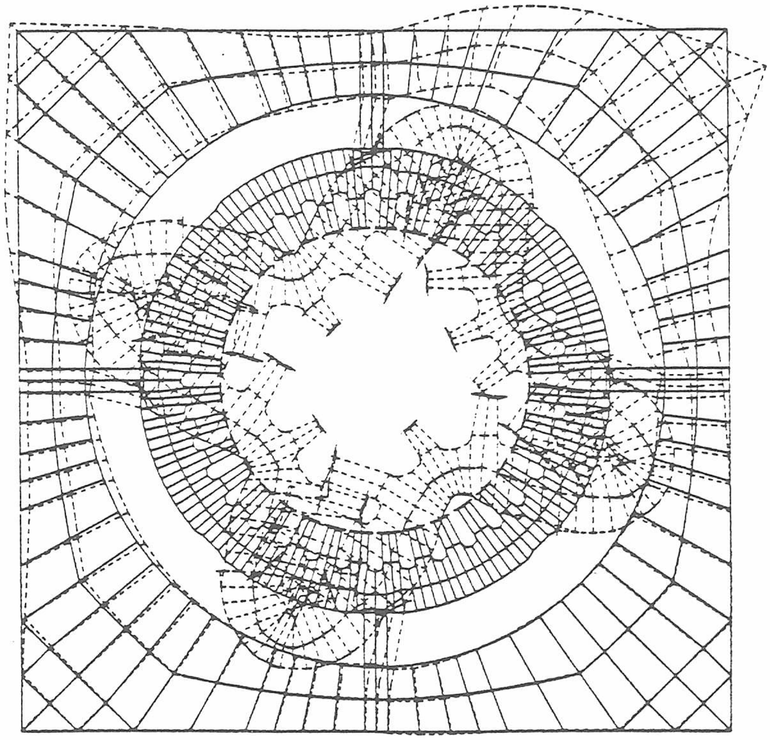

(o) f_n = 6018 Hz.

Figure 5.9

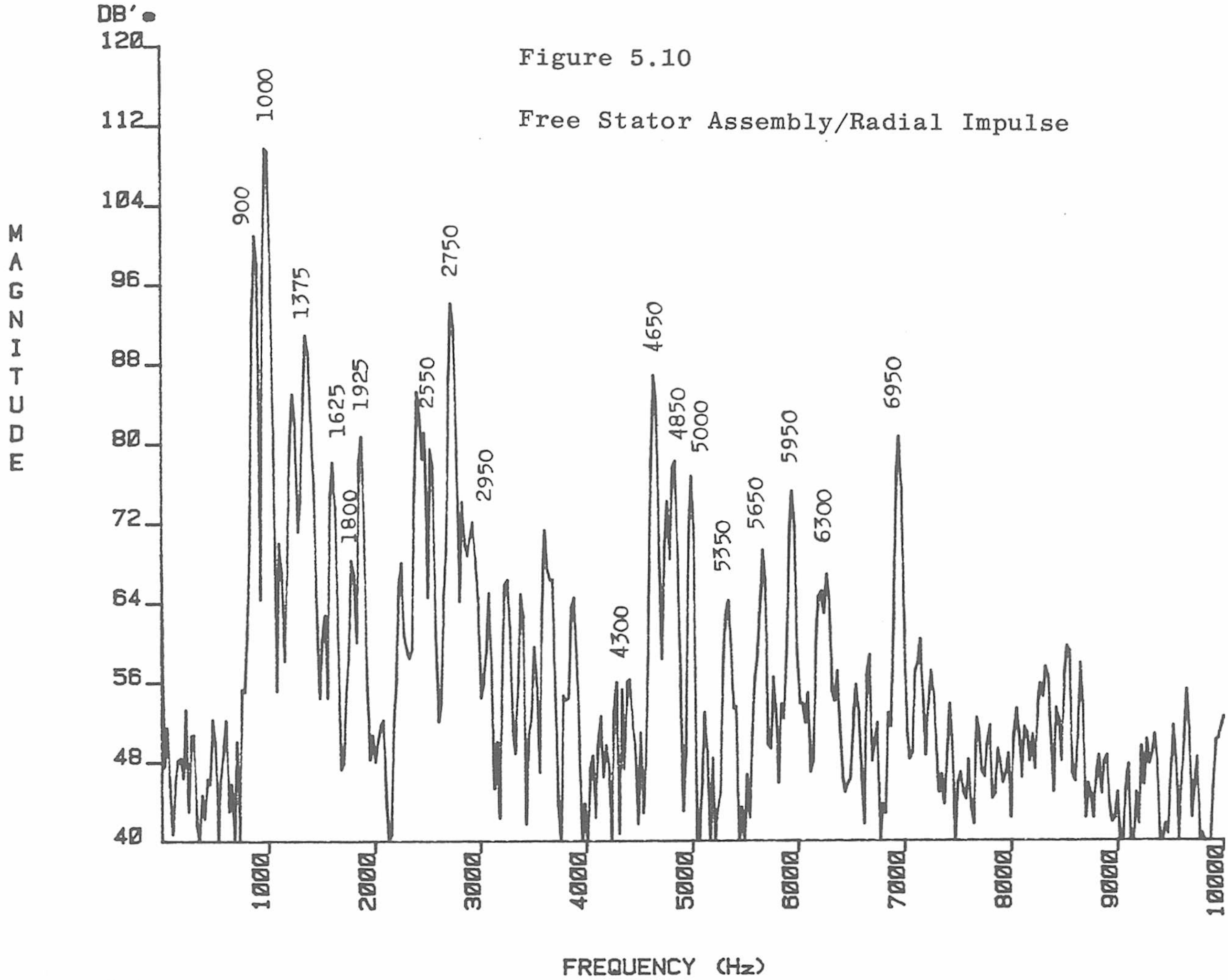
Figure 5.10
Free Stator Assembly/Radial Impulse
DB'
MAGNITUDE
FREQUENCY (Hz)

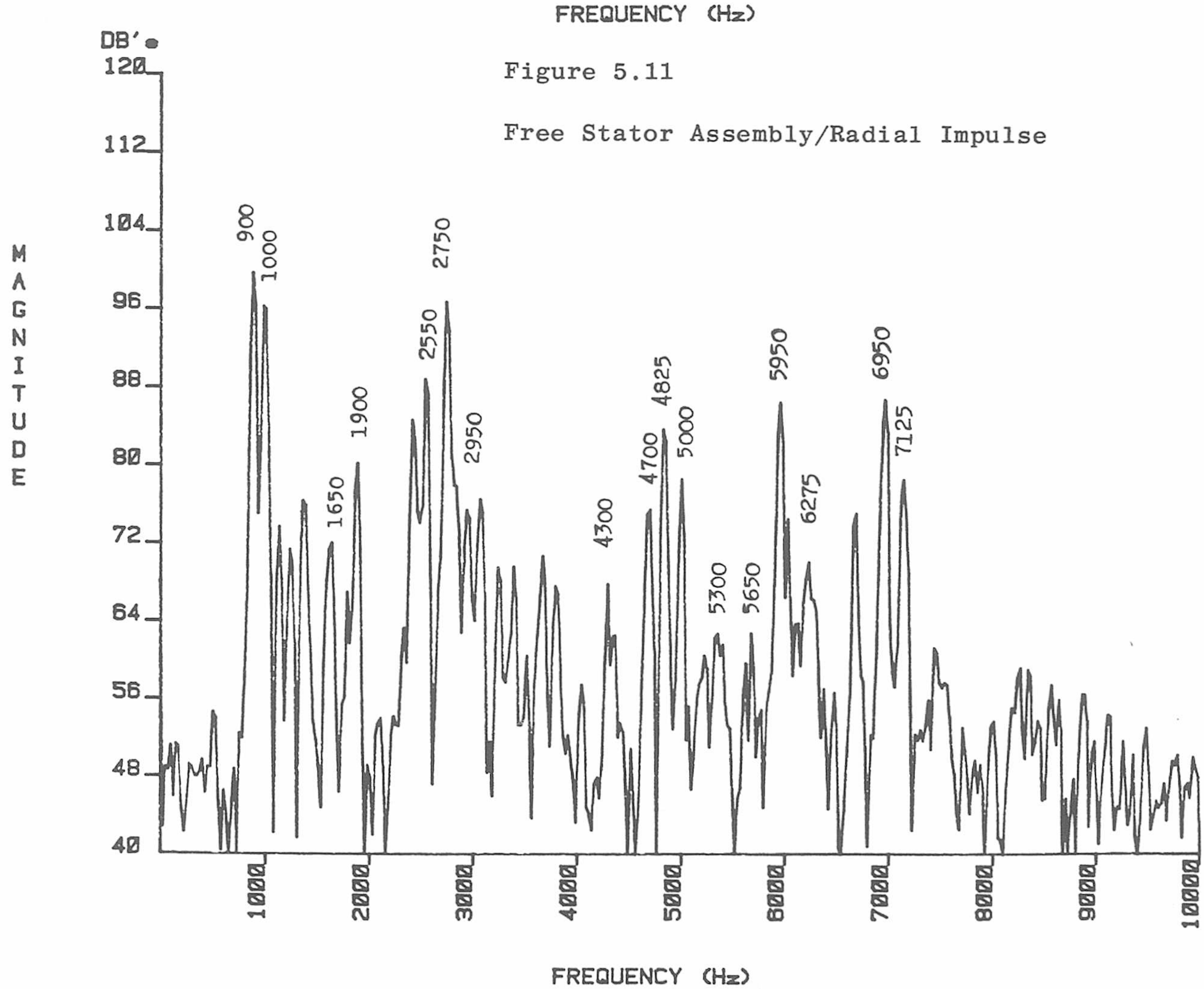
Figure 5.11
Free Stator Assembly/Radial Impulse
DB'
MAGNITUDE
FREQUENCY (Hz)

Figure 5.12

Free Stator Assembly/Axial Impulse

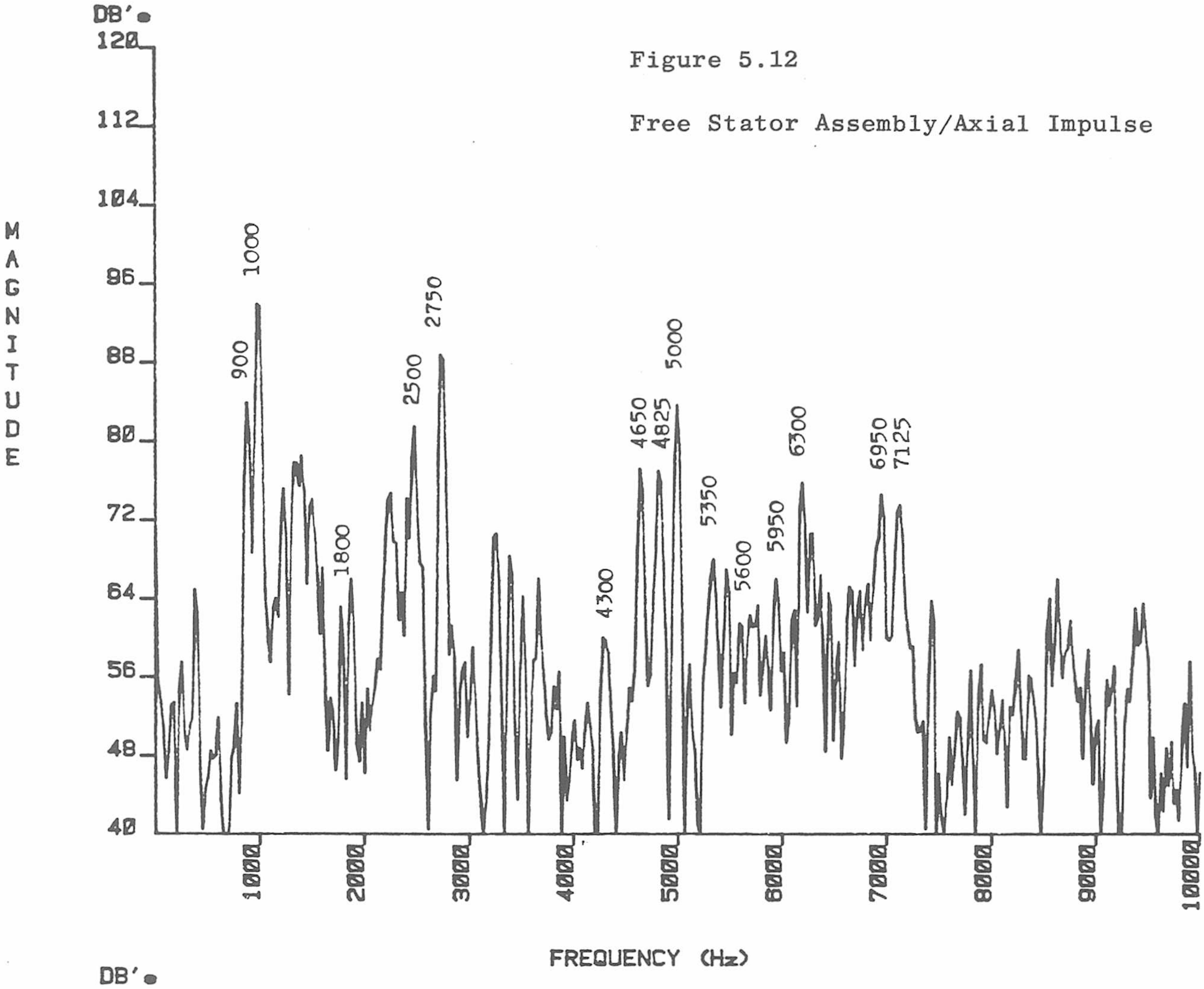

Figure 5.13

Free Stator Assembly/Axial Impulse

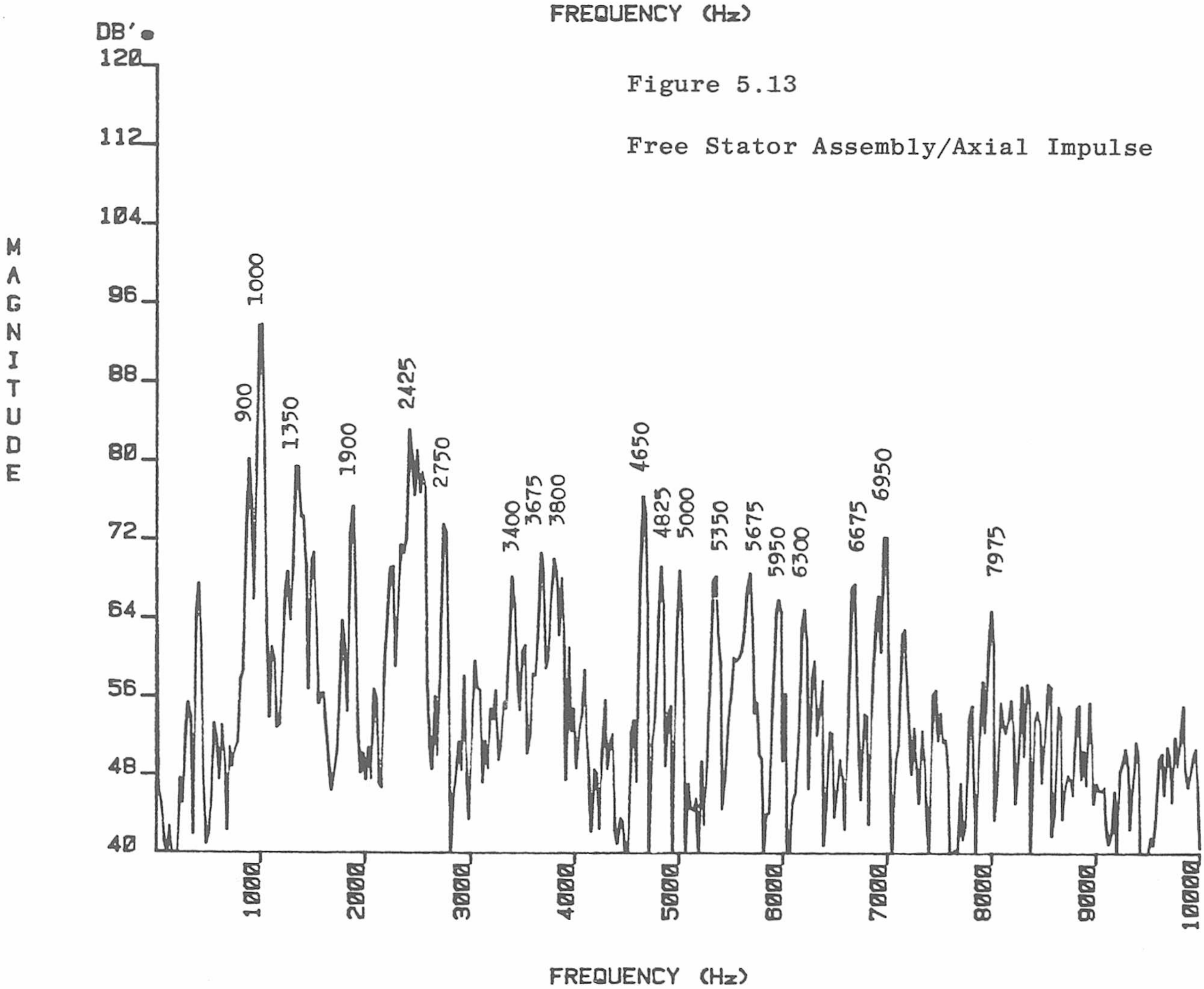

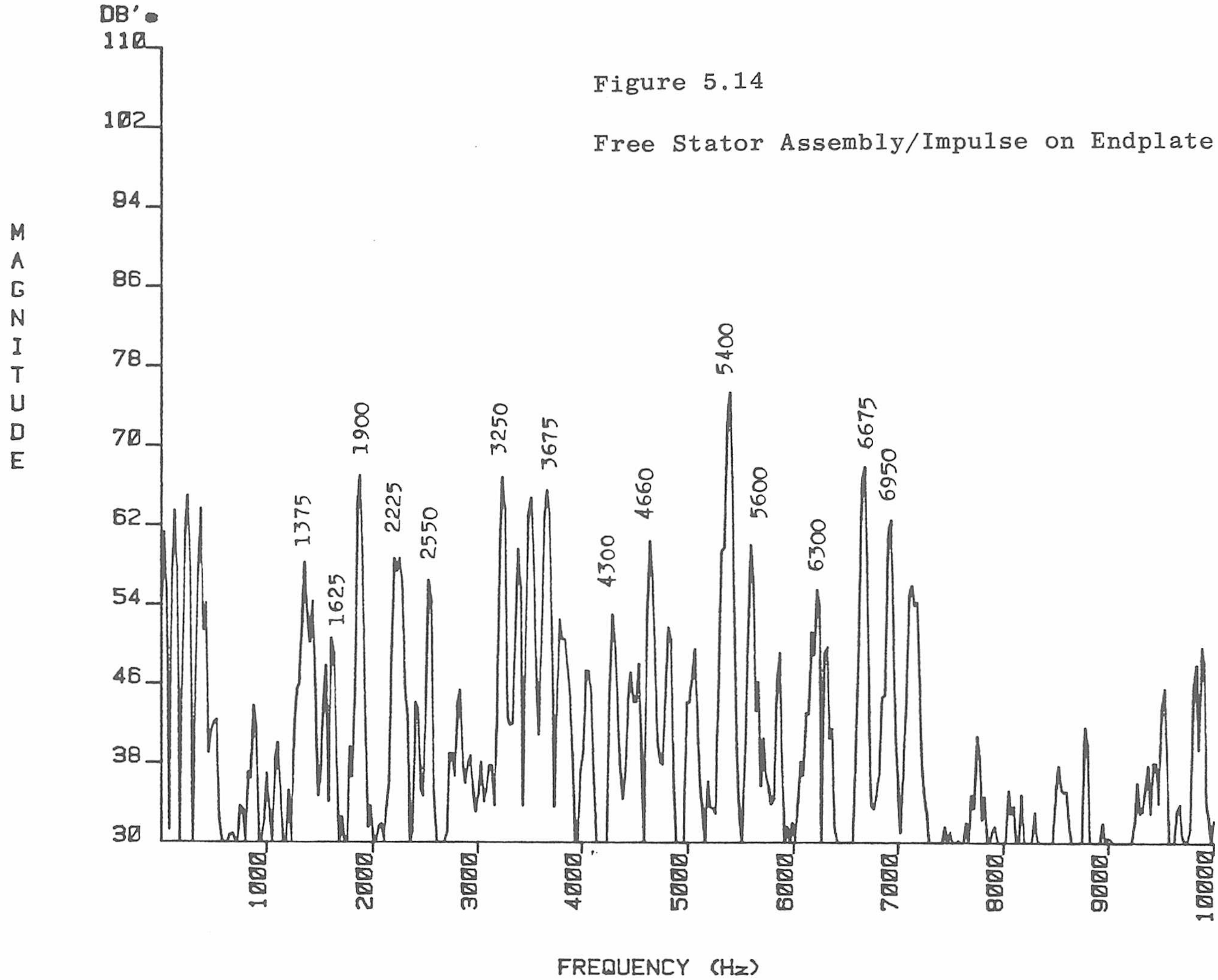

Figure 5.14
Free Stator Assembly/Impulse on Endplate
DB'S
MAGNITUDE
110
102
94
86
78
70
62
54
46
38
30
1375
1625
1900
2225
2550
3250
3675
4300
4660
5400
5600
6300
6675
6950
1000
2000
3000
4000
5000
6000
7000
8000
9000
10000
FREQUENCY (Hz)

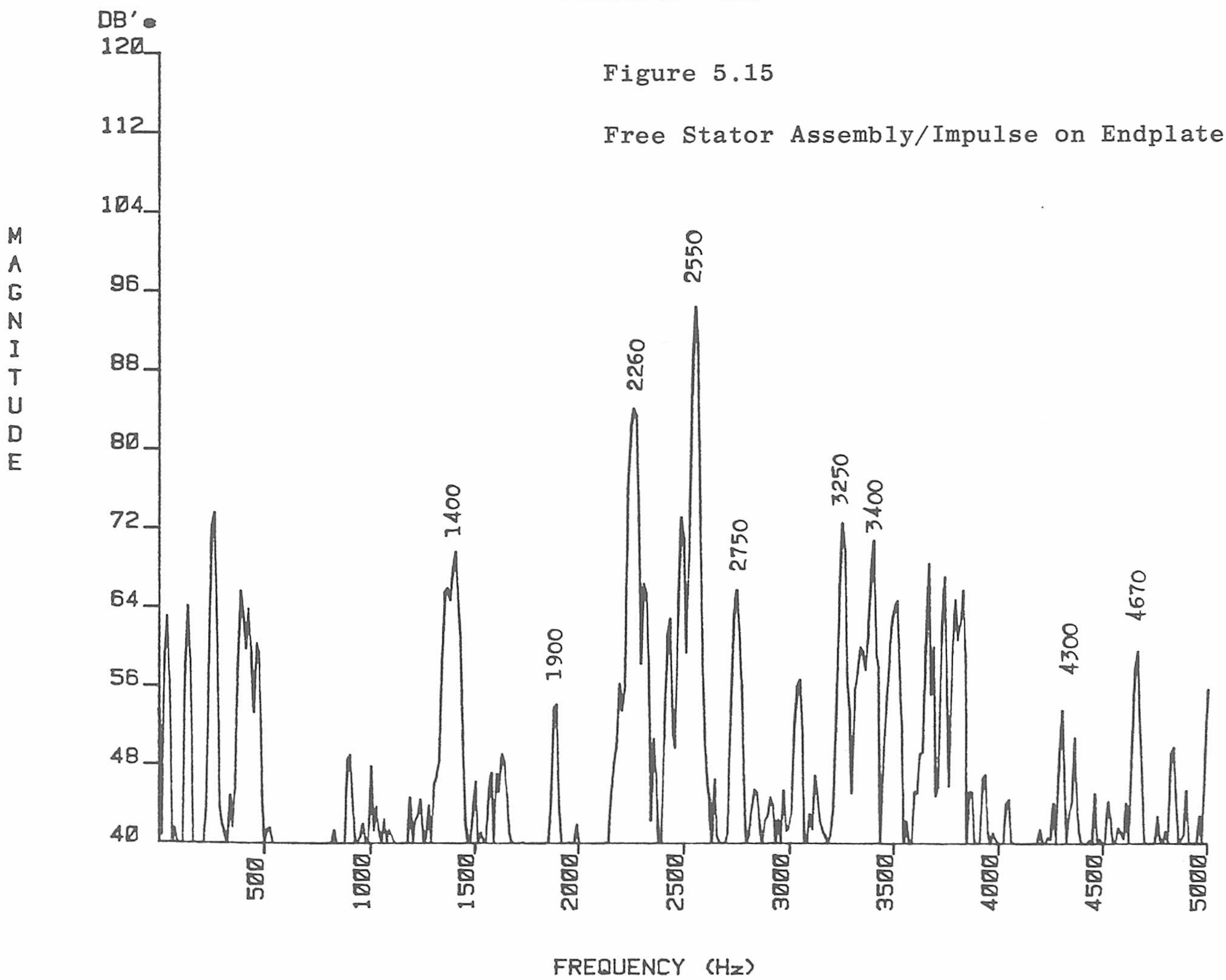

Figure 5.15
Free Stator Assembly/Impulse on Endplate
DB'S
MAGNITUDE
120
112
104
96
88
80
72
64
56
48
40
1400
1900
2260
2550
2750
3250
3400
4300
4670
500
1000
1500
2000
2500
3000
3500
4000
4500
5000
FREQUENCY (Hz)

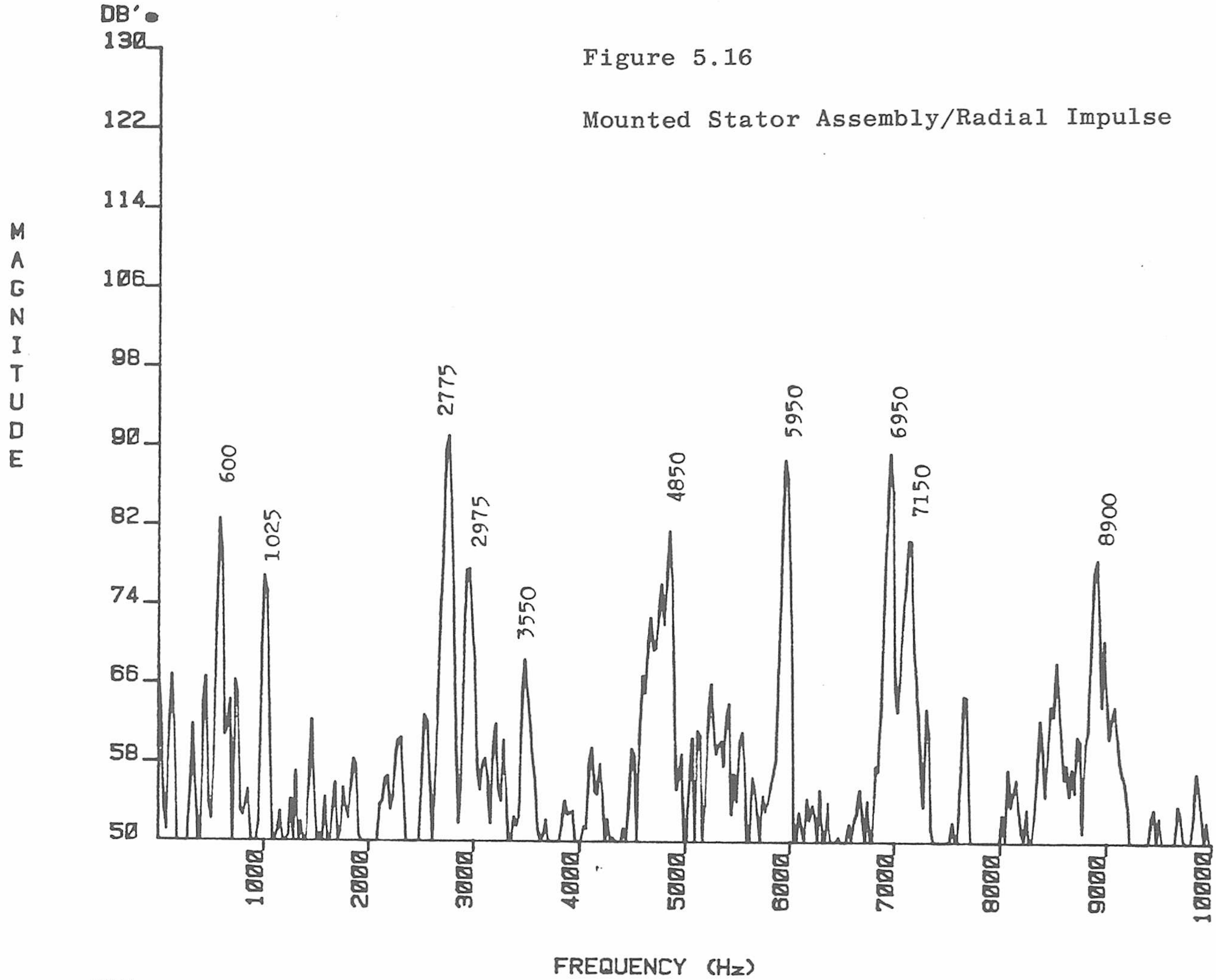

Figure 5.16

Mounted Stator Assembly/Radial Impulse

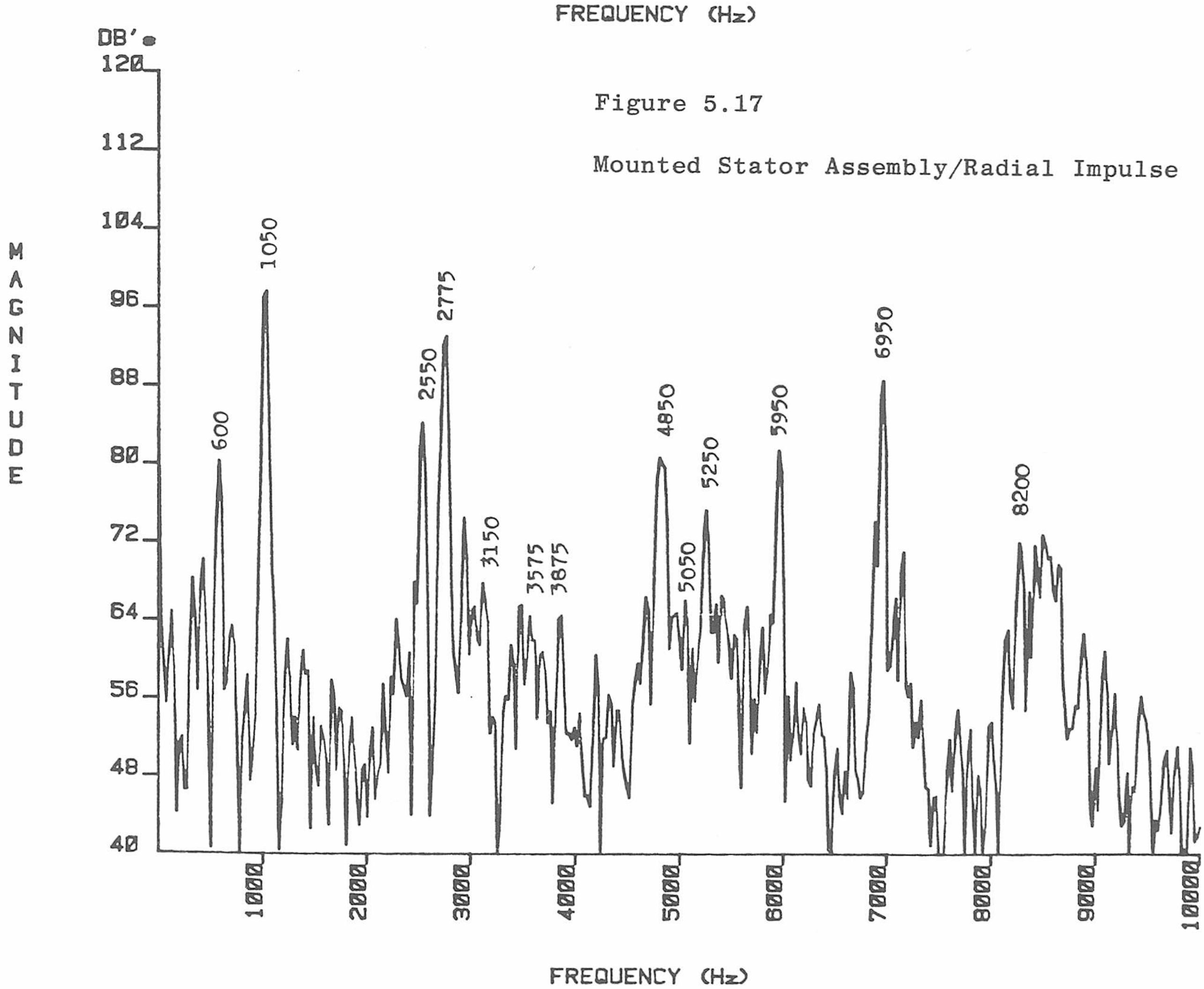

Figure 5.17

Mounted Stator Assembly/Radial Impulse

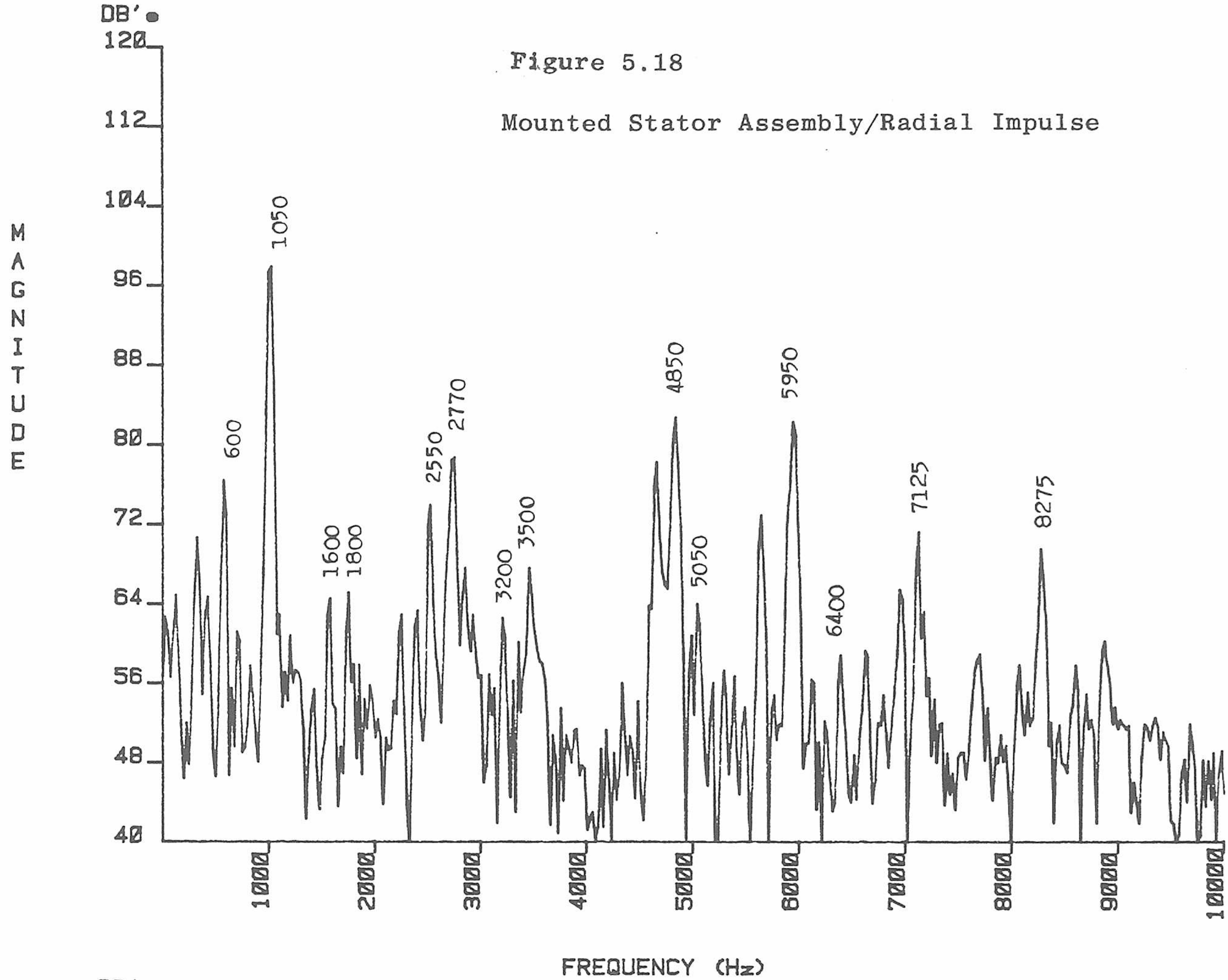

Figure 5.18

Mounted Stator Assembly/Radial Impulse

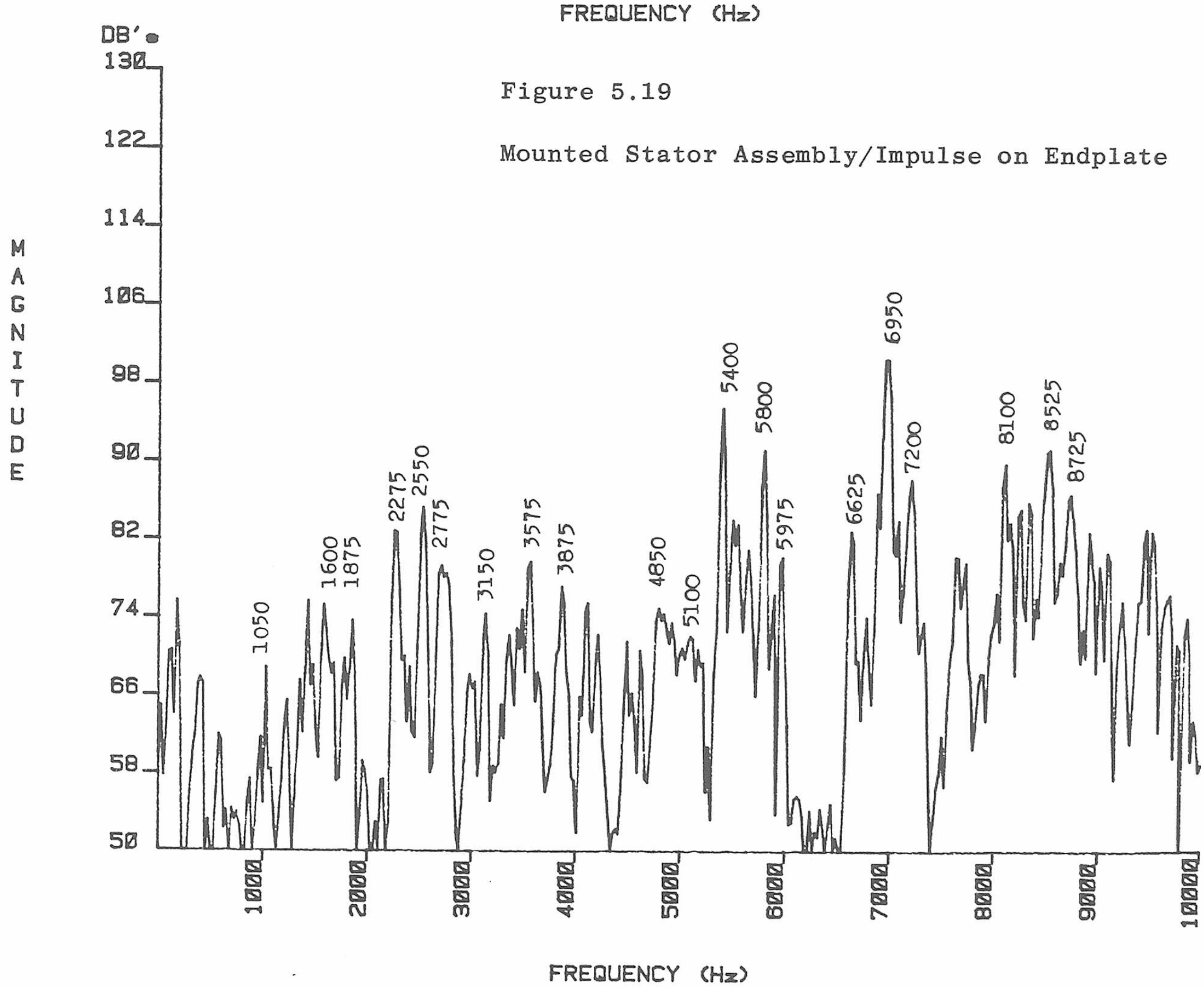

Figure 5.19

Mounted Stator Assembly/Impulse on Endplate

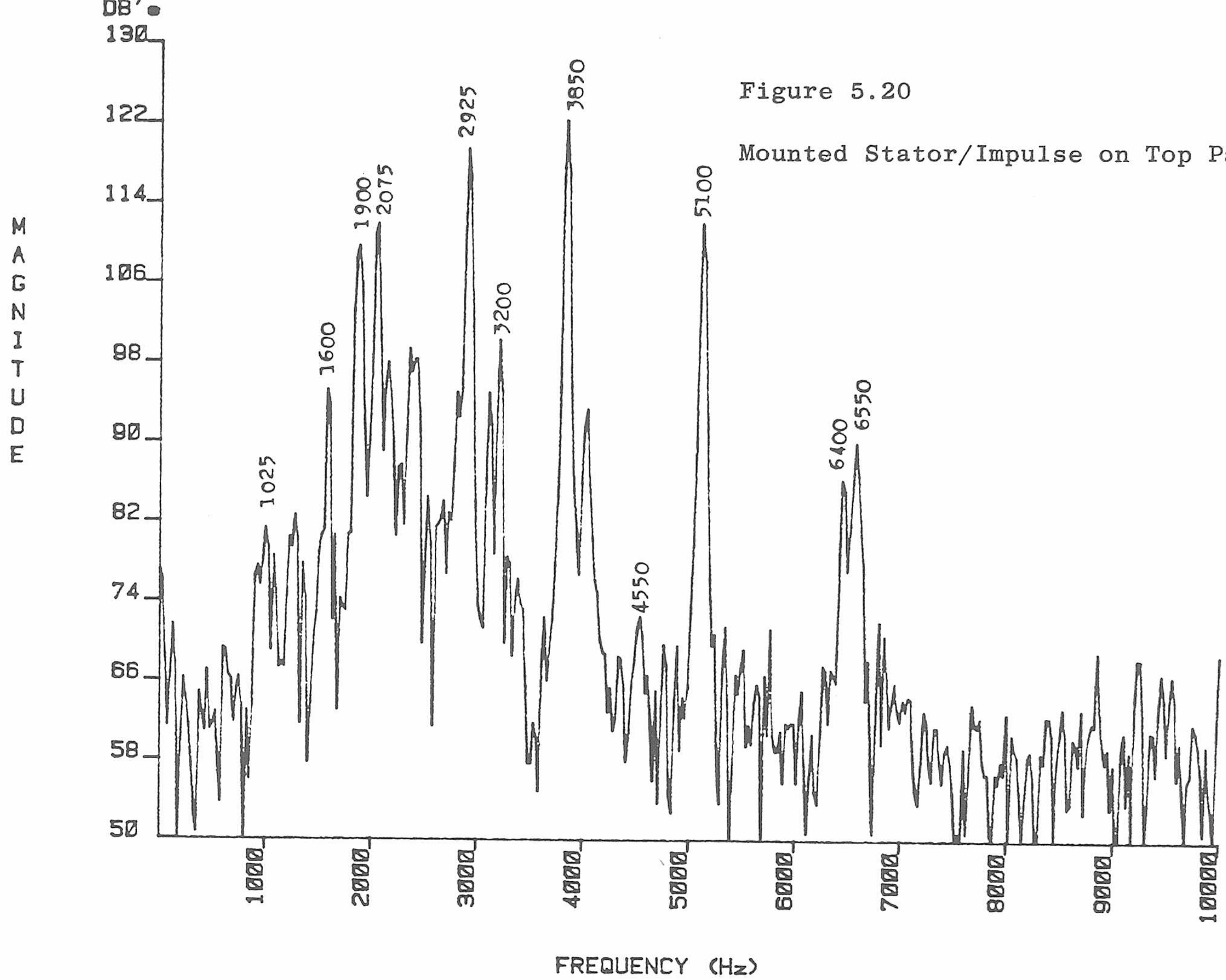

Figure 5.20

Mounted Stator/Impulse on Top Panel

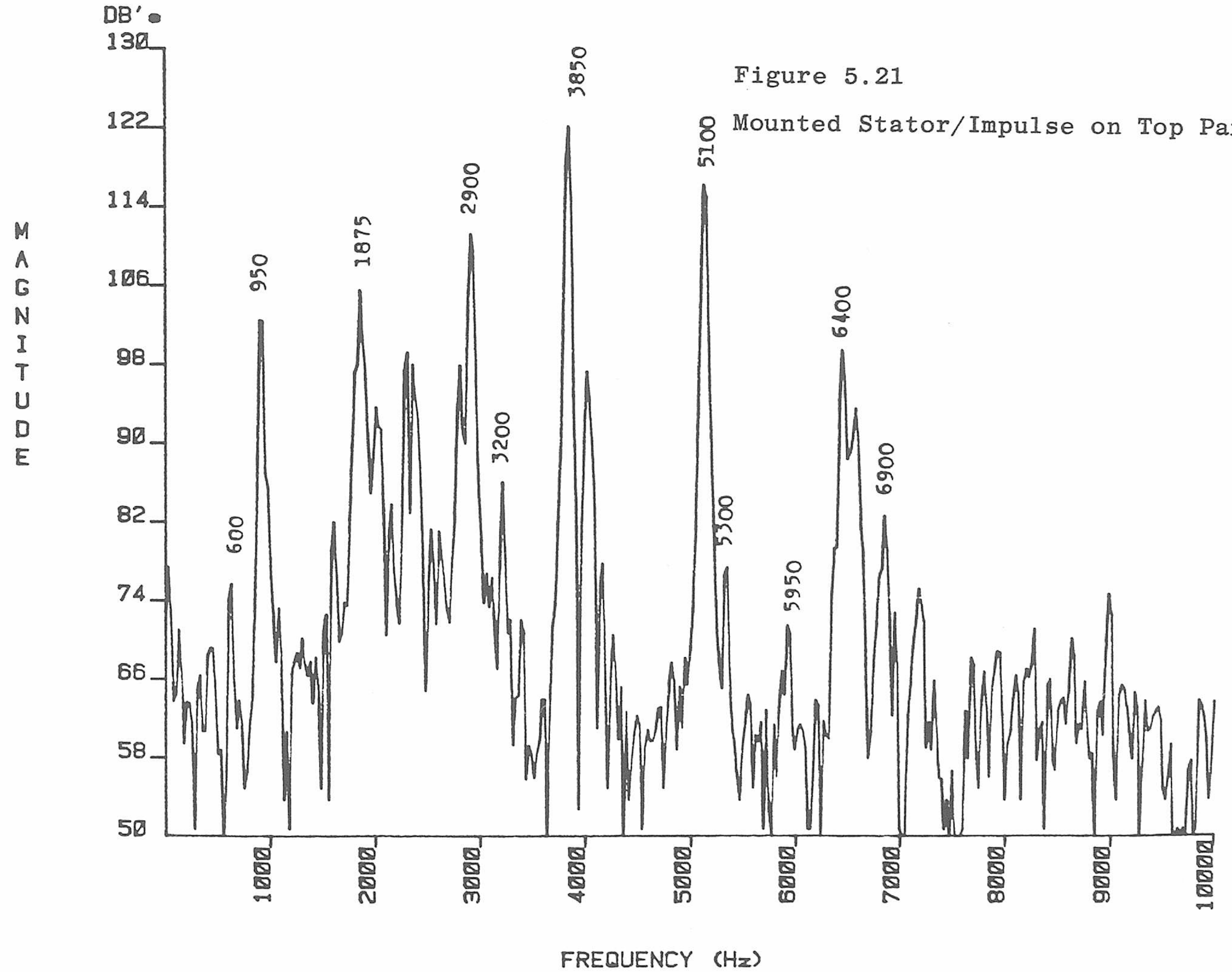

Figure 5.21

Mounted Stator/Impulse on Top Panel

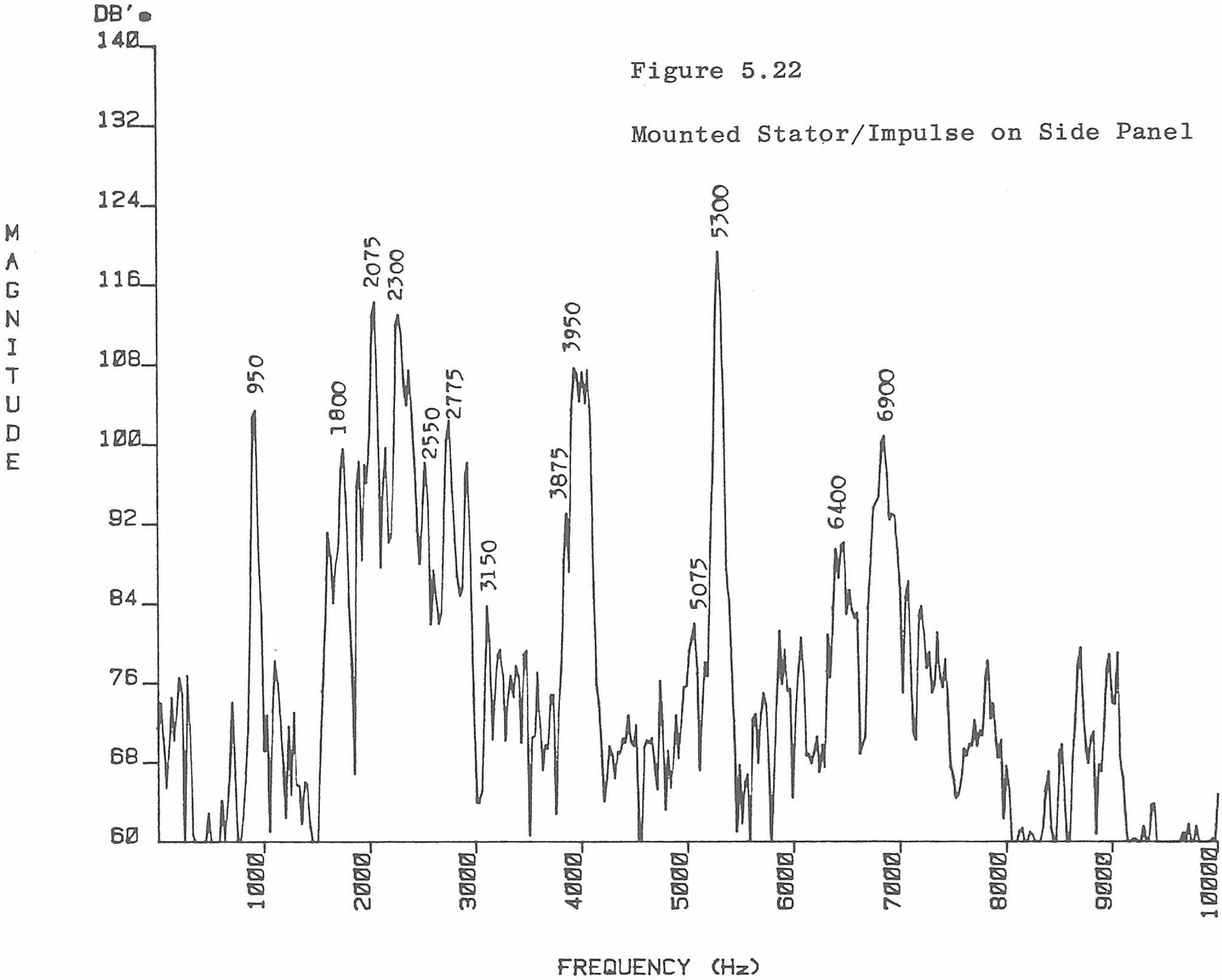

Figure 5.22

Mounted Stator/Impulse on Side Panel

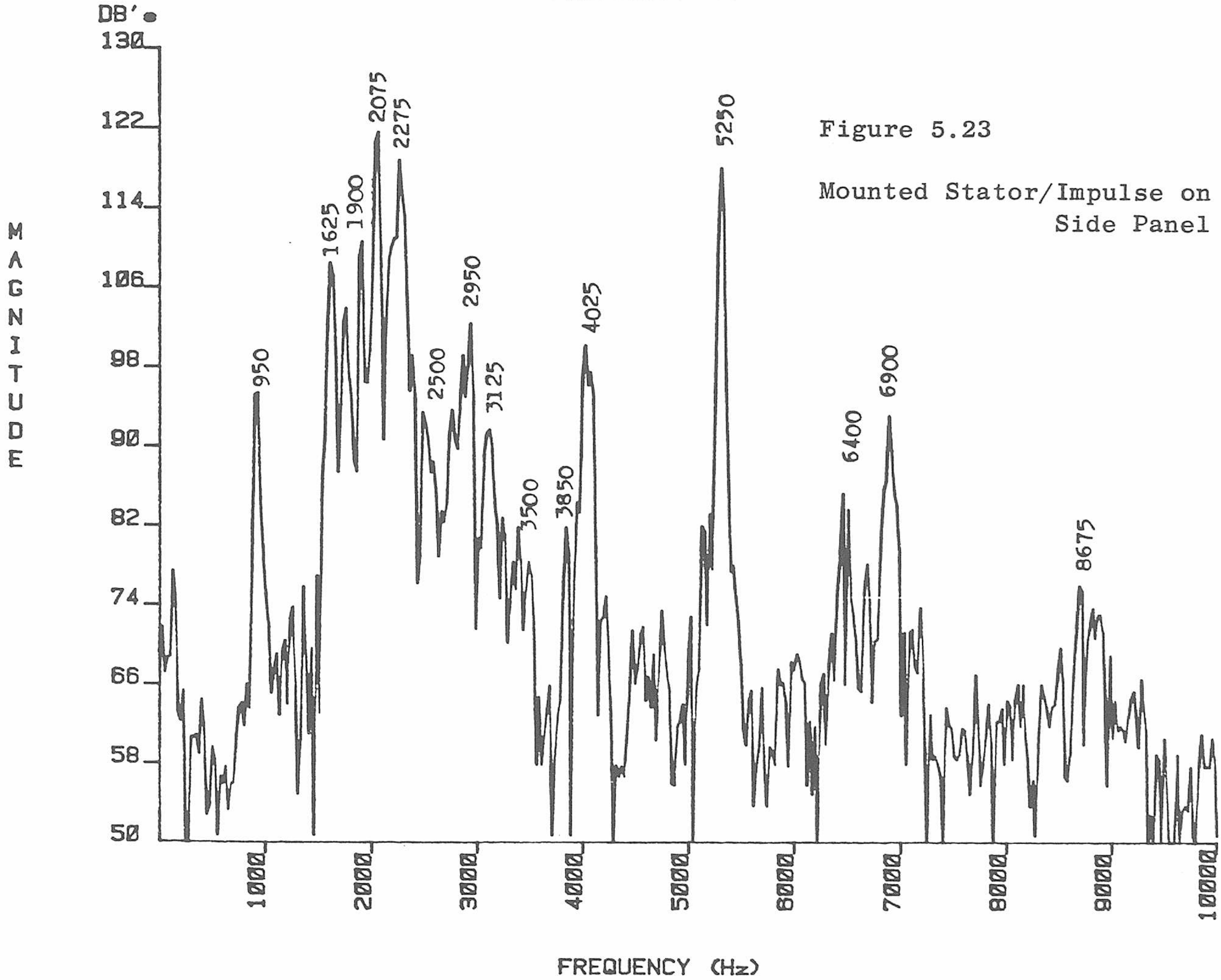

Figure 5.23

Mounted Stator/Impulse on Side Panel

CHAPTER 6. MODELLING THE VIBRATORY RESPONSE CHARACTERISTICS OF A LARGE MOTOR STATOR ASSEMBLY.

6.1 Introduction.

In operation, induction motors are continually subjected to both inherent and external forces which cause the stator core and frame to vibrate.

Electromagnetic forces stem from the revolving mmf waves and their harmonic content which are set up by the air-gap flux distribution when the motor is running. Forces can also be transmitted to the stator core and frame from external vibratory motion, particularly in an offshore installation where drilling operations and sea motion are two such vibration transmitters. The relevance of these forces to the feasibility of introducing a vibration monitoring strategy is that an operator must know in advance the vibration levels which are transmitted to the core and/or frame during normal healthy operation in order to recognise changes in the vibration pattern as being due to a fault condition.

In order to calculate the expected baseline vibratory response of a healthy induction motor in its operating environment, a theoretical analysis would have to include the solution of all the simple and complex pulsating and travelling force waves and a study of force wave transmission to the stator core back and outer frame.

Within the scope of this project, there are two aims concerning response calculations:

(1) To determine the accuracy of sinusoidal response calculations using the Finite Element Method by exciting the stator core model with a single point sinusoidal exciting force of constant magnitude and calculating the response at

the core natural frequencies.

(2) To calculate the vibratory response of the core and frame of the stator assembly model to the fundamental radial component of the electromagnetic forcing function which is a by-product of the square of the air-gap flux density. Also to compare theoretical predictions with experimental measurements.

From these two considerations it will be possible to evaluate the effectiveness of finite element modelling in terms of calculating the response of a stator assembly to external and inherent forcing functions.

6.2 Sinusoidal Response - Finite Element Theory.

In the dynamic analysis outlined in Chapter 3, the natural frequencies of the structure are found by determining the global matrix equation of motion and setting the forces $\{F_s\}$ in equation (28) to zero. For harmonic response calculations $\{U_s\}$ is found for $\{F_s\}$ not equal to zero. In this analysis it is necessary to introduce structural damping into the problem since in the absence of any damping the response of the structure will be infinite if the excitation frequency ω corresponds to a natural frequency. A hysteretic damping factor μ is included by setting the displacements to lead the forces by a phase angle. This is carried out by allowing the material moduli to be complex:

$$\overline{E} = E(1 + \overline{i}\mu) \qquad \text{and} \qquad \overline{G} = G(1 + \overline{i}\mu)$$

where a bar denotes a complex quantity.

If μ is constant for the whole structure then $(1 + \overline{i}\mu)$ is a multiplying factor of the global stiffness matrix. Since the forces will not necessarily be in phase and the response vectors will not all be in phase, the global equation of motion is now complex:

$$\left([S_s](1 + \bar{i}\mu) - \omega^2 [M_s] \right)\{\bar{U}_s\} = \{\bar{F}_s\} \tag{1}$$

Therefore at a frequency ω, the response is given by:

$$\{\bar{U}_s\} = \left([S_s](1 + \bar{i}\mu) - \omega^2 [M_s] \right)^{-1} \{\bar{F}_s\} \quad . \tag{2}$$

For structures where the damping constant is different for each mode of vibration, more meaningful results can be obtained by introducing modal or viscous damping. The dynamic equation becomes:

$$\left([S_s] + \bar{i}\mu[C_s] - \omega^2[M_s] \right) \{\bar{U}_s\} = \{\bar{F}_s\} \tag{3}$$

or the response equation is:

$$\{\bar{U}_s\} = \left([S_s] + \bar{i}\mu[C_s] - \omega^2 [M_s] \right)^{-1}\{\bar{F}_s\} \tag{4}$$

where $[C_s]$ is the global damping matrix.

Both equations (2) and (4) are solved using reduced stiffness, mass and damping matrices which relate just to the degrees of freedom which have been chosen as masters, (39, 42).

6.3 Measuring the Modal Damping Factor.

The response of a structure at or near one of its resonance frequencies is mainly a function of the damping characteristics of the structure. Therefore, in order to calculate the modal response of the stator core around its natural frequencies using the Finite Element Method, it is necessary to determine its modal damping characteristics.

There are several experimental methods for determining the damping in structures (54) and the method which is most suitable will depend on the proximity of the natural frequencies and the effects of off-resonant modes on the resonance curves around each natural frequency. If there is a considerable contribution from off-resonant modes, the resonance peak will be asymmetric since the effects above and below resonance will be different. However it is usual to assume that the off-resonant contribution is constant and the Kennedy-Pancy method can be used to separate and determine the natural frequencies (55). If the modes are fairly isolated from one another so that an approximately symmetrical resonance curve can be plotted and the damping is low at resonance, then the damping property can be determined by the Logarithmic Decrement technique (56, 54).

The logarithmic decrement δ can be found from the decay of a time history curve from:

$$\delta = \frac{1}{n} \ln \frac{u_1}{u_n}$$

where u_1 is the response amplitude at the first cycle of decay and u_n is the amplitude after n cycles.

Alternatively, the logarithmic decrement can be determined from a resonance curve by:

$$\delta = \frac{\pi \Delta_f}{f_{res}}$$

where f res. is the resonance frequency and $\Delta_f = f_2 - f_1$, where f_1 and f_2 are frequencies below and above resonance where the peak response amplitude is reduced by a factor of $\sqrt{2}$, (57).

The experimental technique required to determine the resonance curves is identical to the Sinusoidal Resonance Test procedure. In this case, response levels are measured at frequencies above and below resonance, over a range that includes the two frequencies at which the peak amplitude is reduced by a factor of $\sqrt{2}$. The damping characteristics of both a wound core and an unwound core were investigated. In both cases the stator core was freely suspended and excited by a single point, constant magnitude sinusoidal forcing function.

6.4 Stator Core Damping Characteristics.

All the resonance curves (Figures 6.1 to 6.7) are approximately symmetrical so that the estimate of the damping property using logarithmic decrement measurements is likely to be realistic. The results of δ values are similar to those obtained by Yang (14), for both a core carrying windings and without windings, with some variation in values.

The logarithmic decrement versus frequency curve (Figure 6.8) indicates a gradual rise in δ, as the frequency increases, for a wound core. Much lower damping values are recorded for a core without windings although the rise is more rapid over the frequency range. The increase in damping due to the presence of windings is caused by added energy dissipation.

The damping factor (D) associated with a mode of vibration is determined from the logarithmic decrement curve by:

$$D = \delta/2\pi .$$

6.5 Finite Element Analysis.

Two of the finite element models are adapted to calculate the vibratory response of the stator at resonance:

(1) The response of the free stator core model is calculated. A harmonically varying force of magnitude 19N is applied to an element node on the core circumference. The force level corresponds to the amplitude of the excitation force applied during resonance testing to determine the mode shapes. Therefore the theoretical predictions of stator response at resonance can be compared with experimental measurements. The vibration amplitude round the core periphery is calculated for modes $n = 2$, 3 and 4.

Modal damping factors determined from logarithmic decrement measurements are included in the PAFEC data.

(2) The response of the mounted stator assembly model is calculated at two of its resonance frequencies; namely at 1098 Hz and at 2766 Hz. Both of these frequencies excited relatively high vibration amplitudes during resonance tests. The assembly is excited by a sinusoidal force of amplitude 19N at an element node on the core circumference. Displacement levels are calculated at positions round the core periphery and at positions along the top of the endplate.

A response level calculated by PAFEC is tabulated in the computer output file as a vibration amplitude and a phase angle in terms of the global coordinate system. In order to calculate response levels in a radial direction, as measured by a transducer, local axis systems were introduced at nodes around the core circumference. The calculated phase angles were all either 0^{o} or 180^{o} depending on whether deformation was radially outwards or radially inwards.

Calculated vibration levels corresponding to both finite element models are compared with the measured values obtained from sinusoidal resonance tests.

6.6 Discussion.

The vibration amplitude versus position curves comparing calculated and measured values of response are plotted in Figures 6.9 —— 6.15.

The main problem which is highlighted by this investigation is the difficulty in obtaining accurate response calculations when vibrations excite sub-micrometre levels. Compared to the dimensions of the stator assembly, the vibratory response of the structure is extremely small so that slight incompatibilities in the finite element modelling can lead to large errors in sinusoidal response predictions.

The precise measurement of the vibratory response of the stator at resonance involves finding the exact peak reading on a vibration meter at the exact position on the structure where the vibration amplitude is a maximum. It is therefore also likely that the experimentally obtained results are slightly deviant from the actual response levels.

Taking both these considerations into account, the finite element calculations produce realistic results. The largest error occurs in calculating endplate response. Here the calculated maximum response amplitude at the antinode is 1.9 times the measured value (Figure 6.13). The smallest error at a modal antinode occurs in the finite element model of the free core at $n = 2$ (Figure 6.9). Here the calculated value is 1.4 times the measured value. Furthermore, in each case the theoretically predicted response curve follows the pattern of the measured mode shape and agreement is precise between measured and calculated positions of nodes and antinodes.

If the results are viewed in terms of their relevance to a vibration monitoring strategy, where a natural frequency may occur at or near a frequency being monitored to detect a motor fault, then two pertinent points can be made:

(1) The calculated predictions will give precise indications of modal nodes where the effects of resonance on monitored vibration levels can be avoided.

(2) Since the calculated predictions are greater than measured vibration levels in every case, the effects of resonance are always overestimated rather than underestimated, which introduces a "factor of safety" into the assessment of resonance effects on monitored vibration levels.

A method for calculating the radial deflection of an induction motor stator core, derived from well known beam deflection theory, is put forward by Alger (28). Using his equations, the maximum vibration amplitudes at $n = 2$ and $n = 3$ are 0.11×10^{-6}m and 0.12×10^{-9}m respectively. These predictions represent departure from the measured values by factors of 127 and 1667. As a good approximation for calculating stator core vibratory response, finite element analysis produces much more realistic results then an adaptation of beam theory.

When it comes to calculating the response of a complex structure, the Finite Element Method is the only approximation technique that can adequately simulate the interaction of vibrating components and the restrictions imposed by the boundary conditions. In general, the results of this study show that finite element analysis can be used effectively to calculate the amplitudes of vibration on the core and frame of a stator assembly due to excitation from an external sinusoidal forcing function.

6.7 The Induction Motor Test Rig.

An experimental analysis of the vibratory response of the stator assembly to the inherent electromagnetic forcing function was carried out in compliance with aim (2). To perform the necessary series of running tests, the motor stator assembly was first developed to become a working test rig.

The stator core is wound with a double-layer, delta-connected, 3-phase, standard stator winding with 36 coils and 15 turns per coil. An air-gap of 15 thou lies between the stator bore and the 28 slot squirrel cage rotor. The induction motor has 4 poles and is rated at 11 kw. An automatic starting device connects the motor to a 3-phase, 415 volts, 50 Hz supply. The complete motor and the bearing pedestals are mounted onto a steel bed-plate.

The test rig was specially developed both for experimental studies associated with this research project and to enable future studies of motor faults and vibratory response of a large motor stator structure model to be carried out. For this reason the coil ends are connected via an external connection grid to provide access to the windings for fault simulation. Also, the rotor shaft is coupled to a loading dynamometer for load tests.

The complete installed machine is shown in Figure 6.16.

6.8 The Magnetic Forcing Function.

Now that it has been shown that finite element analysis can calculate the response of the stator core to an external harmonically varying force, the next stage is to model the inherent forcing function.

Analytical methods for calculating the radial magnetic exciting forces from consideration of the air-gap flux distribution have been studied in depth and are well documented (14, 58, 47). The Finite Element Method is to be used here to model the fundamental component of the inherent radial electromagnetic forcing function in order to approximate the dynamic condition of the large induction motor model during normal operation. To model the forcing function mathematically, it is necessary to determine the nature of the force wave.

For a balanced three-phase supply and a delta-connected winding, the phase currents are:

$$Ia = Im \sin \omega t$$

$$Ib = Im \sin (\omega t + 2\pi/3)$$

$$Ic = Im \sin (\omega t - 2\pi/3) \; .$$

The peak mmf produced by one phase is:

$$Mm = Im\, N$$

and therefore the mmf produced in each phase is:

$$Ma = Mm \sin \omega t \cos (\pi x/\tau)$$

$$Mb = Mm \sin (\omega t + 2\pi/3) \cos ((\pi x/\tau) - 2\pi/3)$$

$$Mc = Mm \sin (\omega t - 2\pi/3) \cos ((\pi x/\tau) + 2\pi/3) \; .$$

The sum of the mmf's for the three phases gives the total mmf.

$$M = Ma + Mb + Mc$$

or

$$M = \frac{3}{2} Mm \sin (\omega t - (\pi x/\tau)) \; .$$

The flux density is the product of the mmf and the permeance:

$$B = M\Lambda \; .$$

If the permeance is assumed to be constant, then

$$B = \frac{3}{2} Mm\, \Lambda \sin (\omega t - (\pi x/\tau)) \; .$$

It is well known that the radial pull exerted by the magnetic force across the air-gap is proportional at each point to the square of the flux density. The relationship between the radial force and the flux density is given by:

$$F = \frac{B^2}{2\mu_o} .$$

Therefore the radial force is also given by:

$$F = (\frac{3}{2} \, Mm \, \Lambda)^2 \, \frac{1}{2\mu_o} \quad \sin^2 \, (\omega t - (\pi x/\tau))$$

and the forcing function transmitting vibration to the stator assembly is of the form:

$$\underline{\underline{F = K [1 - \cos(2\omega t - (2\pi x/\tau))}}$$

Neglecting all harmonics except the fundamental component, the equation shows that the forcing function is a constant magnitude uniformly moving wave. As the flux is a wave of supply frequency (50 Hz), the fundamental radial electromagnetic forcing function is a wave of double frequency (100 Hz).

6.9 Modelling the Magnetic Forcing Function.

To model the fundamental magnetic forcing function which transmits radial vibrations to the stator assembly during normal operation, the core must be excited in such a way as to produce a rotating force wave of constant magnitude.

The force pole number will be twice the pole number of the motor. In this case the motor has 2 pole pairs and therefore the force pole number is 8. In a 4 pole motor a complete revolution of the magnetic wave occurs in π mechanical radians. For a motor with p pole pairs:

$$\theta \text{ electrical} = p \, \theta \text{ mechanical}.$$

Therefore one mechanical revolution of the stator core is equivalent to 4π electrical radians.

The force can be modelled by applying four forcing functions to the stator core as follows:

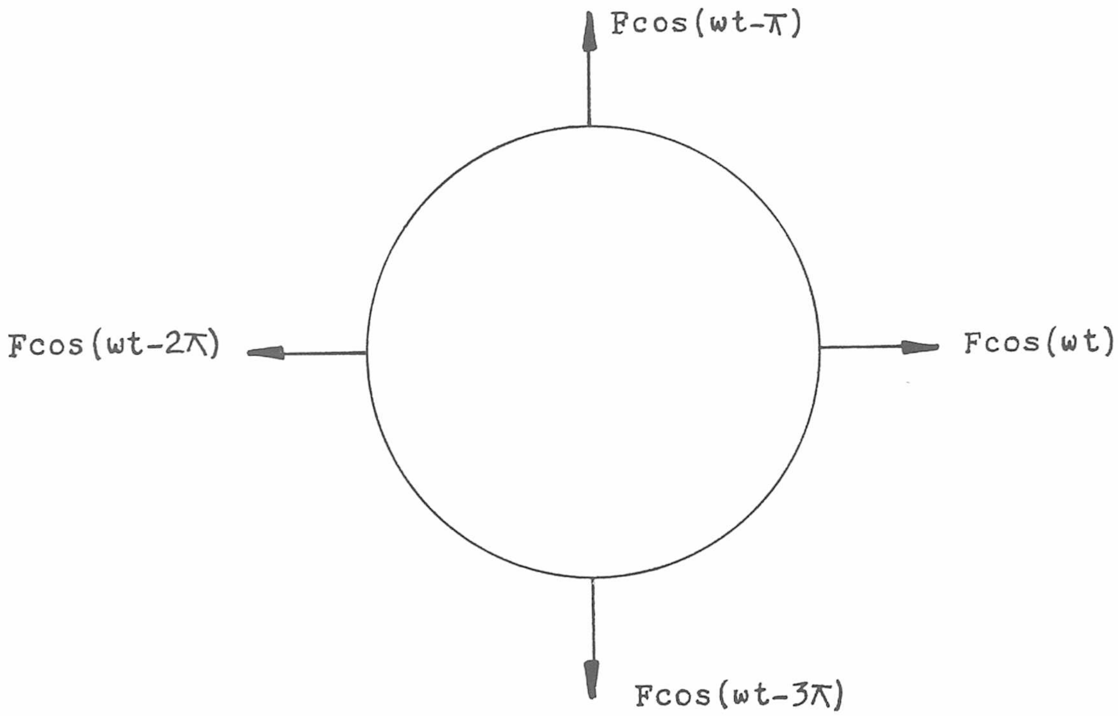

Figure 6.17

The wave pattern due to these forces is a simple approximation of the electromagnetic force wave:

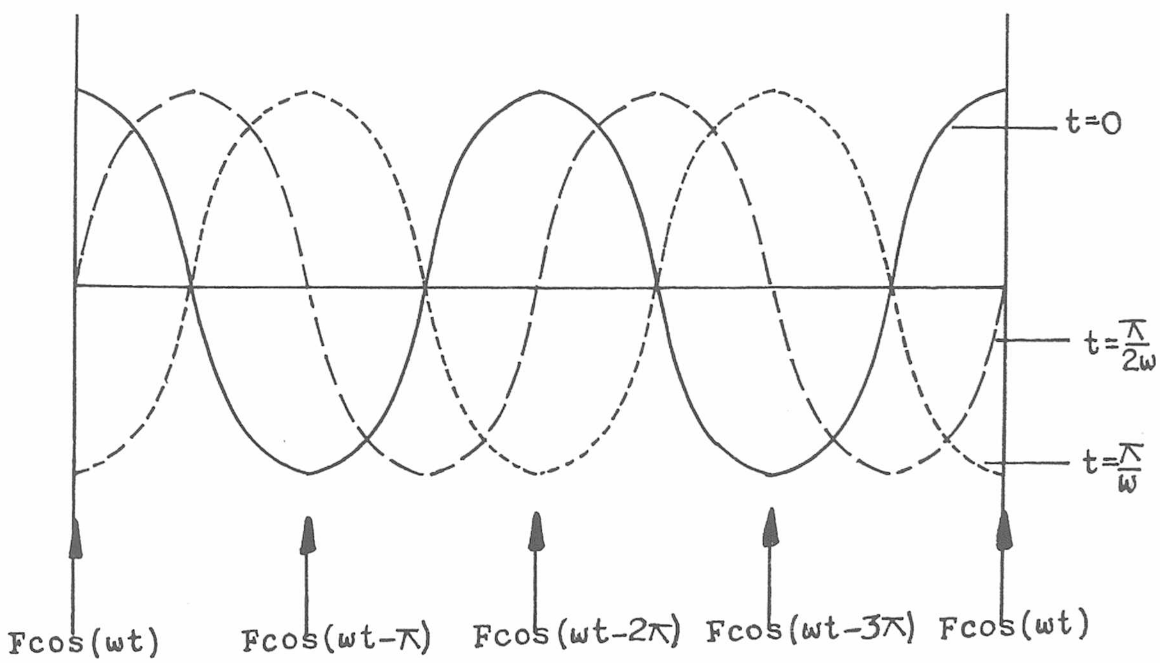

Figure 6.18

These four 100 Hz phase displaced forcing functions can be introduced into the finite element model. The vibratory response of the stator assembly can be calculated from a sinusoidal response analysis. Firstly, the magnitude of the force wave must be determined. This can be achieved by manipulation of the known motor parameters.

6.10 Calculating the Magnitude of the Forcing Function.

Consider the equation for the phase voltage. The phase voltage in terms of the flux per pole is given by:

$$Eph = \sqrt{2}\,\pi\,\phi f\ Tph(k_s k_d) \tag{1}$$

where:

Tph = turns/phase

f = pn

k_s = coil span factor = $\sin(\beta/2)$

k_d = distribution factor = $\sin(\frac{d\theta}{2})\ /\ d\sin(\frac{\theta}{2})$

β = coil span in electrical degrees

d = number of series connected coils per group.

The flux per pole is related to the flux density by:

$$\overline{B} = \frac{\phi}{\gamma L} \tag{2}$$

where: L = effective length

and γ = pole pitch = $\pi D/2p$.

Therefore:

$$\overline{B} = \frac{2p\phi}{\pi DL} \tag{3}$$

$\overline{B}$ is the average flux density so, assuming a sinusoidal distribution, the peak value is given by:

$$\hat{B} = \frac{\pi}{2}\overline{B} = \frac{p\phi}{DL} \tag{4}$$

Therefore the phase voltage can be defined in terms of the peak flux density and the rotor dimensions by:

$$Eph = \frac{\sqrt{2}\ \hat{B}\ L\ Tph\ \pi\ Df\ k_s k_d}{p} \tag{5}$$

and hence the peak flux density can be defined as:

$$\hat{B} = \frac{p\ Eph}{\sqrt{2}\ L\ Tph\ \pi\ Df\ k_s k_d} \ . \tag{6}$$

Since

$$\hat{F} = \frac{\hat{B}^2}{2\mu_o}$$

The peak force is given by:

$$\hat{F} = \frac{1}{2\mu_o}\left(\frac{pEph}{\sqrt{2}\ L\ Tph\ \pi\ Df\ k_s k_d}\right)^2 \ . \tag{7}$$

For the motor under investigation the various terms of the equation are known or can be calculated:

μ_o = magnetic space constant = $\underline{4\pi/10^7}$

p = number of pole pairs = $\underline{2}$

E line = 415 volts.

For a delta connected winding the phase voltage is equal to the line voltage.

Eph = $\underline{415\ \text{volts}}$.

L = rotor length = $\underline{146\ \text{mm}}$.

D = rotor diameter = $\underline{164.34\ \text{mm}}$.

Tph = turns/phase = $\underline{180}$

f = $\underline{50\ \text{Hz}}$.

The coil span factor $k_s = \sin(\frac{\beta}{2})$ where $\beta = 180^\circ$ electrical.

$k_s = \sin 90^\circ = \underline{1}$.

The distribution factor k_d is given by:

$$k_d = \sin\left(\frac{d\theta}{2}\right) / d \sin\left(\frac{\theta}{2}\right)$$

where θ = electrical slot angle = $(2\pi p) / s$.

In electrical degrees the slot angle is $\theta = 360p/s$.

There are 36 slots, i.e. $s = 36$.

Therefore

$$\theta = 20^{\circ} \text{ electrical.}$$

The number of coils per group (d) can be found as follows:

1 group will occupy 2d slots

1 phase will occupy 2dp slots

q phases will occupy 2dpq slots.

Therefore the number of slots s is given by $s = 2dpq$

and

$$d = \frac{s}{2pq} \text{ slots/pole/phase.}$$

$p = 2$, $q = 3$ and $s = 36$ so that $d = 3$.

The distribution factor is calculated to be

$$\underline{kd = 0.9598} \text{ .}$$

Substitution of these motor parameters into equation (6) yields a peak flux density of

$$\underline{\hat{B} = 0.937 \text{ wb/m}^2} \text{ .}$$

The peak value of the radial force is therefore:

$$\underline{\underline{\hat{F} = 323.26 \text{ kN/m}^2}} \text{ .}$$

6.11 Calculating the Vibratory Response at 100 Hz.

The finite element model of the mounted stator assembly was adapted to calculate the vibratory response at 100 Hz to the four phase-displaced harmonically varying forcing functions. The forces were applied at node points on the core teeth of the finite element model. An appropriate damping factor was introduced from extrapolating the logarithmic decrement versus frequency curve for a wound core (the δ value at 100 Hz being 0.08 from Figure 6.8). A sinusoidal response analysis calculated the vibration levels in the radial direction at element nodes round the core periphery and at nodes along the top and side of the endplate.

6.12 Measuring the Response at 100 Hz.

The induction motor is run on no-load. The vibration signal is fed from an accelerometer mounted on the stator assembly via a charge amplifier to a high resolution spectrum analyser where the frequency components of the signal are identified. The vibratory response of the stator assembly is measured at transducer mounting positions round 180° of the stator core circumference, from the top position to the base position. Vibration levels are also measured along the top edge and the side edge of an end-plate. For each transducer position, the vibration amplitude of the 100 Hz component of the response signal is recorded on a decibel scale. The signal output is calibrated by the charge amplifier on an acceleration range and the conversion of dB's to acceleration levels is given by:

$$dB = 20 \log_{10} \left(\frac{X}{X_o}\right)$$

where X is the measured acceleration level and X_o is a reference acceleration level.

Equivalent decibel and acceleration values are presented in Table 10.

Measured response levels are further converted into displacement values for comparison with theoretical findings. The experimental set-up is illustrated in Figure 6.19 .

dB	m/s^2
130	31.6
120	10.0
110	3.16
100	1.00
90	0.316
80	0.100
70	31.6×10^{-3}
60	10.0×10^{-3}
50	3.16×10^{-3}
40	1.00×10^{-3}
30	0.316×10^{-3}

TABLE 10.

Conversion of dB's to m/s^2 .

6.13 Discussion

Comparisons of calculated and measured vibration levels at 100 Hz on the stator core and frame are presented in Figures 6.20 to 6.22. The finite element approximation of the fundamental electromagnetic forcing function produces results in good agreement with measured vibration levels.

On the stator core periphery the differences between predicted and measured response amplitudes are in part due to the mathematical modelling process which neglects all aspects of the forcing function except the fundamental radial component at 100 Hz. Also, the four sinusoidal forces in the theoretical analysis had to be applied at element corner nodes on the finite element mesh. As there were no such nodes at 0°, 90°, 180° and 270°, the excitation forces were applied to the node positions closest to these axes. This accounts for the phase displacement between the two plotted curves and does not indicate inaccuracy in the finite element analysis. The calculated and measured deflection patterns are both waves of the same pole number. The most obvious variations between the two curves occur at the base and top of the stator core. The theoretical analysis predicts a much smaller response ($< 0.01 \times 10^{-6}$ m) near the base of the core. This is most likely due to the rigid restraints imposed at the frame feet of the finite element model. In fact the stator feet have some flexibility which explains the measured response being higher (0.3×10^{-6} m) than the calculated value. However the influence of the mounting arrangement can be seen in the measured response curve where the amplitude of vibration at 180° is more heavily damped than the response at 90° round the core back.

Dissimilarities at the top of the core are due in part to the transducer measurement position being on a core bar but are mainly due to expected errors in response calculations as were outlined in Section 6.6 . The maximum difference between the two response curves occurs at 0° where the calculated vibration amplitude was twice the measured value. At 90° the calculated and measured values differed by only 3.5%. Although the response measurements and calculations are recorded as absolute values, i.e. all positive, the response wave pattern represents ovalising of the stator core due to inherent excitation.

Vibration amplitudes calculated on the top and side of an endplate show the same trend of increasing displacement values as the measured results. However the finite element analysis predicts lower initial response, a larger increase, and higher final response than the measured curves in both cases (Figures 6.20 and 6.21). The sources of error are the same as those discussed previously with added discrepancy due to the effects of the frame panels on endplate movement.

The response analysis has shown that the Finite Element Method can be used to model the 100 Hz fundamental electro-magneticforcing function inherent in all induction motors. The predicted response levels are in good agreement with measured values and the shape of deformation on the core and frame can be determined accurately.

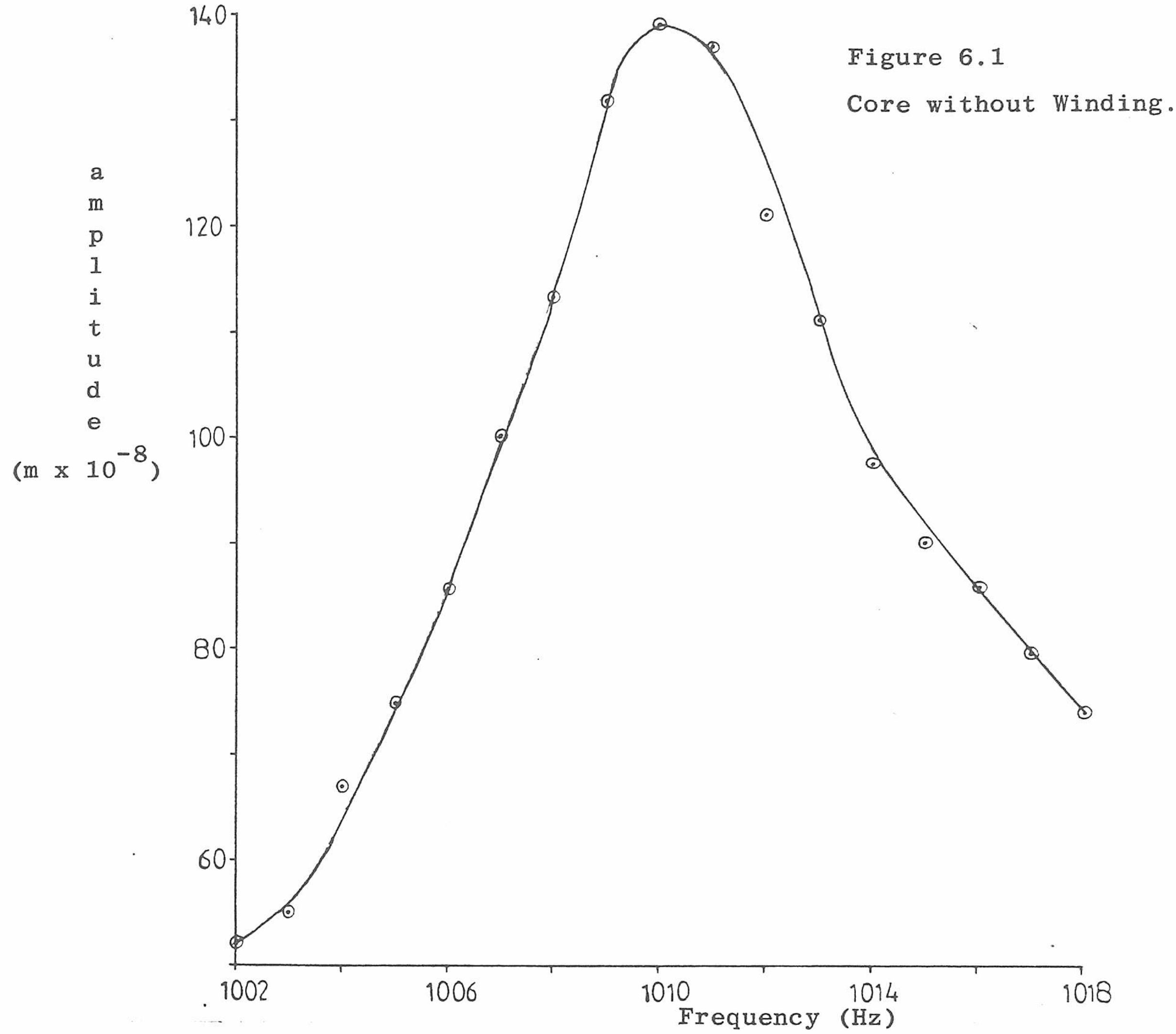
Figure 6.1
Core without Winding.
amplitude
(m x 10^{-8})
140
120
100
80
60
1002
1006
1010
1014
1018
Frequency (Hz)

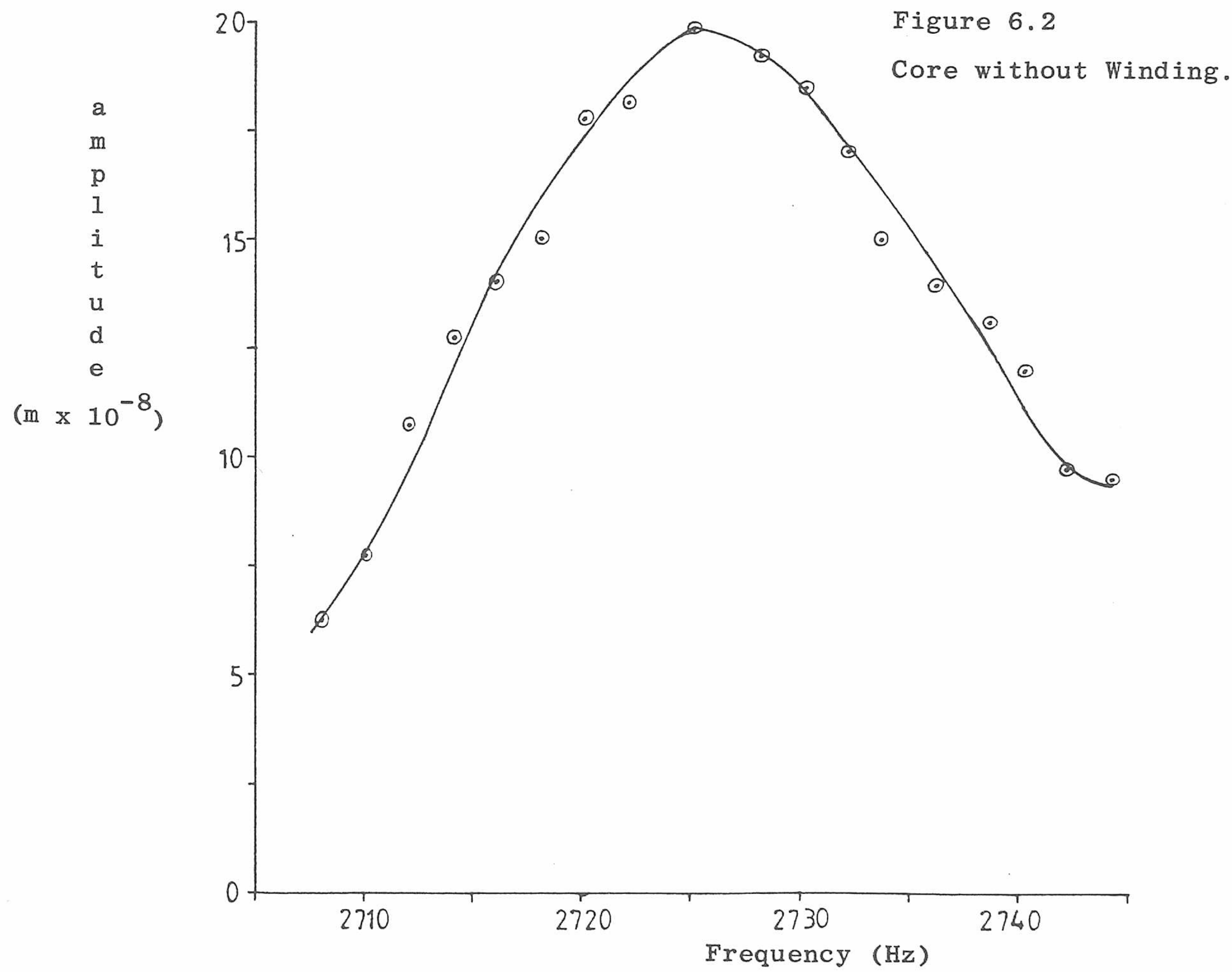
Figure 6.2
Core without Winding.
amplitude
(m x 10^{-8})
20
15
10
5
0
2710
2720
2730
2740
Frequency (Hz)

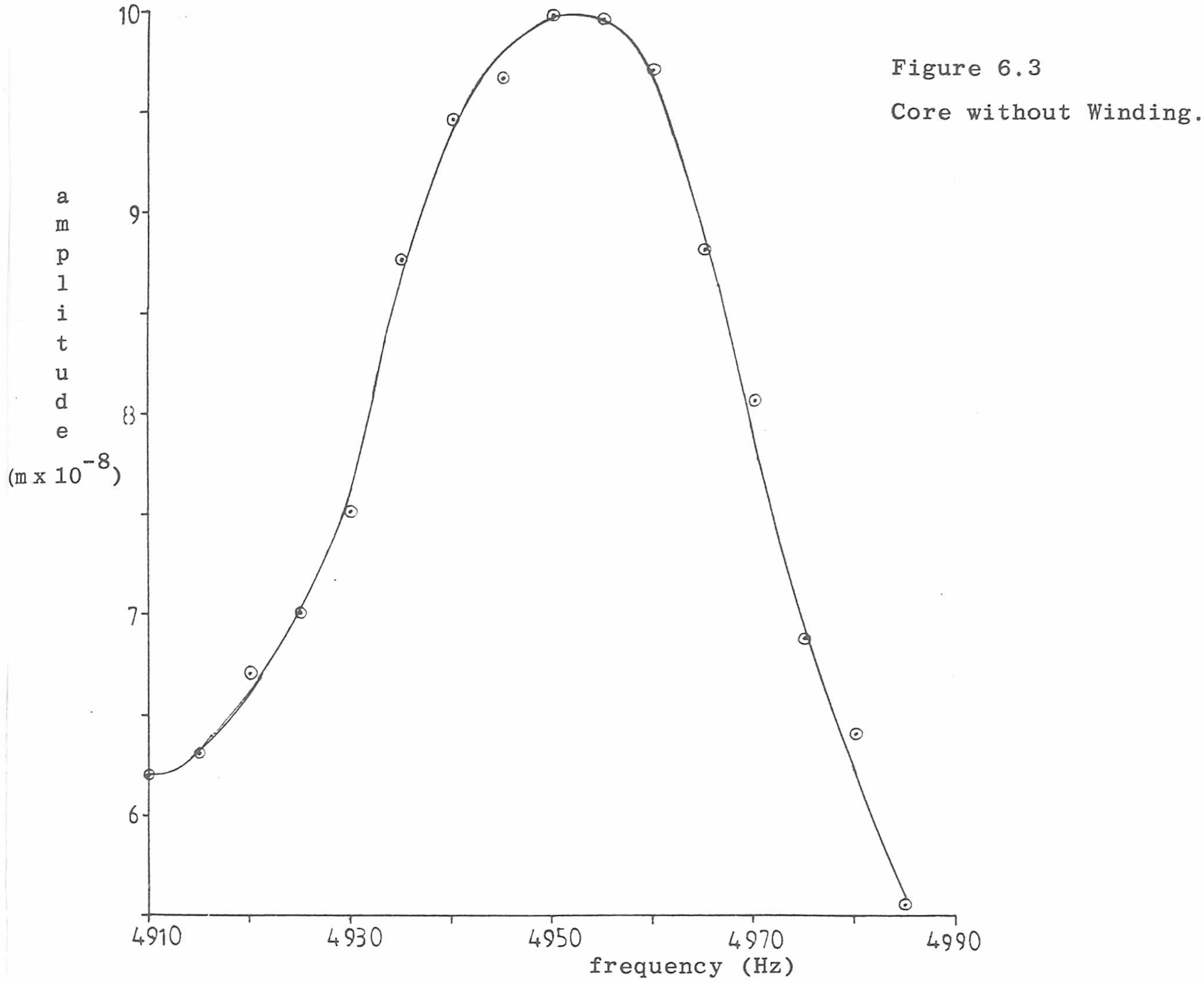

Figure 6.3
Core without Winding.
amplitude
(m x 10^{-8})
10
9
8
7
6
4910
4930
4950
4970
4990
frequency (Hz)

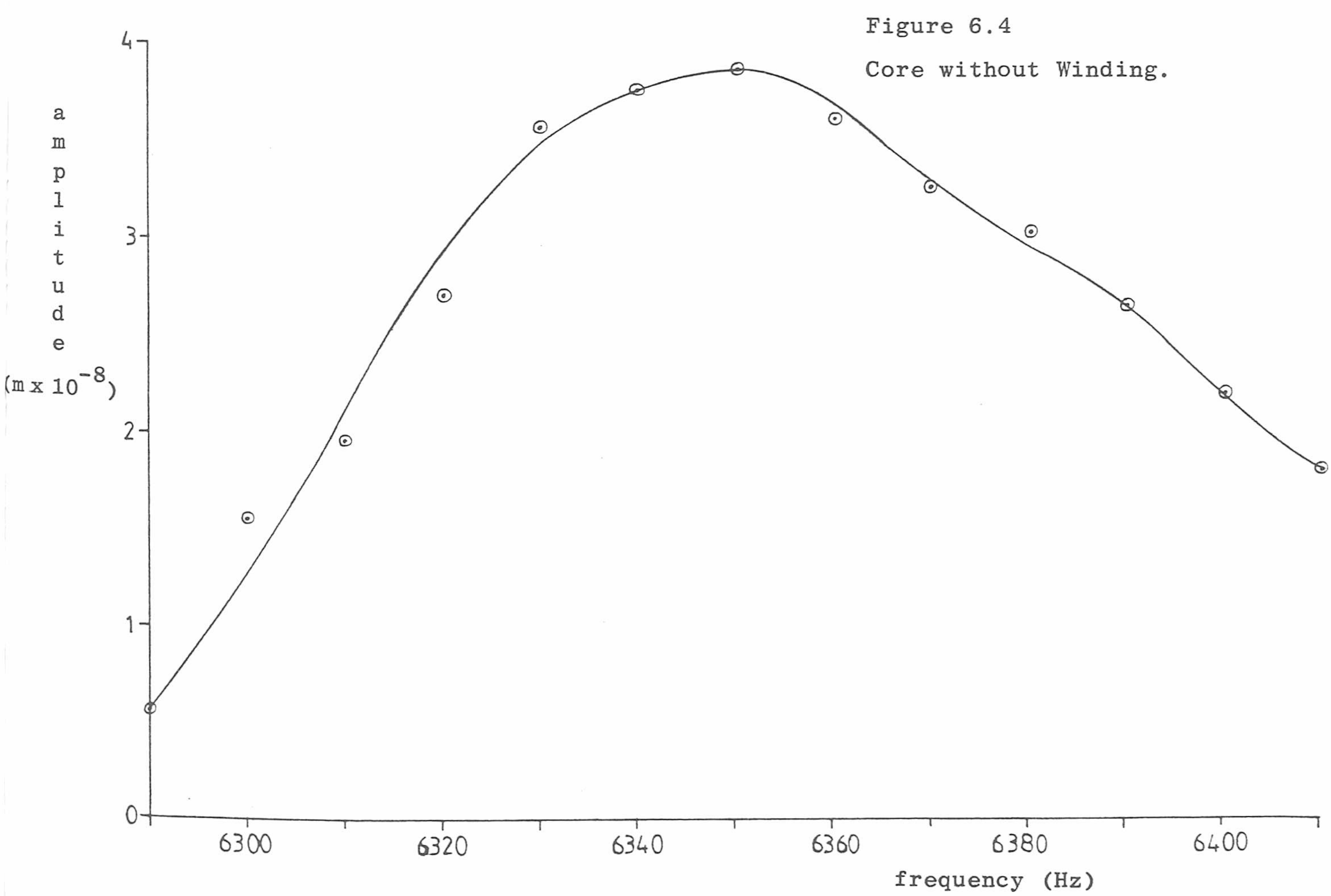

Figure 6.4
Core without Winding.
amplitude
(m x 10^{-8})
4
3
2
1
0
6300
6320
6340
6360
6380
6400
frequency (Hz)

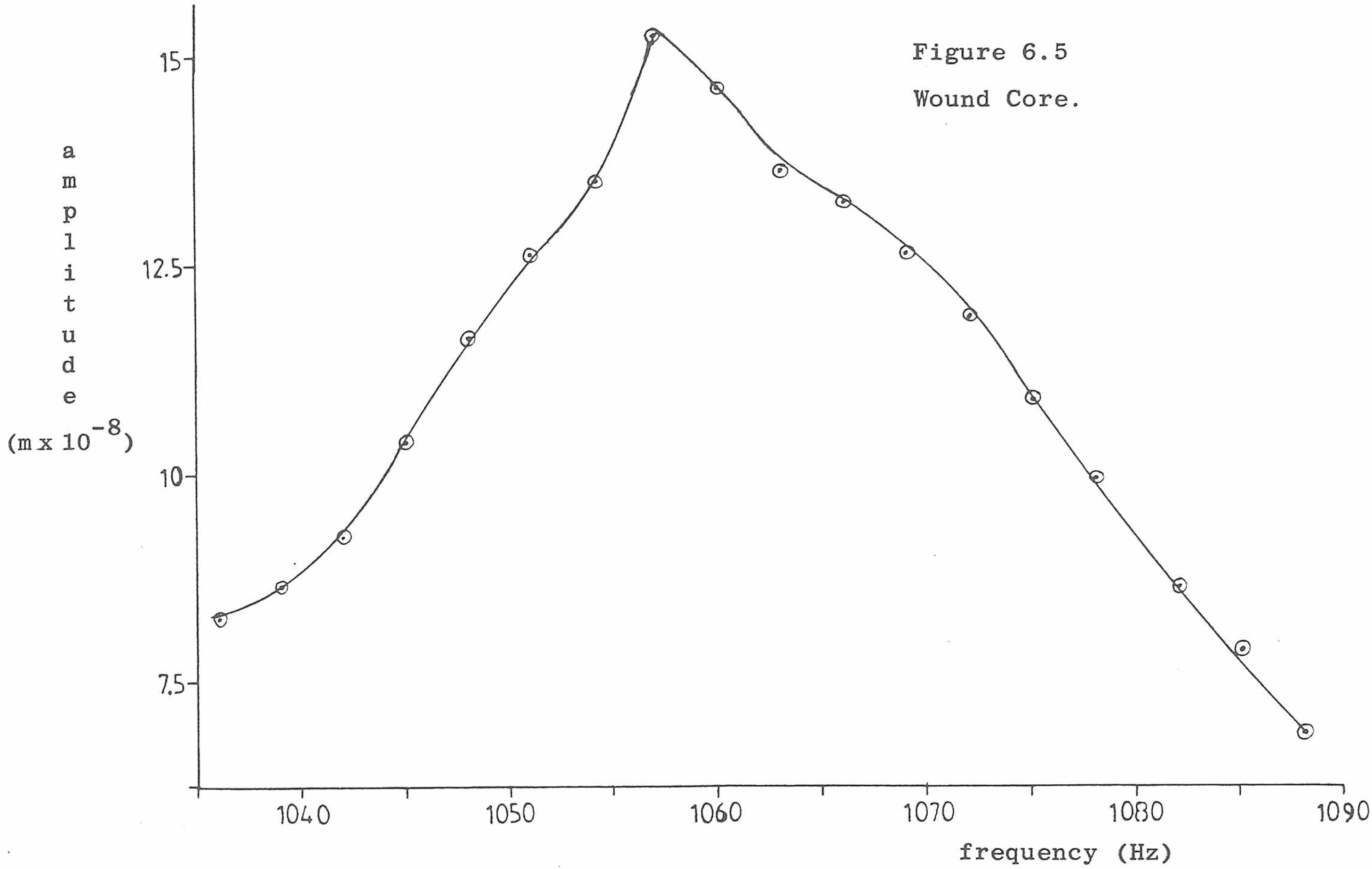

Figure 6.5
Wound Core.

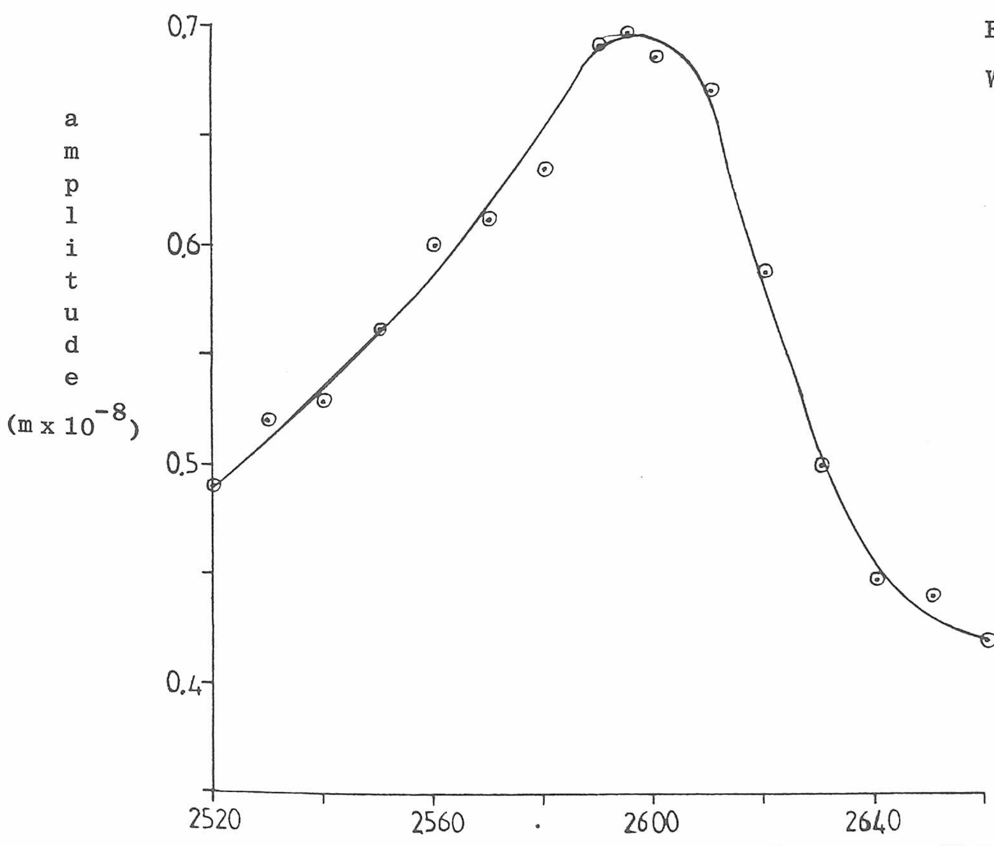

Figure 6.6
Wound Core.

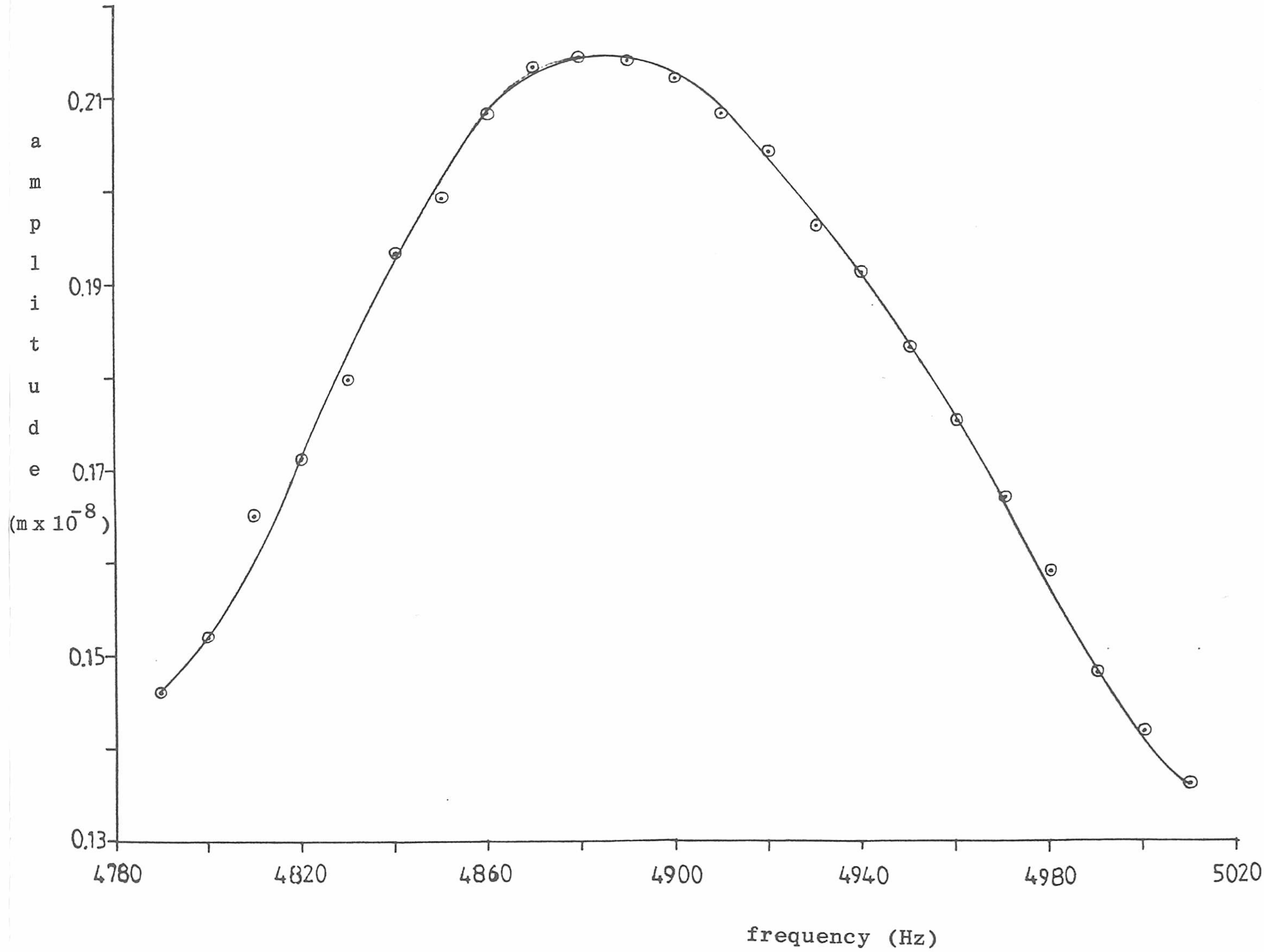

Figure 6.7
Wound Core.

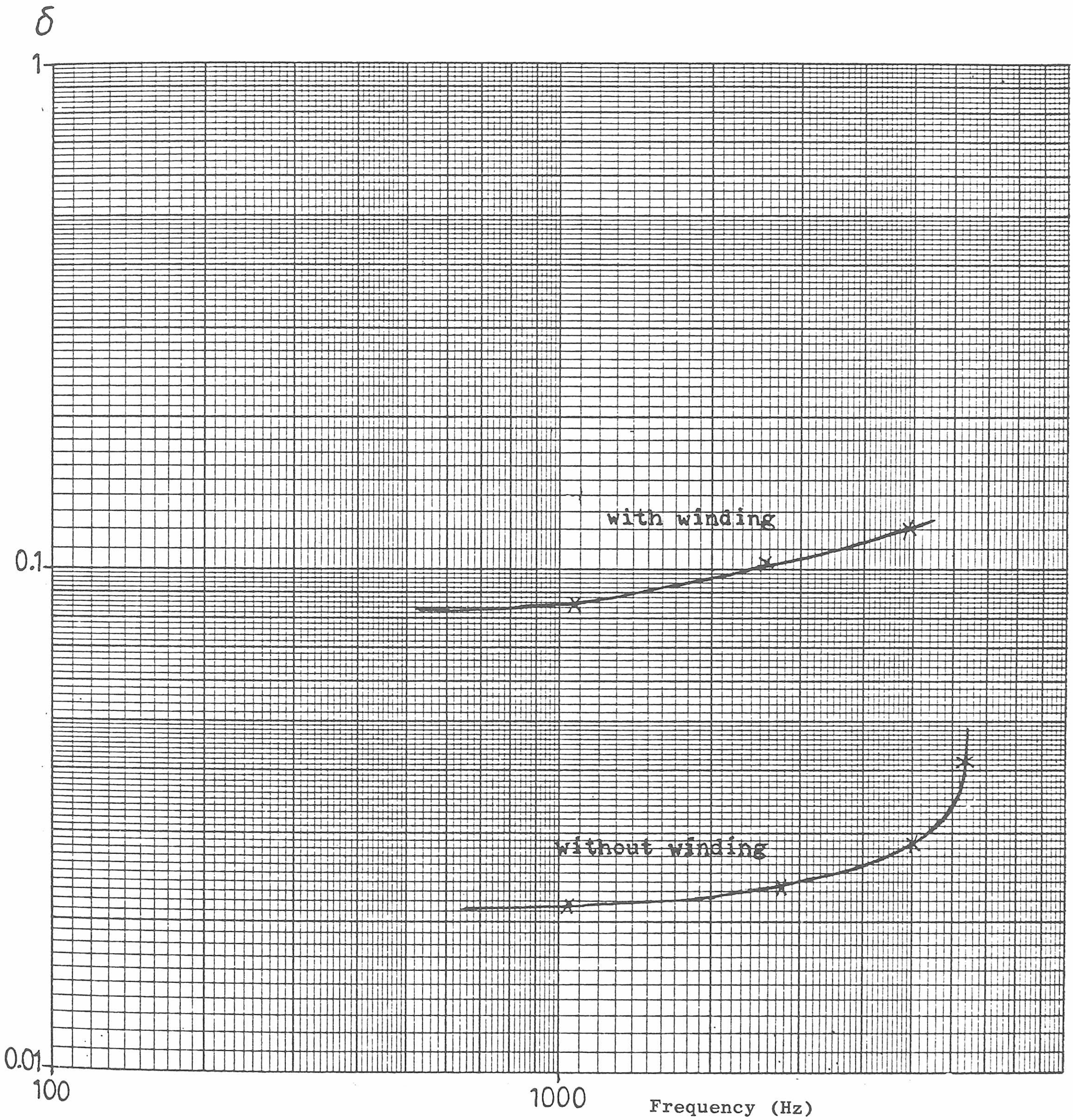

Figure 6.8

Variation of logarithmic Decrement with Frequency.

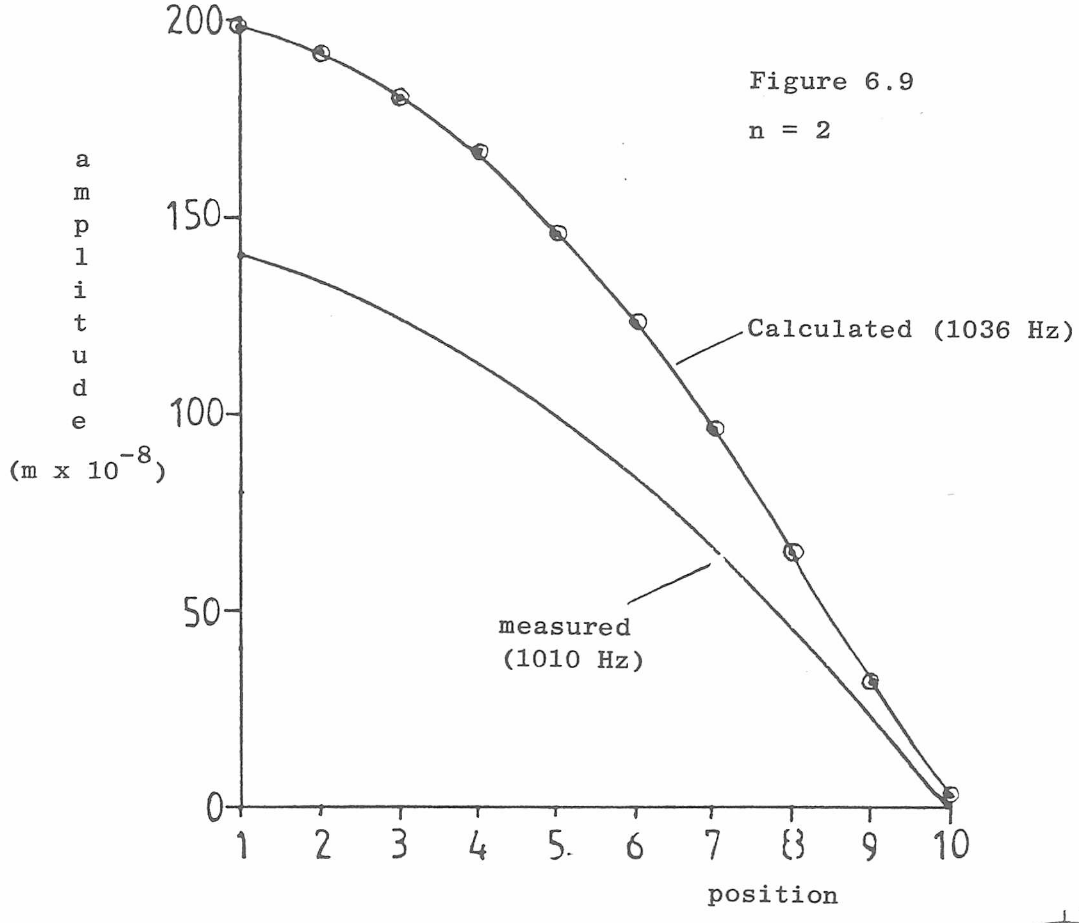
200
150
100
50
0
a
m
p
l
i
t
u
d
e
(m x 10^{-8})
Figure 6.9
n = 2
Calculated (1036 Hz)
measured
(1010 Hz)
1
2
3
4
5
6
7
8
9
10
position

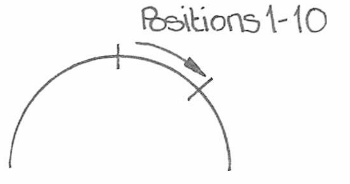
Positions 1-10

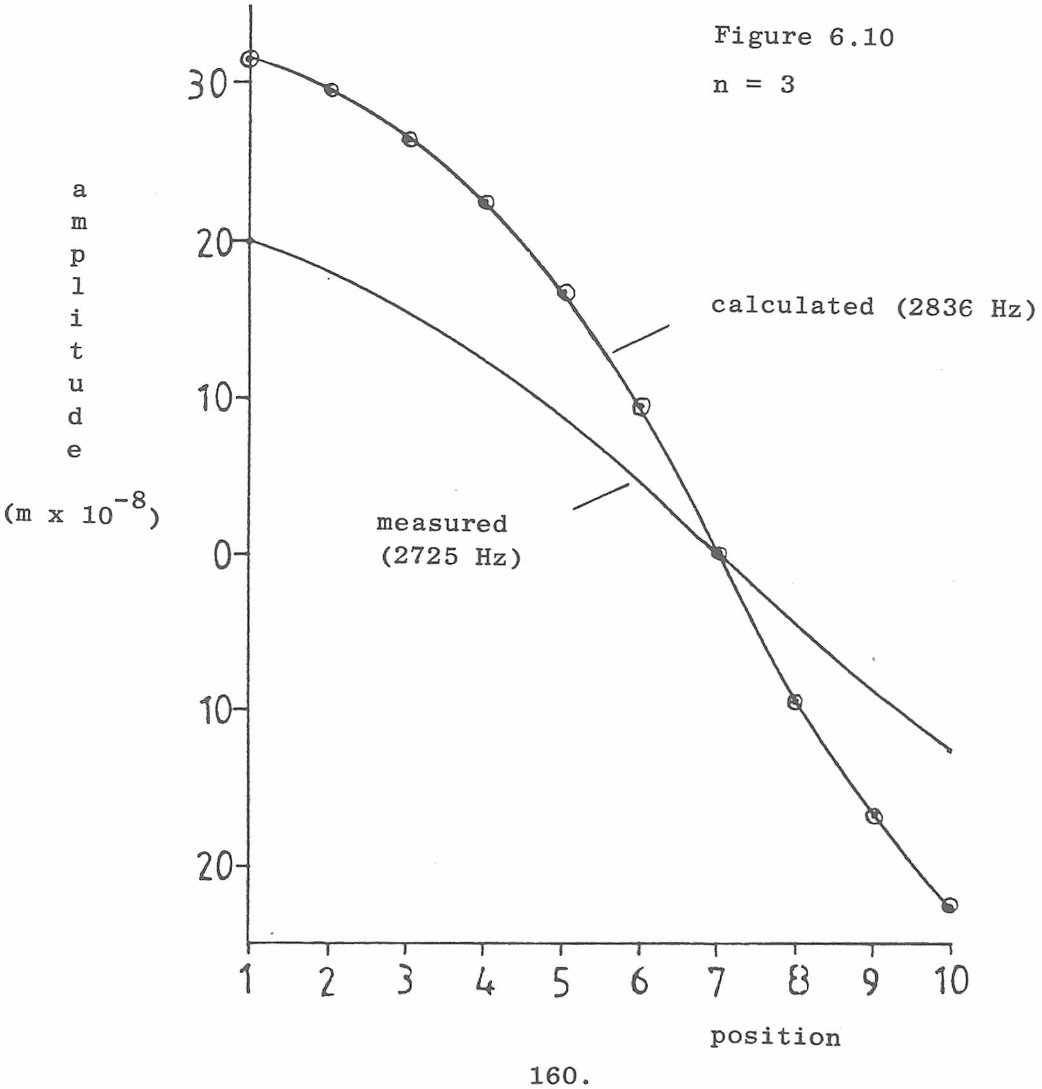
30
20
10
0
10
20
a
m
p
l
i
t
u
d
e
(m x 10^{-8})
Figure 6.10
n = 3
calculated (2836 Hz)
measured
(2725 Hz)
1
2
3
4
5
6
7
8
9
10
position

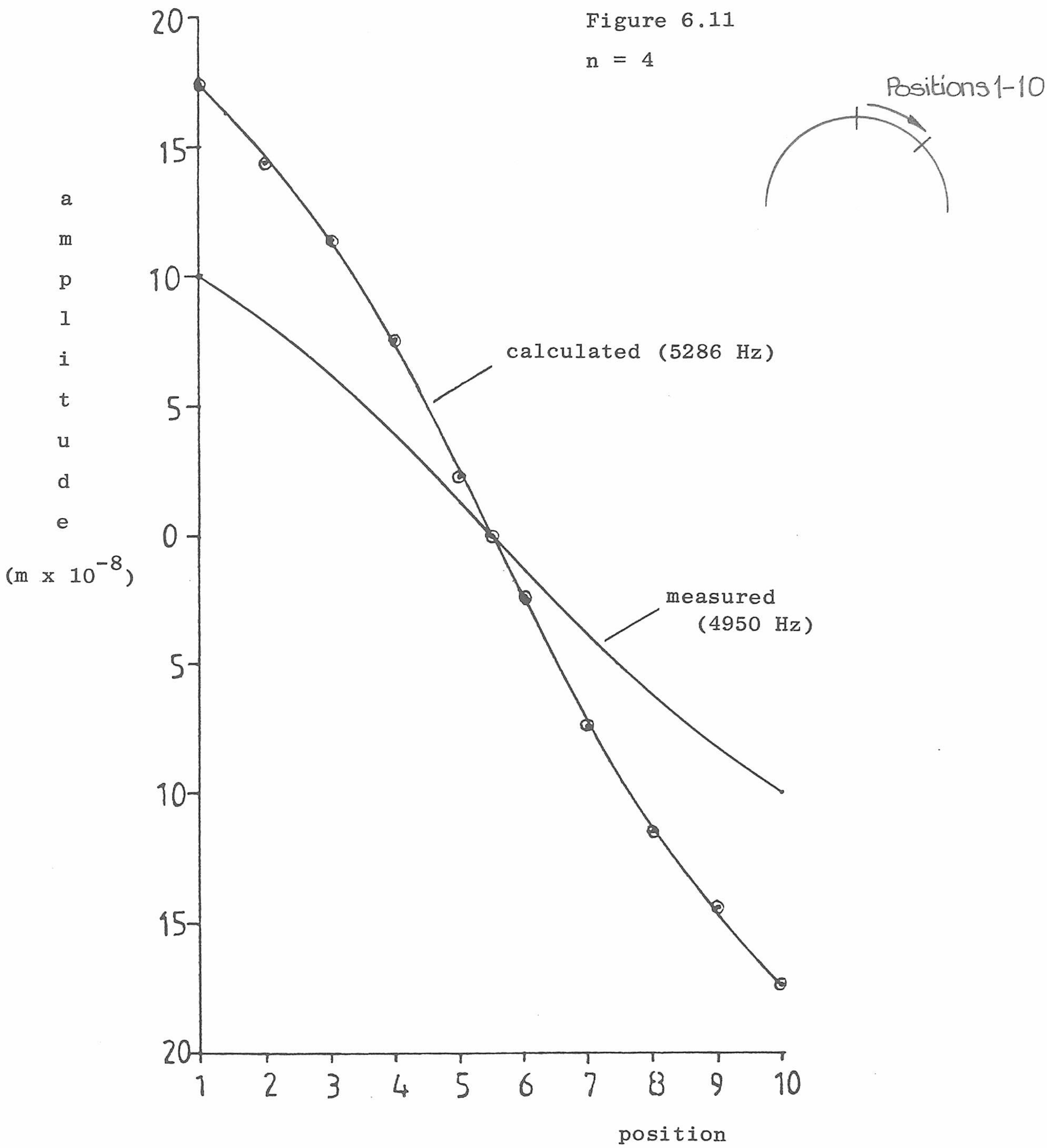
Figure 6.11
n = 4
Positions 1-10
amplitude
(m x 10^{-8})
20
15
10
5
0
5
10
15
20
calculated (5286 Hz)
measured
(4950 Hz)
1
2
3
4
5
6
7
8
9
10
position

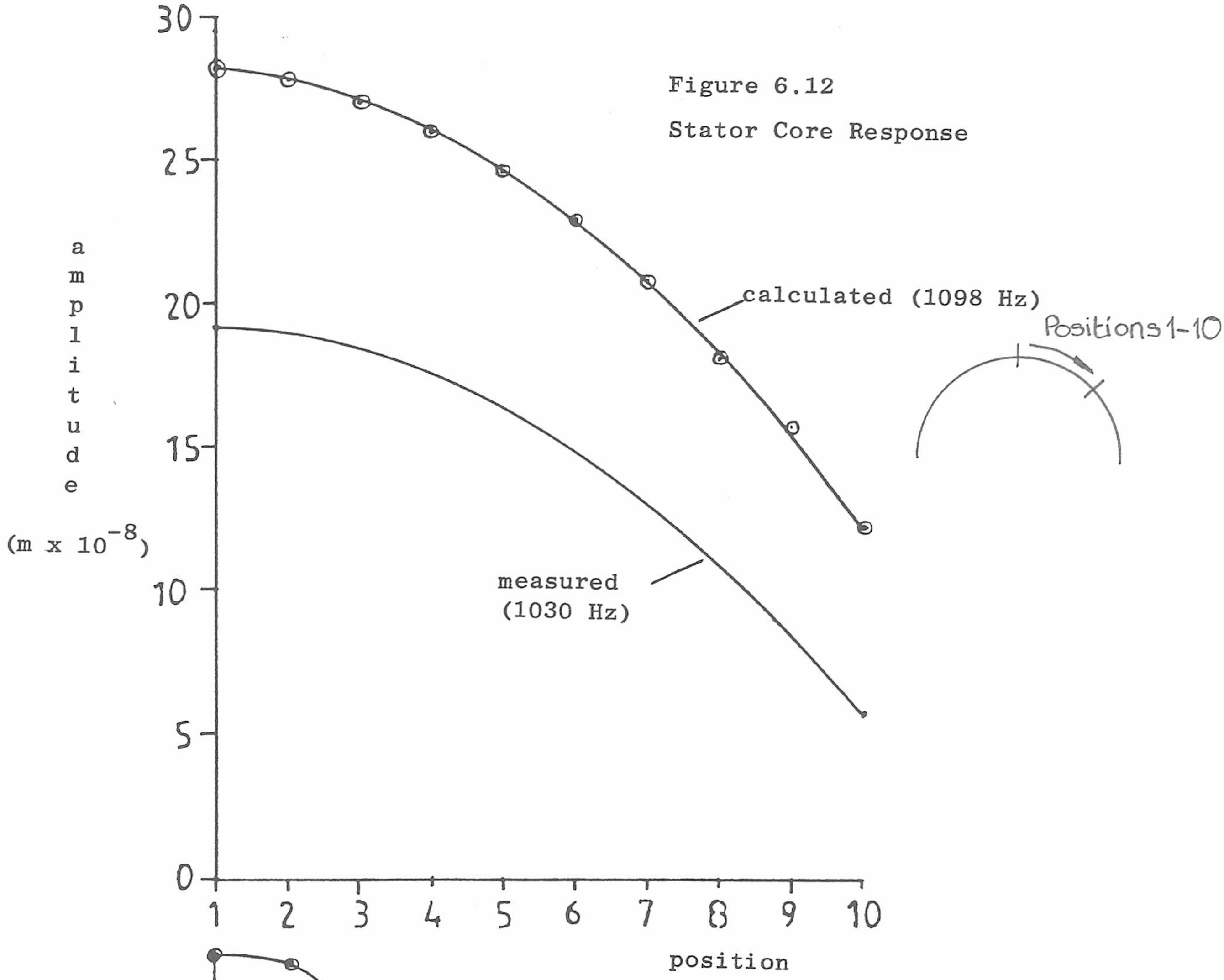

Figure 6.12

Stator Core Response

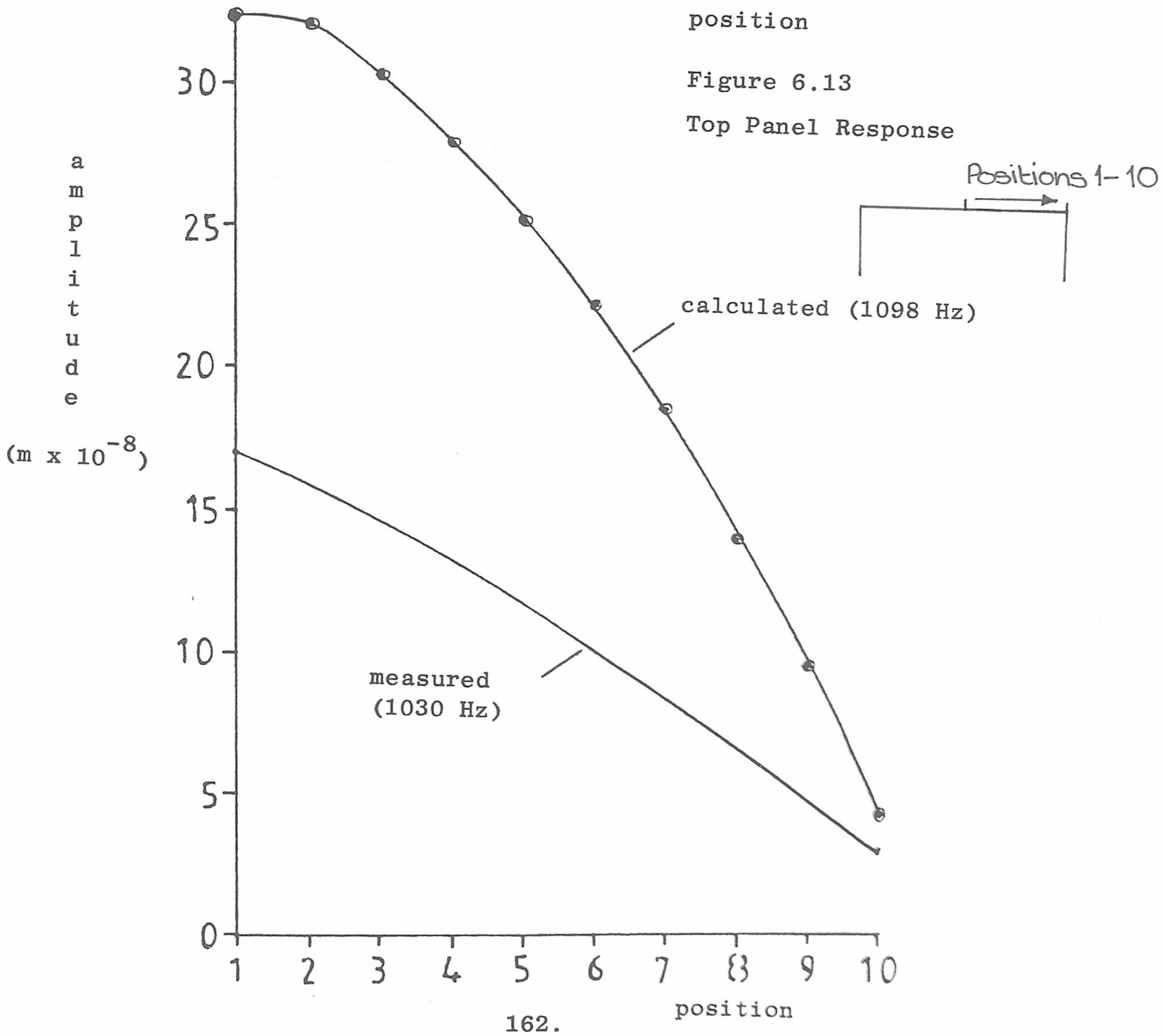

Figure 6.13

Top Panel Response

Figure 6.14

Stator Core Response

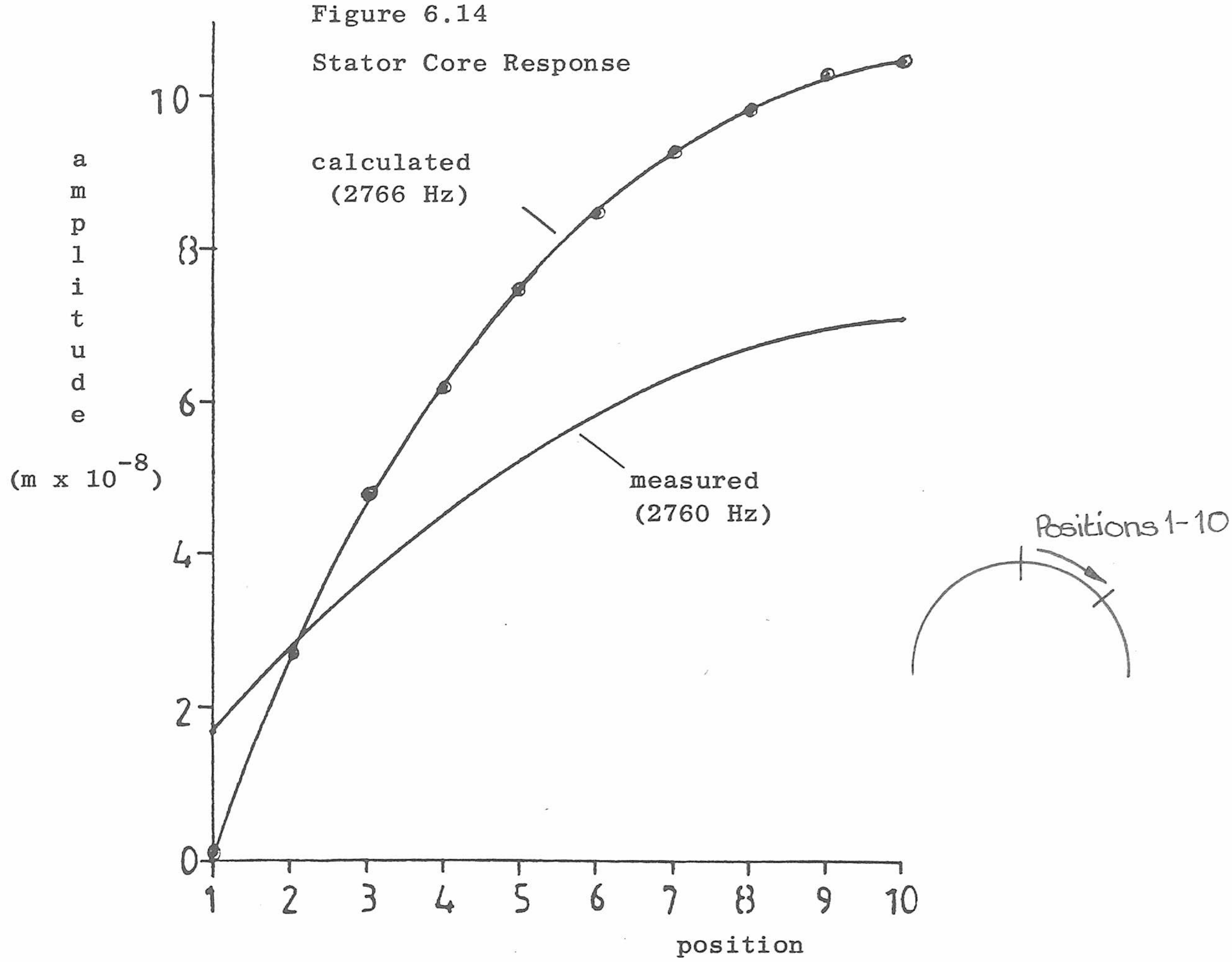

Figure 6.15

Top Panel Response

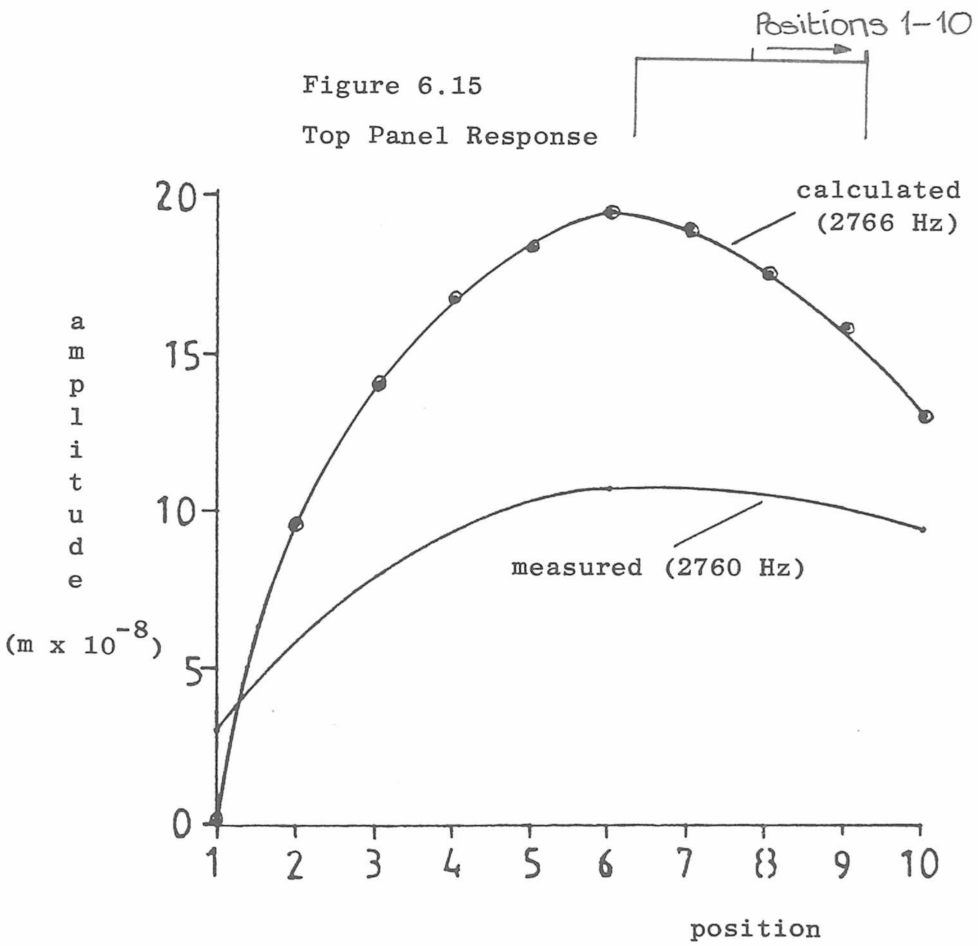

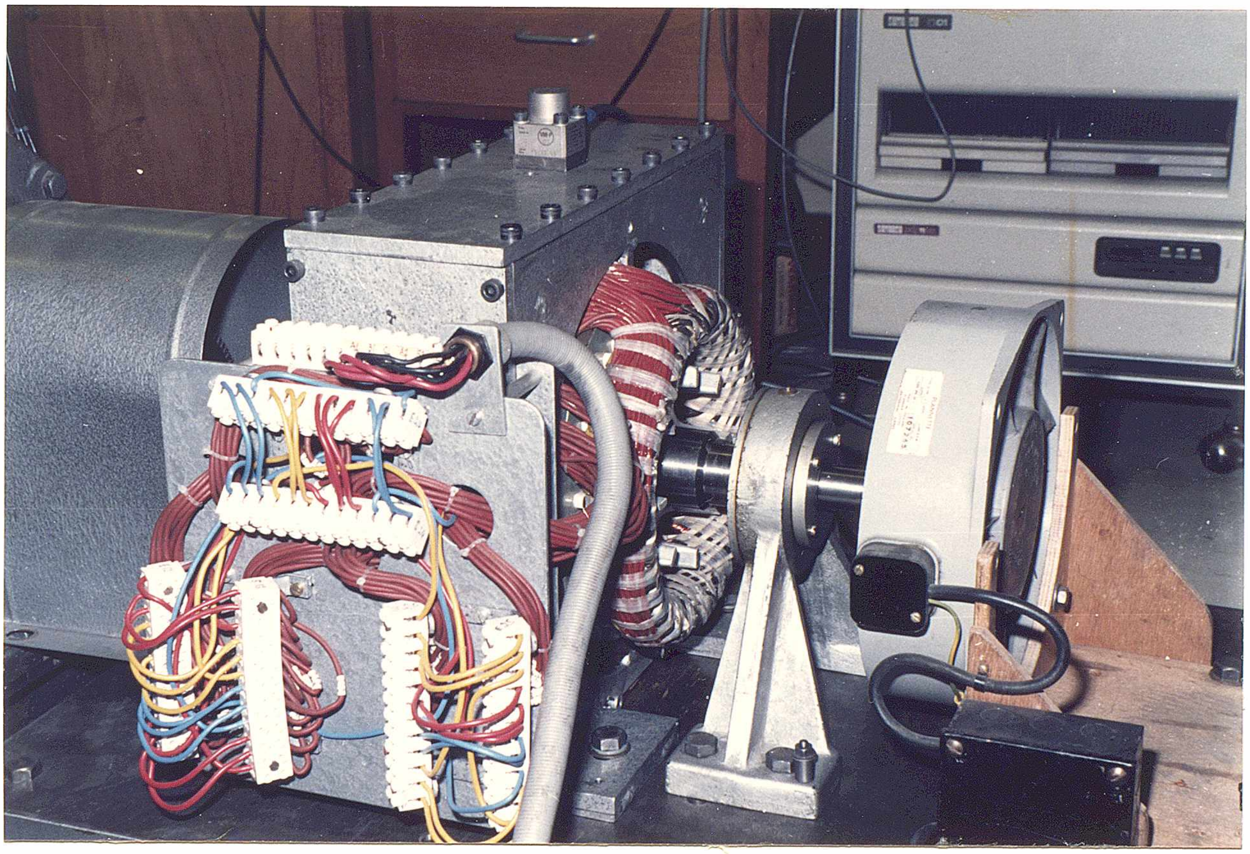

Figure 6.16

(a) The Installed Induction Motor Test Rig.

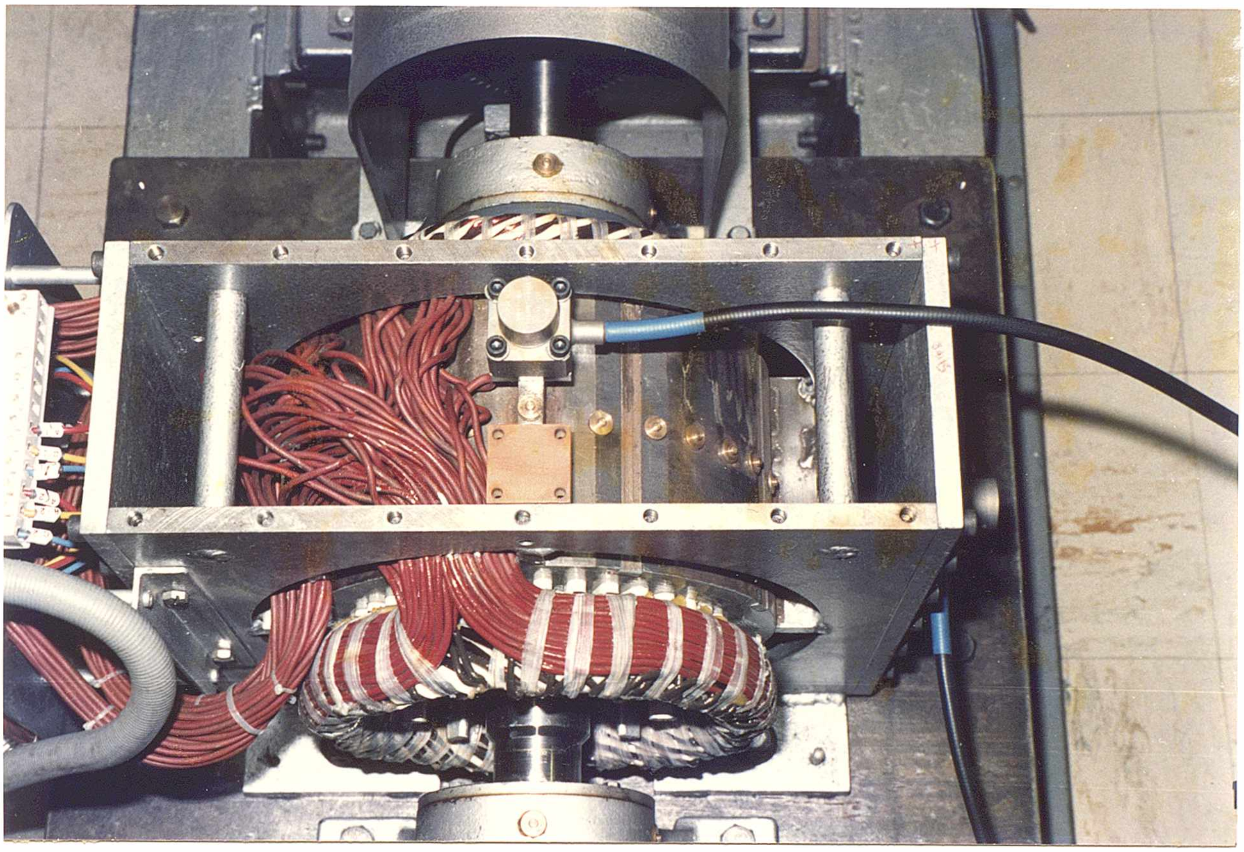

Figure 6.16

(b) The Test Rig with Top Panel Removed Showing
Core Accelerometer Mounting Positions.

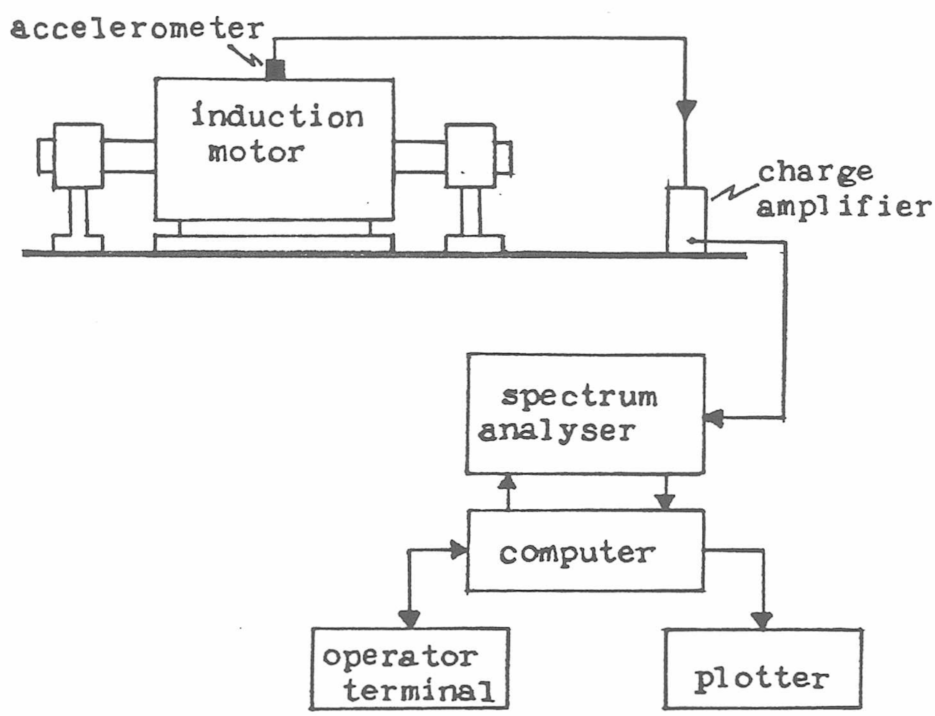

Figure 6.19

Experimental Arrangement for Measuring the Vibration Signal.

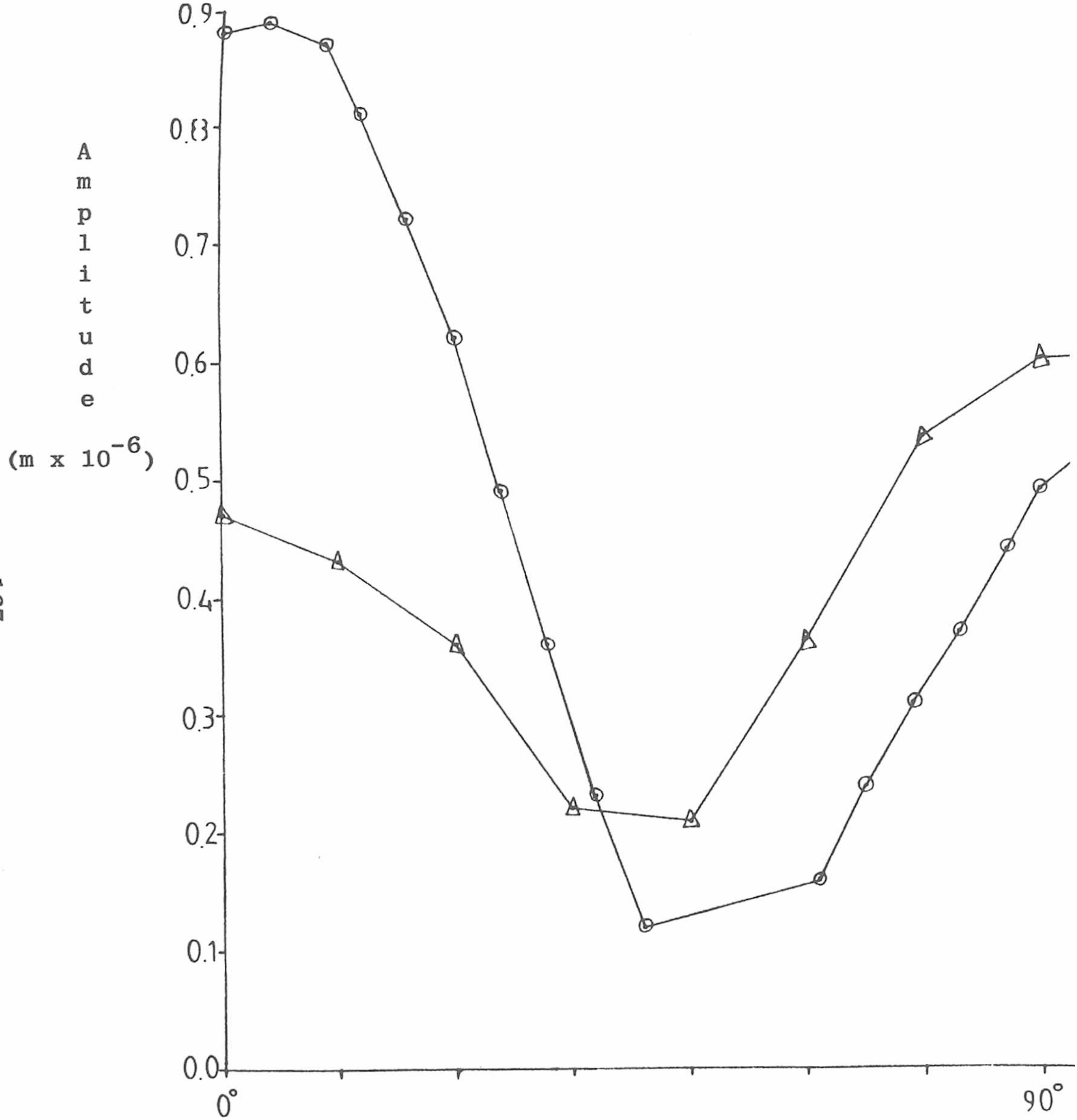

Figure 6.20

Vibratory Response Round the Stator Core at 100 Hz.

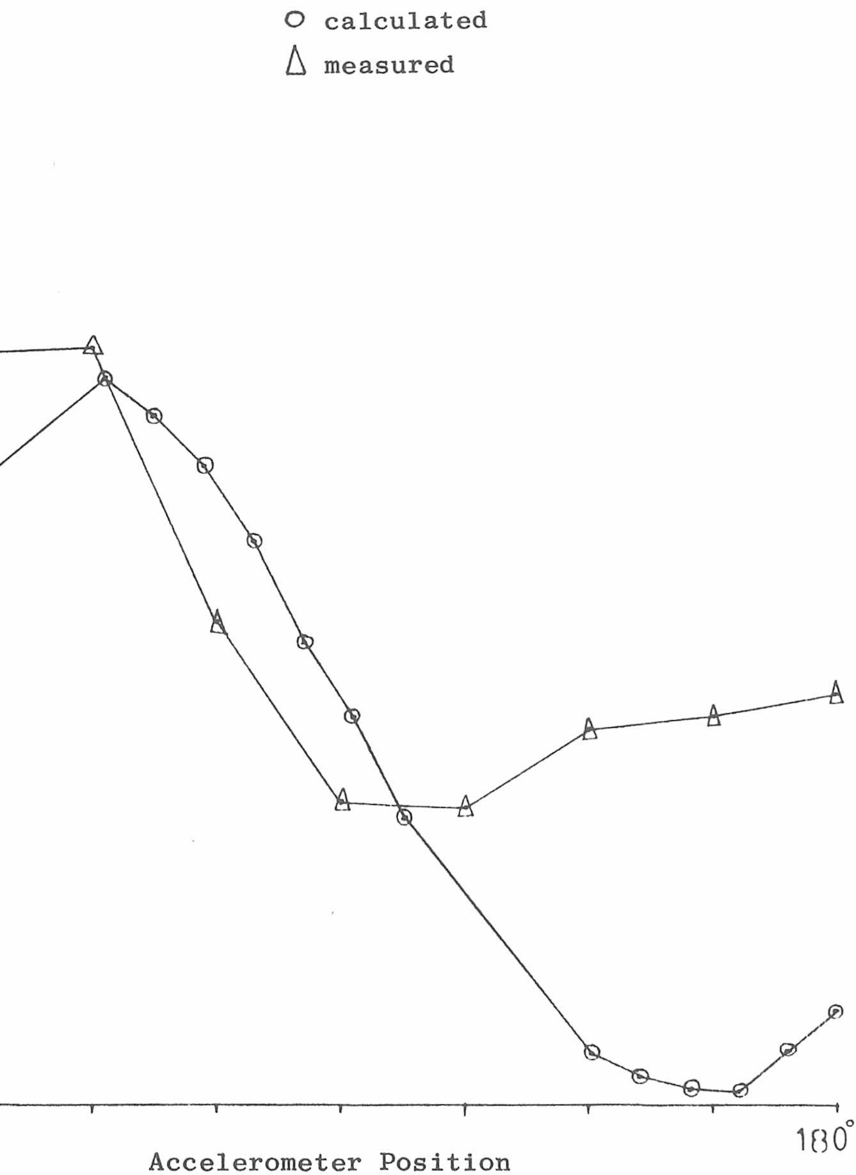
O calculated
Δ measured
180°
Accelerometer Position

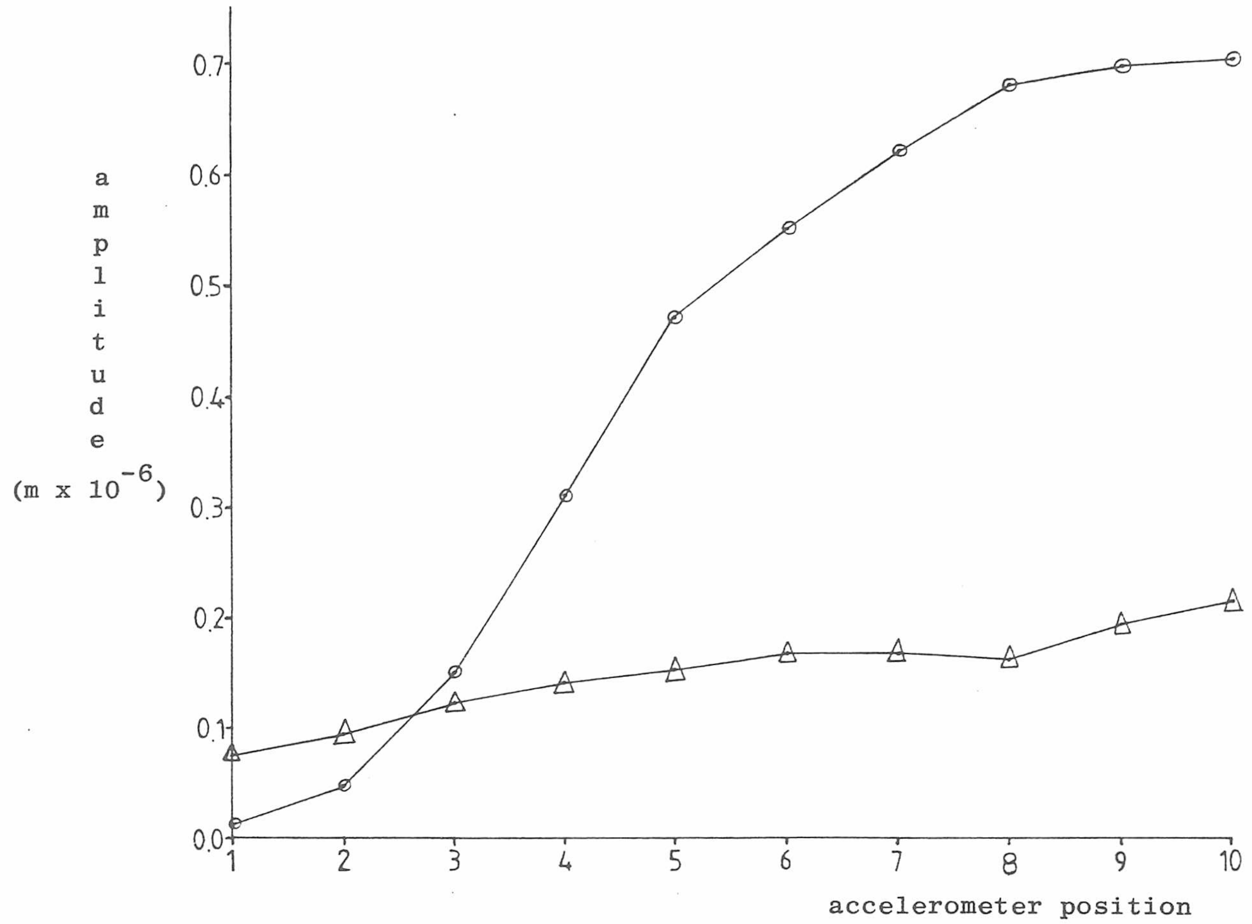

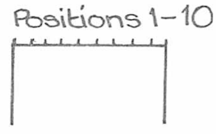

Figure 6.21

Vibratory Response on the Frame Top at 100 Hz.

○ calculated

△ measured

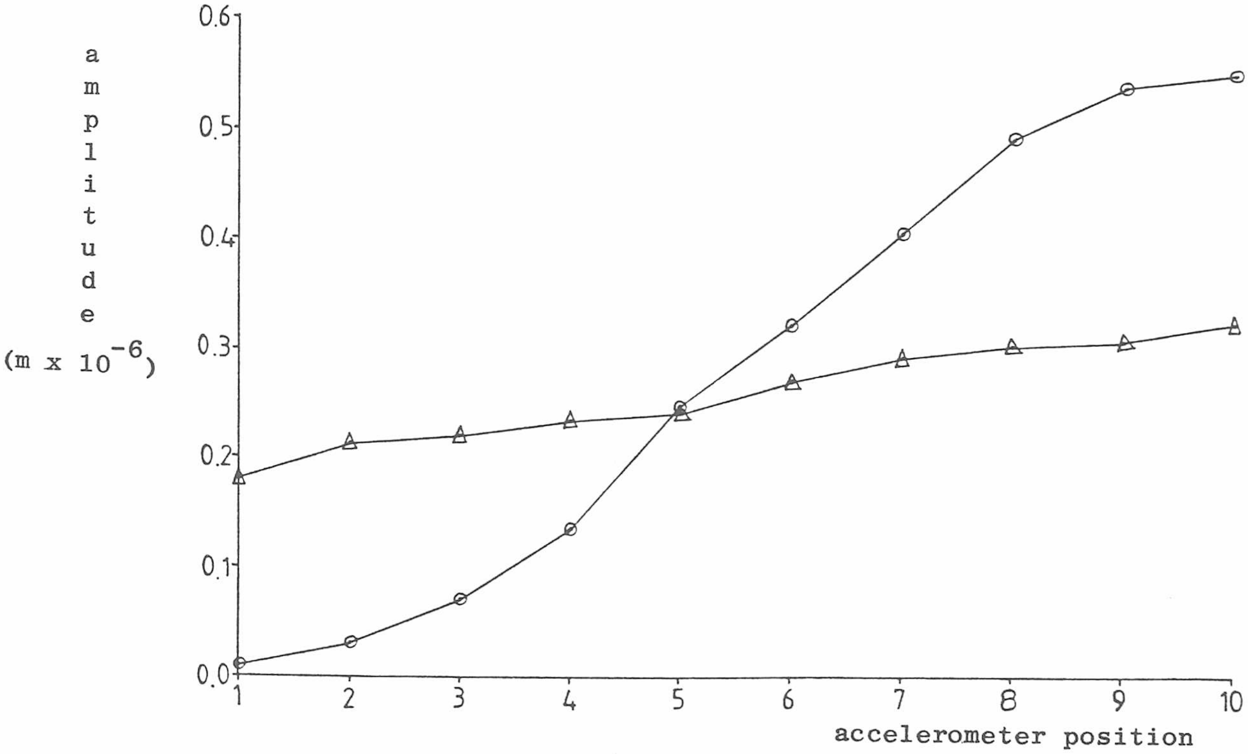

Figure 6.22

Vibratory Response on the Frame Side at 100 Hz.

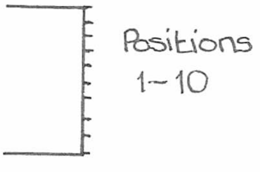

CHAPTER 7. THE EXPERIMENTAL ANALYSIS OF A FAULT CONDITION.

Research into the detection of voltage unbalance and single-phasing in three-phase induction motors (10) has shown that identifiable changes in the 100 Hz component of the radial stator vibration signal are indicative of these fault conditions. The experimental investigation involved measuring vibration levels on the frame of a typical small (11 kw) induction motor.

In this study, an experimental investigation is carried out into the effects of a single-phasing fault on the vibration signal measured on the stator core and frame of a three-phase induction motor test rig incorporating the model of the large motor stator assembly. The aim of the study is to examine the possibilities for monitoring core and/or frame vibration on a large motor stator structure to detect a single-phasing fault.

7.1 Single Phasing.

In the operation of three-phase induction motors, the extreme condition of unbalanced voltage, known as single-phasing, occurs when one of the supply lines is opened by a fuse blowing or when one of the phase windings develops an open circuit. With the loss of one phase, a counter-rotating flux is produced by the voltage unbalance. Under normal balanced operation, the motor develops a positive torque to cause the rotor to spin. A single-phasing fault will cause the motor to develop a negative torque. In order to satisfy the existing load condition, the motor must still produce the same net positive torque which means there must be an increased current in the two remaining phases. In fact the two phase currents must increase by 73% but may increase by 90% at full-load due to increased slip (59,60). A study by McPartland (61) shows that with a medium-sized motor operating unloaded, a single-phasing fault can produce phase currents greater than the normal full-load value. The damaging effects of a single-phasing fault are experienced to some extent at all load conditions and result from the windings overheating and causing thermal ageing, which can lead to insulation failure.

Although many protective devices exist, it is difficult to protect motors over the range of operating conditions (no-load to full-load). Gleason (60) suggests that the phase balance, instantaneous negative sequence overcurrent, and phase failure relays provide the best protection at light loads. However the deficiencies of such protection schemes are discussed by Shan Griffith (62) who reports that the increased current due to single-phasing may not be sufficient to initiate tripping action and that the adequacy of protection will be dependent on the initial shaft load. Vincent (13) reported that 12% of failures from a sample of 380 standard a.c. drives were due to single-phasing. It would seem that the adequate protection of induction motors could only be provided by a scheme incorporating early detection of a single-phasing fault at all load conditions.

Two researchers have investigated the development of on-line condition monitoring strategies to warn of an open phase. Penman (63) has detected single-phasing from changes in the axial flux spectrum and Leonard (10) has shown that changes in the 100 Hz component of the radial vibration spectrum are produced due to a single-phasing fault. The vibration signal can best indicate single-phasing at optimum sensing positions which will depend on the type of frame construction and the accessibility of the core pack. Since the 100 Hz vibration component has amplitude independent of the motor load condition, a detection strategy based on analysing the vibration signal is valid for all load conditions.

7.2 The Radial Force when One Phase is Open-Circuited.

In Chapter 6 the fundamental radial magnetic force wave was determined for a balanced three-phase supply. The forcing function was a time and space dependent travelling wave given by:

$$F = k\left[1 - \cos\left(2\omega t - \frac{2\pi x}{\tau}\right)\right].$$

For a single-phasing condition where one of the phases develops an open-circuit, the three phase currents for a Δ-connected winding are:

$$I_a = I_m \sin \omega t$$

$$I_b = -\frac{I_m}{2} \sin \omega t$$

$$I_c = -\frac{I_m}{2} \sin \omega t \quad .$$

Therefore the mmf's are:

$$M_a = M_m \sin \omega t \cos \frac{\pi x}{\tau}$$

$$M_b = -\frac{M_m}{2} \sin \omega t \cos \left(\frac{\pi x}{\tau} - 2\pi/3\right)$$

$$M_c = -\frac{M_m}{2} \sin \omega t \cos \left(\frac{\pi x}{\tau} + 2\pi/3\right) .$$

The total mmf in this case is:

$$M = \frac{3}{2} M_m \sin \omega t \cos \frac{\pi x}{\tau} \quad .$$

Again for constant permeance,

$$B = \frac{3}{2} M_m \Lambda \sin \omega t \cos \frac{\pi x}{\tau}$$

and the radial air-gap force is:

$$F = \frac{9 M_m^2 \Lambda^2}{8\mu_o} \sin^2 \omega t \cos^2 \frac{\pi x}{\tau} .$$

During a single-phasing fault, the force acting across the air-gap has the form:

$$F = \frac{K}{2}\left[(1 + \cos \frac{2\pi x}{\tau}) - \cos 2\omega t \ (1 + \cos \frac{2\pi x}{\tau})\right] .$$

In this case the force is a standing wave of twice supply frequency. (47).

7.3 Frequency Components in the Vibration Signal.

In the analysis of normal and single-phased operation, the 100 Hz forcing function is derived. In reality the radial forcing function is made up of a fundamental (100 Hz) component and higher harmonics due to slot harmonics in the airgap flux. If single-phasing can be detected by changes in the 100 Hz vibration component then it may also be detected at other harmonic frequencies. Therefore the experimental investigation into the effects of a single-phasing fault on stator vibration levels will measure acceleration amplitudes at the fundamental frequency and at the first three slot harmonic frequencies. The first four expected frequency components are given by:

$$f_1 = 2f_0$$

$$f_2 = f_0(2 - R(1-s)/p)$$

$$f_3 = f_0(R(1-s)/p)$$

$$f_4 = f_0(2 + R(1+s)/p)$$

(14, 47, 58) .

At no-load the slip is approximately zero.

There are 36 stator slots and 28 rotor slots.

Therefore the expected frequency components in the vibration signal at no-load are:

f_1 = 100 Hz

f_2 = 600 Hz

f_3 = 700 Hz

f_4 = 800 Hz.

Measuring the response at each of these frequencies will highlight the differences between monitoring core vibration and frame vibration to detect a motor fault and will determine how each vibration component changes due to a single-phasing fault.

7.4 Experimental Tests.

The experimental analysis can be divided into three groups:

(1) Vibration levels measured at central positions around the core back.

(2) Vibration levels measured at central positions along the frame panels.

(3) Vibration levels measured on a side panel and top panel at axial positions along the length of a core bar.

The accelerometer positions corresponding to each group are illustrated in Figure 7.1 .

For each group four sets of vibration measurements are recorded:

(a) Normal operation.	motor operating at no-load.
(b) Phase A open-circuited.	
(c) Phase B open-circuited.	
(d) Phase C open-circuited.	

Each phase is opened in turn so that any differences in vibratory response between the three operating conditions can be observed.

All the experimental tests are carried out with the motor running at no-load so that the sensitivity of the vibration signal to a single-phasing fault can be investigated without the motor becoming greatly overheated.

Response versus position curves are plotted for each operating condition at 100 Hz, 600 Hz, 700 Hz and 800 Hz.

7.5 Discussion.

Figures 7.2 (a) and (b), show the vibratory response spectra at no-load measured at a transducer position on the frame side panel for the two operating conditions being considered. The most notable difference between normal operation and one open phase is the increase in the 100 Hz vibration component. The greatest increase at this particular transducer position is 17 dB's. The increase due to the fault varies slightly depending on which phase is open-circuited. From measurements taken around the frame, this increase in the 100 Hz component was typical of vibration levels transmitted to the side panel due to the fault condition. However the same magnitude of increases were not found everywhere. Figures 7.3 to 7.5 are plots of vibration levels at 100 Hz varying with transducer position around the core, around the frame and along the core bars.

Figure 7.3 illustrates the wave pattern of the twice supply frequency component of the forcing function around half of the core back, from the centre top (0^o) to the centre bottom (180^o). It has been reported previously (10) that the standing wave vibration pattern around the core due to one open phase is independent of speed and pole number. It was also reported that ideally the vibration levels will be independent of which phase is open. In practice there is some variation in the wave pattern between losing phase A, B or C. This is expected since the supply is not likely to be perfectly symmetrical and any unbalance will cause the force waves to be more complex than the theoretical ideal. However the trend in measured values is as expected. The nodal positions of the forcing function occur at 0^o and 180^o where there is very little if any distinction between normal operation and the fault condition. Good transducer positioning for fault detection in this case would be between +30^{o} and +90^{o}. The maximum recorded increase in the response at 100 Hz was 18 dB's (or 0.6 m/s^2) which represents a vibration level due to one open phase being 8 times the normal level. More typically, increases by a factor of 3 or 4 were measured over this sensing range.

The vibratory force waves transmitted from the core to the outer frame at 100 Hz excite vibration levels on the side panel and top panel which are illustrated graphically in Figure 7.4. Since one of the nodal points of the force wave on the core occurs at 0^{o} and higher vibration levels are measured between 30^{o} and 90^{o}, it is reasonable to expect that fault detection would be more effective on a side panel rather than along the frame top. In fact, along each frame panel the 100 Hz vibration component maintains near constancy due to a fault condition. The level of vibration amplitude increases, associated with losing one phase, are large (typically 0.45 m/s^2) on a side panel and small (typically 0.08 m/s^2) on the top panel. During normal operation the average vibration levels measured on the frame panels (side panel: 0.08 m/s^2, top panel: 0.05 m/s^2) were less than the average level measured on the core (0.14 m/s^2). The average vibration levels due to a single-phasing fault were: side panel: 0.56 m/s^2, top panel: 0.14 m/s^2 and core: 0.48 m/s^2. Firstly this suggests that the core bars, feet and bed-plate act as good vibration transmitters. Secondly, it is possible to conclude that vibration monitoring to detect a single-phasing fault can best be carried out in this case by positioning a transducer on the frame side panel. The detectable changes in the 100 Hz component at the inception of the fault are more significant than those measured on the core, firstly due to their greater magnitude and secondly due to the ease of choosing an accelerometer mounting position which can be situated at any central position along the side panel with equal reliability of sensing the fault. The added advantage of monitoring frame vibration is that the stator frame is accessible for mounting transducers, unlike monitoring core vibration where the monitoring sensors may have to be introduced at the manufacturing stage or even at the design stage.

The investigation into vibration level changes at 100 Hz measured on the stator frame along the length of the core bars showed larger increases in amplitude due to the fault at positions on the side core bar compared to the top core bar (Figure 7.5). The respective average increases were:

side core bar: $0.39\ m/s^2$, top core bar: $0.15\ m/s^2$.

These results would also confirm that transducer positions on the frame side panel are the most suitable for reliable single-phasing fault detection.

The vibration amplitude versus transducer position curves at the other three higher frequency components of the vibration signal are plotted in Figures 7.6 to 7.14 . The only other frequency component of the forcing function which shows significant quantifiable changes in vibration levels due to one open phase is the 700 Hz component. At this frequency the good fault sensing positions are on the frame top panel and on the core between 0^o and 60^o (Figures 7.9 and 7.10). The average measured increases in vibration amplitude due to the fault condition are: core: $0.10\ m/s^2$ and top panel: $0.16\ m/s^2$. It may therefore be useful to monitor 700 Hz stator radial vibration as back-up information for a strategy based around 100 Hz vibration monitoring.

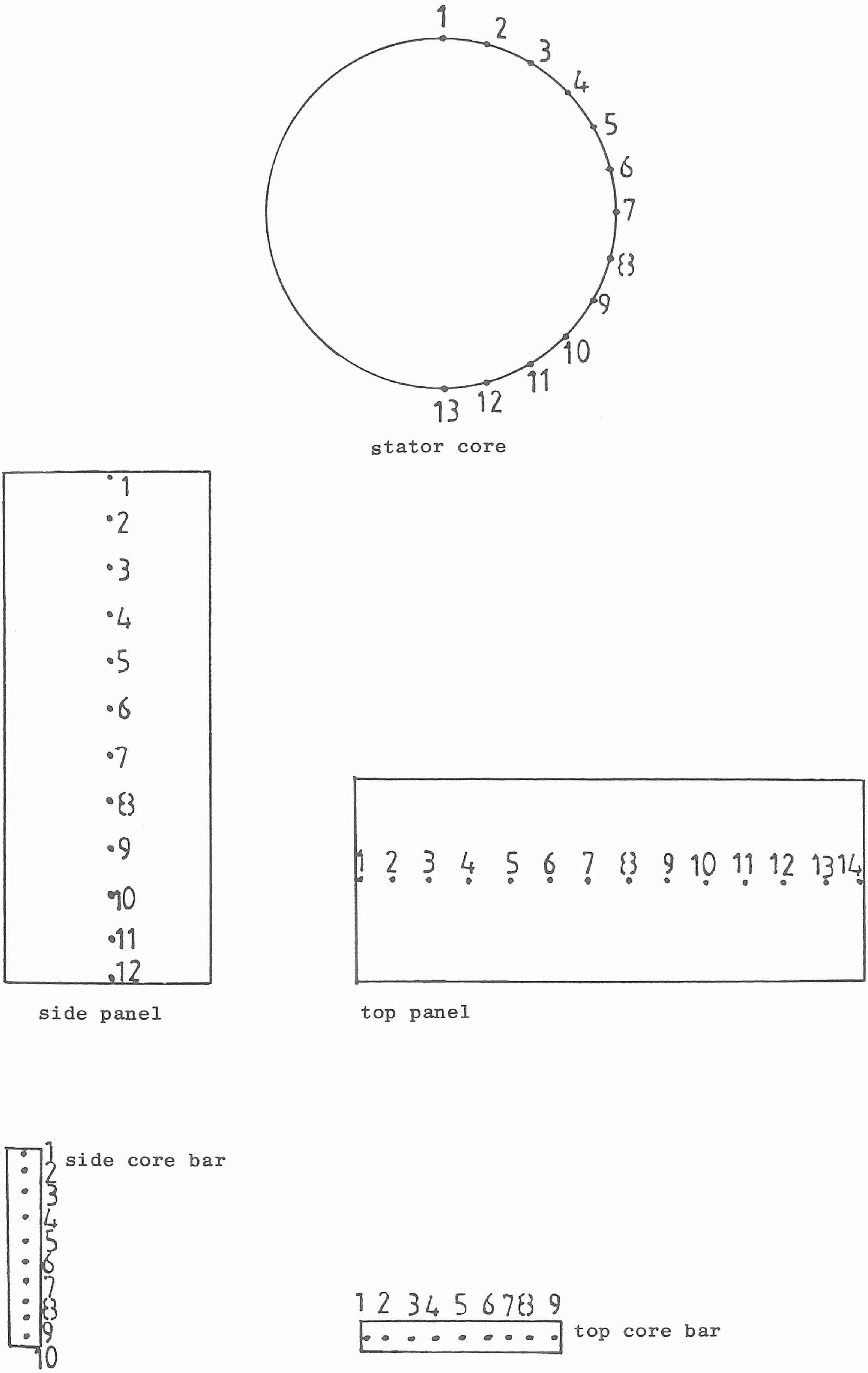

Figure 7.1

Accelerometer Sensing Positions.

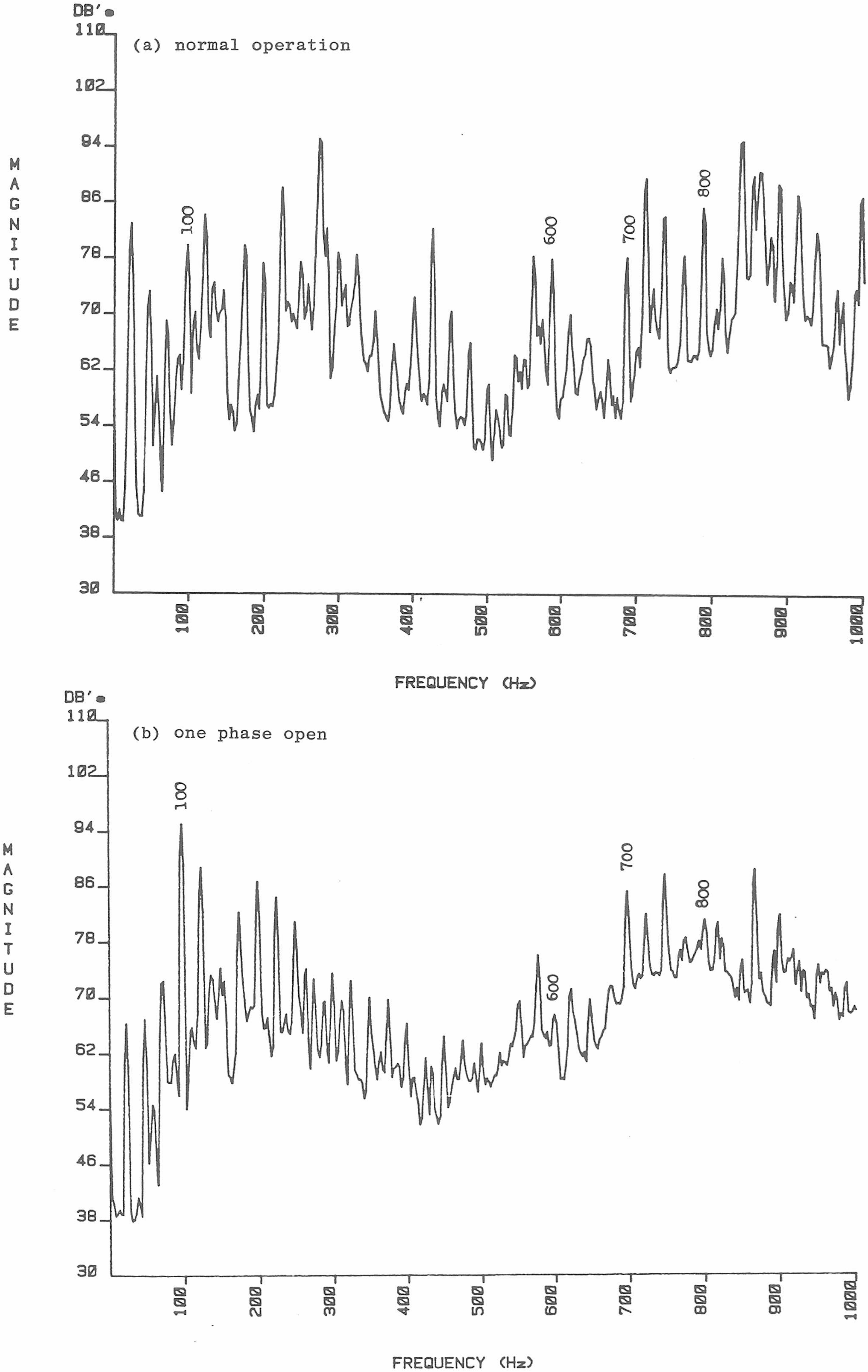
DB's
(a) normal operation
MAGNITUDE
FREQUENCY (Hz)
(b) one phase open
MAGNITUDE
FREQUENCY (Hz)

Figure 7.2

Figure 7.3

100 Hz Vibration on the Core.

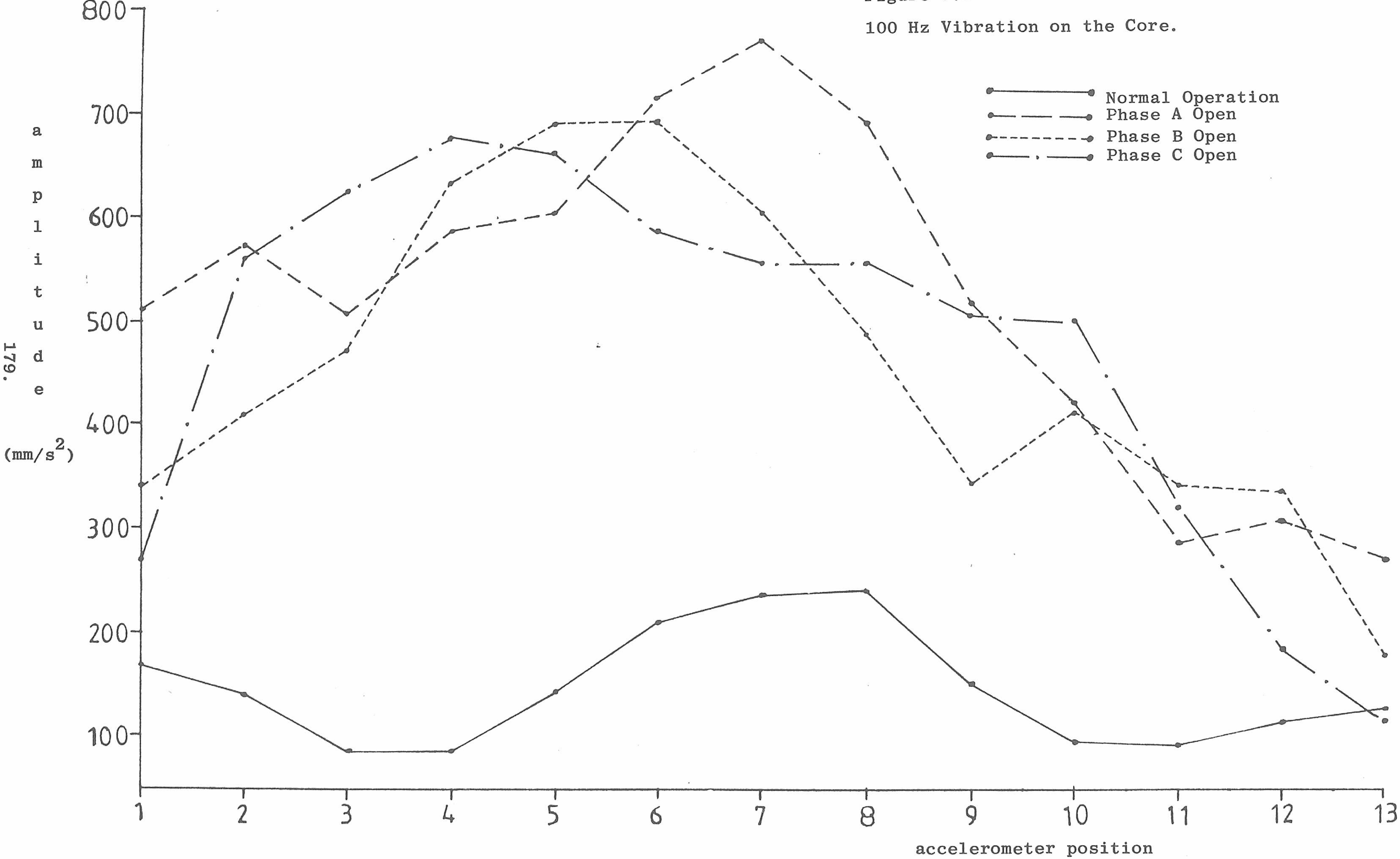

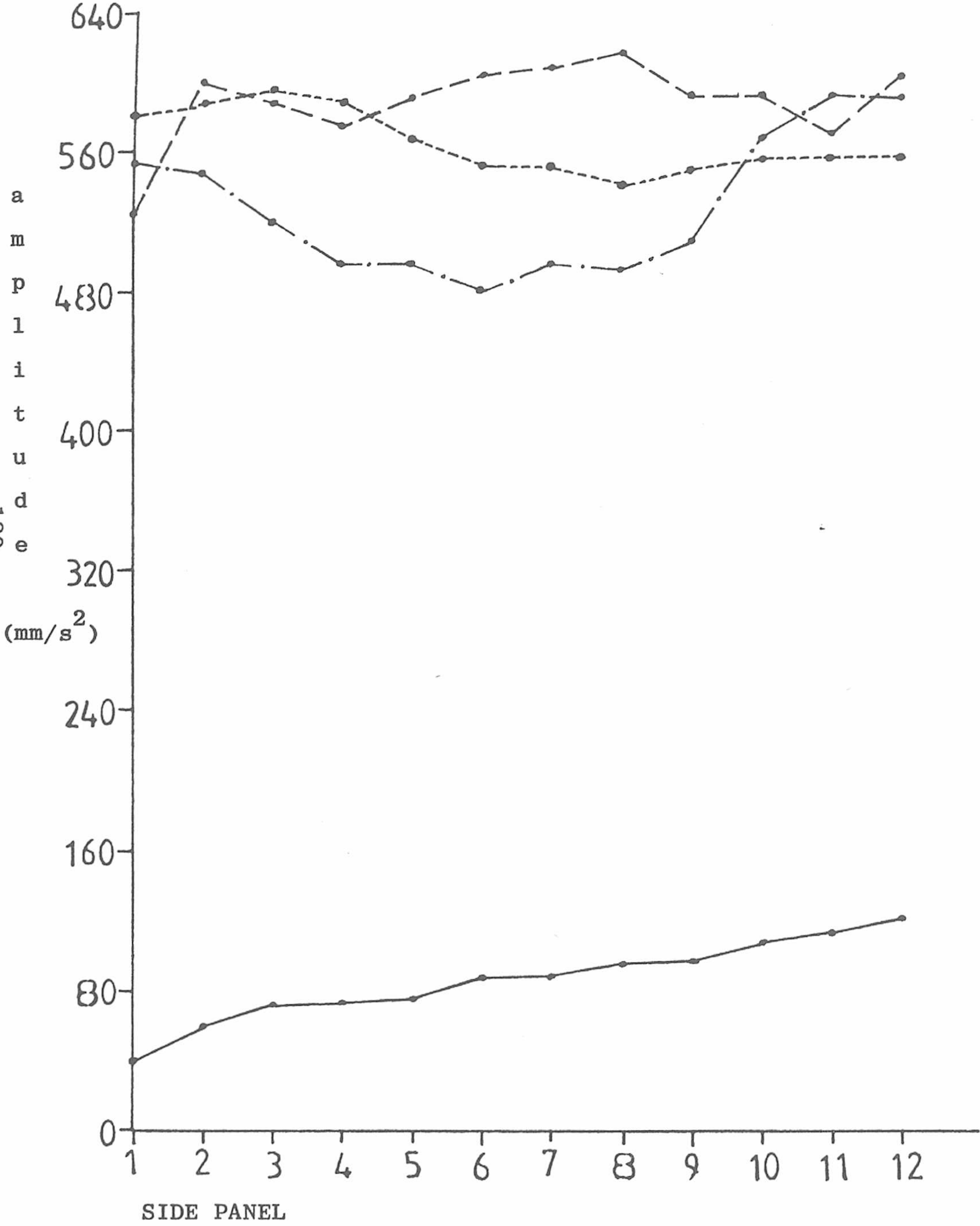

640
560
480
400
320
240
160
80
0
a m p l i t u d e (mm/s^2)
1
2
3
4
5
6
7
8
9
10
11
12
SIDE PANEL

Figure 7.4

100 Hz Vibration on the Frame.

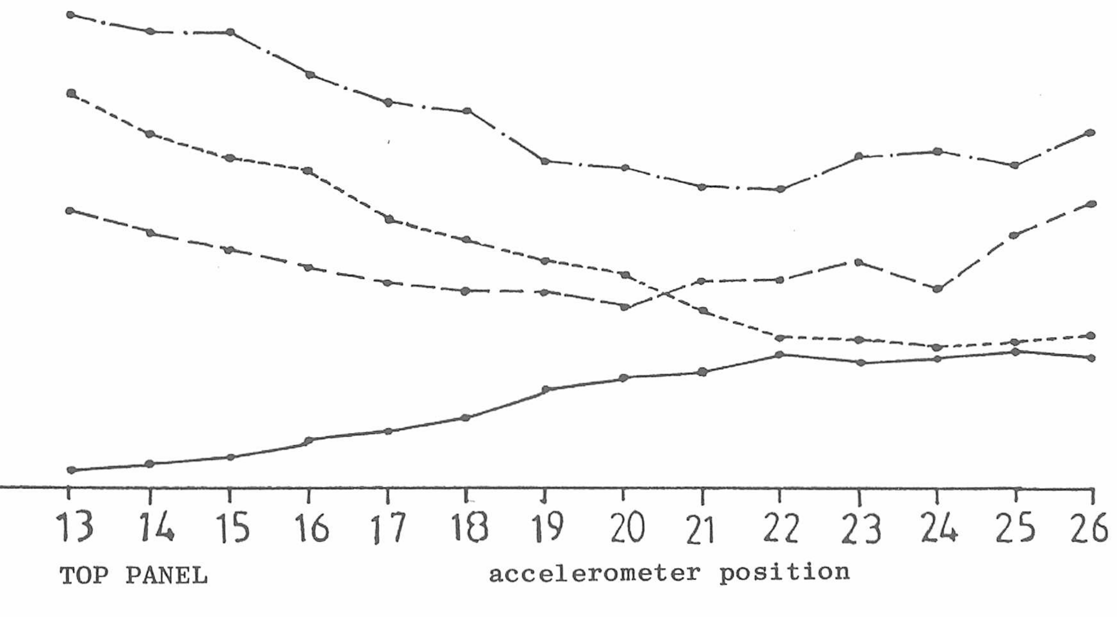

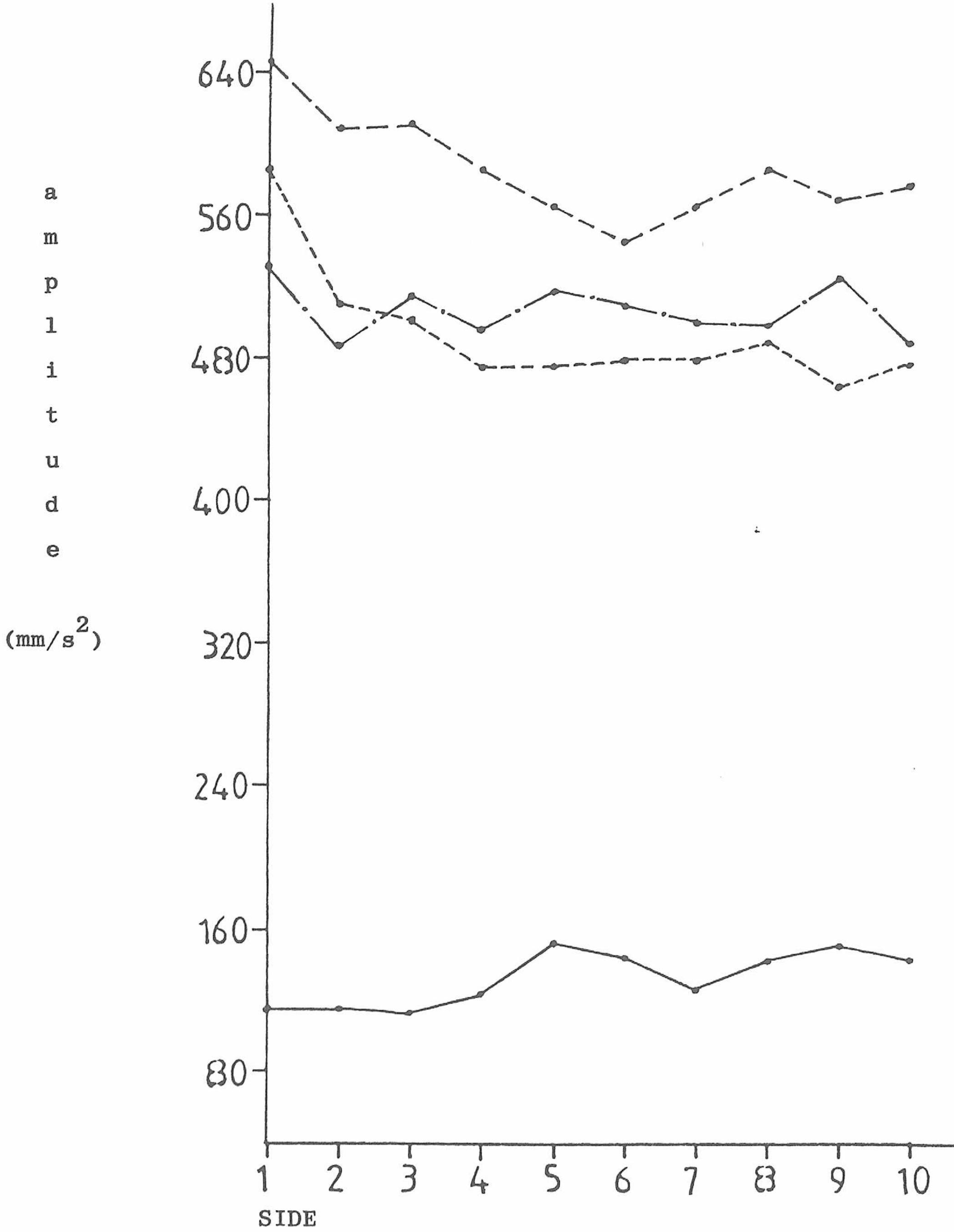
amplitude
(mm/s2)
640
560
480
400
320
240
160
80
1
2
3
4
5
6
7
8
9
10
SIDE

Figure 7.5

100 Hz Vibration on the Core Bars.

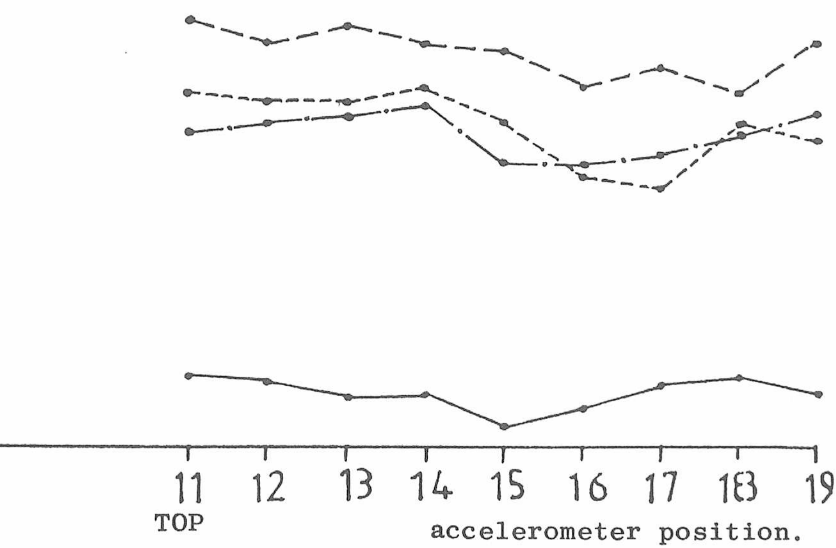

Figure 7.6

600 Hz Vibration on the Core.

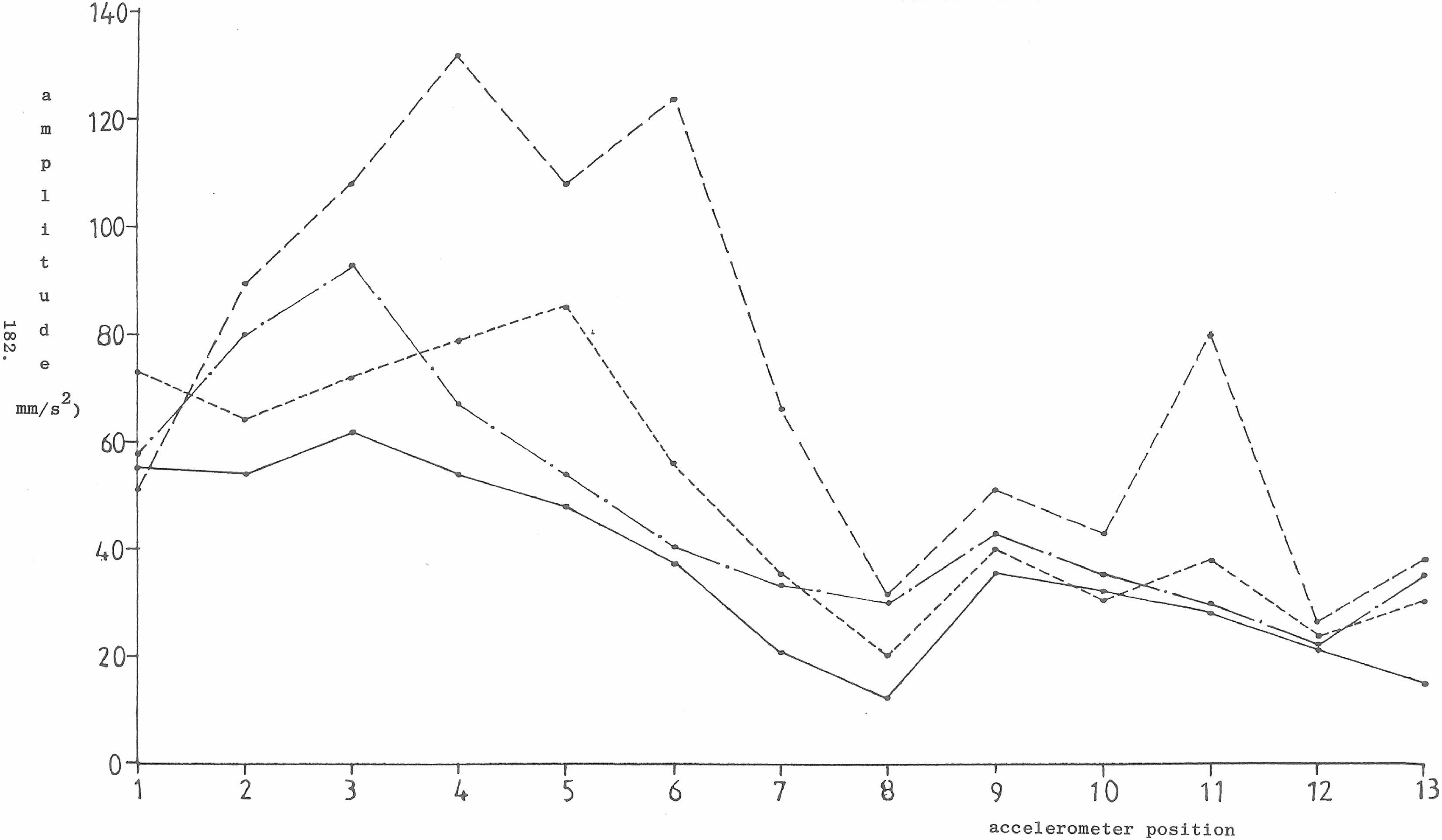

Figure 7.7

600 Hz Vibration on the Frame.

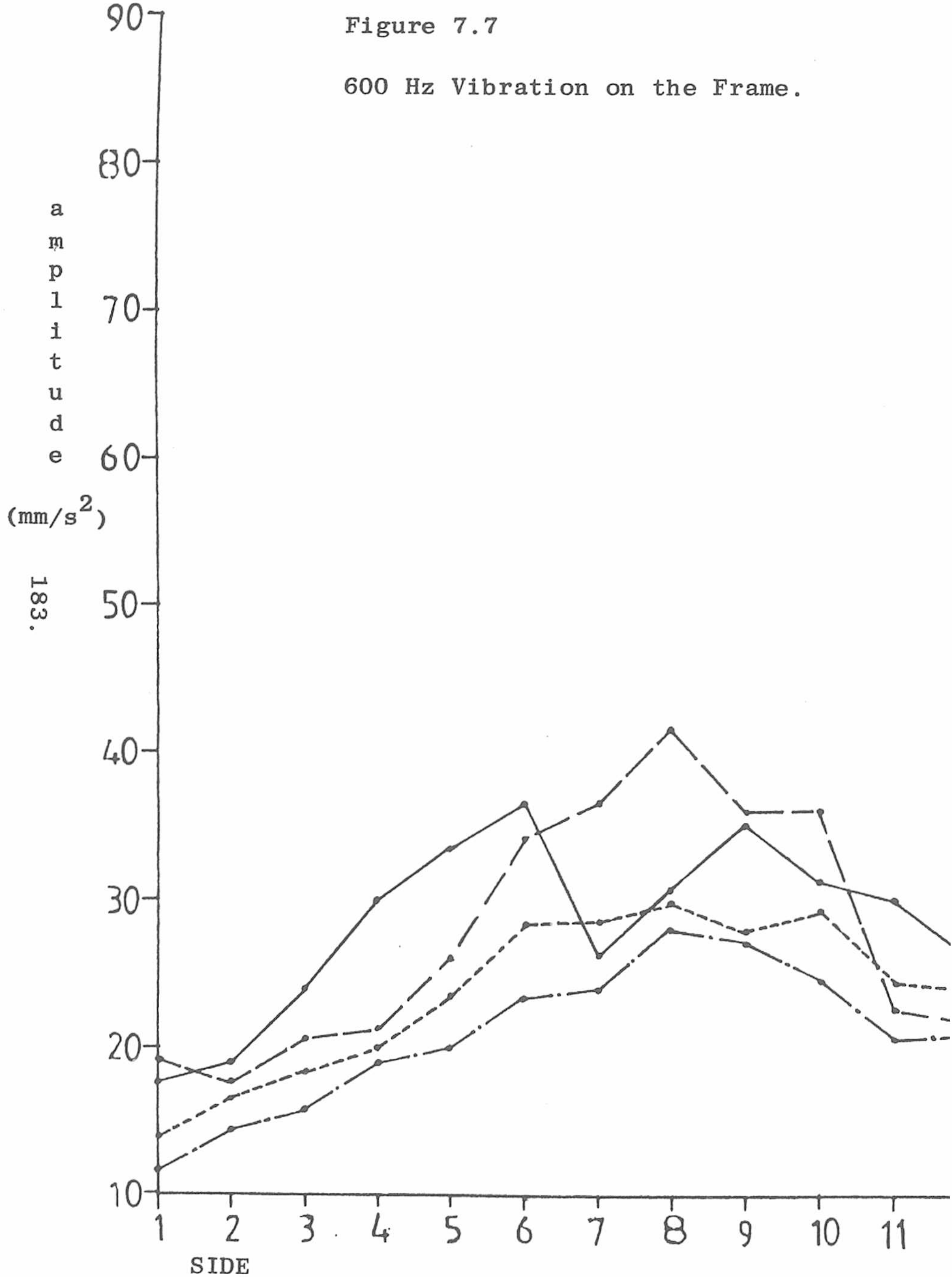

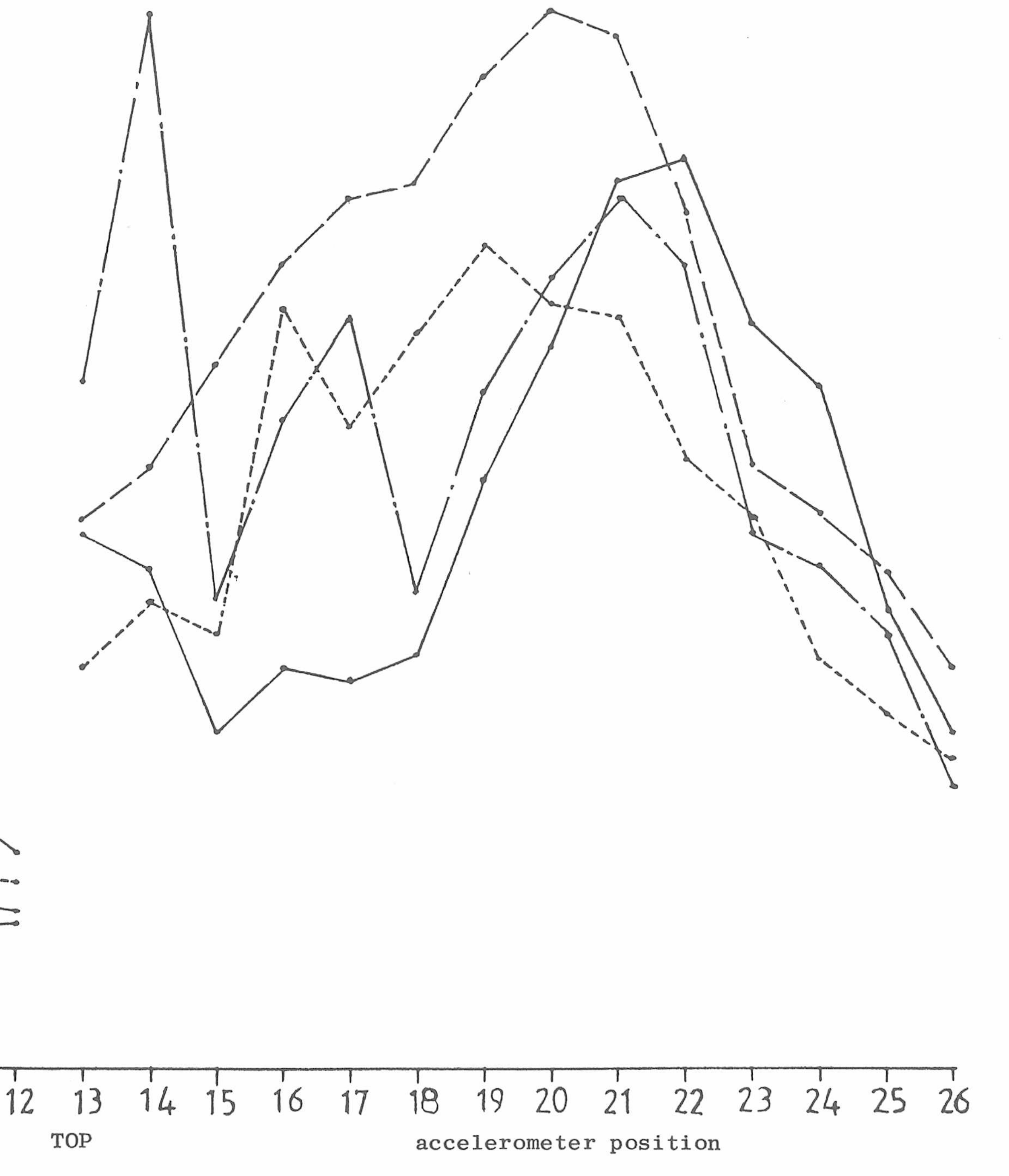

12 13 14 15 16 17 18 19 20 21 22 23 24 25 26
TOP
accelerometer position

Figure 7.8

600 Hz Vibration on the Core Bars.

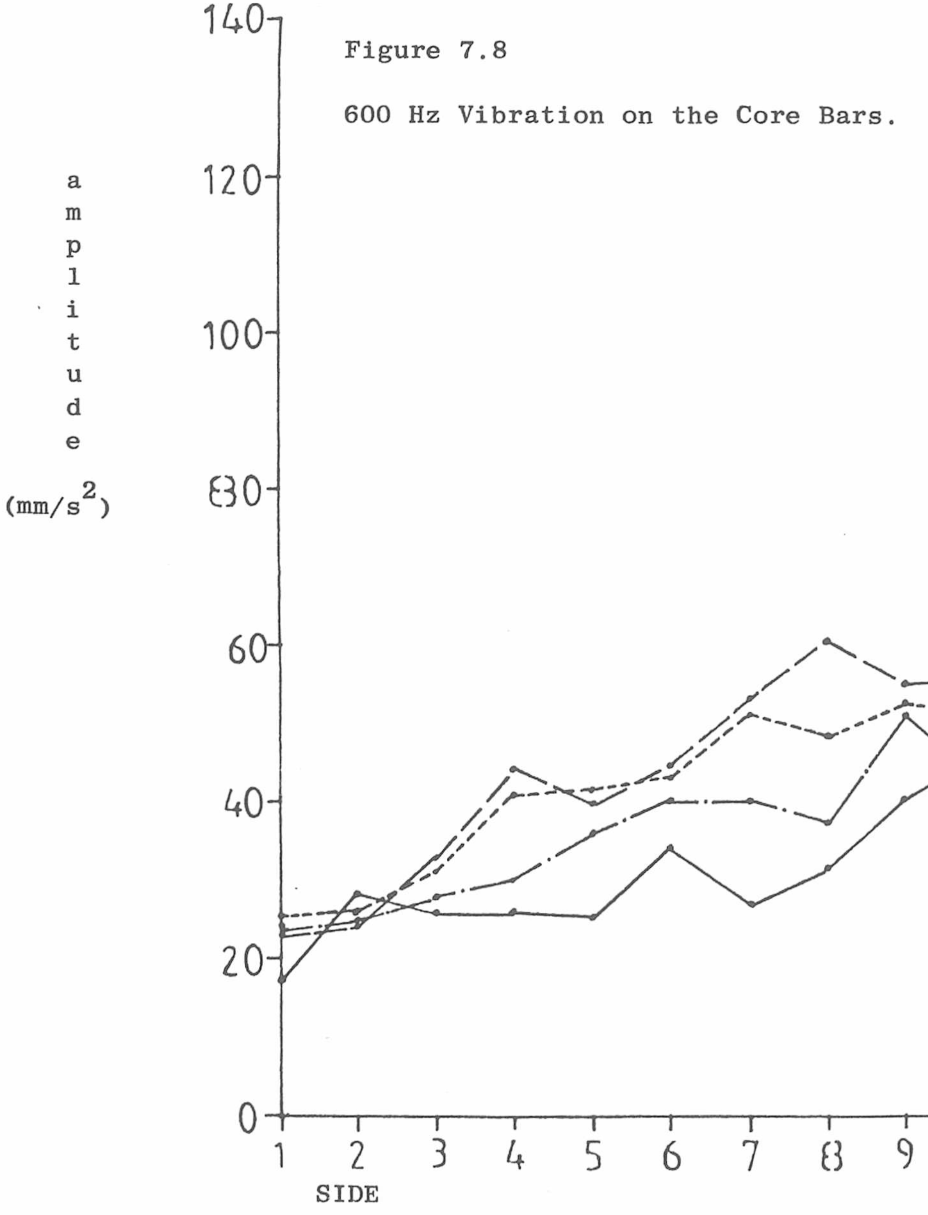

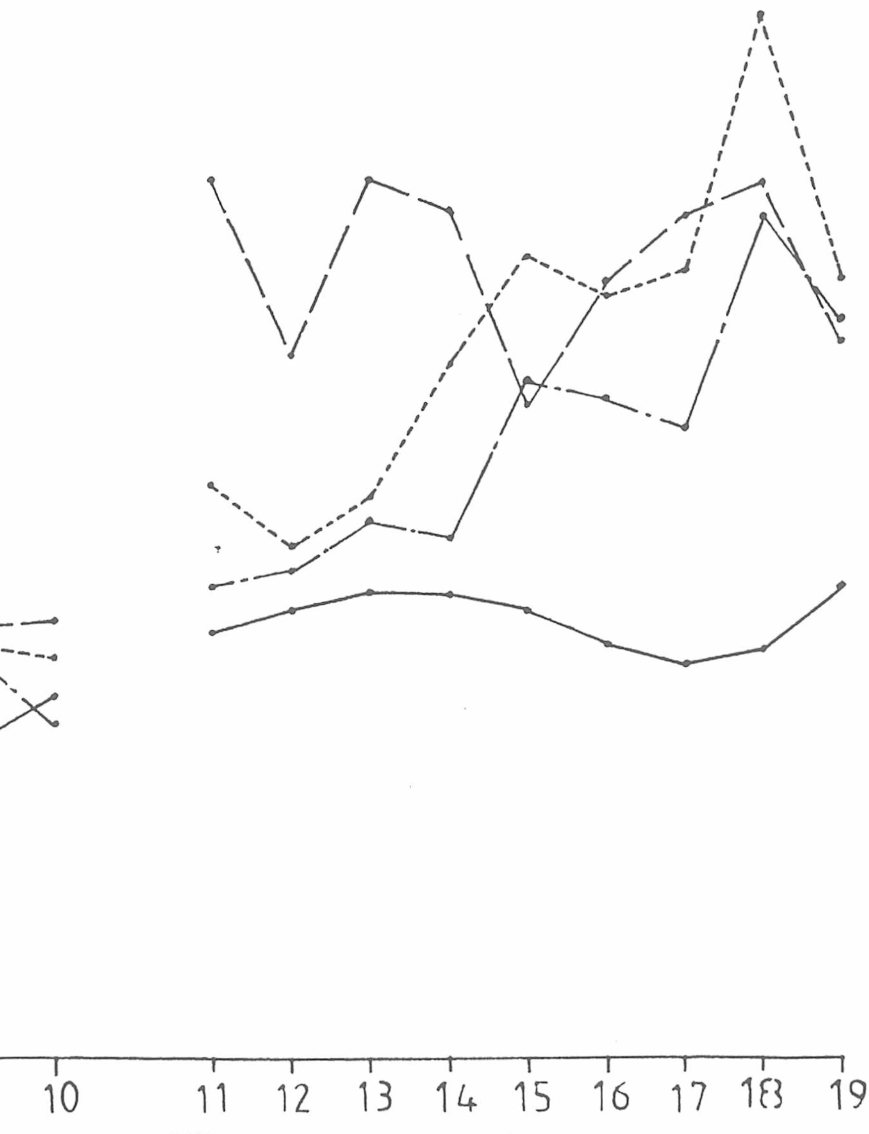
10
11
12
13
14
15
16
17
18
19
TOP
accelerometer position

Figure 7.9

700 Hz Vibration on the Core.

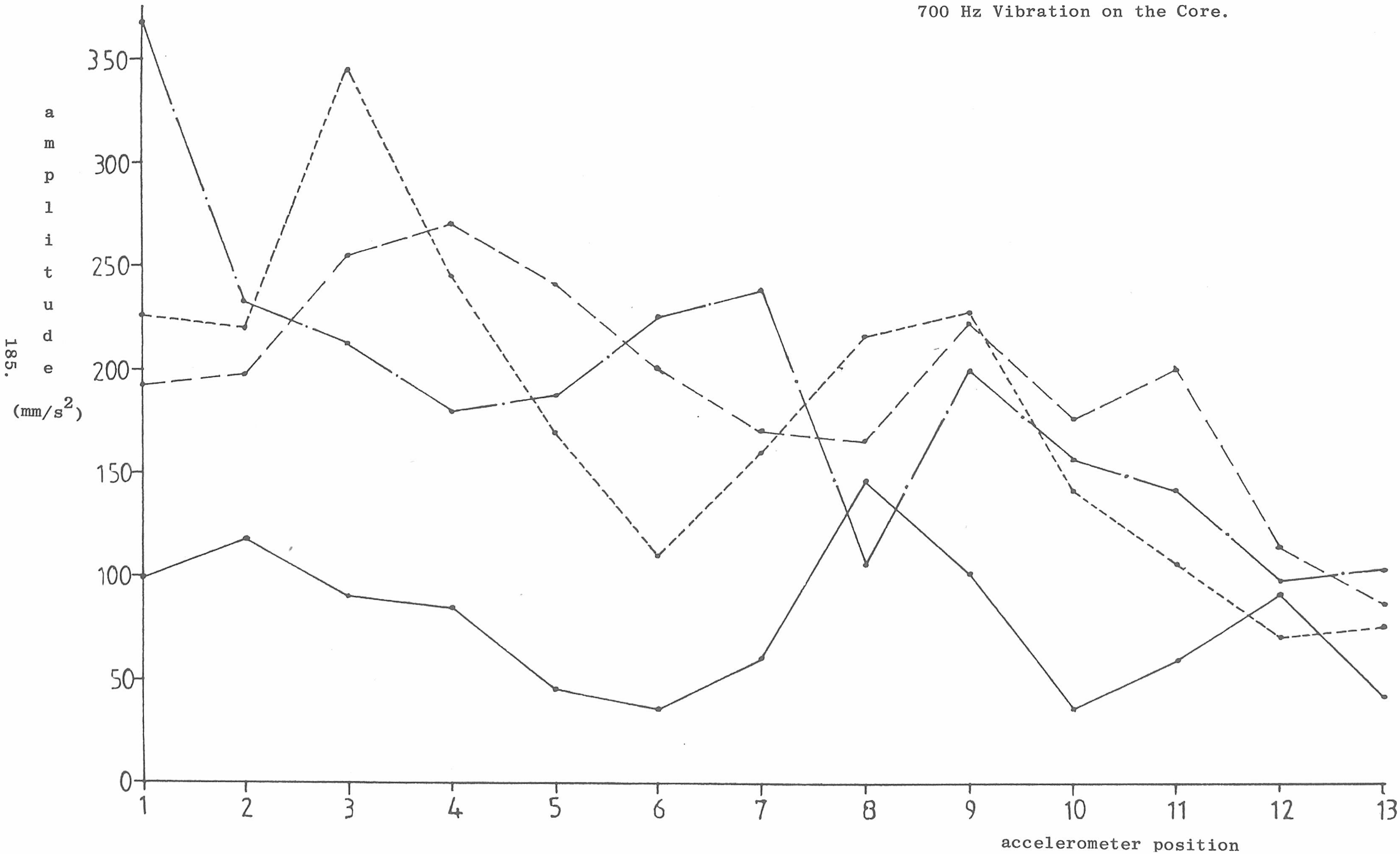

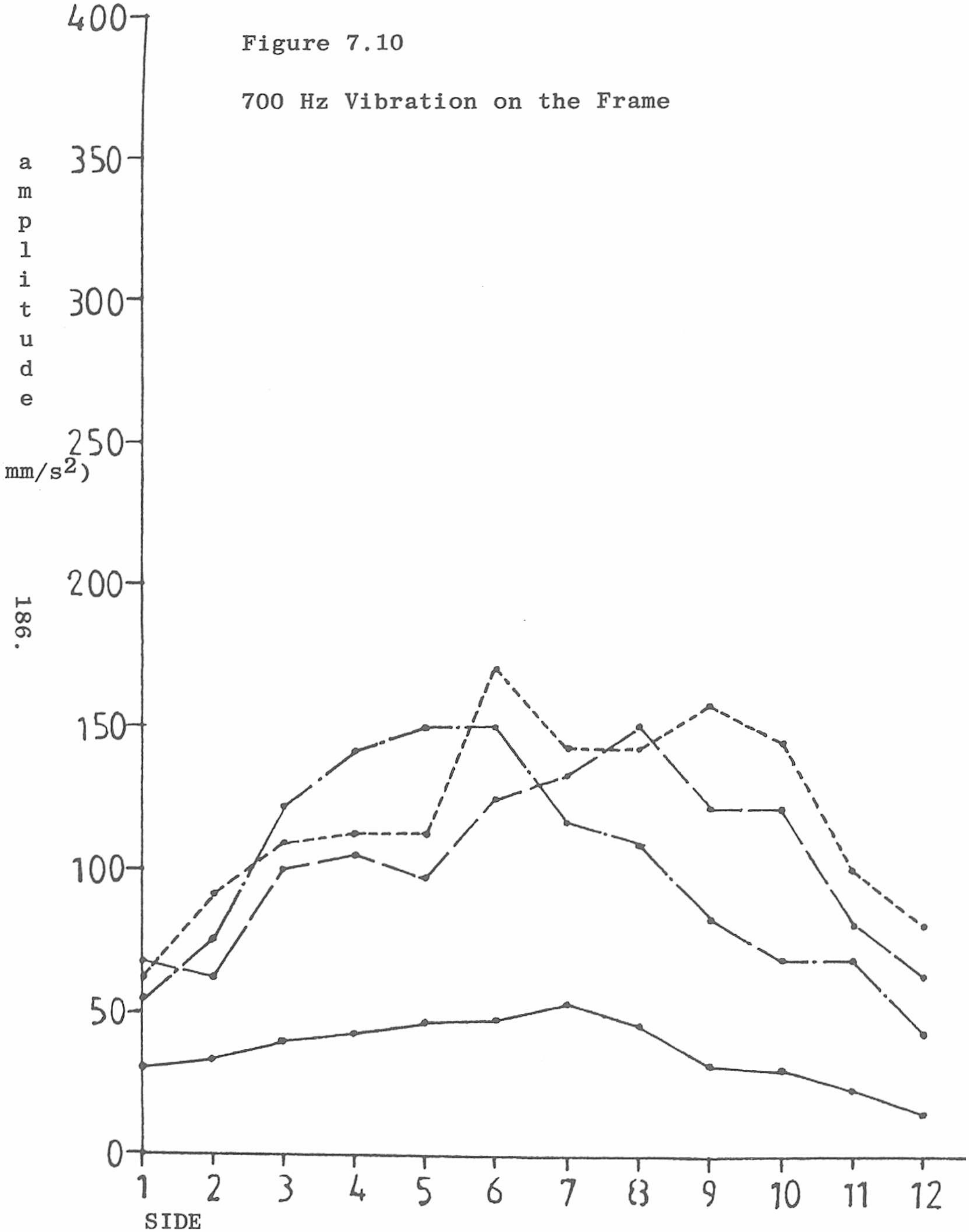
Figure 7.10
700 Hz Vibration on the Frame
amplitude
mm/s²)
400
350
300
250
200
150
100
50
0
1
2
3
4
5
6
7
8
9
10
11
12
SIDE

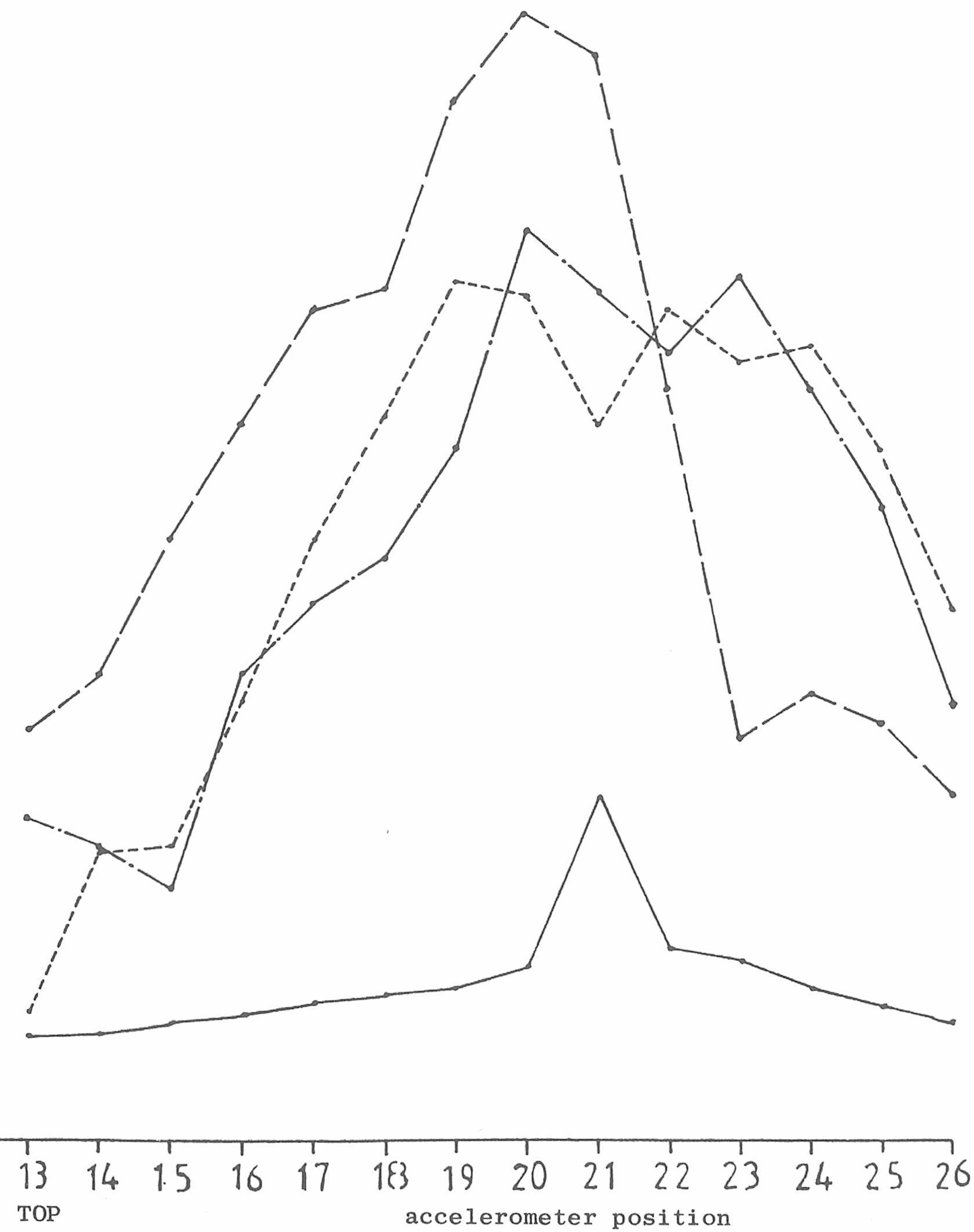
13
14
15
16
17
18
19
20
21
22
23
24
25
26
TOP
accelerometer position

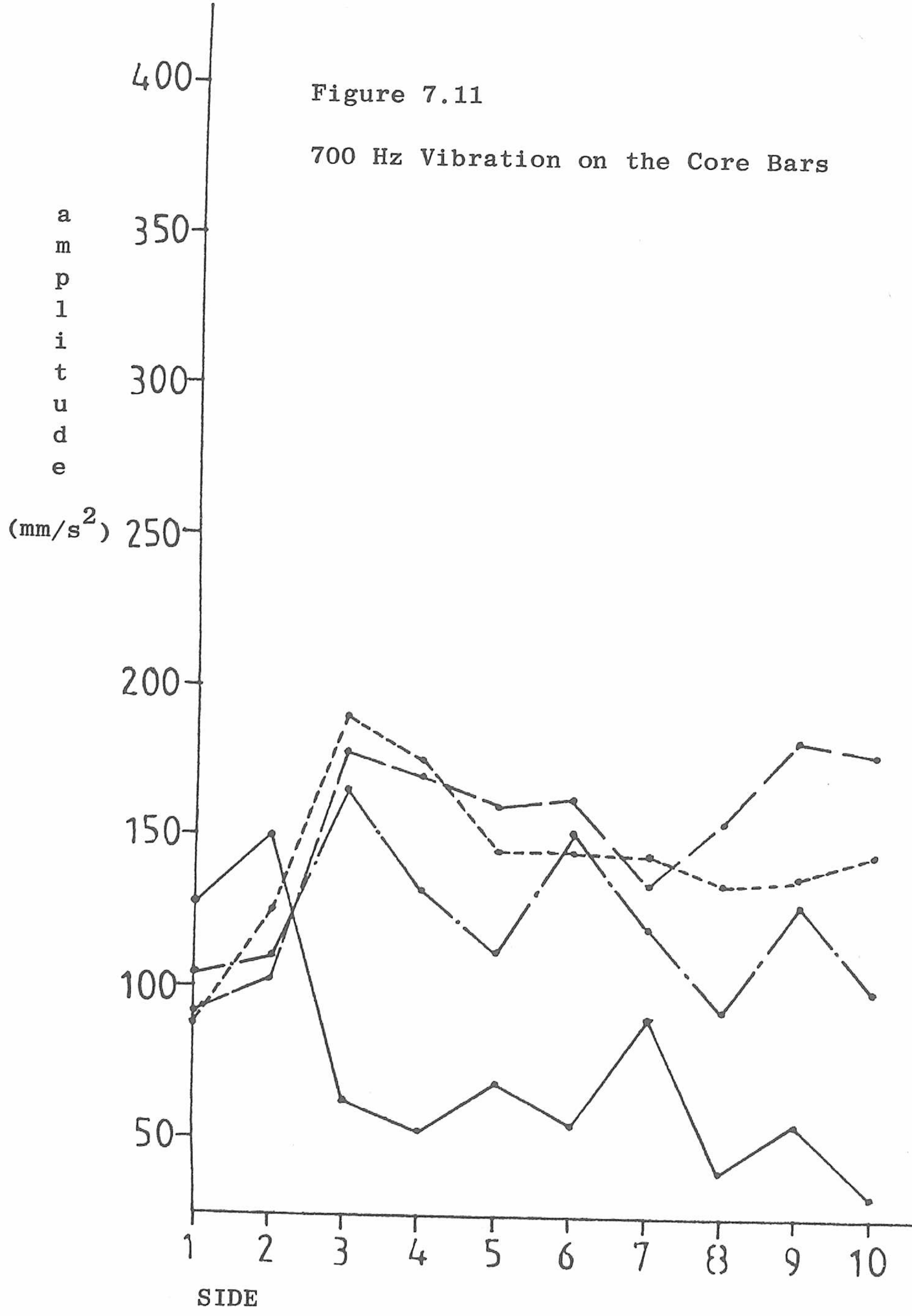

Figure 7.11

700 Hz Vibration on the Core Bars

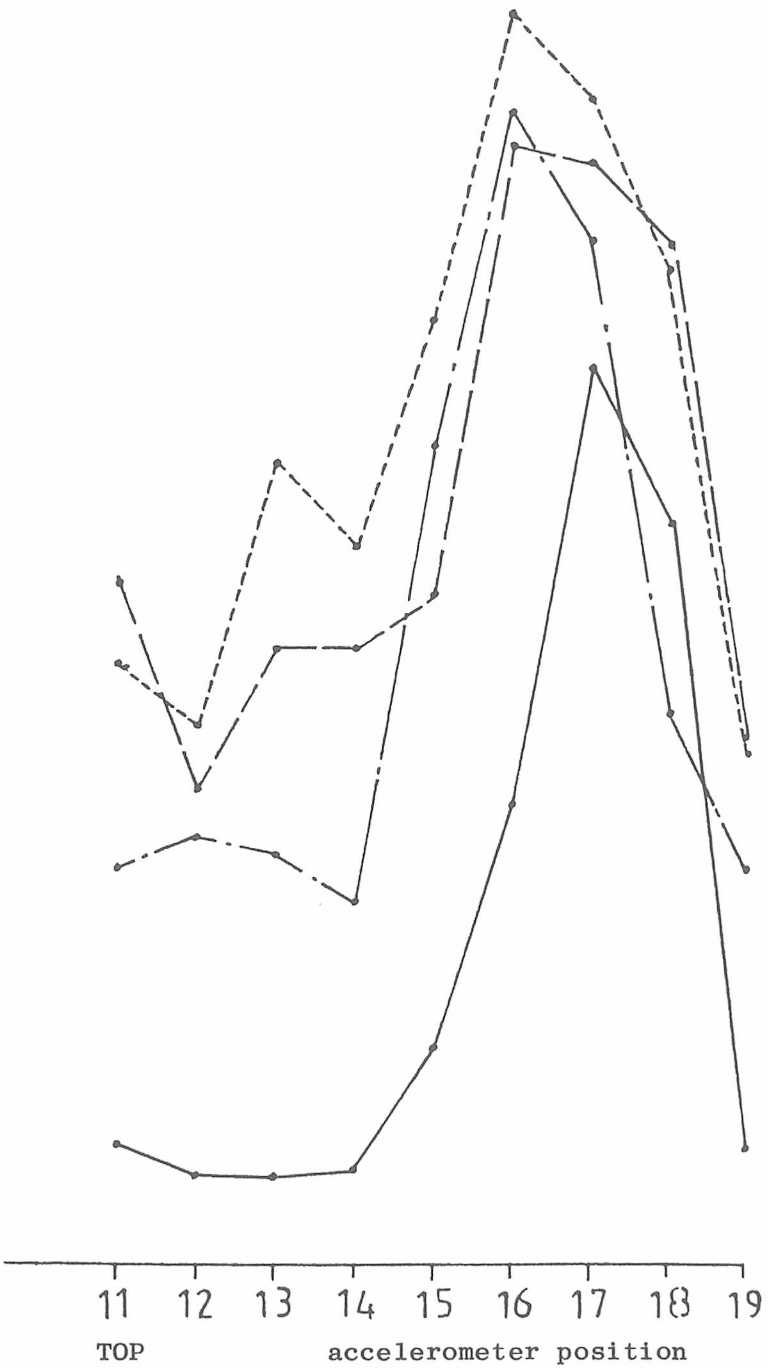
11
12
13
14
15
16
17
18
19
TOP
accelerometer position

Figure 7.12

800 Hz Vibration on the Core.

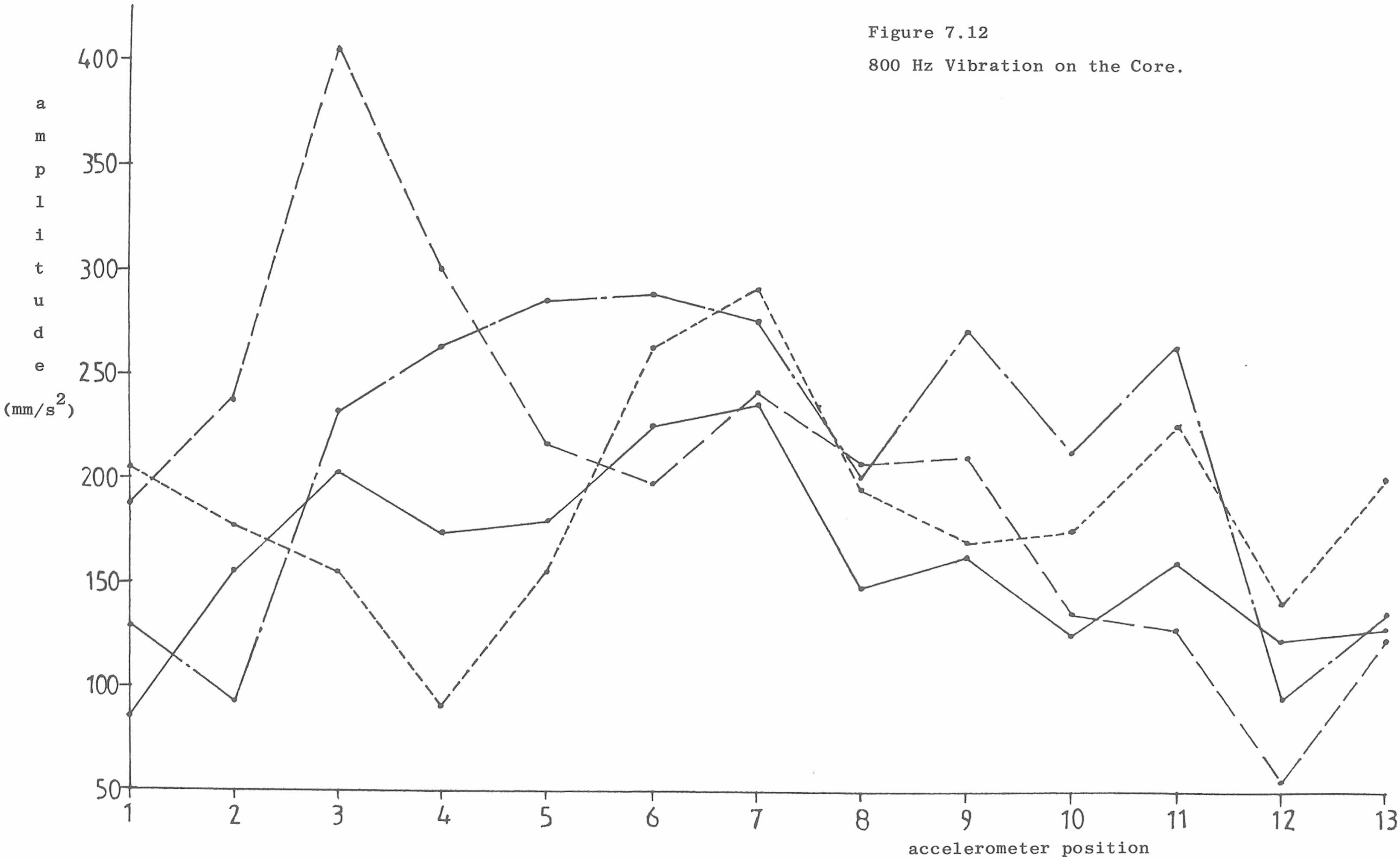

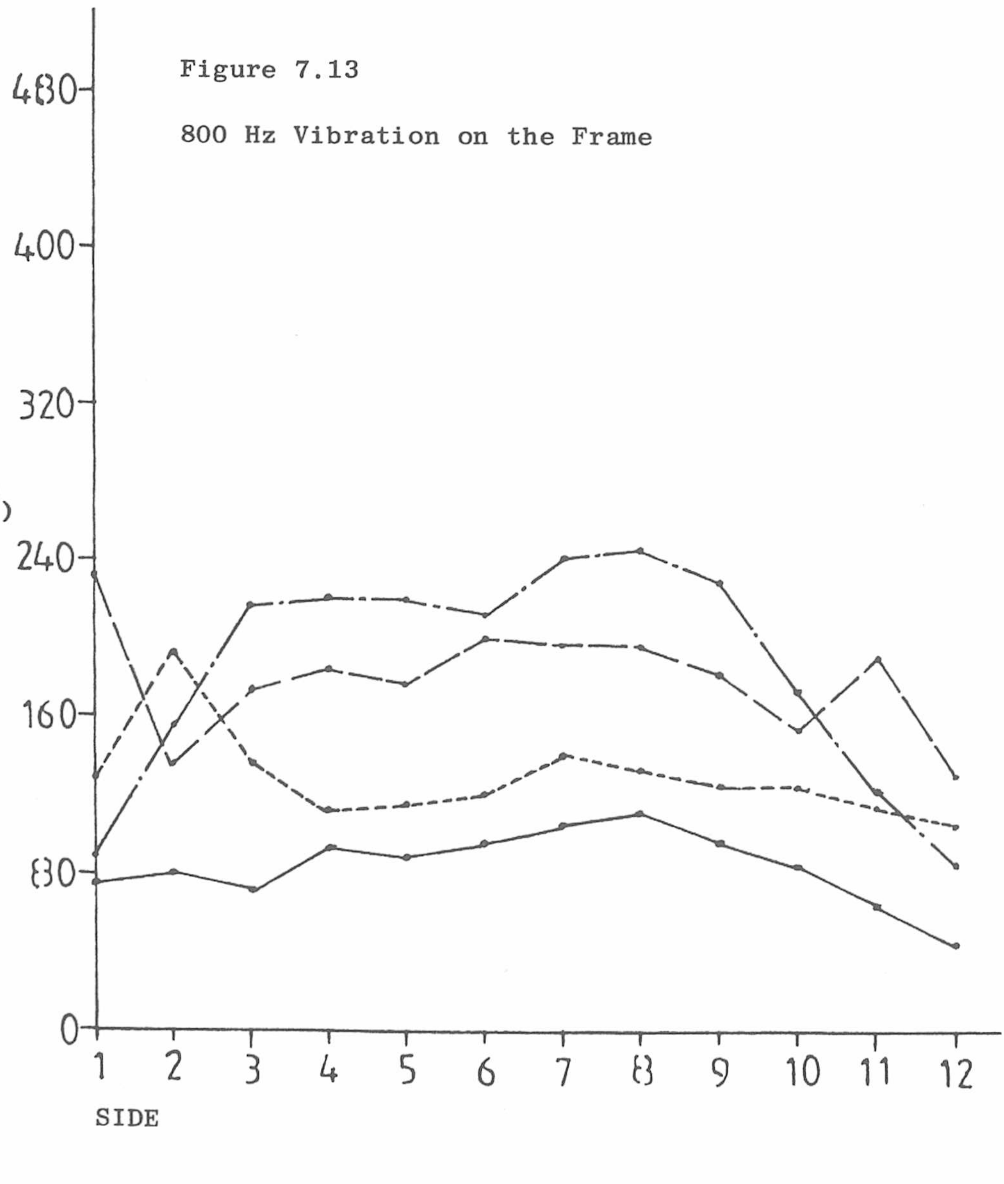

Figure 7.13

800 Hz Vibration on the Frame

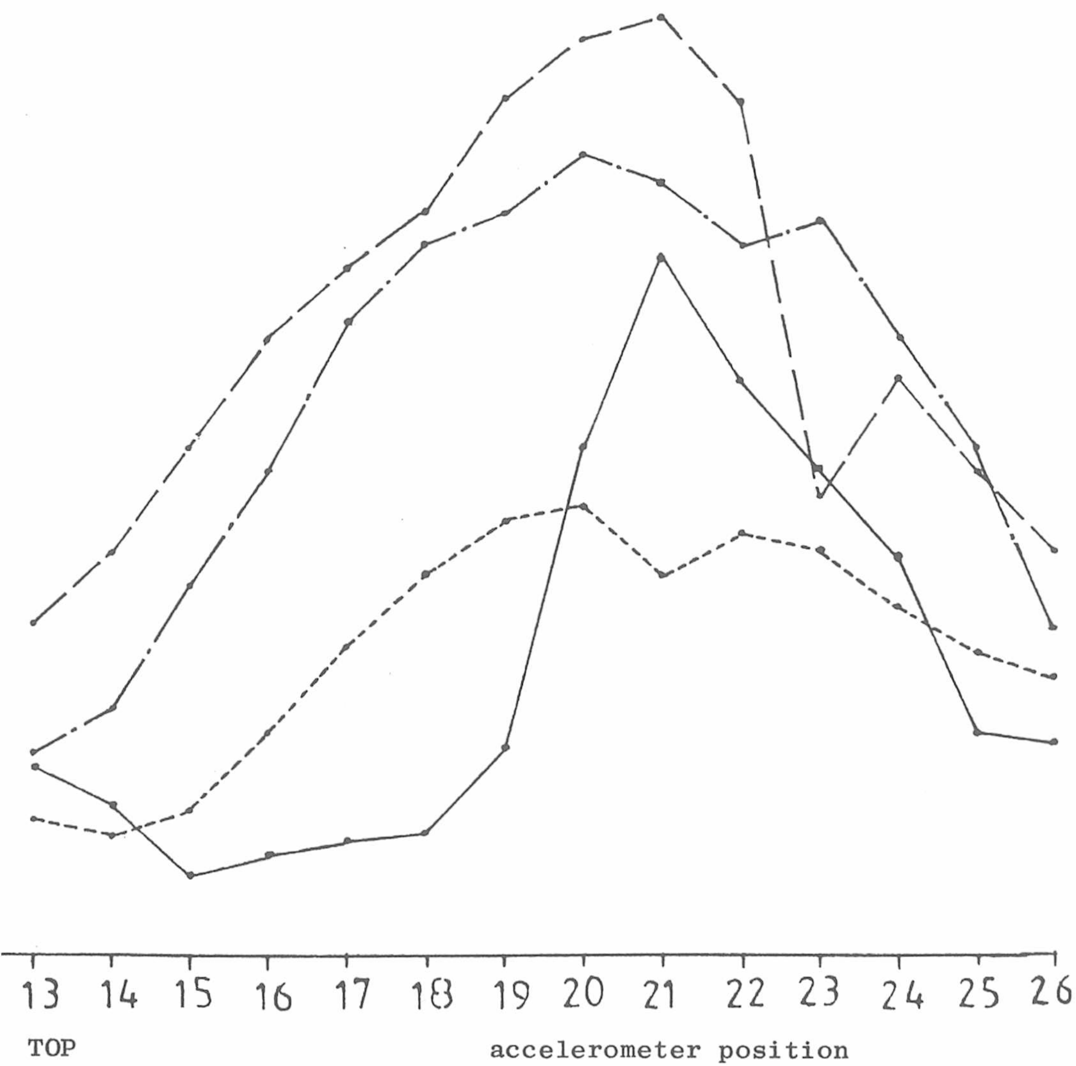
13 14 15 16 17 18 19 20 21 22 23 24 25 26
TOP
accelerometer position

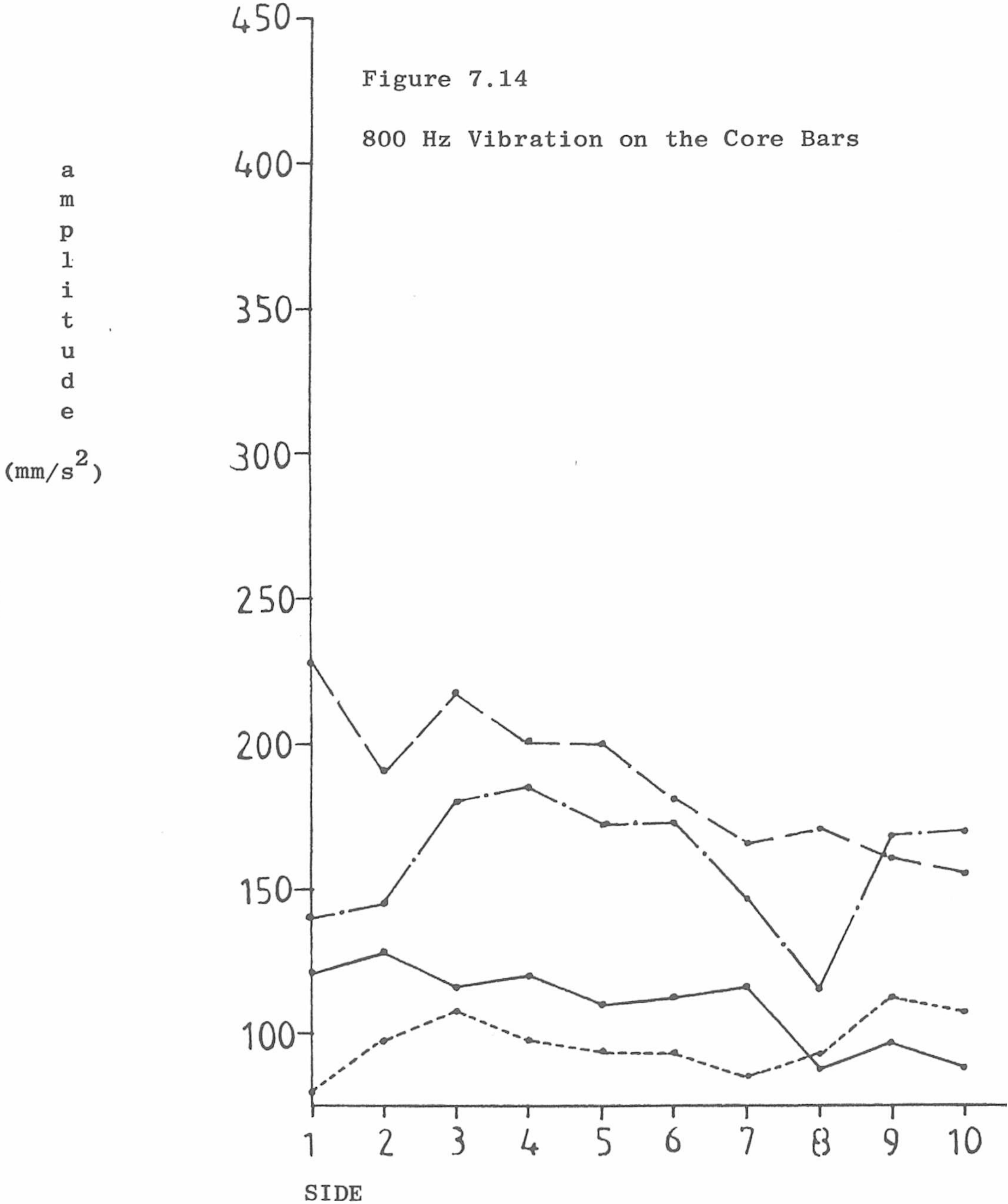

Figure 7.14

800 Hz Vibration on the Core Bars

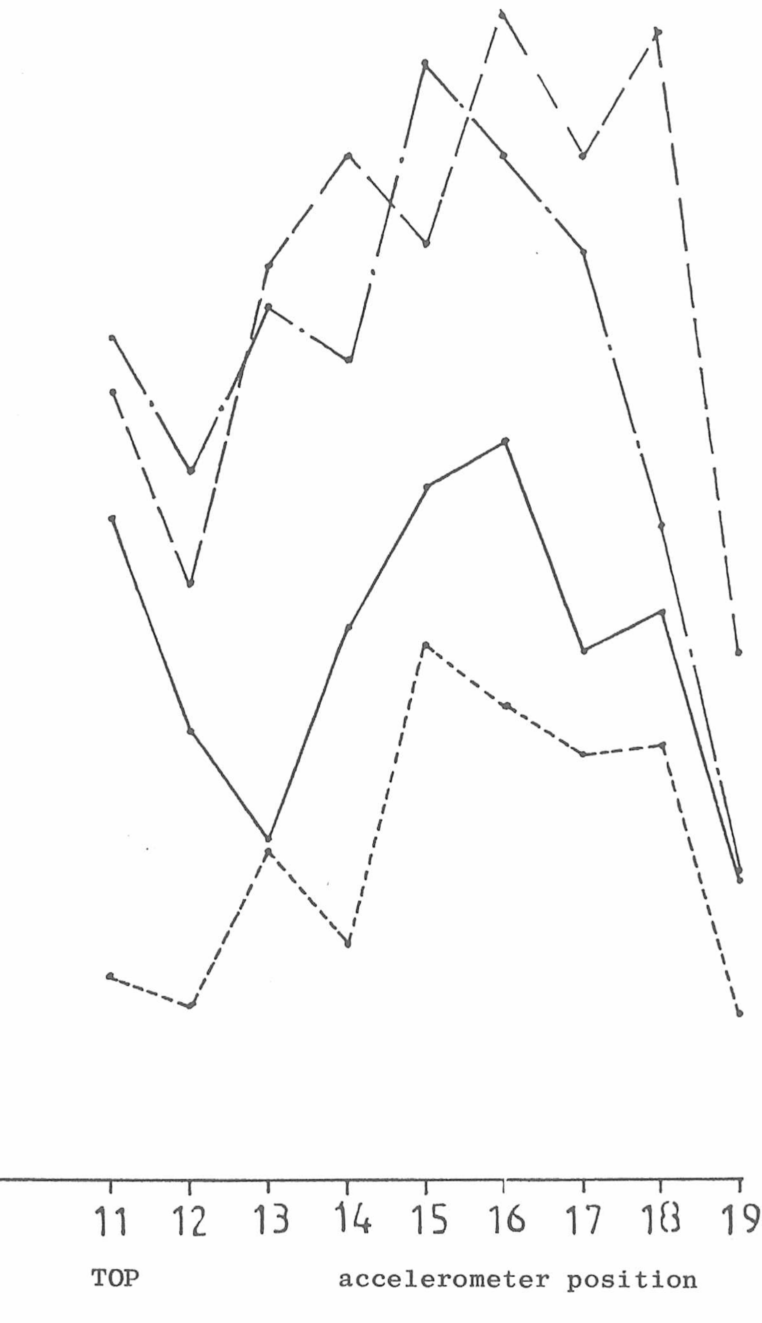

11
12
13
14
15
16
17
18
19
TOP
accelerometer position

CHAPTER 8. CONCLUSIONS ON THE EFFECTIVENESS OF THE FINITE ELEMENT ANALYSIS.

8.1 Conclusions from the Theoretical Calculations.

The main objective of this study was to evaluate the effectiveness of finite element analysis as a mathematical technique for predicting the dynamic characteristics of an induction motor stator assembly. The effectiveness of the numerical approximation method was to be judged in terms of:

(a) the accuracy of the calculated predictions,

and

(b) the relevance of the calculated predictions to the requirements of a vibration monitoring strategy.

Three main conclusions can be drawn from the investigation:

8.1.1 Resonance Frequencies and Mode Shapes.

Although in the majority of cases, calculated natural frequency values were accurate to within 3% of measured values, error margins overall varied between a maximum of 15.6% to a minimum of 0.0%. While the Finite Element Method could be judged in the main to be an accurate technique for calculating stator natural frequencies, the calculated values on their own do not provide reliable information for the purposes of a vibration monitoring strategy. The reason for this can best be explained by example:- If vibration levels on the stator core or frame are being monitored at a certain frequency in order to detect a motor fault, the measured vibration amplitudes are dependent on:

(i) the vibration transmitted to the measurement position due to the fault condition,

and

(ii) the natural dynamic characteristics of the stator assembly at that frequency.

Therefore if the calculations fail to predict that the monitored frequency is occurring at a natural frequency, the reliability of the vibration monitoring system is seriously reduced.

However, the results are accurate enough to predict whether the monitored vibration frequency is in the vicinity of a structural resonance. Also, for every mathematical model, the Finite Element Method accurately predicted the shape of deformation on the stator core and frame at every experimentally identifiable natural frequency. These two factors are important where vibration monitoring is concerned because it allows a motor operator, where appropriate, to position the transducer being used to monitor vibration levels at or near a modal node and hence avoid or reduce the effects of a predicted resonance on vibration amplitude measurements. The use of this approach to monitoring will not always be appropriate. In Chapter 7 it was found that suitable transducer positioning is crucial to the detection of a single-phasing fault. In a case where the fault detecting frequency coincided with a structural resonance, it is possible that the best fault sensing positions occur at or near modal antinodes.

A sensible assessment of appropriate transducer positioning and the avoidance of reasonance effects can only take place if the motor operator has precise information of expected mode shapes. The Finite Element Method is a wholly effective technique for providing this information.

8.1.2 The Response at Resonance.

Comparative theoretical and investigative studies have shown that the Finite Element Method can be used to calculate the response of the stator assembly at resonance due to a simple external sinusoidal forcing function, but that each finite element model calculated a response curve with a maximum amplitude of deformation 1.5 to 2 times greater than the measured level.

If the magnitudes of response levels excited on the stator assembly are viewed in terms of the dimensions of the whole structure, then considerable disparity between calculated and measured vibration amplitudes can be expected due to approximations in the finite element model's dimensions, boundary conditions and loading conditions. However, the accuracy of the response amplitude calculations is not the most important factor when considering the requirements of an analysis which would equip a motor operator with the vibration information essential for the installation of a vibration monitoring system. As was discussed in conclusion 8.1.1, it is sensible, where possible, to position a transducer at a node on the structure's modal wave to avoid the response level increases associated with a resonance. However, the response calculations can provide essential additional information. Since the calculated response levels are consistently between 1.5 and 2 times the measured amplitudes, it is possible to use the results as a guide to the influence of a particular natural frequency. Structural resonances can excite very large increases in vibratory response at some frequencies and almost negligible increases at other frequencies. Therefore the prediction of high or low level vibration at a natural frequency in response to excitation from an external forcing function, can help a motor operator assess the likely significance of resonance effects on the vibration levels being monitored at a particular frequency and alter vibration measurement positions where necessary. In cases where good fault sensing positions coincide with modal antinodes, the significance or insignificance of reasonance effects can be assessed. With the calculated guideline response levels always being higher than actual vibration levels, a "factor of safety" is built in to this assessment procedure.

8.1.3 The Response to the Electromagnetic Forcing Function.

The Finite Element Method has also been used in this study to calculate the response of the stator due to the fundamental electromagnetic travelling wave forcing function. The aim was to predict mathematically, vibration levels excited under normal motor operating conditions.

In this case the accuracy of the calculated results becomes extremely important. It was shown in Chapter 7 that the inception of a single-phasing fault can increase the amplitude of the 100 Hz vibration component typically by a factor of 3 or 4. If calculated predictions of normal vibration levels are inaccurate by a factor of this order then the acceptable range of normal vibration amplitudes would be set above the response excited by the fault condition. Since this would defeat the purpose of a vibration monitoring system, the theoretical analysis of the electromagnetic forces must produce realistic predictions.

If the calculated response values due to the electromagnetic forcing function were to be used as predetermined baseline predictions for the analysis of a single-phasing fault, then the finite element calculations are adequately accurate. The parts of the stator assembly where significant differences occur between calculated and measured values are at the top and base of the core and along the top of the frame. These were the same areas found in Chapter 7 to be least suitable for transducer positioning to detect the single-phasing fault. The parts of the stator assembly most suitable for fault detection were on the side of the frame and between angular positions of 30^{o} and 90^{o} around the core periphery. On these areas of the structure, the finite element calculations and the measured levels of vibratory response were much more compatible.

8.2 The Effectiveness of Finite Element Analysis.

Finite element analysis has been consistently accurate in predicting the deformed shape of the stator assembly, both at resonance and due to electromagnetic excitation. Calculated displaced shapes have matched experimental findings on both the stator core and frame of the stator assembly. Choosing suitable transducer positions has been shown to be an imporatnt consideration for a reliable vibration monitoring system, so that the accurate prediction of stator deformation patterns is of paramount importance. The Finite Element Method is evidently an effective theoretical technique for meeting this requirement.

Furthermore, the Finite Element Method is capable of providing information of the complex interaction of the various components of the stator assembly and of illustrating how each component contributes to the overall vibration characteristics. It is an adaptable modelling technique and has the ability to include complex boundaries in the analysis, which are generally neglected when using other theoretical techniques. Three-dimensional modelling can be employed where axial variations have a significant effect on radial vibration. It is also possible to analyse torsional effects or a combination of radial, axial and torsional vibration. This means that the analysis technique can be applied to large as well as amall induction motor stators.

8.3 The Cost of Finite Element Analysis.

The main drawback of using the Finite Element Method is one of cost, since the analysis is expensive in terms of computer processing time. On the supposition that c.p.u. time is priced at £300 per hour, which is a standard consultancy fee at present, some of the finite element models are valued to provide a guide to the level of costs incurred by this type of dynamic analysis. The c.p.u. time required by four of the finite element models, which include a drawing of the structure and six mode shapes, are given.

F.E. MODEL	c.p.u. time (mins.)	Cost (£)
COR2	197	985
COR3	81	405
STR1	98	490
END1	32	160

Approximately one third of the overall cpu time in each case is utilised in running Phase 3 and Phase 8 to obtain graphic output. The cost is dependent to a large extent on the number of mode shapes required. Two dimensional analysis is considerably less expensive than three-dimensional analysis which makes the former more attractive in financial terms. It is therefore sensible to carry out a two-dimensional dynamic study of a stator assembly unless longitudinal variations are likely to influence significantly the radial vibration behaviour of the structure. The analysis of one component of the structure, such as the core or an endplate, will incur extra cost but provides very useful additional information.

The cost of a finite element study must be viewed in terms of its usefulness to a motor operator. If an operator wishes to invest capital in a vibration monitoring system, it will be invested to make long term savings from early fault detection, planned machine outages and fewer failures. The outlay on initial expenditure would be very large; an estimated 5% of plant value is suggested by Neal and Associates (1). Therefore the amount required to be spent on an initial vibration study would be comparatively small but extremely important to the reliability of the monitoring system.

8.4 Conclusions.

The study of the vibratory characteristics of stators of induction motors operating in an offshore installation can be carried out effectively using the Finite Element Method. The technique can calculate all the structural resonance frequencies to an acceptable level of accuracy but, more importantly, the mode shapes can be predicted precisely. It is possible to determine accurately, the displaced shape of the stator assembly excited by external or inherent forcing functions. The corresponding calculated response amplitudes, although not exact, can be used to indicate the significance of vibration effects due to resonance and aid the appropriate positioning of transducers. The information gathered from a finite element dynamic analysis of a stator assembly is suitable for predetermining the vibration behaviour of an induction motor during healthy operation and can subsequently be used as essential information for a vibration monitoring strategy.

CHAPTER 9.

9. FURTHER WORK.

Vibratory characteristics of a large induction motor stator assembly have been analysed in this study by investigating the dynamic behaviour of a scaled down model. This was to enable laboratory tests to be carried out so that the theoretical approach could be evaluated in terms of accuracy. Further to the findings of this study, future research should involve finite element modelling and the experimental investigation of an actual large motor stator structure in its operating environment to ensure that similar levels of accuracy can be obtained.

It would then be possible to develop the large motor stator finite element model to include the stator windings. The mathematical model of the complete wound core assembly would have to take into account the winding configuration, coil insulation, the restraining influence of the slot wedges and the bracing of the end windings as well as the frame structure and stator mounting arrangement. Previous theoretical investigations of stator vibration behaviour have dealt with some aspects of this requirement (see Chapter 2), but there has not been a complete examination of the dynamic nature of a large induction motor stator assembly which involves the analysis of all its component parts and mounting configuration integrally.

The vibratory response of a large induction motor is characterised by the nature of the inherent and external forces acting on the stator assembly. Under normal operating conditions the solution of these forces is complex due to the harmonic content of the electromagnetic forcing function and the interaction of vibratory forces due to external industrial operations. Further research into the mathematical modelling of these forces by the Finite Element Method is required. Future studies would involve introducing additional computer programs into the finite element package for the specific task of calculating the effects of the forcing functions acting on a particular motor in its industrial environment. From the work carried out in this research project and with an improved analysis of the total response to the various forcing functions, the vibration behaviour of a 'healthy' stator assembly under normal operation could be determined by finite element analysis. This knowledge could then be used as background information for a vibration monitoring strategy.

When an induction motor is mounted on a steel bed-plate, especially in an offshore installation, vibration transmitted from external sources, such as sea motion and drilling operations, can be particularly damaging (see Chapter 1). Vibration problems due to the inception of an electrical or mechanical fault mechanism may be exacerbated by the continuous transmission of vibrations from industrial operations. If external forces excite frequencies close to a stator resonance, there is the added problem of sympathetic vibration. It would seem, therefore, that there is a need for establishing definitions of acceptable levels of stator vibration in terms of longer term mechanical damage to the motor. At present, British standards have recommended vibration levels in terms of motor noise performance and for human hearing of vibrations. In the future, vibration monitoring research could provide recommendations for acceptable principal slot harmonic vibration levels in order to reduce vibration damage, especially to the windings, and reduce the likelihood of insulation failure.

REFERENCES

1. Neale, M. and Associates: 'A guide to the Condition Monitoring of Machinery', HMSO, London, 1979.

2. Neale, M.J. and Woodley, B.J.: 'Condition Monitoring Methods and Economics', Symposium of Environmental Engineers, Bruel and Kjaer, Sept. 1975.

3. Renwick, J.T. and Babson, P.E.: 'Vibration Analysis - A Proven Technique as a Predictive Maintenance Tool', IEEE Transactions, Vol. 1A 21, No. 2, March/April 1985.

4. Hitchen, R.A.: 'Vibration Monitoring for Rotating Machinery', Measurement and Control, Vol. 13, No. 3, March 1980.

5. Stewart, R.M.: 'Vibration Analysis as an Aid to the Detection and Diagnosis of Faults in Rotating Machinery', International Conference on Vibrations in Rotating Machinery, Cambridge, 1976.

6. Taylor, J.I.: 'Fault Diagnosis of Gears Using Spectrum Analysis', International Conference on Vibrations in Rotating Machinery, Cambridge, 1980.

7. Steele, R.M., Ashen, R.A. and Knight, L.G.: 'An Electrical Method for the Condition Monitoring of Motors', IEE International Conference on Electrical Machines, Design and Applications, No. 213, 1982.

8. Thomson, W.T., Leonard, R.A., Milne, A.J. and Penman, J.: 'Failure Identification of Offshore Induction Motor Systems Using On-Condition Monitoring', Fourth National Reliability Conference, Birmingham, July 1983.

9. Thomson, W.T., Deans, N.D., Leonard, R.A. and Milne, A.J.: 'Monitoring Strategy for Discriminating Between Different Types of Rotor Defects in Induction Motors', Universities Power Engineering Conference, University of Surrey, April 1983.

10. Leonard, R.A. and Thomson, W.T.: 'Vibration and Stray Flux Monitoring for Unbalanced Supply and Inter-Turn Winding Fault Diagnosis in Induction Motors', International Conference on Condition Monitoring, Swansea, April 1984.

11. Penman, J., Dey, M. and Smith, J.R.: 'A New Approach to the Protection of Industrial Drives', IEEE-IAS Annual Meeting, Conference Record, 1982.

12. Thomson, W.T., Deans, N.D., Leonard, R.A. and Milne, A.J.: 'Condition Monitoring of Induction Motors for Availability Assessment in Offshore Installations', 4th Euredata Conference, Venice, March 1983.

13. Vincent, C.E.: 'Maintenance of Large Industrial Drives', IEE Colloquium on the Design and Applications of Large Industrial Drives, No. 170, 16-17, 1978.

14. Yang, S.J.: 'Low Noise Electrical Motors', Oxford Science Publications, 1981.

15. Bray, F.M. and Egle, D.M.: 'An Experimental Investigation of the Free Vibration of Thin Cylindrical Shells with Discrete Longitudinal Stiffening', Journal of Sound Vibration, 12(2), 1970.

16. Verma, S.P. and Girgis, R.S.: 'Experimental Verification of Resonant Frequencies and Vibration Behaviour of Stators of Electrical Machines, Part 2 - Experimental Investigations and Results', IEE Proceedings, Vol. 128, Pt.B, No. 1, Jan. 1981.

17. Erdelyi, E. and Horvay, G.: 'Vibration Modes of Stators of Induction Motors', Journal of Applied Mechanics, Trans. ASME, March 1957.

18. Den Hartog, J. P.: 'Vibration of Frames of Electrical Machines', Trans. ASME, APM - 50 - 6, 1928.

19. Den Hartog, J. P.: 'Vibration of Frames of Electrical Machines', Trans. ASME, APM - 50 - 11, 1928.

20. Verma, S.P. and Girgis, R.S.: 'Resonance Frequencies of Electrical Machine Stators having Encased Construction. Part 1 : Derivation of The General Frequency Equation', IEE Trans., Vol. PAS - 92, No. 5, Sept./Oct. 1973.

21. Ellison, A.J. and Yang, S.J.: 'Natural Frequencies of Stators of Small Electric Machines', Proc. IEE, Vol. 118, No. 1, Jan. 1971.

References (contd.)

22. Finch, D.J.: 'Vibration and Noise Response of Electrical Machine Stator Cores Excited by Magnetic Forces', Ph.D. Thesis, Aston University, 1976.

23. Verma, S.P.: 'Resonant Frequencies and Vibration Behaviour of Stators of Electrical Machines', IEE International Conference on Electrical Machines - Design and Applications, 1982.

24. Girgis, R.S. and Verma, S.P.: 'Method for Accurate Determination of Resonant Frequencies and Vibration Behaviour of Stators of Electrical Machines', IEE Proc., Vol. 128, Pt.B, No.1, Jan. 1981.

25. Tsvetkov, V.A. and Pikulskii, V.A.: 'The Effect on the Vibration State of Stator Winding End Coils of Making the Fixing System More Rigid', Elektrotekhnica (USSR), Vol. 53, No.1, 1982.

26. Timoshenko, S., Young, D.H. and Weaver, W.: 'Vibration Problems in Engineering', 4th Edition, John Wiley and Sons, 1974.

27. Flugge, W.: 'Stresses in Shells', Springer-Verlag, Berlin, 1960.

28. Alger, P.L.: 'The Magnetic Noise of Polyphase Induction Motors', AIEE Trans., Vol. 73, Pt. III, PAS, 1954.

29. Seidel, B.S. and Erdelyi, E.A.: 'On the Vibration of a Thick Ring in its Own Plane', Trans. ASME, Journal of Engineering for Industry, Pt. B, 86, Aug. 1964.

30. Buckens, F.: 'Influence of the Relative Radial Thickness of a Ring on its Natural Frequencies', J. Acoustical Society of America, Vol. 22, No. 4, July 1950.

31. Ellison, A.J. and Moore, C.J.: 'Acoustic Noise and Vibration of Rotating Electric Machines', Proc. IEE, Vol. 115, No. 11, Nov. 1968.

32. Verma, S.P. and Girgis, R.S.: 'Theoretical and Experimental Investigations on the Accurate Determination of Resonant Frequencies and Natural Response of Stators', Proc. International Conference on Electrical Machines, Vol. II, Brussels, Sept. 1978.

33. White, J.C.: 'The Flexural Vibrations of Thin Laminated Cylinders', J. of Engineering for Industry, Nov. 1961.

34. Thomson, W.T.: 'Vibration and Noise in Small-Power Electric Motors', MSc Thesis, University of Strathclyde, 1977.

35. Ball, R.E.: 'Dynamic Analysis of Rings by Finite Differences', J. of the Engineering Mechanics Division, Proc. ASCE, Feb.1967.

36. Shumilov, J.A.: 'Calculating Stator Vibrations in Electrical Machines', Proc. International Conference on Electrical Machines, London, 1974.

37. Yang, S.J.: 'Finite Element Method in Evaluating the Stator Natural Frequencies of Small Machines', Proc. International Conference on Electrical Machines, Vol. II, Brussels, Sept. 1978.

38. Watanabe, S., Kenjo, S., Ide, K., Sato, F. and Yamamoto, M.: 'Natural Frequencies and Vibration Behaviour of Motor Stators', IEEE Trans., Vol. PAS - 102, No.4, April 1983.

39. Davies, A.J.: 'The Finite Element Method: A First Approach', Oxford University Press, 1980.

40. Zienkiewicz, O.C.: 'The Finite Element Method in Structural and Continuum Mechanics', McGraw-Hill, 1967.

41. Rao, S.S.: 'The Finite Element Method in Engineering', Pergamon, 1982.

42. 'PAFEC 75 - Theory', PAFEC Ltd., 1984.

43. 'PAFEC 75 - Data Preparation', User Manual Level 5.1, PAFEC Ltd., 1984.

44. Broch, Prof. J.T.: 'Mechanical Vibration and Shock Measurements', Bruel and Kjaer, 1980.

45. Harris, C.M. and Crede, C.E.: 'Shock and Vibration Handbook', Vol. 1, McGraw-Hill, 1961.

46. Cameron, J.R. and Thomson, W.T.: 'Vibration and Current Monitoring for Detecting Airgap Eccentricity in Large Induction Motors', IEE Proc., Vol. 133, Pt. B, No. 3, May 1986.

47. Leonard, R.A.: 'Induction Motor Fault Recognition', MPhil Thesis, Robert Gordon's Institute of Technology, July 1985.

48. Verma, S.P. and Girgis, R.S.: 'Experimental Verification of Resonant Frequencies and Vibration Behaviour of Stators of Electrical Machines, Part 1 - Models, Experimental Procedure and Apparatus', IEE Proceedings, Vol. 128, Pt. B, No. 1, Jan. 1981.

49. Urusov, I.D. and Podrez, V.M.: 'Model Tests for Determining the Rigidity and Vibration Resistance of Electrical Stator Frames', Elektrichestva, 1959 (10), Translation by DSIR, RTS 1609, 1961.

50. Baudry, R.A., Heller, P.R. and Curtis, L.P.: 'Magnetic Vibrations in A-C Generator Stators', Trans. AIEE, 73, Pt. III, June 1954.

51. Barton, S.C. and Taylor, H.D.: Discussion of Reference 50, Trans. AIEE, 73, Pt. III, June 1954.

52. Warburton, G.B.: 'The Vibration of Rectangular Plates', Proceedings of the IMechE, Vol. 168, 1954.

53. Timoshenko, S. and Woinowsky-Krieger, S.: 'Theory of Plates and Shells', 2nd Edition, McGraw-Hill, 1959.

54. Chu, F.H. and Wang, B.P.: 'Experimental Determination of Damping in Materials and Structures', ASME - Damping Applications for Vibration Control, AMD - 38, Nov. 1980.

55. Kennedy, C.C. and Pancu, C.D.P.: 'Use of Vectors in Vibration Measurement and Analysis', J. of Aero Sciences, Vol. 14, No. 11, Nov. 1947.

56. Gladwell, G.M.L.: 'A Refined Estimate for the Damping Coefficient', J. of Royal Aeronautical Soc., Vol. 66, Feb. 1962.

57. Yang, S.J.: 'The Measurement and Calculation of Acoustic Noise from Electric Machines', PhD Thesis, University of London, April 1970.

58. Alger, P.L.: 'The Nature of Induction Machines', Gordon and Breach, 1965.

References (contd.)

59. Linders, J.R.: 'Effects of Power Supply Variations on A.C. Motor Characteristics', IEEE Trans. Vol. IA-8, Pt. 4, 1972.

60. Gleason, L.L. and Elmore, W.A.: 'Protection of 3-Phase Motors Against Single-Phase Operation', AIEE Trans., Power, Apparatus and Systems, Vol. 77, No. 39, Dec. 1958.

61. McPartland, J.F.: 'Motor Burnout on Single-Phasing', Electrical Construction and Maintenance, Vol. 82, Pt. 10, Oct. 1983.

62. Shan Griffith, M.: 'A Penetrating Gaze at One Open Phase; Analysing the Polyphase Induction Motor Dilemma', IEEE Trans., Vol. IA-13, No. 6, Nov./Dec. 1977.

63. Penman, J., Hadwick, J.G. and Stronach, A.F.: 'Protection Strategy Against the Occurrence of Faults in Electrical Machines', IEE Conf. Publication 185, 1980.

BIBLIOGRAPHY

BOOKS:

Collacot, R.A. : 'Mechanical Fault Diagnosis, and Condition Monitoring', Chapman and Hall, 1977.

Owen, D.R.J. and Hinton, E. : 'A Simple Guide to Finite Elements', Pineridge Press, 1980.

Den Hartog, J.P. : 'Mechanical Vibrations', 4th Edition, McGraw-Hill, 1956.

Srinivasulu, P. and Vaidyanathan, C.V. : 'Handbook of Machine Foundations', McGraw-Hill, 1977.

Say, M.G. : 'Alternating Current Machines', 5th Edition, Pitman, 1983.

Hindmarsh, J. : 'Electrical Machines and their Applications', 4th Edition, Pergamon, 1984.

PUBLISHED PAPERS:

Claessens, C. : 'Condition Monitoring of Rotating Equipment with Vibration Measurements', Plant Condition Monitoring Eurotest Seminar, London, Sept. 1979.

'Condition Monitoring: A Step Ahead of Failure', Electrical Review, Vol. 207, No. 18, Nov. 1980.

Webb, R. : 'Frequency Domain Instrumentation Techniques for the Condition Monitoring of Rotating Machinery', Noise and Vibration Worldwide, Oct. 1983.

Rabek, E.E. : 'Machine Vibration Analysis and Monitoring', 18th Annual Petroleum and Chemical Industry Conf., USA, PC1 - 71 - 5, Sept. 1971.

'Vibration Analysis for Condition Monitoring and Component Design', Sensor Review, Jan. 1983.

Knight, A.L. : 'Vibration Monitoring Forewarns of Failure', Design Engineering, Jan. 1978.

White, C.J. and Temple, D.W. : 'Better Fault Analysis from Vibration', Electrical Times, Pt. 4653, April 30th 1982.

Downham, E. : 'Vibration in Rotating Machinery: Malfunction Diagnosis - Art and Science', Int. Conf. on Vibrations in Rotating Machinery, Cambridge, 1976.

Binns, K.J. and Barnard, W.R. : 'Some Aspects of the Use of Flux and Vibration Spectra in Electrical Machines", Conf. on Applications of Time-Series Analysis, Sept. 1977.

Graybeal, T.D. : 'The Nature of Vibration in Electric Machinery', Trans. AIEE, Vol. 63, 1944.

Richardson, P. and Hawley, R. : 'Generator Stator Vibration', IEEE Winter Power Meeting, New York, Jan. 1970.

Robinson, R.C. : 'Line-Frequency Magnetic Vibration of A-C Machines', AIEE Trans., PAS 62-199, Vol. 81, Feb. 1963.

Nagano, S., Tari, M., Nakano, M., Ito, K. and Uto, Y. : 'Early Detection of Excessive Coil Vibration in High-Voltage Rotating Electric Machines', IEEE Trans., Vol. PAS-101, No.6, June 1982.

Lawrenson, P.J. ; 'Forces on Turbogenerator End Windings', Proc. IEE, Vol. 112, No. 6, June 1965.

Campbell, J.J., Clark, P.E., McShane, I.E. and Wakeley, K. : 'Strains on Motor Endwindings', IEEE Conf. Petroleum and Chemical Industry, U.S.A., August 1982.

Dunki-Jacobs, J.R. and Kerr, R.H. : 'A Quantitative Analysis of Grouped Single-Phased Induction Motors', IEEE Trans., Vol. IA-17, No. 2, March/April 1981.

Williams, J.E. : 'Operation of 3-Phase Induction Motors on Unbalanced Voltages', AIEE Trans., Vol. 73, Part III, April 1954.

Ortmeyer, T.H. and Mahmoud, A.A. : 'Induction-Motor Dynamic Analysis during Power Supply Imbalances', International Journal of Electrical Power and Energy Systems, Vol. 13, No.4, Oct. 1981.

Woll, R.F. : 'Effect of Unbalanced Voltage on the Operation of Polyphase Induction Motors', IEEE Trans., Vol. IA-11, No. 1, Jan. 1975.